



UNIVERSIDADE D  
**COIMBRA**

Vanessa Almeida Tomé

**SYNTHESIS OF PROBES FOR CANCER  
MOLECULAR IMAGING**

**Tese no âmbito do doutoramento em Química, ramo de  
especialização em Química Médica orientada pela Professora  
Doutora Maria Miguéns Pereira, co-orientada pelo Professor  
Doutor Pedro Miguel Pimenta Góis e apresentada ao  
Departamento de Química da Faculdade de Ciências e Tecnologia  
da Universidade de Coimbra.**

Julho de 2020

Universidade de Coimbra

Departamento de Química – Faculdade de Ciências e Tecnologia

# **Synthesis of Probes for Cancer Molecular Imaging**

Vanessa Almeida Tomé

Tese no âmbito do doutoramento em Química, ramo de especialização em Química Médica orientada pela Professora Doutora Maria Miguéns Pereira, co-orientada pelo Professor Doutor Pedro Miguel Pimenta Góis e apresentada ao Departamento de Química da Faculdade de Ciências e Tecnologia da Universidade de Coimbra.

**Coimbra, 2020**



## Agradecimentos

Desejo expressar o meu sincero reconhecimento a todos aqueles que contribuíram para o desenvolvimento deste trabalho.

À Doutora Professora Mariette Pereira, minha orientadora, agradeço por me dar a oportunidade de realizar a minha Dissertação de Doutoramento junto do seu grupo de investigação, e pela sapiência que demonstrou para me ajudar a avançar neste trabalho e na minha formação em geral. Agradeço todo o apoio científico e a inestimável ajuda.

Ao Doutor Professor Pedro Góis agradeço pela co-orientação deste trabalho e pela simpatia e forma exemplar como me recebeu no seu laboratório na Universidade de Lisboa.

Não posso também deixar de expressar o meu agradecimento ao Professor Doutor Antero Abrunhosa do Instituto de Ciências Nucleares Aplicadas à Saúde (ICNAS) pela introdução no mundo fantástico que é a radioquímica. Um agradecimento especial à Ângela Neves e ao Vítor Alves pela ajuda e disponibilidade nos estudos de radiomarcagem. Gostaria ainda de agradecer ao Doutor José Sereno pela sua colaboração nos estudos *in vivo*.

Ao Hélder Soares agradeço os estudos *in vitro* e os cálculos teóricos.

Ao Professor Doutor Rui Brito e ao Pedro Cruz do serviço de Ressonância magnética Nuclear de Centro de Química de Coimbra (CCC-NMR) agradeço a colaboração na obtenção dos espectros de RMN.

Agradeço o apoio financeiro da Fundação para a Ciência e Tecnologia (FCT) através da cedência da bolsa de doutoramento do Programa Doutoral MedChemTrain PD/BD/128318/2017.

A todos os meus colegas do laboratório de Catálise e Química Fina Mário Calvete, Rui Carilho, Sara Pinto, César Henriques, Liliana Damas, Andreia Gonzalez, Fábio Rodrigues, Lucas Dias, Guisi Piccirillo, Rafael Aroso, Carolina Vinagreiro e Diana Gomes, obrigado pela boa disposição, espírito de entreajuda e companheirismo. Um agradecimento especial ao Mário pela prestável colaboração para discutir qualquer assunto bem como todo o incentivo e confiança.

Desejo expressar um agradecimento muito especial à Liliana e à Andreia (a minha “nutrição” e o meu “furacão”), pelos preciosos conselhos, pela amizade e o incansável apoio que me deram nesta longa jornada que foi o Doutoramento. Levo-vos comigo!

A todos os meus amigos desejo agradecer a amizade, o carinho, o apoio e a boa disposição que permitiram que esta caminhada fosse, nos seus bons e maus momentos, levada até ao fim. À Adriana, à Tita, à Catarina, à Rosa, à Mariana, à Dani, ao Miguel, ao Jorge, ao Ramirão, à Ema, à Anais e ao Tó, um muito obrigado! Muitos foram os momentos partilhados com vocês ao longo destes anos, e cada um de vocês tem e terá para sempre um lugar muito especial no meu coração. Um agradecimento muito especial à malta das “Cuecas Team”. O monte alentejano espera-nos amigos!

Aos meus Pais e ao meu irmão! Sem vós tudo isto teria sido quase impossível! Obrigado pelo vosso apoio incondicional, compreensão e carinho ao longo destes anos.

Por último, agradeço ao Nuno pelos grandes momentos de felicidade, mas principalmente, pelo apoio nos mais difíceis. Obrigado por todo o amor, paciência e compreensão...enfim, obrigado por tudo.

**Vanessa Almeida Tomé**

Julho de 2020

## Table of contents

Abstract.....	i
Resumo.....	iv
Abbreviations and symbols.....	vii
Nomenclature.....	xi
<b>Chapter 1 – Introduction.....</b>	<b>1</b>
1.1 Phthalocyanines.....	2
1.1.1 Synthetic methods of phthalocyanines.....	7
1.1.2 Biocompatible phthalocyanines.....	11
1.2 Positron Emission Tomography.....	14
1.2.1 Radiopharmaceuticals in Positron Emission Tomography.....	16
1.2.2 Radiopharmaceuticals for cancer Positron Emission Tomography imaging .....	18
1.2.3 Radiopharmaceuticals for brain Positron Emission Tomography imaging.....	23
1.3 Fluorescence Imaging.....	30
1.3.1 Near-infrared fluorophores for fluorescence cancer imaging.....	31
1.4 Aim of this thesis.....	35
1.5 References.....	38
<b>Chapter 2 – Development of <sup>64</sup>Cu-labelled phthalocyanines as potential probes for application in cancer PET imaging.....</b>	<b>50</b>
2.1 Introduction.....	50
2.2 Synthesis and structural modulation of phthalonitriles.....	51
2.3 Synthesis of β-tetra-substituted phthalocyanines.....	60
2.3.1 Synthesis of tetra-choline substituted phthalocyanine.....	68
2.4 Radiolabelling of phthalocyanines with copper-64.....	69
2.4.1 Synthesis of copper(II) metallophthalocyanines (non-radioactive synthesis).....	69

2.4.2 Labelling methodology.....	72
2.4.3 Labelling of phthalocyanines with [ <sup>64</sup> Cu]copper dichloride (radioactive synthesis).....	74
2.4.4 <i>In vitro</i> radiochemical stability studies of <sup>64</sup> Cu-labelled phthalocyanines.....	82
2.5 <i>In vivo</i> PET imaging and biodistribution studies of tetra-choline <sup>64</sup> Cu-labelled phthalocyanine.....	84
2.6 Conclusion.....	87
2.7 References.....	89

### **Chapter 3 – Development of <sup>11</sup>C-labelled β-indolyketones as potential**

probes for application in brain PET imaging.....	91
3.1 Introduction.....	91
3.2 Synthesis of β-indolyketones.....	92
3.3 <i>In vitro</i> cytotoxic studies and computational determination of octan-1-ol/water partition coefficient values of <i>N</i> -methylated β-indolyketones.....	104
3.4 Radiolabelling of β-indolyketones with carbon-11.....	107
3.4.1 Labelling methodology.....	107
3.4.2 Optimization of HPLC conditions.....	111
3.4.3 Labelling of β-indolyketones with [ <sup>11</sup> C]iodomethane.....	116
3.5 Exploratory <i>in vivo</i> PET imaging and biodistribution studies of <sup>11</sup> C-labelled β-indolyketones.....	123
3.6 Conclusion.....	127
3.7 References.....	130

### **Chapter 4 – Structural modulation of glyco-phthalocyanines for the development**

of potential fluorophores for Fluorescence Imaging.....	133
4.1 Introduction.....	133
4.2 Synthesis of α-octa-substituted phthalocyanines.....	135
4.3 UV-Visible absorption and fluorescence emission spectroscopy of synthesized glyco-phthalocyanines.....	144
4.4 Conclusion.....	153

4.5 References.....	155
<b>Chapter 5 – Experimental.....</b>	<b>158</b>
5.1 Instrumentation and methodology.....	158
5.2 Solvents and reagents.....	164
5.3 Experimental (referring to Chapter 2).....	166
5.3.1 Synthesis of 4-substituted phthalonitriles.....	166
5.3.2 Synthesis of $\beta$ -tetra-substituted phthalocyanines.....	170
5.3.3 Radiolabelling studies with copper-64.....	183
5.4 Experimental (referring to Chapter 3).....	186
5.4.1 Synthesis of $\beta$ -indolylketones.....	186
5.4.2 Radiolabelling studies with carbon-11.....	192
5.5 Experimental (referring to Chapter 4).....	193
5.6 References.....	198



## Abstract

The work presented in this thesis is focused on the of design, synthesis and structural modeling studies of phthalocyanines, to obtain new potential probes for cancer diagnosis by molecular imaging, using Positron Emission Tomography (PET) and Fluorescence Optical Imaging (FI) techniques. Furthermore, studies involving the synthesis of small molecules based on the indole and chalcone scaffolds, namely  $\beta$ -indolylketones were also carried out, with the purpose of developing new probes for the diagnosis of brain pathologies, using the PET technique.

In **Chapter 1** the state of the art literature is revised, focusing on the main subjects developed throughout the experimental work, namely on the synthetic methods and structural modulation of phthalocyanines. Furthermore, a literature review on the application of phthalocyanines in PET and FI is also presented, as well as on the application of chalcone and indole derivatives as probes for brain pathologies using PET technique.

**Chapter 2** describes the synthetic methodologies for symmetrical tetra-substituted phthalocyanines in peripheral positions and their metal complexes preparation, aiming at the preparation of potential probes labelled with copper-64 for cancer diagnosis using PET imaging. In a first subtopic, the studies involving the synthesis and structural modeling of phthalonitrile precursors were carried out, involving different substituents – galactose, choline and polyethylene glycol derivatives – whose further cyclotetramerization into phthalocyanines were intended to provide the desired biocompatibility and/or the specificity and selectivity for tumor cells. The second subtopic describes the synthetic methodology that led to the synthesis of the corresponding metal-free phthalocyanines, the precursors for the copper-64 labelling. This methodology was based on the preparation of the corresponding zinc(II) (or alternatively magnesium(II) complexes) from the cyclotetramerization reaction of the previously synthesized phthalonitriles, followed by demetallation with acidic conditions, which yielded the desired metal-free phthalocyanines in isolated yields of 79–85%. The third subtopic present the studies on the development of a synthetic methodology that allowed to obtain the non-radioactive copper(II) phthalocyanine

complexes, with isolated product yields between 86–94%. This methodology was implemented for labelling processes with copper-64, developed at the Institute of Nuclear Sciences Applied to Health (ICNAS), yielding phthalocyanines labelled with copper-64 in moderate to high radiochemical yields (37–98%) and high degree of radiochemical purity (>98%). Furthermore, *in vitro* stability studies of the radioactive phthalocyanine complexes in physiological conditions were carried out, and these studies showed the high stability of copper-64 phthalocyanine complexes. Biodistribution studies in BALB/c mice were performed with one selected phthalocyanine, the tetra-substituted one with choline groups and labelled with copper-64 (**2.14e**), which revealed a high accumulation in the spleen and liver and the hepatobiliary route as its main excretion pathway.

**Chapter 3** describes the optimization of microwave-assisted synthesis of a family of  $\beta$ -indolylketones and their subsequent radiolabelling with carbon-11 aiming at the preparation of new potential PET probes for brain imaging. The  $\beta$ -indolylketones and the corresponding methylated standard compounds were synthesized in 82–91% isolated yields. The lipophilic nature of standard compounds was studied and theoretical values of the octan-1-ol/water partition coefficient (ClogP) between 2.73 e 3.13 were obtained. The development and optimization of analytical and semi-preparative HPLC methods was performed, which allowed an efficient separation/purification of the  $\beta$ -indolylketone 1-(4-fluorophenyl)-3-(1*H*-indol-3-yl)-3-(4-methoxyphenyl)propan-1-one (**3.2c**) and the corresponding standard methylated  $\beta$ -indolylketone 1-(4-fluorophenyl)-3-(4-methoxyphenyl)-3-(1-methyl-1*H*-indol-3-yl)propan-1-one (**3.3c**). Then, the study involving the labelling of compound **3.2** *via* methylation reaction with [<sup>11</sup>C]iodomethane, in an automated radiosynthesis module of ICNAS was carried out, providing the compound 1-(4-fluorophenyl)-3-(4-methoxyphenyl)-3-(1-[<sup>11</sup>C]methyl-1*H*-indol-3-yl)propan-1-one (**3.4c**), analogous to non-radioactive standard **3.3**, in >98% radiochemical purity and chemical purity of  $\approx$ 90%. Preliminary biodistribution studies in BALB/c mice with several carbon-11 labelled  $\beta$ -indolylketones were performed, and the compound 3-(4-bromophenyl)-1-(4-methoxyphenyl)-3-(1-[<sup>11</sup>C]methyl-1*H*-indol-3-yl)propan-1-one (**3.4b**) was shown to display the highest brain uptake.

In **Chapter 4** optimization studies involving the synthesis and structural modeling of symmetrical phthalocyanines were described, aiming at the preparation of new fluorophores for potential application in cancer diagnosis using FI. In order to provide the suitable structural characteristics that could induce an optimal absorption in the near-infrared region of the electromagnetic spectrum, phthalocyanines incorporating eight galactose units in non-peripheral positions were synthesized. The photophysical characterization of the metal-free, zinc(II) and magnesium(II) phthalocyanines was also carried out, which showed promising characteristics for further potential use as fluorophores in FI, such as selective fluorescence emission in the near-infrared region (753–812 nm), large Stokes shifts (17–30 nm) and fluorescence quantum yields between 0.02 and 0.17.

In **Chapter 5**, all experimental procedures and full characterization of all synthesized compounds are described.

**Keywords:** Molecular imaging, Positron Emission Tomography (PET), Fluorescence Optical Imaging (FI), Phthalocyanines, Chalcones.

## Resumo

O trabalho apresentado nesta tese centra-se nos estudos de *design*, síntese e modelação estrutural de ftalocianinas, com vista ao desenvolvimento de potenciais marcadores para diagnóstico de cancro por imagiologia molecular, usando as técnicas de Tomografia por Emissão de Positrões (PET) ou Imagiologia Ótica de Fluorescência (FI). Adicionalmente, procedeu-se a estudos envolvendo a síntese de pequenas moléculas tendo como estrutura base derivados indole e chalcona, nomeadamente as cetonas  $\beta$ -indolilo, com o objetivo de desenvolver marcadores para o diagnóstico de patologias a nível cerebral, usando a técnica de PET.

No **Capítulo 1** apresenta-se uma revisão da literatura sobre as principais temáticas desenvolvidas no decorrer do trabalho experimental, nomeadamente nos métodos de síntese de ftalocianinas. Neste capítulo apresenta-se também uma revisão da literatura da aplicação de ftalocianinas como marcadores em imagiologia por PET e FI, e ainda de derivados de chalconas e indole como marcadores de patologias cerebrais usando a técnica de PET.

No **Capítulo 2** são descritos os métodos utilizados para a síntese de ftalocianinas simétricas tetra-substituídas nas posições periféricas e seus complexos metálicos, com vista à posterior preparação de potenciais marcadores com cobre-64, para aplicação em diagnóstico de cancro usando imagiologia por PET. Num primeiro subtópico, procedeu-se aos estudos envolvendo a síntese e modelação estrutural dos precursores ftalonitrilo, contendo diferentes grupos substituintes – derivados da galactose, colina e polietileno glicol – com o objetivo de obter as correspondentes ftalocianinas com acrescida biocompatibilidade e/ou especificidade para as células tumorais. No segundo subtópico são abordadas as reações de ciclotetramerização que conduziram à síntese das correspondentes ftalocianinas de base livre, precursoras da reação de marcação com cobre-64. Esta metodologia baseou-se na preparação dos respetivos complexos de zinco(II) (ou alternativamente de magnésio(II)) a partir dos ftalonitrilos convenientemente substituídos, seguido de remoção do metal em meio ácido. Com esta metodologia, obtiveram-se as ftalocianinas de base livre pretendidas com rendimentos isolados de 79–85%. No terceiro subtópico apresentam-se os

estudos do método de síntese que permitiu a obtenção dos complexos de cobre(II) de ftalocianinas não radioativos em rendimentos de produto isolado de 86–94%. A metodologia foi transposta para processos de marcação com cobre-64 desenvolvidos no Instituto de Ciências Nucleares Aplicadas à Saúde da Universidade de Coimbra (ICNAS), tendo-se obtido ftalocianinas marcadas com cobre-64 em rendimentos radioquímicos moderados a elevados (37–98%) e com elevado grau de pureza radioquímica (>98%). Adicionalmente, foram efetuados estudos *in vitro* de estabilidade dos complexos de ftalocianina radioativos em condições fisiológicas, tendo-se verificado a elevada estabilidade destes. Foram ainda efetuados estudos de biodistribuição em ratinhos BALB/c, realizados com uma das ftalocianinas selecionadas, a ftalocianina tetra-substituída com grupos colina marcada com cobre-64 (**2.14e**), que revelaram uma elevada acumulação no baço e fígado, tendo-se constatado que a principal via de excreção é a via hepatobiliar.

No **Capítulo 3** apresentam-se estudos de otimização da síntese de uma família de cetonas  $\beta$ -indolilo usando irradiação de micro-ondas e sua posterior marcação com carbono-11, com vista à obtenção de marcadores com potencial aplicação em imagiologia a nível cerebral por PET. As cetonas  $\beta$ -indolilo e os correspondentes compostos padrão metilados foram sintetizados com rendimentos entre 82 e 91%. O carácter lipofílico dos compostos padrão foi também estudado e foram obtidos coeficientes de partição octan-1-ol/água teóricos entre 2,73 e 3,13. Foram ainda optimizadas condições de separação/purificação, por HPLC analítico e semi-preparativo, para o composto 1-(4-fluorofenil)-3-(1*H*-indol-3-il)-3-(4-metoxifenil)propan-1-ona (**3.2c**) e do respetivo composto padrão 1-(4-fluorofenil)-3-(1-metil-1*H*-indol-3-il)-3-(4-metoxifenil)propan-1-ona (**3.3c**). Após esta optimização, procedeu-se então ao estudo de marcação do composto **3.2c** com [<sup>11</sup>C]iodometano, via metilação, num módulo automático de radiosíntese do laboratório do ICNAS, obtendo-se o composto 1-(4-fluorofenil)-3-(1-[<sup>11</sup>C]metil-1*H*-indol-3-il)-3-(4-metoxifenil)propan-1-ona (**3.4c**), análogo do composto padrão não-radioativo **3.3c**, com um grau de pureza radioquímica >98% e uma pureza química de  $\approx$ 90%. Estudos preliminares de biodistribuição em ratinhos BALB/c com várias cetonas  $\beta$ -indolilo marcadas com carbono-11 foram efetuados, tendo-se observado que o composto 3-(4-bromofenil)-3-

(1-[<sup>11</sup>C]metil-1*H*-indol-3-il)-1-(4-metoxifenil)propan-1-ona (**3.4b**) revelou uma maior captação cerebral.

No **Capítulo 4**, descrevem-se os estudos de otimização da síntese e modelação estrutural de derivados simétricos de ftalocianinas e seus complexos metálicos, com vista à preparação de novos fluoróforos para potencial aplicação em diagnóstico de cancro por FI. Por forma a conferir a estas as características estruturais que permitissem absorver luz na região do infravermelho, ftalocianinas contendo oito unidades galactose nas posições não periféricas foram sintetizadas. Procedeu-se também à caracterização fotofísica dos complexos de base livre, zinco(II) e magnésio(II), que revelaram possuir características promissoras para aplicação como fluoróforos em FI, devido à seletiva emissão de fluorescência na região do infravermelho (753–812 nm), elevados desvios de Stokes (17–30 nm) e rendimentos quânticos de fluorescência entre 0.02 e 0.17.

No **Capítulo 5**, apresentam-se os procedimentos experimentais e a completa caracterização química de todos os compostos sintetizados.

**Palavras-chave:** Imagiologia molecular, Tomografia por Emissão de Positrões (PET), Imagiologia Ótica de Fluorescência (FI), Ftalocianinas, Chalconas.

## Abbreviations and Symbols

$\delta$	chemical shifts
$\lambda$	wavelength
$\epsilon$	molar extinction coefficient
$\gamma$	gamma
$\mu\text{Ci}$	microcurie
$\mu\text{M}$	micromolar
$\beta^+$	positron
$\beta^-$	beta emission
Bq	Becquerel
$\Phi_F$	fluorescence quantum yield
br	broad signal
d	doublet
dd	doublet of doublets
$J$	coupling constant
m	multiplet
s	singlet
sl	large singlet
t	triplet
$[\text{M}]^+$	molecular ion
$^1\text{H-NMR}$	proton nuclear magnetic resonance spectroscopy
$^{13}\text{C-NMR}$	carbon 13 nuclear magnetic resonance spectroscopy
3T3 cells	mouse embryo fibroblasts
AcOH	acetic acid
AD	Alzheimer's Disease
BBB	Blood-Brain Barrier
BuOH	butan-1-ol
Ci	Curie
COSY	correlation spectroscopy in nuclear magnetic resonance
CuPc	copper(II) phthalocyanine complex
Da	dalton

DBU	1,8-Diazabicyclo(5.4.0)undec-7-ene
DCTB	Trans-2-[3-(4-tert-butylphenyl)-2-methyl-2-propenylidene]malonitrile
DEAD	diethyl azodicarboxylate
DMAE	<i>N,N</i> -dimethylaminoethanol
DMEM	Dulbecco's modified eagle medium
DMF	<i>N,N</i> -dimethylformamide
DMSO	dimethyl sulfoxide
D <sub>7.4</sub>	octanol-1-ol/water partition coefficient at physiological pH
EC	electron capture
EDTA	ethylenediaminetetraacetic acid
EMA	European Medicines Agency
ESI	Electrospray ionization
EtOH	ethanol
FDA	Food and Drug Administration
FI	Fluorescence Imaging
FT-IR	Fourier-transform infrared spectroscopy
GC	gas chromatography
GC-MS	gas chromatography coupled with mass spectrometry
h	hours
H <sub>2</sub> Pc	metal-free phthalocyanine
HMBC	heteronuclear multiple-bond correlation
HMQC	heteronuclear multiple-quantum correlation
HOMO	highest occupied molecular orbital
HPLC	high performance liquid chromatography
HITIC	1,1',3,3,3',3'-hexamethylindotricarbocyanine iodide
ICG	Indocyanine Green
ICNAS	Institute of Nuclear Sciences Applied to Health (Instituto de Ciências Nucleares Aplicadas à Saúde)
IC <sub>50</sub>	half-maximal inhibitory concentration
<i>i</i> PrOH	isopropanol
LiOPe	lithium pentanolate
LOR	line of response



LUMO	lowest unoccupied molecular orbital
MALDI-TOF	matrix assisted laser desorption/ionization
MB	Methylene Blue
mCi	milicurie
mg	miligrams
MgPc	magnesium(II) phthalocyanine complex
MI	molecular imaging
min	minutes
mL	mililiter
MPc	metallophthalocyanine
MS	mass spectrometry
m/z	mass/charge relation
NIR	near-infrared
nm	nanometer
OcOH	octan-1-ol
P	octan-1-ol/water partition coefficient
PBS	phosphate-buffered saline
Pc	phthalocyanine
PDT	photodynamic therapy
PEG	polyethylene glycol
PET	Positron Emission Tomography
PeOH	pentan-1-ol
Ph. Eur.	European Pharmacopoeia
ppm	parts per million
<i>p</i> -TsOH	<i>para</i> -toluenesulfonic acid
RCC	radiochemical conversion
RCY	radiochemical yield
$R_f$	retention factor (for thin layer chromatography)
RT	room temperature
SPE	Solid Phase Extraction
TFA	trifluoroacetic acid
THF	tetrahydrofuran

TLC	thin-layer chromatography
TMS	tetramethylsilane
$t_R$	retention time
$t_{1/2}$	half-life
UV	Ultraviolet
UV-Vis	Ultraviolet–visible
ZnPc	zinc(II) phthalocyanine complex

## Nomenclature

In this thesis, the IUPAC recommendations were followed to number and name all compounds, with some exceptions. The numbering and nomenclature of each family of compounds synthesized is presented below.

Concerning the synthesized phthalocyanine precursors, trivial names (phthalonitriles)<sup>i</sup> were used instead of IUPAC nomenclature (1,2-dicyanobenzene). The numbering system used for the phthalonitriles is in agreement with the IUPAC nomenclature for aromatic rings,<sup>ii</sup> as shown in **Figure I** for exemplifying 4-nitrophthalonitrile.

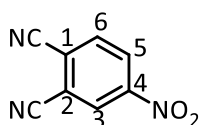


**Figure I.** 4-nitrophthalonitrile.

The adopted nomenclature for phthalocyanines was based on the IUPAC regulations (**Figure II**).<sup>iii</sup>

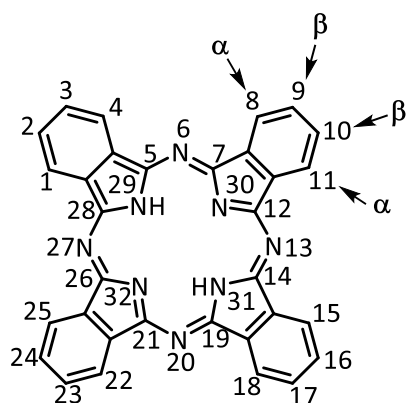


**Figure II.** IUPAC nomenclature of phthalocyanines.

All carbon and nitrogen atoms of phthalocyanine are numbered, with the exception of carbon atoms that correspond to the fusion of pyrrole ring and benzene ring. The numbering is initiated on a carbon of the vicinal benzene ring to a fusion carbon between the pyrrole ring and the benzene ring. After the numbering of the atoms that constitute the external carbons of the macrocycle (1-28), the numbering of the four inside pyrrolic

nitrogen is performed (29-32). For simplicity, the inner and outer positions of the benzene ring are often referred to as  $\alpha$  and  $\beta$  positions, respectively, as shown in **Figure II**.

In this thesis, all the synthesized  $\beta$ -tetra-substituted phthalocyanines are mixture of four positional isomers. So, the alternative positions of the substituent groups occupied in each isomer are indicated in parentheses. As example, the compound shown in **Figure III** is named [2(3),9(10),16(17),23(24)-tetrakis-(methyl)phthalocyaninato] zinc(II).

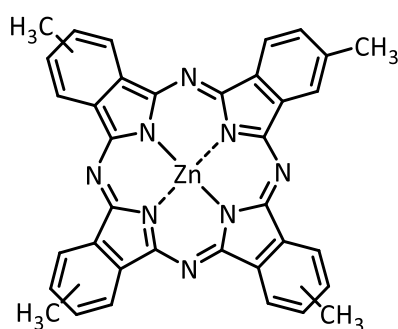


**Figure III.** Structure of [2(3),9(10),16(17),23(24)-tetrakis-(methyl)phthalocyaninato] zinc(II).

The numbering system used for the synthesized  $\beta$ -indolylketone derivatives follows the IUPAC regulations,<sup>iv</sup> as shown in **Figure IV** for 3-(1*H*-indol-3-yl)-1,3-diphenylpropan-1-one. The numbering system used for the A and B rings follow the IUPAC nomenclature for aromatic rings, as well the indole ring (C ring).

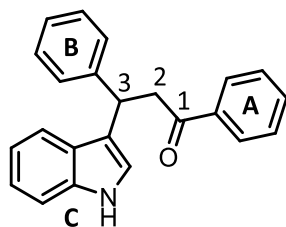


**Figure IV.** 3-(1*H*-indol-3-yl)-1,3-diphenylpropan-1-one.

## References

<sup>i</sup> Kadish, K. M.; Smith, K. M.; Guillard, R., *The Porphyrin Handbook*, volume 15, Academic Press, Amsterdam, **2003**, Chapter 97, 1–60.

---

ii Tomé, A., *Introdução à Nomenclatura dos Compostos Orgânicos*, Escolar Editora, Lisboa, **2010**.

iii Merritt, J. E.; Loening, K. L., *Pure and Applied Chemistry* **1979**, 51, 2251–2304.

iv Rauter, A. P.; Ennis, M.; Hellwich, K.-H.; Herold, B. J.; Horton, D.; Moss, G. P.; Schomburg, I., *Pure and Applied Chemistry* **2018**, 90 (9), 1429–1486.

# CHAPTER 1

---

## *Introduction*

---

Cancer is currently one of the major causes of death worldwide, constituting a large group of heterogeneous diseases characterized by uncontrolled growth and spread of abnormal cells and aberrant cell behavior.<sup>1</sup> It is the most inexorable affliction of our era! Such concern is much evidenced by the vast number of scientific and academic publications, as well as by the numerous initiatives directly sponsored by international entities such as the World Health Organization (WHO). According to WHO, the global burden is expected to grow to 21.4 million new cancer cases and 13.2 million cancer deaths by 2030. In 2018 alone, 18.1 million new cancer cases and 9.6 million cancer deaths have been reported worldwide.<sup>2</sup>

In this respect, it is well accepted in the medical and scientific community that probably the most effective solution to diminish the number of deaths by cancer is based on its early detection. When cancer is diagnosed at an early stage, the more effective the treatment is likely to be, resulting in greater surviving probabilities, as well as less distressful and expensive treatments.<sup>3</sup> Consequently, there is a huge incentive for the development of technologies capable of cancer detection at its earliest stage possible. Among these technologies, Molecular Imaging (MI), a non-invasive technique, has experienced an exponential growth over the last few decades, becoming currently part of standard care in the clinical oncology. Bluntly, MI allows to see, characterize and measure many *in vivo* biological processes at molecular and cellular levels.<sup>4,5</sup> Therefore, the highest advantage of *in vivo* MI is its ability to characterize cancer tissues without invasive biopsies or surgical procedures, allowing a more personalized treatment planning. Additionally, this technology can provide important predictive relevant information regarding therapy response or even disease recurrence monitoring.<sup>6,7</sup>

Such early-stage cancer diagnostic techniques generally require patient intravenous administration of a MI probe, used to allow the visualization and quantification of the biological processes inside the human body, leading to more precise diagnostics. Therefore, the full potential of MI techniques strongly depends on the availability and/or design of proper highly specific and sensitive imaging probes for cellular and molecular processes related to cancer.<sup>8,9</sup>

In this context, the elucidation and development of novel chemical entities with tunable properties for potential application as probes in cancer MI is one of the most important subjects in medicinal chemistry area. Therefore, the main goal of this thesis is to go beyond the state of art regarding the molecular design of ideal MI probes for cancer diagnosis. Our studies started with the selection of promising molecular platforms, whose choice relied on a deep understanding of the structure-property relationships, in order to fine-tune their specific features for the target MI technique. Thus, the work described in this thesis aims the design, synthesis and the study of new: i) macrocyclic compounds such as phthalocyanines and ii) small molecules, based on indole and chalcone scaffolds, as molecular platforms for the development of potential MI probes for Positron Emission Tomography (PET) and/or Fluorescence Imaging (FI) targeting cancer or brain disorders.

## 1.1 Phthalocyanines

Phthalocyanines (Pcs) belong to the broad class of macrocyclic tetrapyrrole compounds, being characterized by having a set of four isoindole rings linked through their 1,3-positions by aza-bridges. Pcs possess a set of conjugated double bonds that form an aromatic ring with eighteen  $\pi$  electrons, delocalized over 32 carbon and 8 nitrogen atoms (**Figure 1.1, a**).<sup>10</sup> Although phthalocyanine structure are related to the naturally occurring porphyrins, such as hemoglobin, (**Figure 1.1, b**) vitamin B<sub>12</sub> or chlorophyll, those cannot be found in nature.

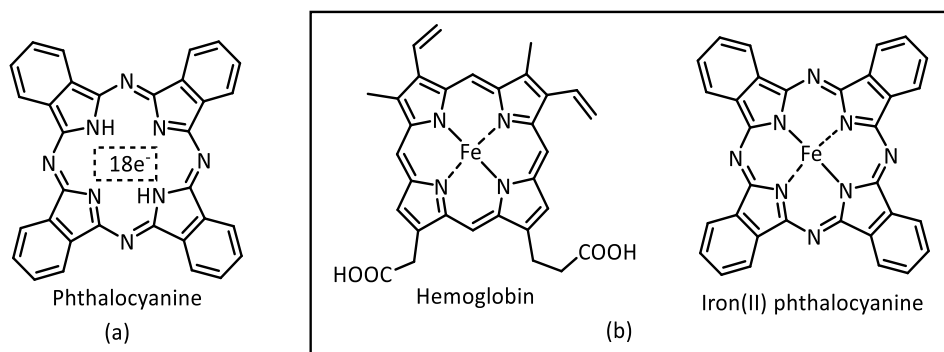


**Figure 1.1** (a) electronic delocalization over the Pc's aromatic ring; (b) structural relationship between hemoglobin and a phthalocyanine.

These macrocycles exist both as free bases (metal-free), with two of the four central ring nitrogen atoms covalently bonded to two hydrogen atoms, and in the form of metal complexes, resulting from the coordination of different metal atoms with the central nitrogen atoms (**Figure 1.2**).

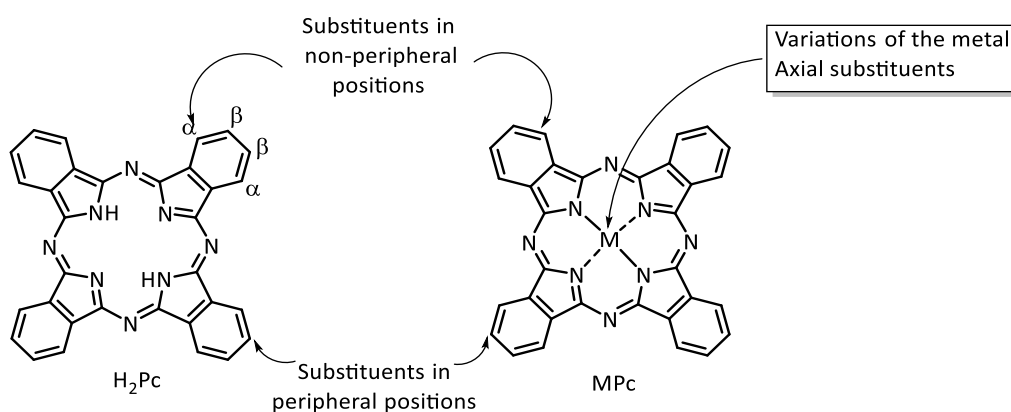


**Figure 1.2.** Structure of metal-free phthalocyanine (left side, H<sub>2</sub>Pc) and metal phthalocyanine complex (right side, MPc), with schematic representation of possible structural modulation sites.

Some of these metal atoms also allow the structural modulation *via* functionalization with axial ligands (**Figure 1.2**). Furthermore, a substantial variety of substituents can be incorporated into the phthalocyanine core at positions designated as  $\alpha$  (non-peripheral) and as  $\beta$  (peripheral) (**Figure 1.2**).<sup>11</sup> This remarkable structural flexibility plays a critical role in the design, solubility and physicochemical and electronic properties of phthalocyanines.<sup>12</sup>



Pcs are intensely blue-green colored aromatic macrocyclic compounds with a typical absorption spectrum. Their electronic absorption spectrum is characterized by two absorption bands in the ultraviolet-visible (UV-Vis) region both attributed to  $\pi \rightarrow \pi^*$  orbital transitions.<sup>13</sup> The first of these bands, named Soret or B-band, is found in the ultraviolet region (around 350 nm), often appearing as a broad band. The second band, called Q-band, is more intense and narrow, appearing in the visible region, around 670–700 nm, also possessing satellite bands between 600–650 nm. While metallophthalocyanines exhibit only a single Q-band, metal-free Pcs have their Q-band split into double bands, due to the lower symmetry of metal-free Pcs ( $D_{2h}$  symmetry), when compared to metallophthalocyanines ( $D_{4h}$  symmetry).<sup>14,15</sup> Nevertheless, these electronic features can be affected by parameters such as presence and nature of the central metal atom (concomitantly with the presence of axial ligands), type and number of peripheral ( $\beta$ ) or non-peripheral ( $\alpha$ ) substituents, macrocyclic aggregation and solvents used, besides the symmetry of the phthalocyanine  $\pi$ -conjugated system.<sup>16-18</sup>

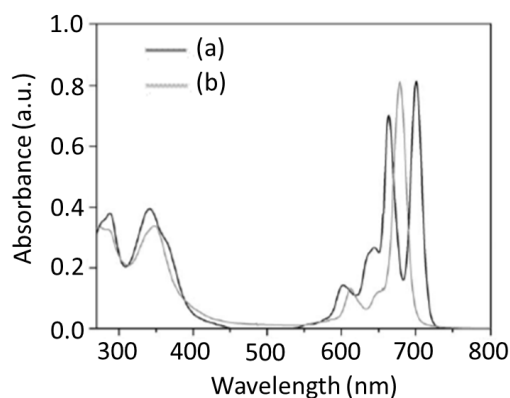


**Figure 1.3.** Typical UV-Vis spectrum for phthalocyanine as (a) metal-free and (b) metal complex.<sup>17</sup>

As for most of non-substituted aromatic compounds, the major disadvantage of unsubstituted Pcs is their sparing solubility both in water and common organic solvents. This is due to the intrinsic hydrophobicity of the aromatic nucleus and its planarity, displaying natural tendency to form molecule stacking ( $\pi$ - $\pi$  stacking) in the form of highly organized aggregates, and it can depend on the concentration, nature of solvent and macrocycle's substitution pattern. Solubility modulation on phthalocyanines mainly focuses on the type of substituents ( $\alpha$  and  $\beta$ ), that can be introduced into the Pc core.

Two different methodologies are classically applied: the first, involving the modification of the already existing Pc using aromatic electrophilic and nucleophilic substitution reactions, holds as main drawback, the proneness to form mixtures with several degrees of substitution, favouring cumbersome purification and low yields. This is due to the chemical stability owned by phthalocyanines, which are quite stable against post-modulation;<sup>19</sup> the second approach involves the cyclotetramerization of substituted phthalocyanine precursors (see **Scheme 1.1** in the following section), leading to an awaited number of substituents on the desired target phthalocyanine (metallated or metal-free). Expectedly, prior modulation of phthalocyanine precursors is the commonly chosen methodology when attempting to introduce significant changes at the phthalocyanine core,<sup>11,20</sup> and will be the approach used in this work.

The most exhaustively investigated soluble substituted phthalocyanines are the symmetrical tetra-substituted and octa-substituted, being the latter of two types depending on the position of the substituents on the isoindole ring (**Figure 1.4**).

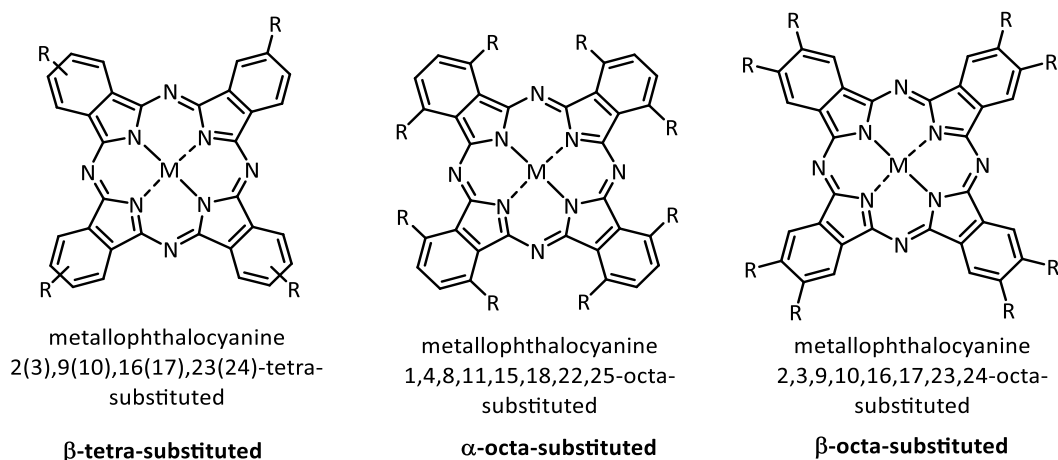


**Figure 1.4.** Common substitution pattern in phthalocyanines.

Generally, the solubility of tetra-substituted phthalocyanines is higher, when compared to octa-substituted ones, because tetra-substituted phthalocyanines consist of an isomeric mixture (**Figure 1.5**), which leads to a lower degree of order in the solid state, when compared to octa-substituted phthalocyanines. It is worth mentioning that the first separation of the four structural isomers of tetra-substituted phthalocyanines was accomplished by Hanack's research group,<sup>21</sup> using preparative HPLC. Notwithstanding

the isomers possible separation, phthalocyanines are commonly used as mixtures of all four isomers in the great majority of their applications.

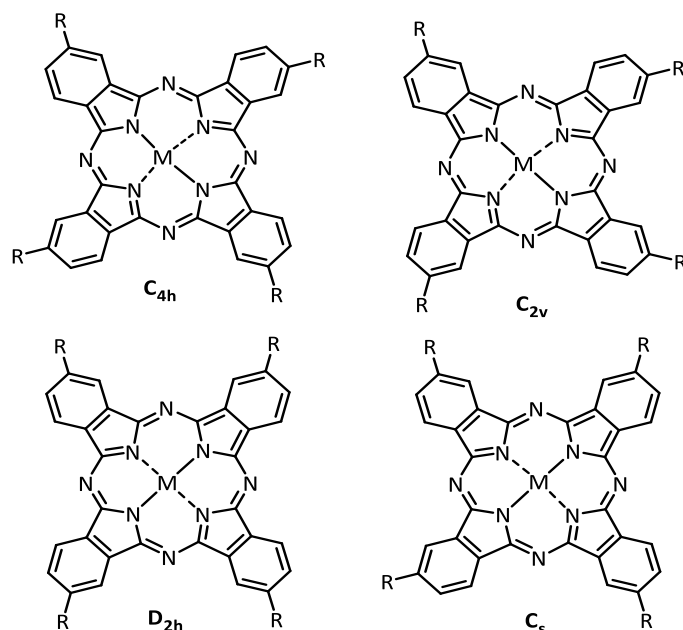


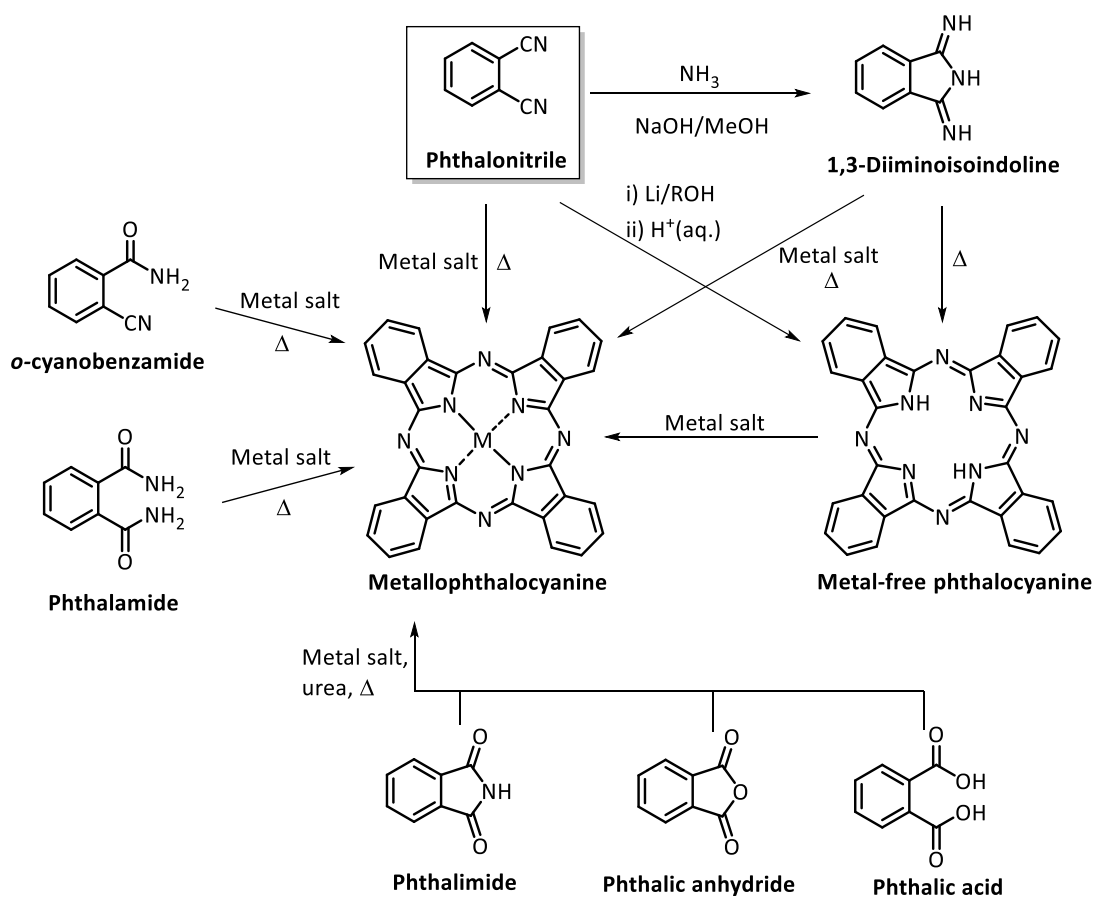
**Figure 1.5.** Constitutional isomers of  $\beta$ -tetra-substituted phthalocyanines.

Since their discovery, phthalocyanines have been a target of intense investigation, particularly considering their properties as dyes. In recent decades, improved synthetic methods demonstrated phthalocyanines remarkable structural flexibility, leading to an expansion of phthalocyanines' potential applications in many fields such as in catalysis,<sup>22</sup> as chemical sensors,<sup>23</sup> as semiconductors,<sup>24</sup> as light-harvesting modules for dye-sensitized solar cells/organic photovoltaics<sup>25</sup> and in nonlinear optics.<sup>26</sup> Furthermore, Pcs also found applications in the medicinal area, including as photosensitizers for Photodynamic Therapy (PDT) of cancer.<sup>27-30</sup>

On the other hand, the application of Pcs in MI has been researched to a much lesser extent, with reports on the utilization of phthalocyanine as potential probes for Magnetic Resonance Imaging (MRI), PET and FI.<sup>31</sup> Since most of the chapters in this thesis deal with the design, synthesis and evaluation of phthalocyanines regarding their potential application in cancer diagnosis as MI probes, a more detailed revision of the prominent literature regarding PET imaging will be given in **section 1.2**. Furthermore, in **section 1.3** a detailed discussion on the phthalocyanines' application in cancer diagnosis as potential FI probes will be also presented.

### 1.1.1 Synthetic methods of phthalocyanines

Phthalocyanines are synthesized by the cyclotetramerization reaction of several aromatic phthalic precursors, as depicted in **Scheme 1.1**, usually using high boiling point solvents.



**Scheme 1.1** Precursors and common synthetic pathways for phthalocyanine synthesis.

The typical precursors are phthalonitriles, 1,3-diiminoisoindolines, phthalic acids, phthalic anhydrides, phthalimides, phthalamides and *o*-cyanobenzamides (**Scheme 1.1**).<sup>32</sup> Among the different precursors available, phthalonitriles are the most frequently used, due to the amenability regarding both the cyclotetramerization reaction, which requires lower temperatures for the phthalocyanine synthesis, and also the presence of cyano groups in *ortho* positions, which are able to participate in the *in situ* formation of isoindol rings and aza-bridges in the template reaction.<sup>33</sup> Occasionally, less reactive phthalonitriles can be further transformed into 1,3-diiminoisoindolines, by

using gaseous ammonia bubbling into a methanolic concentrated sodium hydroxide solution.<sup>11,20,32</sup> This strategy may increase the formation yield of phthalocyanines; however is mostly avoided, given the troublesome reaction conditions required.

Conversely, other aromatic phthalic precursors, like phthalic acid, phthalic anhydride, phthalimide and phthalamide require the presence of an additional source of nitrogen (commonly carried out in melted urea), besides temperatures above 200 °C to provide the desired phthalocyanines, which in turn only allows the presence of a very limited number of possible substituents at the benzene ring.<sup>34</sup>

The amenability in phthalonitriles structural modulation is the main reason why the vast majority of researchers use phthalonitrile precursors, which open the possibility to introduce a vast array of substituents,<sup>11,20</sup> including biocompatible and biologically active groups.<sup>35-37</sup>

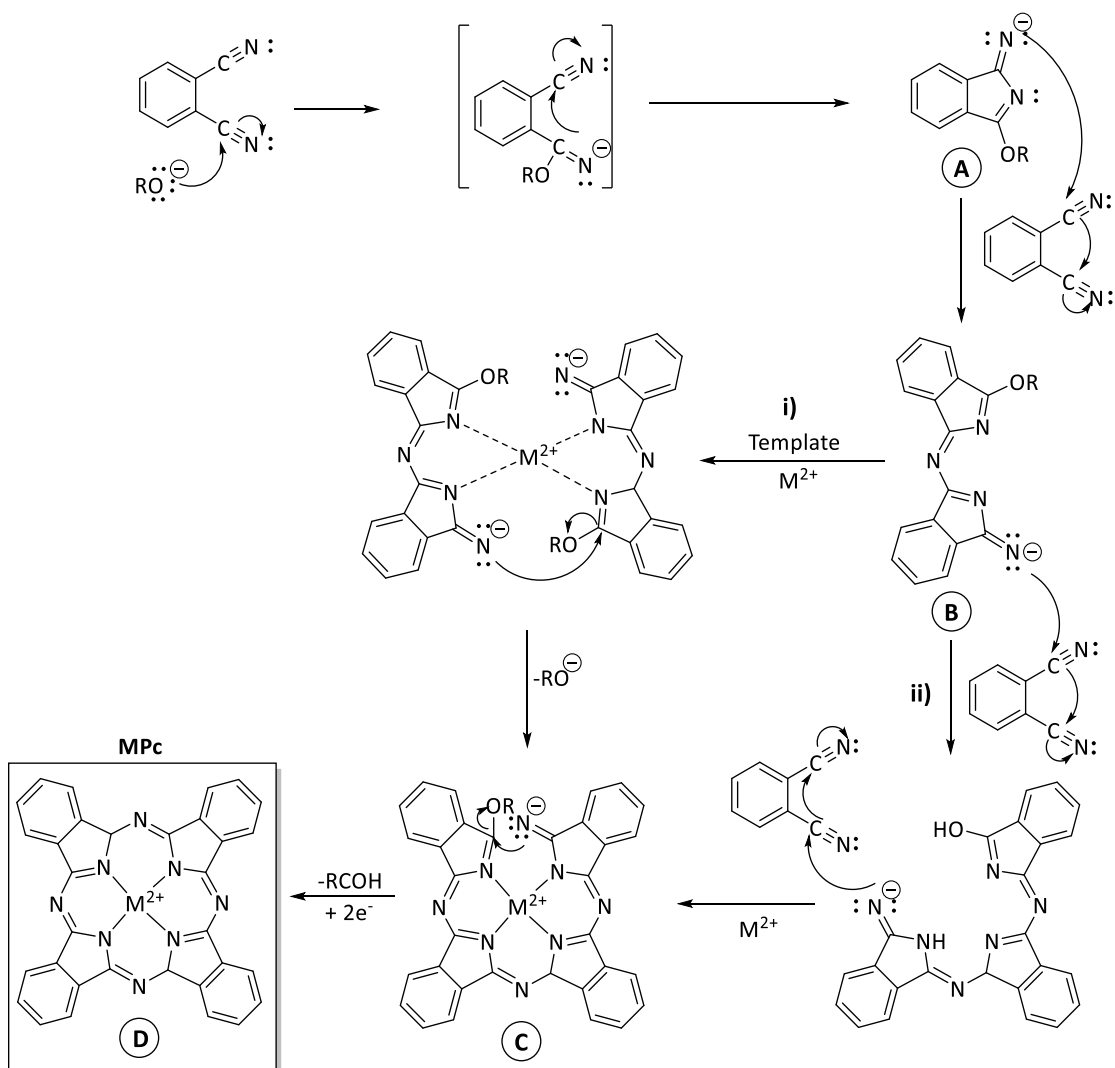
The direct synthesis of symmetric metal-free phthalocyanines can be achieved in low yields from phthalonitrile precursors. A more effective precursor would be 1,3-diiminoisoindoline but, as mentioned above, the difficulties in preparing this precursor conveniently, hampers its common use. The alternative strategy involves the demetallation of labile metallophthalocyanine complexes using acidic work-up.<sup>38</sup> Of particular synthetic value is the Linstead method,<sup>39</sup> in which the phthalonitrile is added to a solution of lithium alkoxide in a primary alcohol, resulting a dilithium phthalocyanine derivative. This complex can be easily demetallated by the addition of diluted aqueous acid, to afford the corresponding metal-free phthalocyanine in reasonable yields (**Scheme 1.1**).<sup>40</sup> More recently, other synthetic approaches, in which magnesium alkoxides<sup>41</sup> or zinc(II) metal salts<sup>42</sup> are first used as templates, with subsequent demetallation have been reported to provide the corresponding metal-free Pcs in higher yields.

As also depicted in **Scheme 1.1**, the synthesis of symmetric metallophthalocyanine complexes generally follows two accepted synthetic methods. One involves the insertion the metal into the metal-free phthalocyanine using an appropriate metal salt.<sup>43</sup> This methodology naturally requires the previous synthesis of the metal-free Pc form which, as described above, is quite demanding to obtain. Hence, this strategy is only useful for the insertion of some specific metals that cannot withstand the somewhat harsher template conditions.<sup>44</sup> The other method, the most

widely used and the one followed in this work, is based on the cyclotetramerization of phthalonitriles (or other precursors) in the presence of a metal salt.<sup>11,20</sup> That said, it is important to state that the conditions used therein for metallophthalocyanine synthesis highly depend on the desired, since the metal acts as template in the cyclotetramerization reaction. For instance, zinc(II) metallophthalocyanine complexes usually require mild reaction conditions when compared to other metals, such as indium(III), aluminum(III), gallium(III),<sup>45</sup> whose phthalocyanine complexes are prepared in much higher boiling solvents.

The cyclotetramerization reactions are usually performed in high boiling point alcohols, such as pentan-1-ol, hexan-1-ol, heptan-1-ol and octan-1-ol or the more basic solvent *N,N*-dimethylaminoethanol (DMAE).<sup>11, 20, 46</sup> In addition, the presence of catalytic amounts of high sterically hindered bases, such as 1,8-diazabicyclo-[5.4.0]-undec-7-ene (DBU) or 1,5-diazabicyclo (4.3.0) non-5-ene (DBN) in combination with a metal salt and the protic solvent contributes significantly for improving the cyclotetramerization yields.<sup>32</sup> Nevertheless, solvents such as quinoline, DMF, 1-methylpyrrolidone and 1-chloronaphthalene can also be employed.

The cyclotetramerization reaction mechanism is not yet fully elucidated and understood. Nevertheless, two distinct mechanisms have been proposed in literature. One suggests the wide possibility that metal ions may work as templates in phthalocyanine synthesis, by promoting a concerted mechanism where four phthalonitrile molecules coordinate with the metal ion to facilitate the cyclization, independently of the solvent used or base, if any.<sup>32,47</sup> The other mechanistic proposal is based on the use of high boiling point alcohols and non-nucleophilic bases, which take part in the mechanistic pathway, as depicted in **Scheme 1.2**.<sup>48</sup>



**Scheme 1.2.** Proposed mechanism for the synthesis of MPcs by cyclotetramerization of phthalonitriles in the presence of a metal salt and an alkoxide anion.<sup>48</sup>

In this case, the mechanism of phthalocyanine formation involves a stepwise dimerization of the precursors, followed by coordination of the central metal ion and ring closure yielding the macrocycle molecule (**Scheme 1.2**). The first step comprises the nucleophilic attack of the alkoxide formed by the alcohol in a basic medium to the carbon of one of the nitrile groups producing the intermediate 1-imido-3-alkoxyisoindoline **A**. Then, the intermediate **A** attacks the nitrile group from other phthalonitrile molecule, forming intermediate **B**, composed of two isoindole units. At this point, the reaction can evolve in two ways: i) *via* condensation of two intermediates **B** or ii) *via* consecutive reaction of intermediate **B** with two phthalonitrile molecules, concomitantly with the coordination with metal salt, affording the

intermediate **C**, composed by four isoindole units. The loss of the alkoxide group in its oxidized form, the aldehyde, together with transfer of two electrons promotes then the ring closure reaction, producing the metallophthalocyanine **D** (**Scheme 1.2**).

### 1.1.2 Biocompatible phthalocyanines

Solubility in physiological media (*e.g.* water) is a crucial issue to consider when designing phthalocyanines for medicinal applications, including MI. In order to confer water solubility to Pcs two major strategies can be applied: i) their functionalization with ionic substituents, namely cationic or anionic charged groups or (ii) the introduction of non-ionic but highly hydrophilic substituents, such as the polyethylene glycol (PEG) and carbohydrates.<sup>36</sup>

This section elucidates on the strategies used so far for the synthesis of water-soluble phthalocyanines. Regarding anionic substituents, the most commonly used groups to increase phthalocyanine's aqueous solubility are carboxylic acids,<sup>49</sup> sulfonic acids<sup>50</sup> and phosphonic acids,<sup>51</sup> either directly linked to the Pc macrocycle, or through spacers. The solubility of this type of phthalocyanines is usually quite dependent on the pH value, since the conjugated acid forms are not necessarily water-soluble. Among them, the anionic water soluble sulfonated Pcs has been extensively studied due particularly to their application as photosensitizers for PDT. For instance, **Photosens**<sup>®</sup>, a clinical-approved photosensitizer in Russia, is a mixture of tetra-, tri-, di- and mono-sulfonated aluminum(III) chloride Pc derivatives (**Figure 1.6**), which has shown to be effective in the treatment of breast, skin, gastrointestinal tract and lung cancers.<sup>52</sup>

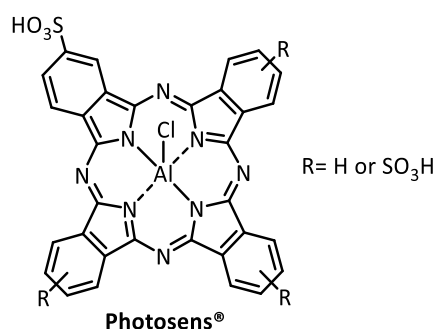


**Figure 1.6.** Selected example of anionic charged functionalized Pc.<sup>52</sup>



Another approach to promote the solubilization of Pcs in aqueous media involves the cationization of their substituents at the periphery of the ring structure. Cationic phthalocyanines are classically obtained by quaternization of aliphatic or aromatic nitrogen atoms substituents. This process generally occurs at the end of the synthetic sequence, at the formed phthalocyanine. Commonly used cationic substituents are ammonium,<sup>53</sup> pyridinium,<sup>54</sup> imidazolium,<sup>55</sup> quinolinium,<sup>56</sup> piperidinium<sup>57</sup> and morpholinium<sup>58</sup> groups. Furthermore, cationic moieties have been attached as axial ligands to the central metal atom silicon(IV).<sup>59,60</sup> As a selected example, Wohrle's group<sup>61</sup> synthesized a set of  $\beta$ -tetra-cationic Pcs with variations in the aliphatic chain's size at the quaternary nitrogen of amino groups (**Figure 1.7**). The compounds with larger aliphatic side chains (**Figure 1.7**, b-c) exhibited higher *in vitro* photodynamic activity, superior to Photofrin II, a clinically approved PDT photosensitizer.<sup>61</sup>

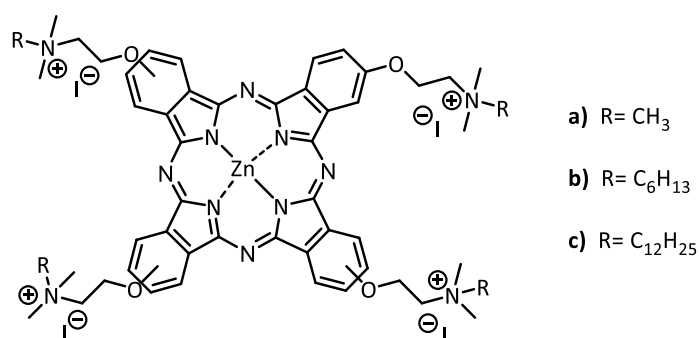


**Figure 1.7.** Selected example of cationic charged functionalized Pc.<sup>61</sup>

As reviewed in literature, a variety of cancer cells overexpress the choline transport receptors on their cell membranes. Subsequently, cancer cell have increased levels of choline uptake in order to provide sufficient metabolic energy to sustain their proliferation.<sup>62,63</sup> Thus, the inclusion of choline moieties into Pcs structures (**Figure 1.7**, a) could attract considerable interest, with the aim of enhancing their cellular uptake and consequently the diagnosis efficacy. This is also one of the main goals of the Pc compounds developed in this work, whose studies are presented in Chapter 2.

Another common strategy to improve the biocompatibility of phthalocyanines is the attachment of polyethylene glycol (PEG) units to the macrocycle's periphery. PEG is a hydrophilic polymer that has been often used in pharmaceutical applications<sup>64</sup> as an effective drug vehicle (*e.g.* nanoparticles and polymeric micelles) or covalently attached

for drug delivery to target tissues. Besides improving drug's water solubility, the incorporation of PEG increases drug's blood circulating lifetime, allowing the minimization of non-specific uptake, which in turn results in a higher concentration of the drug at the targeted cancer cells.<sup>65</sup>

Several works using this type of substituents either at the Pc ring's peripheral positions<sup>66</sup> or in axial position of the central metal atoms<sup>67</sup> have been recently reported. For instance, Lv's group<sup>68</sup> reported a water-soluble  $\beta$ -tetra-substituted zinc(II) phthalocyanine containing PEG chains with MW  $\approx 800$  g.mol<sup>-1</sup> (**Figure 1.8**). The authors described its photophysical properties and investigated its *in vivo* biodistribution in normal mice using FI.

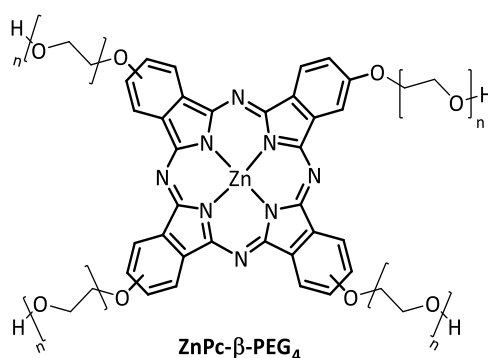


**Figure 1.8.** Selected example of PEG functionalized Pc.<sup>68</sup>

The incorporation of carbohydrate moieties is another possible strategy to provide water solubility to phthalocyanines. This, together with the fact that cancer cells overexpress carbohydrate transport receptors on their cell membranes in order to maintain their highly increased glycolysis activity and sustain their high proliferation rate,<sup>69</sup> has attracted the interest of several research groups. Several examples in literature show the incorporation of carbohydrates directly linked or linked by a spacer to Pc macrocycle through peripheral substitution.<sup>70,71</sup> Pcs axially substituted with carbohydrates have also been described.<sup>72-74</sup> For instance, Lv's group<sup>75</sup> reported the preparation of water-soluble zinc(II) Pc bearing four *D*-galactose units linked by the hydroxyl group located in carbon C-6 (**Figure 1.9, a**) and the *in vivo* studies in tumor-bearing mice revealed its potential use as *in vivo* FI probe for liver cancer imaging.

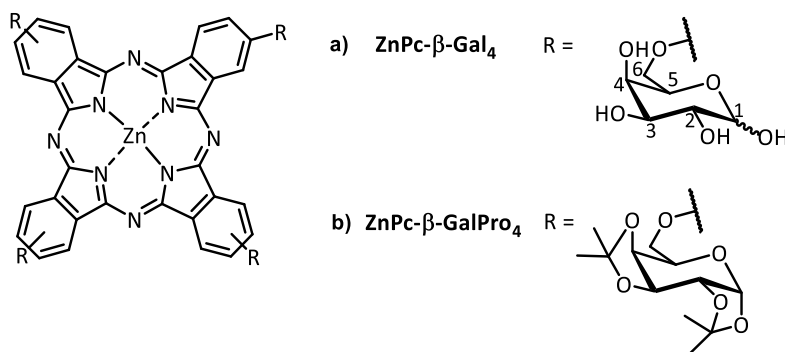


**Figure 1.9.** Selected example of carbohydrate functionalized Pc.<sup>75,76</sup>

More recently, Kimani *et al.*<sup>76</sup> reported that water-soluble **ZnPc- $\beta$ -Gal<sub>4</sub>** (Figure 1.9, a) shows negligible *in vitro* uptake in MCF-7 cells (human breast cancer cell line), 100-fold less than the isopropylidene protected corresponding Pc (**ZnPc- $\beta$ -GalPro<sub>4</sub>**; Figure 1.9, b). The **ZnPc- $\beta$ -GalPro<sub>4</sub>** also demonstrated a high *in vitro* photodynamic cytotoxicity make it attractive photosensitizer for PDT.

## 1.2 Positron Emission Tomography

Positron emission tomography (PET) is a nuclear-medicine-based molecular imaging technique that produces a three-dimensional image of functional processes (*e.g.* cellular metabolism, receptor/enzyme function) by the direct detection and quantification of positron-emitting probes' (radiopharmaceuticals) distribution pattern in the human body. A radiopharmaceutical is prepared by the linking of biological molecules able to target a specific physiological process, organ or tissue to positron-emitting radioisotopes.<sup>77,78</sup>

The clinical PET imaging is mainly used in the area of oncology, both in the identification/localization of cancer tissues and in monitoring therapy's progress,<sup>79</sup> but also in the detection and evaluation of various neurodegenerative diseases (such as Alzheimer's and Parkinson's diseases),<sup>80</sup> as well as in psychiatric disorders.<sup>80</sup> It is also used in cardiology,<sup>81</sup> and it has been applied to measure other organs function such as thyroid, kidneys, liver and lungs. Furthermore, the PET imaging has shown potential at various stages along the drug development pipeline as means to monitor *in vivo* drug

pharmacokinetics.<sup>82</sup> Additionally, pre-clinical PET imaging could also be used to image small animals and obtain real-time information.<sup>83</sup>

PET technique is characterized by a high level of sensitivity ( $10^{-11}$  to  $10^{-12}$  mol/L), therefore allowing accurate quantification and precise disease diagnostics. Radiopharmaceuticals can be detected in nano to picomolar ranges, generally avoiding unwanted pharmacological side effects caused by the radiopharmaceutical and interferences with the physiological processes under study.<sup>84</sup> Briefly, the principle of PET imaging is depicted in **Figure 1.10**.

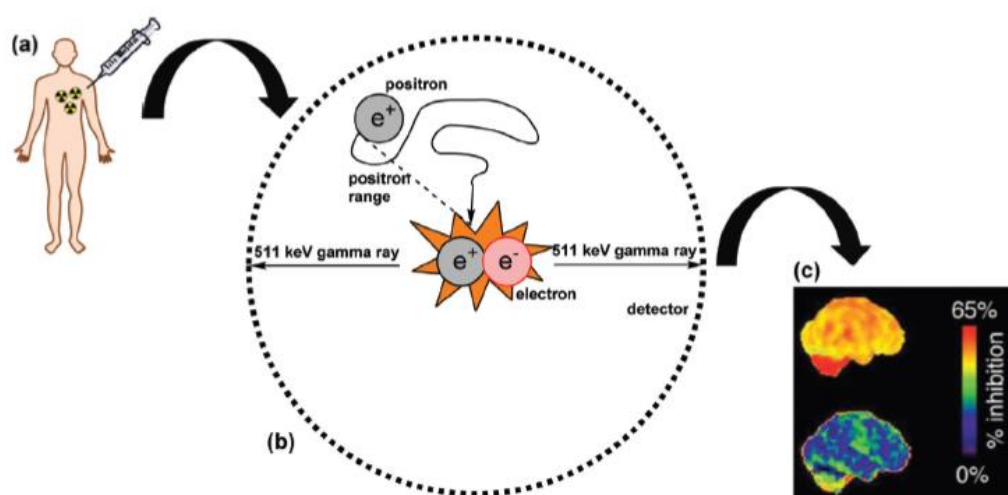


**Figure 1.10.** The principle behind of PET imaging.<sup>85</sup>

The PET exam begins with the administration of a positron-emitting radiopharmaceutical to the patient (**Figure 1.10**, a). After its administration, an induction period occurs, to allow the radiopharmaceutical to concentrate in the target tissues. Then, the radioisotope atom in the radiopharmaceutical will decay to its most stable form with emission of a positron (antiparticle of the electron), that travels for a short distance and interacts with an electron. Then, the two particles are annihilated by each other, producing a pair of 511 keV gamma rays that travel in the opposite direction (180 degrees) to each other (**Figure 1.10**, b). A circular array of detectors that surround the patient allows to locate the source of the annihilation process by drawing a set of straight lines, called lines of response (LORs).<sup>86,87</sup> Nevertheless, the emitted pair of gamma rays on the annihilation process needs to be detected simultaneously (coincidence) by the circular array of detectors, to be considered valid in the PET imaging

equipment. Thus, based on the generated LORs and by mathematical equations and computing, a three-dimensional image containing information about the distribution of the radiopharmaceutical in the patient (**Figure 1.10, c**) is generated.<sup>88</sup> Nevertheless, PET technology can be combined with computed tomography (CT) techniques, thus obtaining images that allow the attenuation correction of PET data and the anatomical location of detected pathologies.

### 1.2.1 Radiopharmaceuticals in Positron Emission Tomography

As stated before, PET technique relies, from a chemical point of view, on the use and preparation of positron-emitting radiopharmaceuticals. This process starts with the production of the positron-emitting radioisotope of interest (typically in a cyclotron using nuclear reactions in the targets of stable isotopes),<sup>89</sup> followed by its incorporation in targeted biologically active molecules using specific radiolabelling procedures carried out in a radiochemistry laboratory. The next step involves the purification, formulation and quality control analysis (to assure the safety of the formulated product prior to *in vivo* injection) of the radiopharmaceutical, and its delivery to the clinical PET facility.<sup>90</sup> Indeed, the production of the radiopharmaceuticals is usually one of the most difficult steps in PET imaging. Since the amount of the radiopharmaceutical required for the evaluation of the functional processes in human body is reduced, the radiopharmaceutical does not interfere with the physiological systems under study. However, its handling requires special attention both in *pre*- and *post*-synthesis, following rigorous rules on radiation protection as well as protocols for working under sterile conditions with Good Manufacturing Practice (GMP), which are regulated by the competent authorities.<sup>91</sup>

As mentioned earlier, only positron-emitting radioisotopes can be used on PET imaging, with the most common being fluorine-18 (<sup>18</sup>F), nitrogen-13 (<sup>13</sup>N), carbon-11 (<sup>11</sup>C) and oxygen-15 (<sup>15</sup>O) (**Table 1.1**), all showing high percentage of decay by positron emission ( $\beta^+$ ) and a short half-life. Naturally, this places limitations about the synthesis time, purification and clinical use. Conversely, there are other positron-emitting radioisotopes, such as copper-64 (<sup>64</sup>Cu), which displays long half-life (768 minutes), but only 17.8% decay by positron emission.<sup>92</sup>

**Table 1.1** Production and characteristics of common positron-emitting radioisotopes.<sup>92,93</sup> [ $\beta^+$ : positron emission;  $\beta^-$ : beta emission; EC: electron capture]

Radioisotope	Half-life (min)	Mode of decay (%)	Common production method	Product decay
$^{15}\text{O}$	2	$\beta^+$ (100)	Cyclotron, $^{15}\text{N}(\text{p},\text{n})^{15}\text{O}^{\text{a}}$	$^{15}\text{N}$
$^{13}\text{N}$	10	$\beta^+$ (100)	Cyclotron, $^{16}\text{O}(\text{p},\alpha)^{13}\text{N}^{\text{a}}$	$^{13}\text{C}$
$^{11}\text{C}$	20.4	$\beta^+$ (99.8); EC (0.2)	Cyclotron, $^{14}\text{N}(\text{p},\alpha)^{11}\text{C}^{\text{a}}$	$^{11}\text{B}$
$^{18}\text{F}$	109.8	$\beta^+$ (97); EC (3)	Cyclotron, $^{18}\text{O}(\text{p},\text{n})^{18}\text{F}^{\text{a}}$	$^{18}\text{O}$
$^{68}\text{Ga}$	68.3	$\beta^+$ (89); EC (11)	Cyclotron, $^{68}\text{Zn}(\text{p},\text{n})^{68}\text{Ga}^{\text{a}}$	$^{68}\text{Zn}$
$^{64}\text{Cu}$	768	$\beta^+$ (17.8); $\beta^-$ (39.4); EC (43.8)	Cyclotron, $^{64}\text{Ni}(\text{p},\text{n})^{64}\text{Cu}^{\text{a}}$	$^{64}\text{Ni}$

<sup>a</sup> The nuclear reaction is written as: target atom (bombarding particle, emitted particle) radioisotope product.

Since one of the objectives of the work developed in this thesis is the development of carbon-11 and copper-64 labelled radiopharmaceuticals as potential PET probes, this literature review is more focused on these two radioisotopes.

Carbon-11 is one of the most commonly used PET radioisotopes, since it can be incorporated into nearly any organic molecule without significant affect its chemical properties and biological activity. This characteristic is especially important in compounds for brain imaging studies, as the preservation of physicochemical characteristics is essential for Blood-Brain Barrier (BBB) permeability and for the affinity to specific molecular targets in the brain. Moreover, its short half-life (20.4 minutes), reduces patient's radioisotope exposure to a minimum, even allowing hypothetical exam repetition. Nevertheless, its short half-life restricts PET imaging studies to radiopharmaceuticals of fast pharmacokinetics, and limits the clinical exams to PET facilities with on-site cyclotrons.<sup>94,95</sup> Furthermore, its short half-life confines the  $^{11}\text{C}$ -radiochemistry to simple and rapid reactions such as methylation of alcohols or amines. As preparation times of two to three half-lives are acceptable to obtain sufficient amounts of radiopharmaceutical for clinical studies,<sup>95,96</sup> one of the major challenges in the use of carbon-11 is the development of increasingly fast, reliable, versatile and automated radiosynthesis procedures.

Copper-64 is one of the most promising PET radioisotopes, due to its suitable half-life (768 minutes; 12.7 h) and decay properties ( $\beta^+$ , 17.8%;  $\beta^-$ , 38.4 %; 43.9% is electron capture) which provide an adequate time for synthetic and imaging of functional processes (as well for radiotherapy), allowing its application as radiopharmaceutical outside of the production facility. Its long half-life makes it versatile for both radiopharmaceuticals with rapid pharmacokinetics such as small molecules, as well as slow pharmacokinetic agents such as monoclonal antibodies, peptides and nanoparticles.<sup>97</sup> Moreover, the advantageous and versatile coordination chemistry of copper allows its reaction with a wide variety of macrocycle chelating systems, with formation of stable complexes.<sup>98-100</sup>

### 1.2.2 Radiopharmaceuticals for cancer Positron Emission Tomography imaging

The most widely used PET radiopharmaceutical in oncology is the fluorine-18-fluorodeoxyglucose ( $[^{18}\text{F}]\text{FDG}$ ), due to the ubiquitous use of glucose by the human body (**Figure 1.11**).

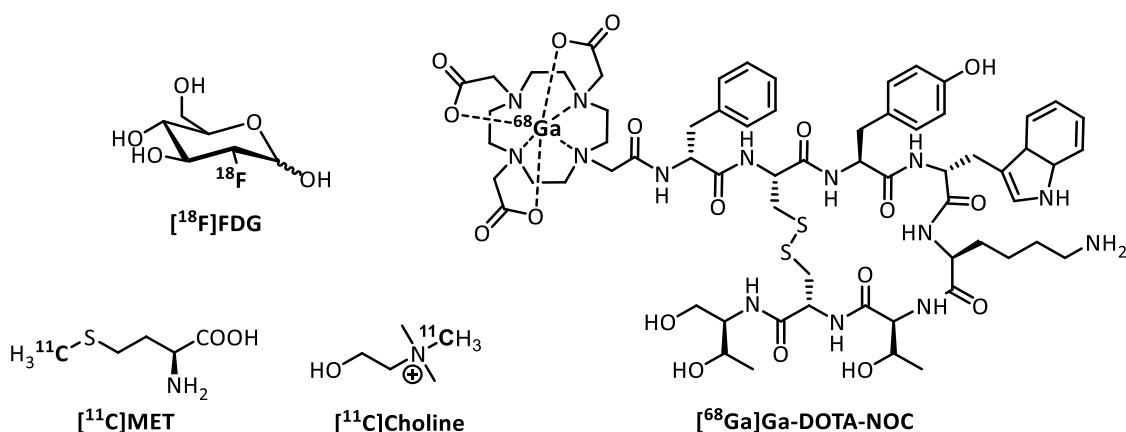


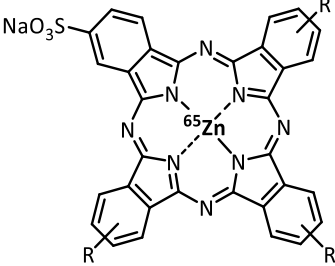
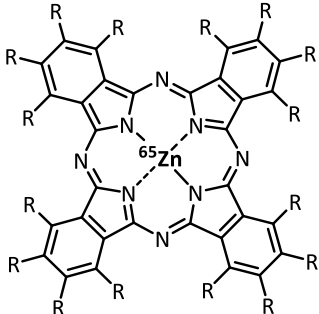
**Figure 1.11** Selected clinical-approved PET radiopharmaceuticals (listed in European Pharmacopoeia Monograph) for oncology.

$[^{18}\text{F}]\text{FDG}$  clinical application includes many types of cancers, such as lung, esophageal, breast, head, neck, colorectal cancers, malignant lymphoma and melanoma, among others.<sup>101,102</sup> However, it is important to recognize that, being a glucose metabolism

tracer, [ $^{18}\text{F}$ ]FDG is not a specific radiopharmaceutical, since many benign and malignant conditions lead to increased uptake of this radiopharmaceutical. Currently, other radiopharmaceuticals for cancer diagnosis include the  $^{68}\text{Ga}$ -labelled [1,4,7,10-tetraazacyclododecane-1,4,7,10-tetraacetic acid]-1-NaI<sub>3</sub>-octreotide ([ $^{68}\text{Ga}$ ]Ga-DOTA-NOC) for neuroendocrine tumors, the L-[methyl- $^{11}\text{C}$ ]Methionine ([ $^{11}\text{C}$ ]MET) for the diagnosis of brain, urinary, liver and lung cancer<sup>103</sup> and the [ $^{11}\text{C}$ ]Choline for prostate, brain, lung and bladder cancer (**Figure 1.11**).<sup>104</sup>

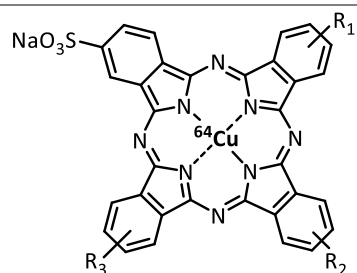
The success of PET imaging upholds in the continued development and application of novel and biologically relevant radiopharmaceuticals. As such, the properties of Pcs presented above, evoke the interest in developing synthetic and labelling methodologies for phthalocyanines with radioisotopes for potential application in cancer diagnosis as PET probes. To the best of our knowledge, there are only few examples in the literature reporting PET probes incorporating Pcs, as shown in **Table 1.2**, where three of them consist of  $^{64}\text{Cu}$ -labelled phthalocyanines (entries 3 and 4, **Table 1.2**).

**Table 1.2.** Radiolabelled phthalocyanines with positron-emitting radioisotopes reported in literature.

Entry	Radiolabelled phthalocyanines	Studies/application
1	 <p>[<math>^{65}\text{Zn}</math>][Zn(PcS<sub>n</sub>)]; R= H or SO<sub>3</sub>Na</p>	Synthesis and evaluation ( <i>in vitro</i> ) as potential PET probe for assessment of its photodynamic activity <sup>105</sup>
2	 <p>[<math>^{65}\text{Zn}</math>][Zn(Pc)]; R= H or F</p>	Synthesis and evaluation ( <i>in vivo</i> ) as potential probe for PET image-guided photodynamic therapy response to tumors <sup>106</sup>

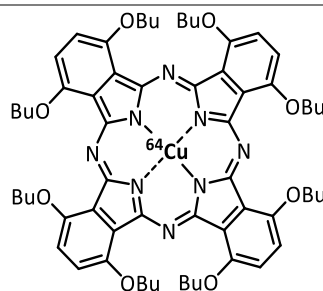


3


 $[^{64}\text{Cu}][\text{Cu}(\text{PcS}_{1-4})]$   $R_1=R_2=R_3= \text{H or SO}_3\text{Na}$ 
 $[^{64}\text{Cu}][\text{Cu}(\text{PcS}_4)]$   $R_1=R_2=R_3= \text{SO}_3\text{Na}$ 
 $[^{64}\text{Cu}][\text{Cu}(\text{PcS}_3)]$   $R_1=R_2=\text{SO}_3\text{Na}; R_3= \text{H}$ 
 $[^{64}\text{Cu}][\text{Cu}(\text{PcS}_2)]$   $R_1= \text{SO}_3\text{Na}; R_2=R_3= \text{H}$ 
 $[^{64}\text{Cu}][\text{Cu}(\text{PcS}_3\text{C}_6)]$   $R_1=R_2=\text{SO}_3\text{Na}; R_3=\text{C}_6\text{H}_{11}$ 

Synthesis and evaluation (*in vivo*) as potential probe for PET image-guided photodynamic therapy response to tumors<sup>107,108</sup>

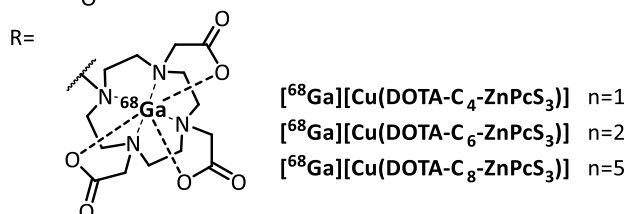
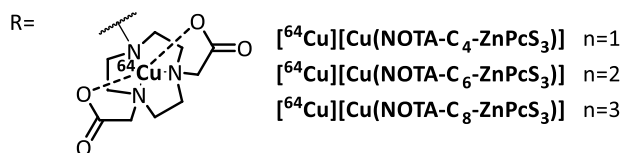
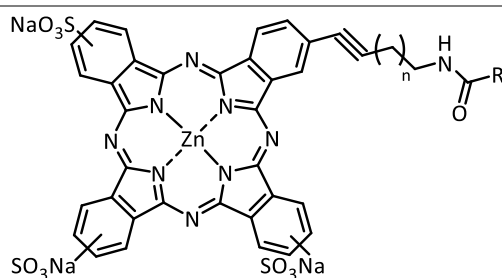
4



encapsulated in PEG-coated nanoparticle

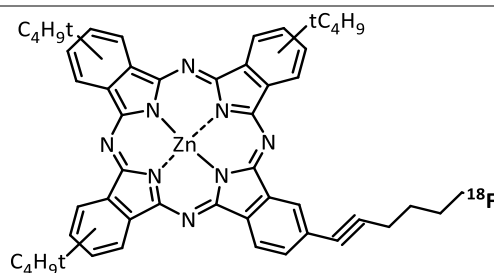
Only synthesis was reported<sup>109</sup>

5



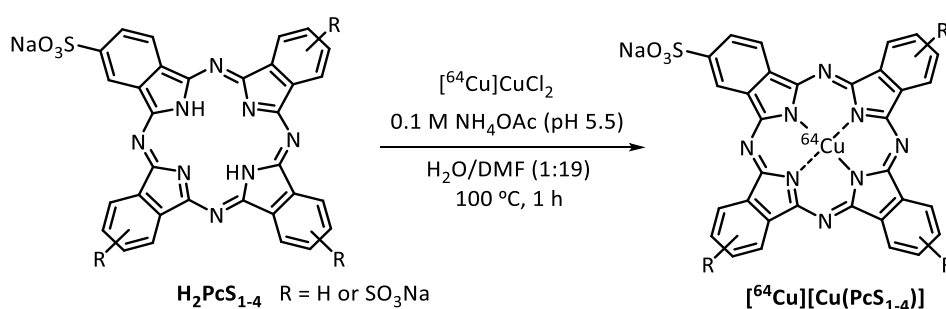
Synthesis and evaluation (*in vivo*; only  $[^{64}\text{Cu}][\text{Cu}(\text{NOTA-C}_4\text{-ZnPcS}_3)]$ ) as potential probe for bimodal FI/PET image-guided tumor diagnosis<sup>110</sup>

6



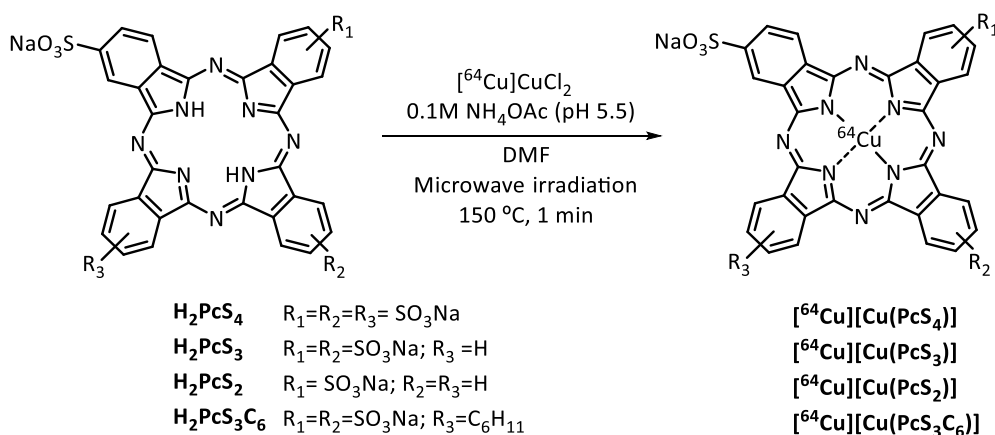
Only synthesis was reported<sup>111</sup>

One of the studies reported the radiolabelling reaction of a metal-free Pc substituted with several degrees of sulfonic acid groups, in the form of a mixture, with  $[^{64}\text{Cu}]\text{CuCl}_2$  to yield  $[^{64}\text{Cu}][\text{Cu}(\text{PcS}_{1-4})]$ , which was employed for biodistribution studies in tumor-bearing rats using PET imaging (**Scheme 1.3**).<sup>107</sup> The comparison of the pharmacokinetics of the  $[^{64}\text{Cu}][\text{Cu}(\text{PcS}_{1-4})]$  with free  $[^{64}\text{Cu}]\text{CuCl}_2$  suggested no *in vivo* Pc demetallation. The biodistribution patterns showed low tumor uptake and most  $[^{64}\text{Cu}][\text{Cu}(\text{PcS}_{1-4})]$  was taken up by the kidneys and liver. The authors attributed these poor results to the complexity of the radiolabelled mixture.<sup>107</sup>



**Scheme 1.3** Synthesis methodology of  $^{64}\text{Cu}$ -labelled Pc.<sup>107</sup>

Later, the same research group reported an optimization of the synthetic methodology of the sulfonated metal-free Pc mixture, achieving the pure isolated metal-free sulfonated bearing two ( $\text{H}_2\text{PcS}_2$ ), three ( $\text{H}_2\text{PcS}_3$ ) or four ( $\text{H}_2\text{PcS}_4$ ) sulfonate groups (**Scheme 1.4**).<sup>108</sup>



**Scheme 1.4.** Synthesis methodology of  $^{64}\text{Cu}$ -labelled Pcs.<sup>108</sup>

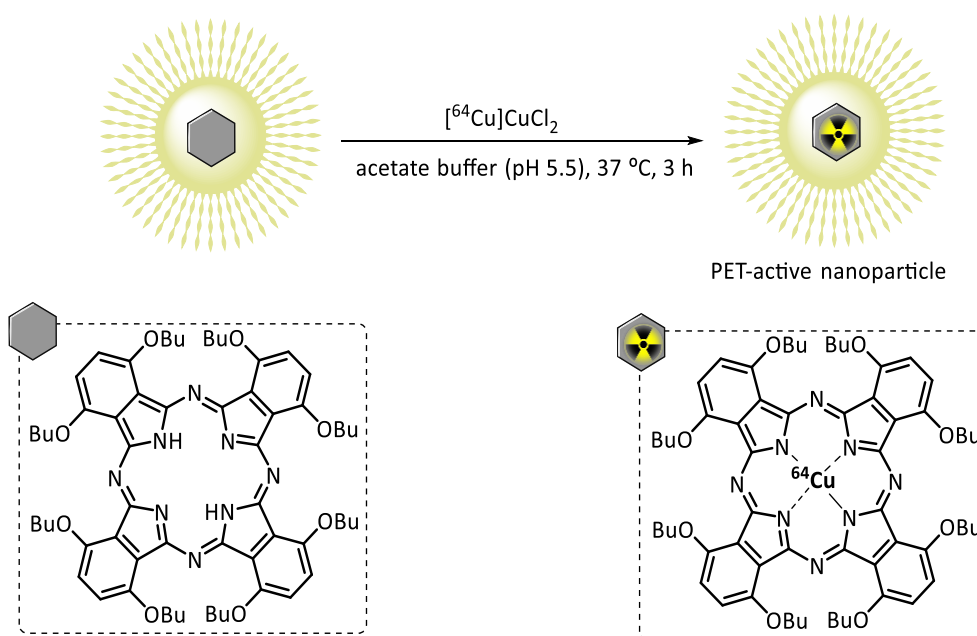
Additionally, to further evaluate the amphiphilic character, the  $\text{H}_2\text{PcS}_3\text{C}_6$  derivative was also synthesized, and its *in vivo* biodistribution studies were also described (**Scheme 1.4**). The above mentioned metal-free phthalocyanines were radiolabelled with  $^{64}\text{Cu}$  under microwave irradiation, producing the desired  $^{64}\text{Cu}$ -labelled Pcs ( $^{64}\text{Cu}[\text{Cu}(\text{PcS}_n)]$ ) in 40–50% isolated yields and >98% radiochemical purities (**Scheme 1.4**). The *in vivo* biodistribution studies in tumor-bearing rats using PET imaging showed that the most hydrophilic derivatives  $^{64}\text{Cu}[\text{Cu}(\text{PcS}_4)]$  and  $^{64}\text{Cu}[\text{Cu}(\text{PcS}_3)]$  exhibited a significant bladder and kidney uptake; however no tumor uptake was observed. On the other hand, the more lipophilic derivatives  $^{64}\text{Cu}[\text{Cu}(\text{PcS}_2)]$  and  $^{64}\text{Cu}[\text{CuPc}(\text{S}_3\text{C}_6)]$  exhibited a good tumor and liver uptake, with best PET image being obtained for the amphiphilic derivative  $^{64}\text{Cu}[\text{Cu}(\text{PcS}_3\text{C}_6)]$ .<sup>108</sup>

Another significant report describes the synthesis of a  $^{64}\text{Cu}$ -labelled Pc encapsulated on PEG coated nanoparticle, affording a PET-active nanoparticle (**Scheme 1.5**). The nanoparticle loaded with the Pc was incubated with  $^{64}\text{Cu}$  under microwave irradiation, producing the desired  $^{64}\text{Cu}$ -labelled Pcs ( $^{64}\text{Cu}[\text{Cu}(\text{PcS}_n)]$ ) in 40–50% isolated yields and >98% radiochemical purities (**Scheme 1.4**). The *in vivo* biodistribution studies in tumor-bearing rats using PET imaging showed that the most hydrophilic derivatives  $^{64}\text{Cu}[\text{Cu}(\text{PcS}_4)]$  and  $^{64}\text{Cu}[\text{Cu}(\text{PcS}_3)]$  exhibited a significant bladder and kidney uptake; however no tumor uptake was observed. On the other hand, the more lipophilic derivatives  $^{64}\text{Cu}[\text{Cu}(\text{PcS}_2)]$  and  $^{64}\text{Cu}[\text{CuPc}(\text{S}_3\text{C}_6)]$  exhibited a good tumor and liver uptake, with best PET image being obtained for the amphiphilic derivative  $^{64}\text{Cu}[\text{Cu}(\text{PcS}_3\text{C}_6)]$ .<sup>108</sup>

Another significant report describes the synthesis of a  $^{64}\text{Cu}$ -labelled Pc encapsulated on PEG coated nanoparticle, affording a PET-active nanoparticle (**Scheme 1.5**). The nanoparticle loaded with the Pc was incubated with  $^{64}\text{Cu}$  under microwave irradiation, producing the desired  $^{64}\text{Cu}$ -labelled Pcs ( $^{64}\text{Cu}[\text{Cu}(\text{PcS}_n)]$ ) in 40–50% isolated yields and >98% radiochemical purities (**Scheme 1.4**). The *in vivo* biodistribution studies in tumor-bearing rats using PET imaging showed that the most hydrophilic derivatives  $^{64}\text{Cu}[\text{Cu}(\text{PcS}_4)]$  and  $^{64}\text{Cu}[\text{Cu}(\text{PcS}_3)]$  exhibited a significant bladder and kidney uptake; however no tumor uptake was observed. On the other hand, the more lipophilic derivatives  $^{64}\text{Cu}[\text{Cu}(\text{PcS}_2)]$  and  $^{64}\text{Cu}[\text{CuPc}(\text{S}_3\text{C}_6)]$  exhibited a good tumor and liver uptake, with best PET image being obtained for the amphiphilic derivative  $^{64}\text{Cu}[\text{Cu}(\text{PcS}_3\text{C}_6)]$ .<sup>108</sup>

The nanoparticle loaded with the Pc was incubated with  $^{64}\text{Cu}$  under microwave irradiation, producing the desired  $^{64}\text{Cu}$ -labelled Pcs ( $^{64}\text{Cu}[\text{Cu}(\text{PcS}_n)]$ ) in 40–50% isolated yields and >98% radiochemical purities (**Scheme 1.4**). The *in vivo* biodistribution studies in tumor-bearing rats using PET imaging showed that the most hydrophilic derivatives  $^{64}\text{Cu}[\text{Cu}(\text{PcS}_4)]$  and  $^{64}\text{Cu}[\text{Cu}(\text{PcS}_3)]$  exhibited a significant bladder and kidney uptake; however no tumor uptake was observed. On the other hand, the more lipophilic derivatives  $^{64}\text{Cu}[\text{Cu}(\text{PcS}_2)]$  and  $^{64}\text{Cu}[\text{CuPc}(\text{S}_3\text{C}_6)]$  exhibited a good tumor and liver uptake, with best PET image being obtained for the amphiphilic derivative  $^{64}\text{Cu}[\text{Cu}(\text{PcS}_3\text{C}_6)]$ .<sup>108</sup>

After 3 hours of incubation, the desired radiolabelled nanoparticle was obtained in 98% isolated labelling yield.<sup>109</sup>



**Scheme 1.5.** Synthesis methodology of  $^{64}\text{Cu}$ -labelled Pc encapsulated in PEG-coated nanoparticle.<sup>109</sup>

In conclusion, Pcs form stable copper-64 complexes with the *in vivo* biodistribution studies showing that their stability prevents the *in vivo* release of the metal ion. These relevant properties prompted us to select copper-64 as the radioisotope of choice for further radiolabelling studies, using Pcs as chelating agents. However, it should be emphasized that none of the reported studies have ever exploited the targeting ability in the synthesis of phthalocyanine as PET probes, with the aim of improving tumor uptake and enhancing PET image quality. The synthesis of  $^{64}\text{Cu}$ -labelled phthalocyanines suitably functionalized with biocompatible and/or cancer-targeting groups is described in Chapter 2 of this thesis.

### 1.2.3 Radiopharmaceuticals for brain Positron Emission Tomography imaging

The brain PET imaging field has grown exponentially in recent years. The advances in drug development for the treatment and/or diagnosis of several human brain disorders such as Alzheimer's disease, Parkinson's disease, depression, brain cancer, epilepsy, brain inflammation and infections, among others, resulted strongly from the improvement of small PET radiopharmaceuticals targeting diverse receptors, transporters, enzymes, and other molecular targets within the human brain.<sup>112</sup> Since the radiolabelling of molecules of interest with carbon-11 normally provides radiopharmaceuticals with unchanged pharmacokinetics and pharmacodynamics,<sup>113</sup> when compared with the parent compound, the  $^{11}\text{C}$ -labelled radiopharmaceuticals are usually preferred as probes for brain PET imaging. Currently, there are several radiopharmaceuticals bearing carbon-11 (**Figure 1.12**), such as 2- (4- $N$ - $^{11}\text{C}$ )-methylaminophenyl)-6-hydroxybenzothiazole ( $^{11}\text{C}$ )-PIB) for the diagnosis of Alzheimer's disease,  $^{11}\text{C}$ -Raclopride for the assessment of Parkinson's disease, Huntington's disease, Wilson's disease and schizophrenia, and  $^{11}\text{C}$ -Flumazenil ( $^{11}\text{C}$ )-FMZ), which is widely used for the assessment of epilepsy, schizophrenia, post-traumatic stress disorder and Alzheimer's disease.<sup>114</sup>

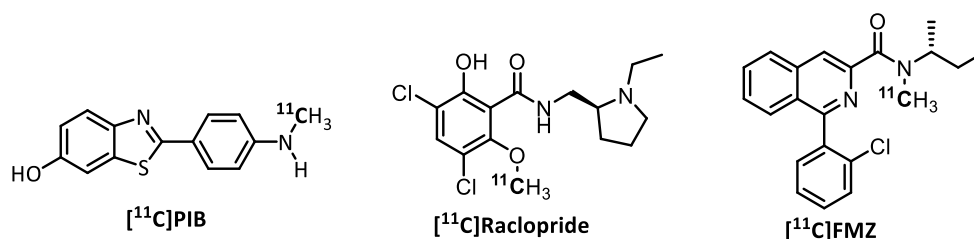


**Figure 1.12.** Selected clinical-approved  $^{11}\text{C}$ -labelled PET radiopharmaceuticals (listed in European Pharmacopoeia Monograph) for brain disorders/pathologies.

Furthermore, the radiopharmaceuticals [ $^{11}\text{C}$ ]MET and [ $^{18}\text{F}$ ]FDG (**Figure 1.11**), along with  $^{18}\text{F}$ -fluoroethyltyrosine ([ $^{18}\text{F}$ ]FET),  $^{18}\text{F}$ -labelled 3'-deoxy-3'-fluorothymidine ([ $^{18}\text{F}$ ]FLT) and  $^{18}\text{F}$ -fluorodihydroxyphenylalanine ([ $^{18}\text{F}$ ]DOPA; fluorodopa) are also currently used for brain cancer imaging.<sup>115</sup>

Regardless of the advances in this field, the ability to image fundamental aspects of neurological diseases is still a great challenge. To penetrate into the brain, a PET radiopharmaceutical must possess suitable physicochemical properties to cross the BBB by passive diffusion. This is the most common obstacle to the development of *in vivo* brain PET radiopharmaceuticals, alluring many research groups to define the optimal physicochemical properties for brain-penetrating PET radiopharmaceuticals,<sup>116</sup> using these criteria to filter the number of compounds further evaluated *in vitro* or *in vivo*.<sup>117</sup> There are several radiopharmaceutical physicochemical properties that might govern its passive diffusion across the BBB. Generally, such compounds have low molecular weights ( $< 500 \text{ g.mol}^{-1}$ ), low number of hydrogen bond donor and acceptors ( $< 3$  H-bond donors and  $< 7$  H-bond acceptors) and lack of charge.<sup>118</sup> Additionally, lipophilicity is probably, the most important physicochemical property. The commonly used index of lipophilicity is the LogP, where P is the octan-1-ol/water partition coefficient of the non-ionized species. The corresponding partition coefficient at physiological pH is named LogD<sub>7.4</sub>. Passive diffusion across the BBB might be expected to increase with radiopharmaceutical lipophilicity, since entry first requires partitioning of the radiopharmaceutical from plasma into the lipid bilayer of the BBB. However, a radiopharmaceutical showing high lipophilicity may also become extensively bound to blood proteins, thereby reducing its ability to permeate the BBB. Bluntly, it is accepted that LogD<sub>7.4</sub> values of 2–3.5 show optimal passive diffusion across the BBB with high brain uptake and non-specific binding.<sup>119</sup>

In the search of novel small-molecule PET probes, we highlighted those which include in their structure two aromatic groups joined by an  $\alpha,\beta$ -unsaturated ketone of the chalcone-type, as well as, molecules based on indole nucleus, to function as new scaffolds for the development of potential MI probes for brain PET imaging.

Chalcones are aromatic ketones, where two aromatic rings are linked by a highly electrophilic three carbon  $\alpha, \beta$ -unsaturated carbonyl system. The presence of two electrophilic reactive centers in these compounds, due to delocalization of electron density in the  $\alpha, \beta$ -unsaturated carbonyl system, allows them to participate in addition reactions via attack to the carbonyl group (1,2-addition) or involving the  $\beta$ -carbon (1,4-addition), leading to the synthesis of novel bioactive heterocyclic compounds.<sup>120</sup> Chalcones have been reported to possess a broad spectrum of biological and pharmacological activities, depending on the substitution made on the aromatic rings,<sup>121</sup> and also, even by  $\alpha$ -position substitution of the double bond of the  $\alpha,\beta$ -unsaturated carbonyl system.<sup>122</sup>

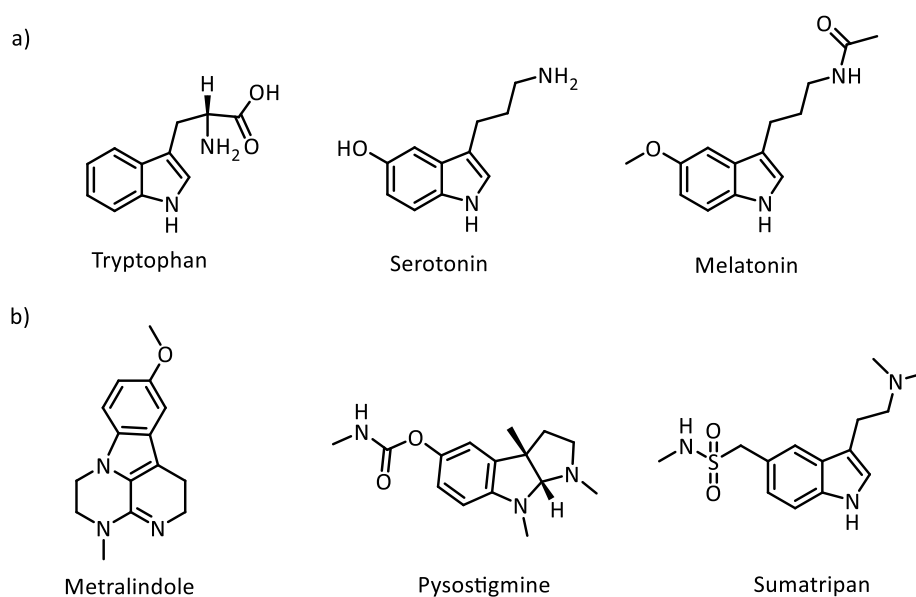
Besides the therapeutic potential of chalcones, a literature survey revealed that the chalcone backbone has been explored for the diagnosis of human brain disorders through PET imaging technique, aiming, mainly, the detection of  $\beta$ -amyloid plaques in Alzheimer's disease (AD). Chalcone derivatives radiolabelled with fluorine-18, carbon-11 and gallium-68, as depicted in **Table 1.3**, have been reported in literature and, in general, they displayed favorable characteristics as  $\beta$ -amyloid imaging probes, showing high affinity for  $\beta$ -amyloid plaques and both high uptake into and good clearance from the brain.

**Table 1.3.** Radiolabelled chalcones with positron-emitting radioisotopes for targets within brain reported in literature.

Radiolabelled chalcones	Log D <sub>7.4</sub>	Studies/application
	---	Synthesis and evaluation ( <i>in vitro</i> and <i>in vivo</i> ) as potential PET probes for $\beta$ -amyloid plaques imaging in AD <sup>123</sup>
	1.58	Synthesis and evaluation ( <i>in vitro</i> and <i>in vivo</i> ) as potential PET probe for $\beta$ -amyloid plaques imaging in AD <sup>124</sup>
	---	Synthesis and evaluation ( <i>in vitro</i> and <i>in vivo</i> ) as potential PET probes for $\beta$ -amyloid plaques imaging in AD <sup>125</sup>
<p>R= NMe<sub>2</sub> R= NHMe</p>	2.25 - 2.64	Synthesis and evaluation ( <i>in vitro</i> and <i>in vivo</i> ) as potential PET probes for $\beta$ -amyloid plaques imaging in AD <sup>126</sup>

Additionally, indole is a fused six-membered benzene with five-membered pyrrole rings, being an aromatic heterocyclic system containing 10  $\pi$  electrons. Indole is a quite important scaffold in medicinal chemistry, since it can be ubiquitously found in living organisms including the essential amino acid tryptophan, the neurotransmitter

serotonin, and the mammalian hormone melatonin, suggesting a proper biocompatibility for the indole nucleus (**Figure 1.13, a**).<sup>127</sup> This, combined with the well described nucleus electrophilicity (which leads to synthetic manipulation of various indoles derivatives), a wide variety of drugs bearing indole motif were synthesized up to now, and are currently used in clinical for human brain disorders, such as Pysostigmine (Alzheimer's disease), Metralindole (depression) and Sumatripan (migraine) (**Figure 1.13, b**).<sup>127</sup>

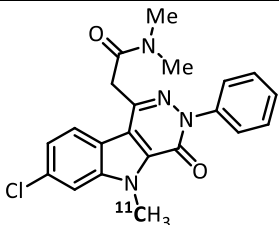
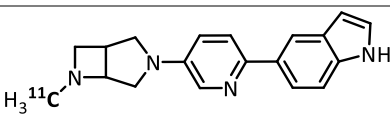
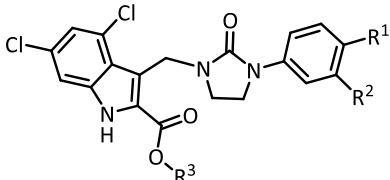
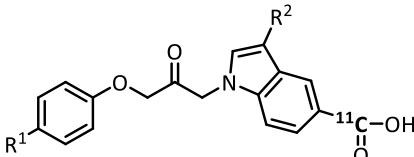
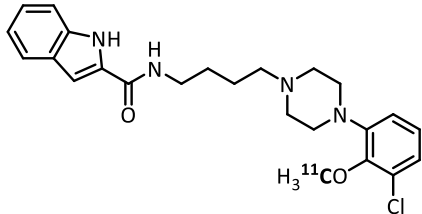
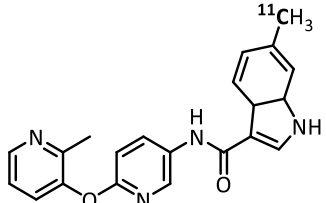


**Figure 1.13.** Examples of molecules containing indole nucleus: a) natural compounds and b) synthetic marketed drugs.<sup>127</sup>

Moreover, a number of indole derivatives have also been explored as potential PET probes for different targets within brain, such as, the serotonin receptors<sup>128,129</sup>, the cannabinoid receptors,<sup>130-132</sup> the dopamine receptors<sup>133</sup> and the  $\beta$ -amyloid plaques in Alzheimer's disease.<sup>134</sup> Selected examples of the application of indoles derivatives radiolabelled with the common positron-emitting radioisotopes, fluorine-18 and carbon-11, for brain PET imaging based on publications from the last decade are shown in **Table 1.4**.



**Table 1.4.** Radiolabelled indoles with positron-emitting radioisotopes for targets within brain reported in literature.

Radiolabelled indoles	LogD <sub>7.4</sub>	Studies/application
	1.86	Only synthesis was reported. Potential PET probe for TSPO (peripheral benzodiazepine) receptor imaging <sup>135</sup>
	---	Synthesis and evaluation ( <i>in vivo</i> ) as potential PET probe for nicotinic acetylcholine receptors imaging <sup>136</sup>
 <p> <math>R^1=O(CH_2)_2\ ^{18}F</math>; <math>R^2=H</math>; <math>R^3=C_2H_5</math>  <math>R^1=H</math>; <math>R^2=O(CH_2)_2\ ^{18}F</math>; <math>R^3=C_2H_5</math>  <math>R^1=O^{11}CH_3</math>; <math>R^2=H</math>; <math>R^3=C_2H_5</math>  <math>R^1=O(CH_2)_2\ ^{18}F</math>; <math>R^2=H</math>; <math>R^3=H</math>  <math>R^1=O^{11}CH_3</math>; <math>R^2=H</math>; <math>R^3=H</math>. </p>	1.51- 2.56 <sup>a</sup>	Synthesis and evaluation ( <i>in vitro</i> ) as potential PET probes for N-methyl-D-aspartate (NMDA) receptor imaging <sup>137</sup>
 <p> <math>R^1=PhO</math>; <math>R^2=COPr</math>  <math>R^1=4-CF_3PhO</math>; <math>R^2=COMe</math>  <math>R^1=PhO</math>; <math>R^2=3-Me-1,2,4-oxadiazole</math>  <math>R^1=n-C_8H_{17}</math>; <math>R^2=3-Me-1,2,4-oxadiazole</math> </p>	1.94- 2.43	Synthesis and evaluation ( <i>in vitro</i> an <i>in vivo</i> ) as potential PET probes for cytosolic phospholipase A2 $\alpha$ enzyme imaging <sup>138</sup>
	3.33	Synthesis and evaluation ( <i>in vitro</i> an <i>in vivo</i> ) as potential PET probe for dopamine receptors imaging <sup>139</sup>
	2.79 <sup>a</sup>	Synthesis and evaluation ( <i>in vitro</i> an <i>in vivo</i> ) as potential PET probe for serotonin receptors imaging <sup>140</sup>

<p>R<sup>1</sup> = 2-Br or H or 4-iPr or 4-F</p>	2.59- 3.83	Only synthesis was reported. Potential PET probes for serotonin receptors imaging <sup>141</sup>
	3.61	Synthesis and evaluation ( <i>in vitro</i> an <i>in vivo</i> ) as potential PET probe for $\beta$ -amyloid plaques imaging in AD <sup>142</sup>

<sup>a</sup> LogD<sub>7.4</sub> values for the corresponding non-radioactive standard reference compounds.

Considering the privileged biological properties of chalcone and indole scaffolds in brain imaging (**Tables 1.3** and **1.4**), we turned our attention to a new indole core based on conjugate addition reaction of indoles to chalcones, the  $\beta$ -indolylketone (**Figure 1.14**).  $\beta$ -indolylketones (**Figure 1.14**), generally accessed by Michael addition reaction of indoles to chalcones using an acid catalyst,<sup>143</sup> may represent a valuable, yet unexplored, scaffold for medicinal/synthetic organic chemists, as only a few examples on their antibacterial,<sup>144</sup> antimicrobial<sup>145</sup> and anticancer activity<sup>146</sup> as well acetylcholinesterase inhibitory effect in AD<sup>147</sup> have been reported in literature. So far to the best of our knowledge, their use as potential PET probe for human brain disorders/pathologies imaging has never been reported. Thus, the simple and synthetically produced  $\beta$ -indolylketone could represent a new challenge for the medicinal chemistry field with the possibility of extending the scientific importance of these compounds. In Chapter 3 of this thesis we describe the synthesis and <sup>11</sup>C-labelling methodologies of  $\beta$ -indolylketones as potential PET probes for brain imaging.

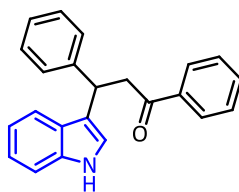


**Figure 1.14.** Structure of a  $\beta$ -indolylketone.

### 1.3 Fluorescence Imaging

Fluorescence Imaging (FI) involves the use of fluorescence-emitting probes (fluorophores) that accumulates in the target tissues and is further detected and quantified by a specialized imaging system, providing a simple and direct visualization of specific molecular targets or biological pathways *in vitro* and *in vivo*.<sup>148,149</sup> The fluorescence quantum yield ( $\Phi_F$ ) is representative property of the fluorophore molecule and can be defined as the ratio of the number of photons emitted through fluorescence, to the number of photons absorbed by the fluorophore.<sup>150</sup>

The FI technique has an high sensitivity ( $10^{-9}$  to  $10^{-12}$  mol/L) and it is a relatively low cost technique.<sup>84</sup> Nevertheless, the poor depth tissue penetration properties of light, especially in the UV-Vis range of spectrum (300–650 nm), limits FI application to study surface malignancies (limited types of cancers). In the UV-Vis range, the light in tissues it is absorbed and scattered by the endogenous biological chromophores (such as hemoglobin, vitamins and bilirubin) (**Figure 1.15**). In addition, the endogenous chromophores may also contribute to auto-fluorescence, which significantly hinders the discrimination between diseased and healthy tissue. One way to overcome these limitations is to use light in the near-infrared (NIR) window, the so called “phototherapeutic window”, which appears around 700–900 nm in the electromagnetic spectrum (**Figure 1.15**).<sup>148,149</sup>

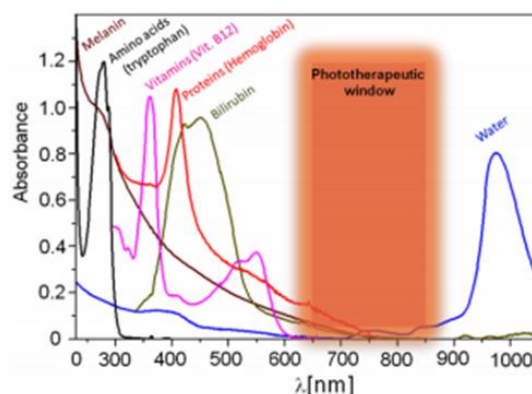


**Figure 1.15.** “Phototherapeutic window”.<sup>151</sup>

In the “phototherapeutic window”, the tissues have a minimal light absorption and scattering, and therefore enable deepest tissue penetration by light and minimum

background auto-fluorescence, when compared with UV-Vis light wavelengths. All these factors make the NIR light the most suitable for *in vivo* FI.<sup>152,153</sup>

The NIR FI has not yet been in standard clinical practice as a tool for cancer diagnostics. Nonetheless, it is widely used for *in vitro* and *in vivo* preclinical studies and it has been clinically useful in intraoperative fluorescence-guided oncologic surgery when combined with corresponding fluorophores.<sup>154,155</sup> This imaging technology allows real-time visualization of tumors and, potentially, lymph nodes and metastatic lesions, allowing surgeons to perform complete tumor resections without affecting the surrounding healthy organs. The successful implementation of deep-tissue FI with high resolution and sensitivity into standard clinical settings depends on of two key issues: (i) the development of NIR fluorescence imaging systems and (ii) the design of new sensitive and specific NIR fluorophores with improved photophysical properties.<sup>156,157</sup>

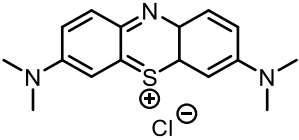
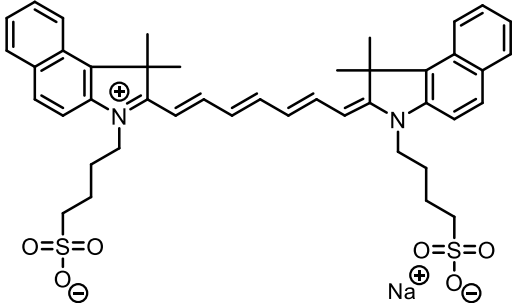
### 1.3.1 Near-infrared fluorophores for fluorescence cancer imaging

An ideal NIR fluorophore for fluorescence cancer imaging must possess the following features: 1) biocompatibility; 2) enhanced selectivity to cancer cells, which would improve the fluorescent signal-to-background ratio, allowing for sharper contrast between diseased and healthy tissue; 3) strong absorption (molar extinction coefficients  $\approx 10^5 \text{ M}^{-1} \text{ cm}^{-1}$ ) in the “phototherapeutic window”; 4) large fluorescence quantum yields to increase the sensitivity; 5) large Stokes shift, with both absorption and fluorescence in the “phototherapeutic window”, 6) photostability and 7) low toxicity.<sup>158</sup>

Currently, methylene blue (MB) and indocyanine green (ICG) are the only two NIR fluorophores available in clinical use for cancer detection (**Table 1.5**). Both NIR fluorophores are not specific-targeted for any cancer tissue<sup>159</sup> but, because they are the only clinically approved NIR fluorophores, significant research and clinical studies have been completed with both fluorophores and many intraoperative fluorescence-guided oncologic surgery uses have been found (**Table 1.5**).<sup>160</sup> Furthermore, MB use is limited because it lacks the favorable photophysical properties of NIR fluorophores, it is rapidly eliminated from the body and its rapid inactivation due to the enzymatic reduction leads to fluorescence quenching.<sup>161</sup> Additionally, ICG clinical application is also hampered by

its low stability in an aqueous medium and by its high binding affinity to non-specific blood proteins (98%), inducing rapid body clearance (half-life of 2-4 min).<sup>162,163</sup>

**Table 1.5.** Clinically approved NIR fluorophores for cancer detection.<sup>164-166</sup> [ $\lambda_{\text{abs}}$ : wavelength of maximum absorption;  $\lambda_{\text{em}}$ : wavelength of maximum fluorescence emission;  $\epsilon$ : molar extinction coefficient;  $\Phi_{\text{F}}$ : fluorescence quantum yield]

NIR fluorophores	Photophysical properties <sup>a</sup>	Cancer indication <sup>b</sup>
 <p style="text-align: center;"><b>MB</b></p>	$\lambda_{\text{abs}}$ : 670 nm $\lambda_{\text{em}}$ : 690 nm Stokes shift: 20 nm $\epsilon$ : $7.12 \times 10^4 \text{ M}^{-1} \text{ cm}^{-1}$ $\Phi_{\text{F}}$ : 0.038	- Sentinel lymph nodes mapping (breast cancer and melanoma); - Neuroendocrine, thyroid and parathyroid tumors.
 <p style="text-align: center;"><b>ICG</b></p>	$\lambda_{\text{abs}}$ : 807 nm $\lambda_{\text{em}}$ : 822 nm Stokes shift: 15 nm $\epsilon$ : $1.21 \times 10^5 \text{ M}^{-1} \text{ cm}^{-1}$ $\Phi_{\text{F}}$ : 0.093	- Sentinel lymph nodes mapping (breast cancer and melanoma); - Hepatocellular carcinoma; - Liver metastases; - Ovarian and pancreatic cancers.

<sup>a</sup> In Fetal Bovine Serum (pH 7.4).

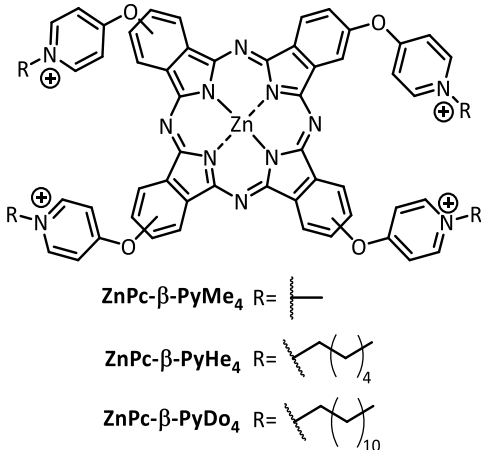
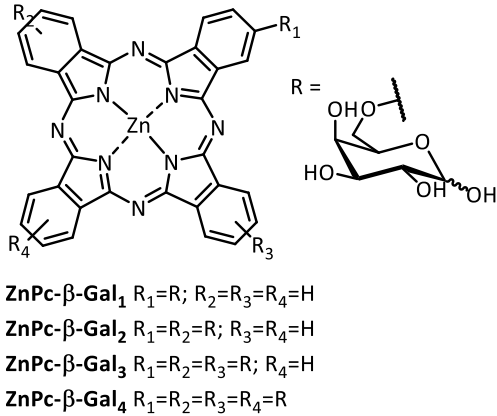
<sup>b</sup> Cancers in which intraoperative fluorescence-guided surgery has been performed with these fluorophores.

Although MB and ICG have found clinical use due to their FDA and EMA approval (**Table 1.5**), their features are far from the ideal NIR fluorophore as they cannot be easily conjugated to other molecules, an essential part for the development of novel cancer-targeted NIR fluorophores. Thus, there is clearly a clinical need to design and synthesize new NIR fluorophores with ideal photophysical properties, optimal pharmacokinetics, and with improved cancer-targeting capability.

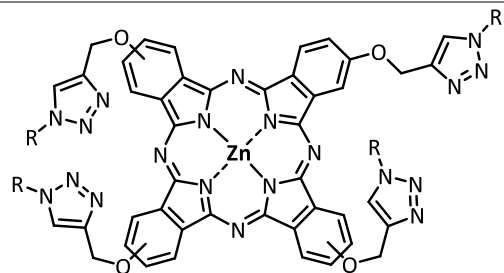
To this respect, Pcs exhibit singular properties that have prompted their study as potential NIR fluorophores for the detection of cancer. Their strong Q-band absorption close to NIR region (“phototherapeutic window”) and their high molar extinction

coefficients ( $\epsilon$ ) of typically  $\approx 10^5 \text{ M}^{-1}\text{cm}^{-1}$  are of extreme relevance for FI application. As stated before, one of the key advantages of these compounds is their easy structural modulation to achieve suitable biocompatibility and tumor selectivity by introducing the desired substituents. Selected examples of phthalocyanines application as NIR fluorophores for *in vivo* fluorescence cancer imaging based on publications from the last fifteen years are shown in **Table 1.6**.

**Table 1.6.** Pcs as potential NIR fluorophores for *in vivo* fluorescence cancer imaging reported in literature. [ $\lambda_{\text{abs}}$ : wavelength of maximum absorption;  $\lambda_{\text{em}}$ : wavelength of maximum fluorescence emission;  $\epsilon$ : molar extinction coefficient;  $\Phi_{\text{F}}$ : fluorescence quantum yield]

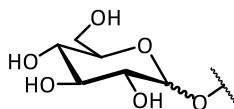
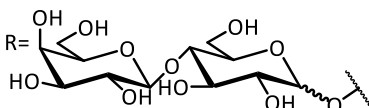
Entry	Phthalocyanines	Photophysical properties/cancer indication
1	 <p>ZnPc-<math>\beta</math>-PyMe<sub>4</sub> R = <math>\text{---CH}_3</math></p> <p>ZnPc-<math>\beta</math>-PyHe<sub>4</sub> R = <math>\text{---(CH}_2\text{)}_4\text{---}</math></p> <p>ZnPc-<math>\beta</math>-PyDo<sub>4</sub> R = <math>\text{---(CH}_2\text{)}_{10}\text{---}</math></p>	<p><math>\lambda_{\text{abs}}</math>: 671-675 nm; <math>\lambda_{\text{em}}</math>: 688-691 nm; Stokes shift: 15-20 nm; <math>\epsilon</math>: <math>0.53\text{-}1.08 \times 10^5 \text{ M}^{-1} \text{ cm}^{-1}</math>; <math>\Phi_{\text{F}}</math>: 0.29- 0.33. (in DMF)</p> <p>- Potential NIR fluorophores for <i>in vivo</i> melanoma cancer imaging, with <b>ZnPc-<math>\beta</math>-PyHe<sub>4</sub></b> demonstrating the best tumor uptake profile.<sup>167</sup></p>
2	 <p>ZnPc-<math>\beta</math>-Gal<sub>1</sub> R<sub>1</sub>=R; R<sub>2</sub>=R<sub>3</sub>=R<sub>4</sub>=H</p> <p>ZnPc-<math>\beta</math>-Gal<sub>2</sub> R<sub>1</sub>=R<sub>2</sub>=R; R<sub>3</sub>=R<sub>4</sub>=H</p> <p>ZnPc-<math>\beta</math>-Gal<sub>3</sub> R<sub>1</sub>=R<sub>2</sub>=R<sub>3</sub>=R; R<sub>4</sub>=H</p> <p>ZnPc-<math>\beta</math>-Gal<sub>4</sub> R<sub>1</sub>=R<sub>2</sub>=R<sub>3</sub>=R<sub>4</sub>=R</p>	<p><math>\lambda_{\text{abs}}</math>: 674-682 nm; <math>\lambda_{\text{em}}</math>: 680-700 nm; <math>\epsilon</math>: <math>1.07\text{-}1.77 \times 10^5 \text{ M}^{-1} \text{ cm}^{-1}</math>; <math>\Phi_{\text{F}}</math>: 0.22-0.27. (in DMSO)</p> <p>- Potential NIR fluorophores for <i>in vivo</i> liver cancer imaging, with <b>ZnPc-<math>\beta</math>-Gal<sub>3-4</sub></b> demonstrating the best tumor uptake profile.<sup>75</sup></p>

3

**ZnPc-β-Gluc<sub>4</sub>**

$\lambda_{\text{abs}}$ : 682 nm;  $\lambda_{\text{em}}$ : 690 nm; Stokes shift: 8 nm;  $\Phi_{\text{F}}$ : 0.48. (in DMSO)

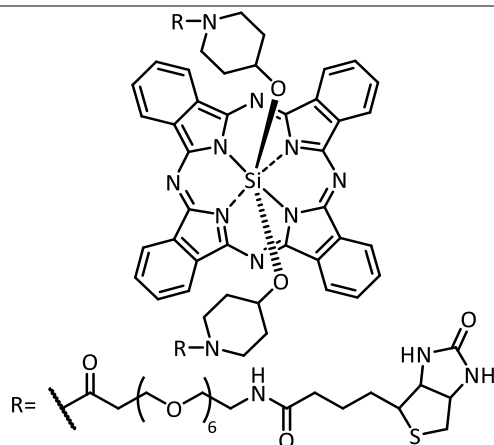
- Potential NIR fluorophore for *in vivo* liver cancer imaging.<sup>168</sup>

ZnPc-β-Gluc<sub>4</sub> R=ZnPc-β-Lac<sub>4</sub> R=**ZnPc-β-Lac<sub>4</sub>**

$\lambda_{\text{abs}}$ : 682 nm;  $\lambda_{\text{em}}$ : 690 nm; Stokes shift: 8 nm;  $\Phi_{\text{F}}$ : 0.27. (in DMSO)

- Potential NIR fluorophore for *in vivo* liver cancer imaging<sup>169</sup> and sentinel lymph node imaging.<sup>170</sup>

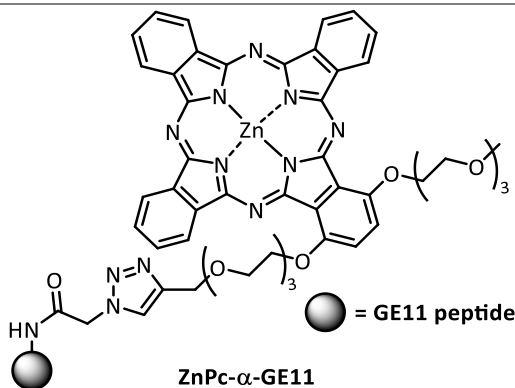
4

**SiPc-Biotin**

$\lambda_{\text{abs}}$ : 675 nm;  $\lambda_{\text{em}}$ : 680 nm; Stokes shift: 5 nm;  $\epsilon$ :  $2.2 \times 10^5 \text{ M}^{-1} \text{ cm}^{-1}$ ;  $\Phi_{\text{F}}$ : 0.35. (in DMF)

- Potential NIR fluorophore for *in vivo* cervical cancer imaging.<sup>171</sup>

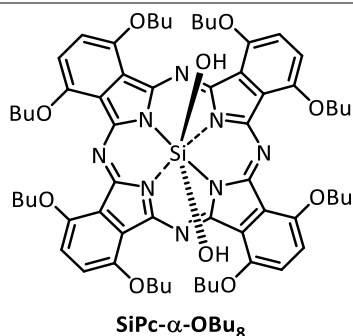
5

**ZnPc-α-GE11**

$\lambda_{\text{abs}}$ : 691 nm;  $\lambda_{\text{em}}$ : 708 nm; Stokes shift: 17 nm;  $\epsilon$ :  $2.2 \times 10^5 \text{ M}^{-1} \text{ cm}^{-1}$ ;  $\Phi_{\text{F}}$ : 0.10. (in DMF)

- Potential NIR fluorophore for *in vivo* EGFR-overexpressing tumors imaging.<sup>172</sup>

6

**SiPc-α-OBu<sub>8</sub>**

$\lambda_{\text{abs}}$ : 743 nm;  $\lambda_{\text{em}}$ : 759 nm; Stokes shift: 16 nm;  $\epsilon$ :  $1.07 \times 10^5 \text{ M}^{-1} \text{ cm}^{-1}$ ;  $\Phi_{\text{F}}$ : 0.22. (in THF)

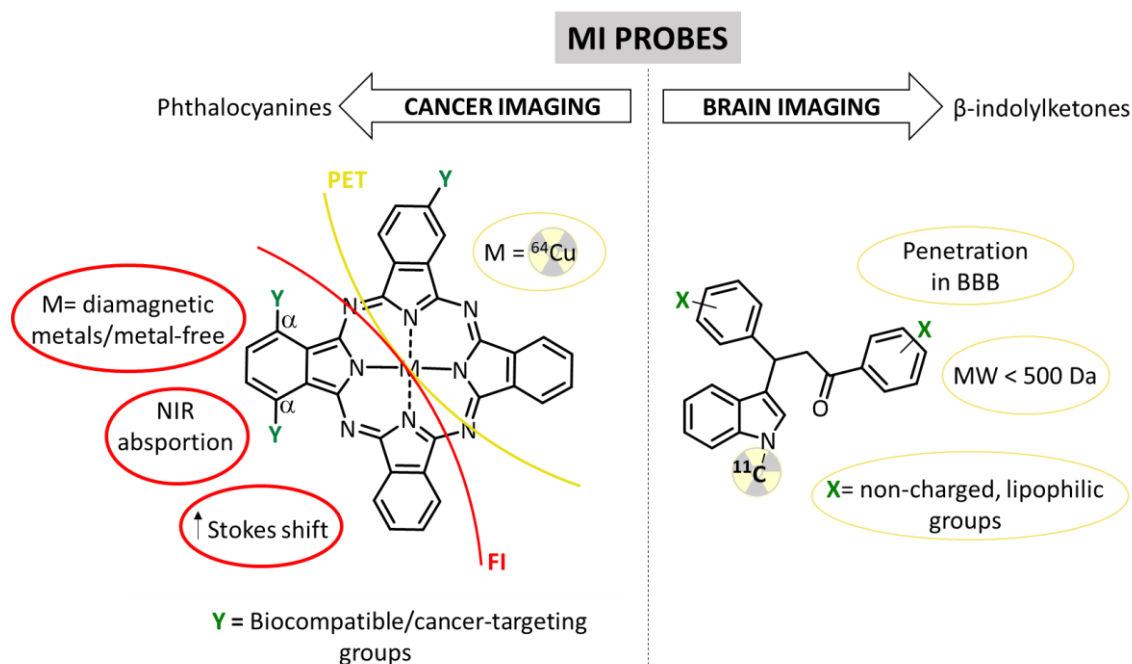
- Potential NIR fluorophore for *in vivo* breast cancer imaging.<sup>31c</sup>

Zinc(II) complexes of  $\beta$ -tetra-substituted Pcs, suitably functionalized with carbohydrate targeting moieties have been widely explored as fluorophores, due to acceptable fluorescent efficiency, mainly for liver cancer diagnosis (entries 2-3, **Table 1.6**). However, even if these zinc(II) Pc derivatives proved to show good tumor localization by FI, their photophysical properties were not ideal, as the Q-band absorptions appeared at 674-682 nm, displaying small Stokes shifts (entries 2-3, **Table 1.6**). These shortcomings were also observed for the  $\beta$ -tetra-substituted pyridinium Pcs (entry 1, **Table 1.6**) and the **SiPc-Biotin** (entry 4, **Table 1.6**). The desired red-shift of the Q-band absorption, into NIR region, can be optimized by the number, position ( $\alpha$  or  $\beta$ ) and electronic nature of the introduced substituents, along with central moiety exchange.<sup>17,173,174</sup> Previous reports suggest that tetra- or octa-substitution in the  $\alpha$  position with electron-donor substituents (*e.g.* thioalkyl and alkoxy groups) result in a large red-shift of Pc Q-band absorption into NIR region, when compared with the equivalent substitution in the  $\beta$  position.<sup>17,175-177</sup> Particularly, many researchers have reported remarkable red-shift of the Q-band absorption up to 820 nm, as well large Stokes shifts (up to 35 nm), for the  $\alpha$ -octa-substitution pattern with electron-donor moieties.<sup>18,177-180</sup> In this respect, we highlight the Arnaut and collaborators<sup>31c</sup> work, who synthesized a silicon(IV)  $\alpha$ -octa-substituted Pc bearing eight butoxy groups **SiPc- $\alpha$ -OBu<sub>8</sub>** (entry 6, **Table 1.6**). This **SiPc- $\alpha$ -OBu<sub>8</sub>** showed relevant photophysical properties for NIR fluorescence imaging and *in vivo* imaging studies in tumor breast-bearing nude mice reveals its intrinsic ability to accumulate in the tumor. However, **SiPc- $\alpha$ -OBu<sub>8</sub>** is relatively hydrophobic requiring additional structural modification to enhance its biocompatibility for FI application. Still, this specific structural modification in Pc core open interesting perspectives for the use of Pcs as NIR fluorophores for FI, and our results regarding this subject are presented in Chapter 4.

## 1.4 Aim of this thesis

**Scheme 1.6** shows the design of the compounds that were the subject of the studies in this thesis, as suitable tunable molecular platforms for potential application as MI probes for PET and FI techniques.





**Scheme 1.6.** Design of the molecular platforms as potential MI probes for PET or FI techniques.

Regarding the use of Pc as molecular platform, two main strategies were followed for its structural modulation, taking into account the target MI technique. In the case of the potential application in PET technique, our aim was to synthesize a new family of copper-64 labelled tetra-substituted phthalocyanines incorporating, through one-step approach, biocompatible and/or cancer-targeting groups at  $\beta$  positions of the macrocycle. In order to provide them with the suitable photophysical properties for potential application in FI, namely deviation of the spectral absorption range to NIR window and large Stokes shifts, we also aimed to develop a new family of phthalocyanines with octa-substitution pattern, incorporating biocompatible and/or cancer-targeting electron-donor substituents in the  $\alpha$ -positions.

At last, in an effort to discover more effective small molecules radiolabelled with short-lived positron-emitting radioisotopes as potential probes for *in vivo* brain PET imaging, a family of  $\beta$ -indolylketones was synthesized, taking into account the common structural requirements described in literature related to their ability to successfully penetrate the BBB (non-charged, lipophilic and low molecular weight compounds). Further functionalization of the  $\beta$ -indolylketones with short-lived PET radioisotope

carbon-11 could possibly led to a new generation of *in vivo* MI probes for brain PET imaging.

## 1.5 References

- <sup>1</sup> Mansoori, B.; Mohammadi, A.; Davudian, S.; Shirjang, S.; Baradaran, B., *Advanced Pharmaceutical Bulletin* **2017**, 7 (3), 339–348.
- <sup>2</sup> Bray, F.; Ferlay, J.; Soerjomataram, I.; Siegel, R. L.; Torre, L. A.; Jemal A., *CA: A Cancer Journal for Clinicians* **2018**, 68 (6), 394–424.
- <sup>3</sup> Siegel, R. L.; Miller, K. D.; Jemal, A., *CA: A Cancer Journal for Clinicians* **2019**, 69 (1), 7–34.
- <sup>4</sup> Lewis, J. S.; Keshari, K. R., *Imaging and Metabolism*, Springer International Publishing AG, Cham, Switzerland, **2018**, Chapter 1, 3–27.
- <sup>5</sup> Alcantara, D.; Leal, M. P.; García-Bocanegra, I.; García-Martín, M. L., *Frontiers in Chemistry* **2014**, 2, 112.
- <sup>6</sup> Miladinova, D., *European Journal of Nuclear Medicine Molecular Imaging* **2019**, 53 (5), 313–319.
- <sup>7</sup> Otsuka, H., *Journal of Medical Investigation* **2019**, 66 (1.2), 31–34.
- <sup>8</sup> Ghamsari, M. S., *State of the Art in Nano-Bioimaging*, IntechOpen, London, UK, **2018**, Chapter 2, 11–33.
- <sup>9</sup> Chen, K.; Chen, X., *Current Topics in Medicinal Chemistry* **2010**, 10 (12), 1227–1236.
- <sup>10</sup> Leznoff, C. C.; Lever, A. B. P. *Phthalocyanines, Properties and Applications*, Vol. 1–4, Wiley-VCH, New York, USA, **1989–1996**.
- <sup>11</sup> Luk'yanets, E. A.; Nemykin, V. N., *Journal of Porphyrins and Phthalocyanines* **2010**, 14 (01), 1–40.
- <sup>12</sup> Kadish, K. M.; Smith, K. M.; Guillard, R., *The Porphyrin Handbook: Applications of Phthalocyanines*, Vol. 19, Elsevier Science, USA, **2003**, Chapter 119, 105–149.
- <sup>13</sup> (a) Gouterman, M.; Wagnière, G. H.; Synder, L. C., *Journal of Molecular Spectroscopy* **1963**, 11 (1–6), 108–127; (b) Weiss, C.; Kobayashi, H.; Gouterman, M., *Journal of Molecular Spectroscopy* **1965**, 16 (2), 415–450; (c) McHugh, A. J.; Gouterman, M., *Theoretica Chimica Acta* **1972**, 24, 346–370.
- <sup>14</sup> Isago, H., *Optical Spectra of Phthalocyanines and Related Compounds*, Springer, Tsukuba, Japan, **2015**, Chapter 2, 21–40.
- <sup>15</sup> de laTorre, G.; Vazquez, P.; Agullo-Lopez, F.; Torres, T., *Chemical Reviews* **2004**, 104 (9), 3723–3750.
- <sup>16</sup> Mack, J.; Kobayashi, N., *Chemical Reviews* **2011**, 111 (2), 281–321.
- <sup>17</sup> Rio, Y.; Rodríguez-Morgade, M. S.; Torres, T., *Organic & Biomolecular Chemistry* **2008**, 6 (11), 1877–1894.
- <sup>18</sup> Kobayashi, N.; Ogata, H.; Nonaka, N.; Luk'yanets, E. A., *Chemistry – A European Journal* **2003**, 9, 5123–5134.
- <sup>19</sup> Tomé, V. A.; Calvete, M. J. F.; Vinagreiro, C. S.; Aroso, R. T.; Pereira, M. M., *Catalysts* **2018**, 8 (10), 480.
- <sup>20</sup> Nemykin, V. N.; Luk'yanets, E. A., *ARKIVOC* **2010**, 136–208.

- <sup>21</sup> (a) Sommerauer, M.; Rager, C.; Hanack, M., *Journal of American Chemical Society* **1996**, 118 (42), 10085–10093; (b) Hanack, M.; Schmid, G.; Sommerauer, M., *Angewandte Chemie International Edition* **1993**, 32 (10), 1422–1424.
- <sup>22</sup> (a) Sorokin, A., *Chemical Reviews* **2013**, 113 (10), 8152–8191; (b) Silva, M.; Calvete, M. J. F.; Pereira, M. M.; Burrows, H. D., *RSC Advances* **2013**, 3 (45), 22774–22789; (c) Silva, M.; Calvete, M. J. F.; Gonçalves, N. P. F.; Azenha, M. E.; Burrows, H. D.; Sarakha, M.; Ribeiro, M. F.; Fernandes, A.; Pereira, M. M., *Journal of Hazardous Materials* **2012**, 233–234, 79–88.
- <sup>23</sup> (a) Bouvet, M.; Gaudillat, P.; Suisse, J. M., *Journal of Porphyrins and Phthalocyanines* **2013**, 17 (10), 913–919; (b) Paoletti, A. M.; Pennesi, G.; Rossi, G.; Generosi, A.; Paci, B.; Albertini, V. R., *Sensors* **2009**, 9 (7), 5277–5297; (c) Guillaud, G.; Simon, J.; Germain, J. P., *Coordination Chemistry Reviews* **1998**, 178–180 (2), 1433–1484.
- <sup>24</sup> (a) Valli, L., *Advances in Colloid and Interface Science* **2005**, 116 (1–3), 1–344; (b) Papageorgiou, N.; Salomon, E.; Angot, T.; Layet, J. M.; Giovanelli, L.; Le Lay, G., *Progress in Surface Science* **2004**, 77 (5–8), 139–170.
- <sup>25</sup> Bottari, G.; de la Torre, G.; Guldi, D. M.; Torres, T., *Chemical Reviews* **2010**, 110, 6768–6816; (b) Pereira, A. M. V. M.; Soares, A. R. M.; Calvete, M. J. F.; de la Torre, G., *Journal of Porphyrins and Phthalocyanines* **2009**, 13 (04–05), 419–428.
- <sup>26</sup> (a) Calvete, M. J. F.; Dini, D., *Journal of Photochemistry and Photobiology C: Photochemistry Reviews* **2018**, 35, 56–73; (b) Dini, D.; Calvete, M. J. F.; Hanack, M., *Chemical Reviews* **2016**, 116 (22), 13043–13233.
- <sup>27</sup> Lo, P. C.; Rodríguez-Morgade, M. S.; Pandey, R. K.; Ng, D. K. P.; Torres, T.; Dumoulin, F., *Chemical Society Reviews* **2020**, Advance Article. DOI: 10.1039/C9CS00129H.
- <sup>28</sup> (a) Li, X.; Zheng, B.-D.; Peng, X.-H.; Li, S.-Z.; Ying, J.-W.; Zhao, Y.; Huang, J.-D.; Yoon, J., *Coordination Chemistry Reviews* **2019**, 379, 147–160; (b) Roguin, L. P.; Chiarante, N.; Vior, M. C. G.; Marino, J., *International Journal of Biochemistry & Cell Biology* **2019**, 114, 105575.
- <sup>29</sup> Pandey, R. K.; Kessel, D.; Dougherty, T. J., *Handbook of Photodynamic Therapy: Updates on Recent Applications of Porphyrin-Based Compounds*, World Scientific, Singapore, **2016**, Chapter 5, 173–235.
- <sup>30</sup> Zhang, Y.; Lovell, J. F., *Wiley Interdisciplinary Reviews: Nanomedicine and Nanobiotechnology* **2017**, 9 (1), 1–15.
- <sup>31</sup> (a) Calvete, M. J. F.; Pinto, S. M., *Current Organic Synthesis* **2017**, 14 (5), 704–714; (b) Calvete, M. J. F.; Pinto, S. M. A.; Pereira, M. M.; Geraldès, C. F. G. C., *Coordination Chemistry Reviews* **2017**, 333, 82–107; (c) Lobo, A. C. S.; Silva, A. D.; Tomé, V. A.; Pinto, S. M. A.; Silva, E. F. F.; Calvete, M. J. F.; Gomes, C. M. F.; Pereira, M. M.; Arnaut, L. G., *Journal of Medicinal Chemistry* **2016**, 59 (10), 4688–4696; (d) Calvete, M. J. F.; Simões, A. V. C.; Henriques, C. A.; Pinto, S. M. A.; Pereira, M. M., *Current Organic Synthesis* **2014**, 11, 127–140.
- <sup>32</sup> Calvete, M. J. F., *Future Trends for Top Materials*, Bentham e-Books, Bentham Science Publishers, **2016**, Chapter 1, 3–77.

- <sup>33</sup> Schubert, U.; Hüsing, N.; Laine, R., *Materials Syntheses: A Practical Guide*, Springer-Verlag Wien, Germany, **2008**, Chapter 28, 217–225.
- <sup>34</sup> Schaumann, E., *Methoden der Organischen Chemie (Houben–Weyl)*, Vol. E9d: Hetarenes IV, 4<sup>th</sup> edition, Thieme-Verlag Stuttgart, Germany, **1997**, 717–766.
- <sup>35</sup> (a) Pinto, S. M. A.; Tomé, V. A.; Calvete, M. J. F.; Pereira, M. M.; Burrows, H. D.; Cardoso, A. M. S.; Pallier, A.; Castro, M. M. C. A.; Tóth, É.; Geraldés, C. F. G. C., *Journal of Inorganic Biochemistry* **2016**, 154, 50–59; (b) Singh, S.; Aggarwal, A.; Bhupathiraju, N. V. S. D. K.; Arianna, G.; Tiwari, K.; Drain, C. M., *Chemical Reviews* **2015**, 115 (18), 10261–10306.
- <sup>36</sup> Dumoulin, F.; Durmuş, M.; Ahsen, V.; Nyokong, T., *Coordination Chemistry Reviews* **2010**, 254 (23–24), 2792–2847.
- <sup>37</sup> Hanack, M.; Crucius, G.; Calvete, M. J. F.; Ziegler, T., *Current Organic Synthesis* **2014**, 11 (1), 59–66.
- <sup>38</sup> Lever, A. B. P., *Advances in Inorganic Chemistry and Radiochemistry* **1965**, 7, 27–114.
- <sup>39</sup> Barrett, P. A.; Frye, D. A.; Linstead, R. P., *Journal of Chemical Society (Resumed)* **1938**, 1157–1163.
- <sup>40</sup> (a) Özçeşmeci, M.; Sorar, I.; Özçeşmeci, I.; Hamuryudan, E., *Journal of Coordination Chemistry* **2018**, 71 (15), 2281–2292; (b) Fukuda, T.; Ishiguro, T.; Kobayashi, N., *Tetrahedron Letters* **2005**, 46 (16), 2907–2909; (c) Brewis, M.; Clarkson, G. J.; Humberstone, P.; Makhseed, S.; McKeown, N. B., *Chemistry: A European Journal* **1998**, 4, 1633–1640; (d) Cook, M. J.; Daniel, M. F.; Harrison, K. J.; McKeown, N. B.; Thomson, A. J., *Journal of the Chemical Society-Chemical Communications* **1987**, 14, 1086–1088.
- <sup>41</sup> Calvete, M. J. F.; Dini, D.; Hanack, M.; Sancho-Garcia, J. C.; Chen, W.; Ji, W., *Journal Molecular Modeling* **2006**, 12 (5), 543–550; (b) Dini, D.; Calvete, M. J. F.; Hanack, M.; Chen, W.; Ji, W., *ARKIVOC* **2006**, 3, 77–96; (c) Calvete, M. J. F.; Dini, D.; Flom, S. R.; Hanack, M.; Pong, R. G. S.; Shirk, J. S., *European Journal of Organic Chemistry* **2005**, 16, 3499–3509.
- <sup>42</sup> Alzeer, J.; Roth, P. J. C.; Luedtke, N. W., *Chemical Communications* **2009**, 15, 1970–1971.
- <sup>43</sup> Haruhiko, T.; Shojiro, S.; Shinsaku, S., *Chemistry Letters* **1983**, 12 (3), 313–316.
- <sup>44</sup> Joyner, R. D.; Linck, R. G.; Esposito, J. N.; Kenney, M. E., *Journal of Inorganic and Nuclear Chemistry* **1962**, 24 (3), 299–302.
- <sup>45</sup> Chauke, V.; Ogunsipe, A.; Durmuş, M.; Nyokong, T., *Polyhedron* **2007**, 26 (12), 2663–2671.
- <sup>46</sup> Smith, K. M.; Guillard, R., *The Porphyrin Handbook*, Vol. 15, Academic Press, Amsterdam, **2003**, Chapter 97, 1–60.
- <sup>47</sup> Rager, C.; Schmid, G.; Hanack, M., *Chemistry – A European Journal* **1999**, 5 (1), 280–288.
- <sup>48</sup> Oliver, S. W.; Smith, T. D., *Journal of Chemical Society, Perkin Transactions 2* **1987**, 11, 1579–1582.

- <sup>49</sup> Setaro, F.; Ruiz-González, R.; Nonell, S.; Hahn, U.; Torres, T., *Journal of Inorganic Biochemistry* **2014**, 136, 170–176.
- <sup>50</sup> Wei, S.; Zhou, J.; Huang, D.; Wang, X.; Zhang, B.; Shen, J., *Dyes and Pigments* **2006**, 71 (1), 61–67.
- <sup>51</sup> Venkatramaiah, N.; Pereira, P. M. R.; Almeida Paz, F. A.; Ribeiro, C. A. F.; Fernandes, R.; Tomé, J. P. C., *Chemical Communications* **2015**, 51 (85), 15550–15553.
- <sup>52</sup> (a) Yano, S.; Hirohara, S.; Obata, M.; Hagiya, Y.; Ogura, S.; Ikeda, A.; Kataoka, H.; Tanaka, M.; Joh, T., *Journal of Photochemistry and Photobiology C: Photochemistry Reviews* **2011**, 12 (1), 46–67; (b) Serra, A.; Piñeiro, M.; Pereira, N.; Gonsalves, A. R.; Laranjo, M.; Abrantes, M.; Botelho, F., *Oncology Reviews* **2008**, 2, 235–239; (c) Allison, R. R.; Downie, G. H.; Cuenca, R.; Hu, X.-H.; Childs, C. J.; Sibata, C. H., *Photodiagnosis and Photodynamic Therapy* **2004**, 1 (1), 27–42.
- <sup>53</sup> Machacek, M.; Cidlina, A.; Novakova, V.; Svec, J.; Rudolf, E.; Miletin, M.; Kučera, R.; Simunek, T.; Zimcik, P., *Journal of Medicinal Chemistry* **2015**, 58 (4), 1736–1749.
- <sup>54</sup> Mantareva, V.; Angelov, I.; Kussovski, V.; Dimitrov, R.; Lapok, L.; Wöhrle, D., *European Journal of Medicinal Chemistry* **2011**, 46 (9), 4430–4440.
- <sup>55</sup> Aroso, R. T.; Calvete, M. J. F.; Pucelik, B.; Dubin, G.; Arnaut, L. G.; Pereira, M. M.; Dąbrowski, J. M., *European Journal of Medicinal Chemistry* **2019**, 184, 111740.
- <sup>56</sup> Kutlu, O. D.; Avcil, D.; Erdoğan, A., *Main Group Chemistry* **2019**, 18 (2), 139–151.
- <sup>57</sup> Özel, A.; Demirbaş, Ü.; Barut, B.; Kantekin, H., *Journal of Molecular Structure* **2019**, 1186, 325–332.
- <sup>58</sup> Barut, B.; Demirbaş, Ü.; Özel, A.; Kantekin, H., *International Journal of Biological Macromolecules* **2017**, 105, 499–508.
- <sup>59</sup> (a) Lo, P.-C.; Huang, J.-D.; Cheng, D. Y. Y.; Chan, E. Y. M.; Fong, W.-P.; Ko, W.-H.; Ng, D. K. P., *Chemistry: A European Journal* **2004**, 10 (19), 4831–4838; (b) Huang, J.-D.; Lo, P.-C.; Chen, Y.-M.; Lai, J. C.; Fong, W.-P.; Ng, D. K. P., *Journal of Inorganic Biochemistry* **2006**, 100 (5-6), 946–951; (c) Jiang, X.-J.; Huang, J.-D.; Zhu, Y.-J.; Tang, F.-X.; Ng, D. K. P.; Sun, J.-C., *Bioorganic and Medicinal Chemistry Letters* **2006**, 16 (9), 2450–2453; (d) Li, H.; Jensen, T. J.; Fronczek, F. R.; Vicente, M. G. H., *Journal of Medicinal Chemistry* **2008**, 51 (3), 502–511; (e) Mao, J.; Zhang, Y.; Zhu, J.; Zhang, C.; Guo, Z., *Chemical Communications* **2009**, 8, 908–910.
- <sup>60</sup> Furuyama, T.; Ishii, T.; Leda, N.; Maeda, H.; Segi, M.; Uchiyama, M.; Nakagawa, H., *Chemical Communications (Camb)* **2019**, 55 (51), 7311–7314.
- <sup>61</sup> Wöhrle, D.; Iskander, N.; Grasczew, G.; Sinn, H.; Friedrich, E. A.; Maier-Borst, W.; Stern, J.; Schlag, P., *Photochemistry and Photobiology* **1990**, 51 (3), 351–356.
- <sup>62</sup> (a) Cheng, M.; Bhujwala, Z. M.; Glunde, K., *Frontiers in Oncology* **2016**, 6, 266; (b) Glunde, K.; Penet, M. F.; Jiang, L.; Jacobs, M. A.; Bhujwala, Z. M., *Expert Review of Molecular Diagnostics* **2015**, 15 (6), 735–747.
- <sup>63</sup> (a) Inazu, M., *Biopharmaceutics & Drug Disposition* **2014**, 35 (8), 431–449; (b) Glunde, K.; Bhujwala, Z. M.; Ronen, S. M., *Nature Reviews Cancer* **2011**, 11 (12), 835–848.
- <sup>64</sup> D'souza, A. A.; Shegokar, R., *Expert Opinion on Drug Delivery* **2016**, 13 (9), 1257–1275.

- <sup>65</sup> (a) Liu, J.-Y.; Jiang, X.-J.; Fong, W.-P.; Ng, D. K. P., *Organic & Biomolecular Chemistry* **2008**, 6 (24), 4560–4566; (b) van Vlerken, L. E.; Vyas, T. K.; Amiji, M. M., *Pharmaceutical Research* **2007**, 24, 1405–1414.
- <sup>66</sup> (a) Uslan, C.; Köksoy, B.; Durmuş, M.; Durmuş, İ. N.; Öztürk, Y.; Çakar, Z. P.; Gürsel, Y. H.; Sesalan, B. S., *Journal of Biological Inorganic Chemistry* **2019**, 24 (2), 191–210; (b) Şahin, S.; Açar, E., *Journal of Molecular Structure* **2019**, 1187, 121–131.
- <sup>67</sup> (a) Lo, P.-C.; Wang, S.; Zeug, A.; Meyer, M.; Röder, B.; Ng, D. K. P., *Tetrahedron Letters* **2003**, 44, 1967–1970; (b) Huang, J.-D.; Wang, S.; Lo, P.-C.; Fong, W.-P.; Ko, W.-P.; Ng, D. K. P., *New Journal of Chemistry* **2004**, 28 (3), 348–354; (c) Bandera, Y.; Burdette, M. K.; Shetzline, J. A.; Jenkins, R.; Creager, S. E.; Foulger, S. H., *Dyes and Pigments* **2016**, 125, 72–79; (d) Uslan, C.; İşleyen, N. D.; Öztürk, Y.; Yildiz, B. T.; Çakar, Z. P.; Göksel, M.; Durmuş, M.; Gürsel, Y. H.; Sesalan, B. S., *Journal of Porphyrins and Phthalocyanines* **2018**, 22 (01–03), 10–24.
- <sup>68</sup> Lv, F.; Cao, B.; Cui, Y.; Liu, T., *Molecules* **2012**, 17 (6), 6348–6361.
- <sup>69</sup> (a) Barrona, C. C.; Bilan, P. J.; Tsakiridis, T.; Tsiani, E., *Metabolism Clinical and Experimental* **2016**, 65, 124–139; (b) Calvo, M. B.; Figueroa, A.; Pulido, E. G.; Campelo, R. G.; Aparicio, L. A., *International Journal of Endocrinology* **2010**, 205357; (c) Airley, R. E.; Mobasheri, A., *Chemotherapy* **2007**, 53 (4), 233–256.
- <sup>70</sup> (a) Hanack, M., *Molecules* **2015**, 20 (11), 20173–20185; (b) Lourenço, L. M. O.; Neves, M. G. P. M. S.; Cavaleiro, J. A. S.; Tomé, J. P. C., *Tetrahedron*, **2014**, 70, 2681–2698.
- <sup>71</sup> Mori, S.; Yoshiyama, H.; Tokunaga, E.; Iida, N.; Hayashi, M.; Obata, T.; Tanaka, M.; Shibata, N., *Journal of Fluorine Chemistry* **2015**, 174, 137–141.
- <sup>72</sup> (a) Chan, C. M. H.; Lo, P.-C.; Yeung, S.-L.; Ng, D. K. P.; Fong, W.-P., *Cancer Biology & Therapy* **2010**, 10 (2), 126–134; (b) Lo, P.-C.; Leung, S. C. H.; Chan, E. Y. M.; Fong, W.-P.; Ko, W.-H.; Ng, D. K. P., *Photodiagnosis and Photodynamic Therapy* **2007**, 4 (2), 117–123; (c) Lo, P.-C.; Chan, C. M. H.; Liu, J.-Y.; Fong, W.-P.; Ng, D. K. P., *Journal of Medicinal Chemistry* **2007**, 50 (9), 2100–2107; (d) Lee, P. P. S.; Lo, P.-C.; Chan, E. Y. M.; Fong, W.-P.; Ko, W.-H.; Ng, D. K. P., *Tetrahedron Letters* **2005**, 46 (9), 1551–1554.
- <sup>73</sup> (a) Cooper, S. A. L.; Graepel, K. W.; Steffensa, R. C.; Dennisc, D. G.; Cambroneoa, G. A.; Wiggins, R. Q.; Ruppel, J. V.; Snyder, N. L., *Journal of Porphyrins and Phthalocyanines* **2019**, 23 (07–08), 850–855; (b) Bispo, M.; Pereira, P. M. R.; Setaro, F.; Rodríguez-Morgade, M. S.; Fernandes, R.; Torres, T.; Tomé, J. P. C., *ChemPlusChem* **2018**, 83 (9), 855–860; (c) Galstyan, A.; Block, D.; Niemann, S.; Grüner, M. C.; Abbruzzetti, S.; Oneto, M.; Daniliuc, C. G.; Hermann, S.; Viappiani, C.; Schäfers, M.; Löffler, B.; Strassert, C. A.; Faust, A., *Chemistry – A European Journal* **2016**, 22 (15), 5243–5252.
- <sup>74</sup> (a) Ferreira, J. T.; Pina, J.; Ribeiro, C. A. F.; Fernandes, R.; Tomé, J. P. C.; Rodríguez-Morgade, M. S.; Torres, T., *Chemistry – A European Journal* **2020**, 26 (8), 1789–1799; (b) Ferreira, J. T.; Pina, J.; Ribeiro, C. A. F.; Fernandes, R.; Tomé, J. P. C.; Rodríguez-Morgade, M. S.; Torres, T., *ChemPhotoChem* **2018**, 2 (7), 640–654.
- <sup>75</sup> Lv, F.; Li, Y.; Cao, B.; Liu, T., *Journal of Materials Science: Materials in Medicine* **2013**, 24 (3), 811–819.

- <sup>76</sup> Kimani, S. G.; Shmigol, T. A.; Hammond, S.; Phillips, J. B.; Bruce, J. I.; MacRobert, A. J.; Malakhov, M. V.; Golding, J. P., *Photochemistry and Photobiology* **2013**, 89 (1), 139–149.
- <sup>77</sup> Dollé, F., *Journal of Labelled Compounds and Radiopharmaceuticals* **2013**, 56 (3–4), 65–67.
- <sup>78</sup> Ametamey, S. M.; Honer, M.; Schubiger, P. A., *Chemical Reviews* **2008**, 108 (5), 1501–1516.
- <sup>79</sup> Derlin, T.; Grünwald, V.; Steinbach, J.; Wester, H. J.; Ross, T. L., *Deutsches Arzteblatt International* **2018**, 115 (11), 175–181.
- <sup>80</sup> Khalil, M. M., *Basic Science of PET Imaging*, Springer, Cham, Switzerland, **2017**, Chapter 20, 485–535.
- <sup>81</sup> Khalil, M. M., *Basic Science of PET Imaging*, Springer, Cham, Switzerland, **2017**, Chapter 19, 451–483.
- <sup>82</sup> Son, H.; Jang, K.; Lee, H.; Kim, S. E.; Kang, K. W.; Lee, H., *Nuclear Medicine and Molecular Imaging* **2019**, 53 (3), 208–215.
- <sup>83</sup> Schnöckel, U.; Hermann, S.; Stegger, L.; Law, M.; Kuhlmann, M.; Schober, O.; Schäfers, K.; Schäfers, M., *European Journal of Pharmaceutics and Biopharmaceutics* **2010**, 74 (1), 50–54.
- <sup>84</sup> Lu, F. M.; Yuan, Z., *Quantitative Imaging in Medicine and Surgery* **2015**, 5 (3), 433–447.
- <sup>85</sup> Karamé, I.; Shaya, J.; Srour, H., *Carbon Dioxide Chemistry, Capture and Oil Recovery*, IntechOpen, London, UK, **2018**, Chapter 7, 123–138.
- <sup>86</sup> Dresel, S., *PET in Oncology*, Springer-Verlag Berlin Heidelberg, **2008**, Chapter 1, 1–23.
- <sup>87</sup> Saha, G. B., *Basics of PET Imaging: Physics, Chemistry and Regulations*, 3<sup>rd</sup> edition, Springer, New York, USA, **2016**, Chapter 2, 19–54.
- <sup>88</sup> Saha, G. B., *Basics of PET Imaging: Physics, Chemistry and Regulations*, 3<sup>rd</sup> edition, Springer, New York, USA, **2016**, Chapter 4, 91–107.
- <sup>89</sup> Powsner R. A.; Powsner E. R.; Palmer, M. R., *Essential Nuclear Medicine Physics and Instrumentation*, 3<sup>rd</sup> edition, Wiley-Blackwell Publishing, Malden, USA, **2013**, Chapter 3, 32–40.
- <sup>90</sup> (a) Attard, M., *Radiopharmacy: An update - A Technologist's Guide*, European Association of Nuclear Medicine, Vienna, Austria, **2019**, Chapter 6, 72–92; (b) Ha, N. S.; Sadeghi, S.; van Dam, R. M., *Micromachines (Basel)* **2017**, 8 (11), E337; (c) Saha, G. B., *Basics of PET Imaging: Physics, Chemistry and Regulations*, 3<sup>rd</sup> edition, Springer, New York, USA, **2016**, Chapter 8, 161–178.
- <sup>91</sup> (a) Shahzad, A.; Bashir, S., *Nuclear Medicine Physics*, IntechOpen, London, UK, **2019**, Chapter 5, 59–80; (b) Khalil, M. M., *Basic Science of PET Imaging*, Springer, Cham, Switzerland, **2017**, Chapters 6–7, 127–170.
- <sup>92</sup> Saha, G. B., *Basics of PET Imaging: Physics, Chemistry and Regulations*, 3<sup>rd</sup> edition, Springer, New York, USA, **2016**, Chapter 7, 143–160.
- <sup>93</sup> Kadrmas, D. J.; Hoffman, J. M., *Theranostics* **2013**, 3 (10), 757–773.



- <sup>94</sup> Neumann, K.; Flavell, R.; Wilson, D. M., *Seminars in Nuclear Medicine* **2017**, 47 (5), 461–473.
- <sup>95</sup> Dahl, K.; Halldin, C.; Schou, M., *Clinical and Translational Imaging* **2017**, 5 (3), 275–289.
- <sup>96</sup> Lewis, J. S.; Windhorst, A. D.; Zeglis, B., *Radiopharmaceutical Chemistry*, Springer, Cham, Switzerland, **2019**, Chapter 11, 207–220.
- <sup>97</sup> Paterson, B. M.; Donnelly, P. S., *Advances in Inorganic Chemistry* **2016**, 68, 223–251.
- <sup>98</sup> Lewis, J. S.; Windhorst, A. D.; Zeglis, B., *Radiopharmaceutical Chemistry*, Springer, Cham, Switzerland, **2019**, Chapter 19, 335–358.
- <sup>99</sup> Aguilar-Ortíz, E.; Jalilian, A. R.; Ávila-Rodríguez, M. A., *MedChemComm* **2018**, 9 (10), 1577–1588.
- <sup>100</sup> Smith, S. V., *Journal of Inorganic Biochemistry* **2004**, 98 (11), 1874–1901.
- <sup>101</sup> Derlin, T.; Grünwald, V.; Steinbach, J.; Wester, H.; Ross, T. L., *Deutsches Arzteblatt International* **2018**, 115 (11), 175–181.
- <sup>102</sup> Bennett, P.; Oza, U., *Diagnostic Imaging: Nuclear Medicine*, 2<sup>nd</sup> edition, Elsevier, Canada, **2016**, Chapter 11, 310–467.
- <sup>103</sup> Shahzad, A.; Bashir, S., *Nuclear Medicine Physics*, IntechOpen, London, UK, **2019**, Chapter 4, 35–58.
- <sup>104</sup> Strauss, H. W.; Mariani, G.; Volterrani, D.; Larson, S. M., *Nuclear Oncology*, Springer, Cham, Switzerland, **2017**, Chapter 4, 85–98.
- <sup>105</sup> Obochi, M. O.; Boyle, R. W.; van Lier, J. E., *Photochemistry and Photobiology* **1993**, 57 (4), 634–640.
- <sup>106</sup> Boyle, R. W.; Rousseau, J.; Kudrevich, S. V.; Obochi, M.; van Lier, J. E., *British Journal of Cancer* **1996**, 73 (1), 49–53.
- <sup>107</sup> Soucy-Faulkner, A.; Rousseau, J. A.; Langlois, R.; Berard, V.; Lecomte, R.; Bénard, F.; van Lier, J. E., *Journal of Porphyrins and Phthalocyanines* **2008**, 12 (01), 49–53.
- <sup>108</sup> Ranyuk, E. R.; Cauchon, N.; Ali, H.; Lecomte, R.; Guérin, B.; van Lier, J. E., *Bioorganic & Medicinal Chemistry Letters* **2011**, 21 (24), 7470–7473.
- <sup>109</sup> Lu, H. D.; Wang, L. Z.; Wilson, B. K.; McManus, S. A.; Jumai'na, J.; Padakanti, P. K.; Alavi, A.; Mach, R. H.; Prud'homme, R. K., *ACS Applied Materials & Interfaces* **2018**, 10 (4), 3191–3199.
- <sup>110</sup> Ranyuk, E.; Lebel, R.; Bérubé-Lauzière, Y.; Klarskov, K.; Lecomte, R.; van Lier, J. E.; Guérin, B., *Bioconjugate Chemistry* **2013**, 24 (9), 1624–1633.
- <sup>111</sup> Ranyuk, E.; Ali, H.; Guérin, B.; van Lier, J. E., *Journal of Porphyrins and Phthalocyanines* **2013**, 17 (08–09), 850–856.
- <sup>112</sup> (a) McCluskey, S. P.; Plisson, C.; Rabiner, E. A.; Howes, O., *European Journal of Nuclear Medicine and Molecular Imaging* **2020**, 47, 451–489; (b) Suridjan, I.; Comley, R. A.; Rabiner, E. A., *Brain Imaging and Behavior* **2019**, 13, 354–365.
- <sup>113</sup> (a) Miller, P. W.; Long, N. J.; Vilar, R.; Gee, A. D., *Angewandte Chemie International Edition* **2008**, 47 (47), 8998–9033; (b) Roeda, D.; Kuhnast, B.; Hammadi, A.; Dollé, F., *Journal of Labelled Compounds and Radiopharmaceuticals* **2007**, 50 (9–10), 848–866.

- <sup>114</sup> Fragoso, P. C.; Santos, A.; Borut, V., *Brain Imaging*, European Association of Nuclear Medicine, Vienna, Austria, **2016**, Chapter 2, 12–25.
- <sup>115</sup> Fragoso, P. C.; Santos, A.; Borut, V., *Brain Imaging*, European Association of Nuclear Medicine, Vienna, Austria, **2016**, Chapter 4, 33–53.
- <sup>116</sup> Rankovic, Z., *Journal of Medicinal Chemistry* **2015**, 58 (6), 2584–2608.
- <sup>117</sup> Need, A.; Kant, N.; Jesudason, C.; Barth, V., *Clinical and Translational Imaging* **2017**, 5, 265–274.
- <sup>118</sup> (a) McCluskey, S. P.; Plisson, C.; Rabiner, E. A.; Howes, O., *European Journal of Nuclear Medicine and Molecular Imaging* **2020**, 46, 451–489; (b) Fong, C. W., *Journal of Membrane Biology* **2015**, 248, 651–669.
- <sup>119</sup> (a) Lewis, J. S.; Windhorst, A. D.; Zeglis, B., *Radiopharmaceutical Chemistry*, Springer, Cham, Switzerland, **2019**, Chapter 34, 583–606; (b) Pike, V. W. *Trends in Pharmacological Sciences* **2009**, 30 (8), 431–440.
- <sup>120</sup> (a) Ovonramwen, O. B.; Owolabi, B. J.; Oviawe, A. P., *Asian Journal of Chemical Sciences* **2019**, 6 (3), 1–16; (b) Albuquerque, H. T.; Santos, H. M. M.; Cavaleiro, J. A. S.; Silva, A. M. S., *Current Organic Chemistry* **2014**, 18 (21), 2750–2775.
- <sup>121</sup> (a) Rammohan, A.; Reddy, J. S.; Sravya, G.; Rao, C. N.; Zyryanov, G. V., *Environmental Chemistry Letters* **2020**, 28, 433–458; (b) Sahu, N. K.; Balbhadra, S. S.; Choudhary, J.; Kohli, D. V., *Current Medicinal Chemistry* **2012**, 19 (2), 209–225.
- <sup>122</sup> (a) Amslinger, S.; Al-Rifai, N.; Winter, K.; Wörmann, K.; Scholz, R.; Baumeister, P.; Wild, M., *Organic & Biomolecular Chemistry* **2013**, 11 (4), 549–554; (b) Romagnoli, R.; Baraldi, P.G.; Carrion, M. D.; Cara, C. L.; Cruz-Lopez, O.; Preti, D.; Tolomeo, M.; Grimaudo, S.; Cristina, A. D.; Zonta, N.; Balzarini, J.; Brancale, A.; Sarkar, T.; Hamel, E., *Bioorganic & Medicinal Chemistry* **2008**, 16 (10), 5367–5376; (c) Lawrence, N. J.; Patterson, R. P.; Ooi, L.-L.; Cook, D.; Ducki, S., *Bioorganic & Medicinal Chemistry Letters* **2006**, 16 (22), 5844–5848.
- <sup>123</sup> Ono, M.; Watanabe, R.; Kawashima, H.; Cheng, Y.; Kimura, H.; Watanabe, H.; Mamoru, H.; Saji, H.; Nakayama, M., *Journal of Medicinal Chemistry* **2009**, 52 (20), 6394–6401.
- <sup>124</sup> Chauhan, K.; Datta, A.; Adhikari, A.; Chuttani, K.; Singh, A. K.; Mishra, A. K., *Organic & Biomolecular Chemistry* **2014**, 12 (37), 7328–7337.
- <sup>125</sup> Chauhan, K.; Tiwari, A. K.; Chadha, N.; Kaul, A.; Singh, A. K.; Datta, A., *Molecular Pharmaceutics* **2018**, 15 (4), 1515–1525.
- <sup>126</sup> Kaide, S.; Ono, M.; Watanabe, H.; Shimizu, Y.; Nakamoto, Y.; Togashi, K.; Yamaguchi, A.; Hanaoka, H.; Saji, H., *Bioorganic & Medicinal Chemistry* **2018**, 26 (12), 3352–3358.
- <sup>127</sup> Silakari, O., *Key Heterocycle Cores for Designing Multitargeting Molecules*, 1<sup>st</sup> edition Elsevier, **2018**, Chapter 8, 285–321.
- <sup>128</sup> Roeda, D.; Tavitian, B.; Coulon, C.; David, F.; Dollé, F.; Fuseau, C.; Jobert, A.; Crouzel, C., *Bioorganic & Medicinal Chemistry* **1997**, 5 (2), 397–403.
- <sup>129</sup> Ben-Daniel, R.; Deuther-Conrad, W.; Scheunemann, M.; Steinbach, J.; Brust, P.; Mishani, E., *Bioorganic & Medicinal Chemistry* **2008**, 16 (12), 6364–6370.

- <sup>130</sup> Donohue, S. R.; Halldin, C.; Schou, M.; Hong, J.; Phebus, L.; Chernet, E.; Hitchcock, S. A.; Gardinier, K. M.; Ruley, K. M.; Krushinski, J. H.; Schaus, J.; Pike, V. W., *Journal of Labelled Compounds and Radiopharmaceuticals* **2008**, 51 (3), 146–152.
- <sup>131</sup> Finnema, S. J.; Donohue, S. R.; Zoghbi, S. S.; Brown, A. K.; Gulyás, B.; Innis, R. B.; Halldin, C.; Pike, V. W., *Synapse* **2009**, 63 (1), 22–30.
- <sup>132</sup> Willis, P. G.; Pavlova, O. A.; Chefer, S. I.; Vaupel, D. B.; Mukhin, A. G.; Horti, A. G., *Journal of Medicinal Chemistry* **2005**, 48 (18), 5813–5822.
- <sup>133</sup> Tietze, R.; Hocke, C.; Löber, S.; Hübner, H.; Kuwert, T.; Gmeiner, P.; Prante, O., *Journal of Labelled Compounds and Radiopharmaceuticals* **2006**, 49 (1), 55–70.
- <sup>134</sup> Qu, W.; Choi, S. R.; Hou, C.; Zhuang, Z.; Oya, S.; Zhang, W.; Kung, M. P.; Manchandra, R.; Skovronsky, D. M.; Kung, H. F., *Bioorganic & Medicinal Chemistry Letters* **2008**, 18 (17), 4823–4827.
- <sup>135</sup> Thominaux, C.; Damont, A.; Kuhnast, B.; Demphel, S.; Le Helleix, S.; Boisnard, S.; Rivron, L.; Chauveau, F.; Boutin, H.; Van Camp, N.; Boisgard, R.; Roy, S.; Allen, J.; Rooney, T.; Benavides, J.; Hantraye, P.; Tavitian, B.; Dollé, F., *Journal of Labelled Compounds and Radiopharmaceuticals* **2010**, 53 (13), 767–773.
- <sup>136</sup> Gao, Y.; Ravert, H. T.; Valentine, H.; Scheffel, U.; Finley, P.; Wong, D. F.; Dannals, R. F.; Horti, A. G., *Bioorganic & Medicinal Chemistry* **2012**, 20 (12), 3698–3702.
- <sup>137</sup> Bauman, A.; Piel, M.; Höhnemann, S.; Krauss, A.; Jansen, M.; Solbach, C.; Dannhardt, G.; Rösch, F., *Journal of Labelled Compounds and Radiopharmaceuticals* **2011**, 54 (10), 645–656.
- <sup>138</sup> Fisher, M. J.; McMurray, L.; Lu, S.; Morse, C. L.; Liow, J.-S.; Zoghbi, S. S.; Kowalski, A.; Tye, G. L.; Innis, R. B.; Aigbirhio, F. I.; Pike, V. W., *ChemMedChem* **2018**, 13 (2), 138–146.
- <sup>139</sup> Liow, J.-S.; Morse, C. L.; Lu, S.; Frankland, M.; Tye, G. L.; Zoghbi, S. S.; Gladding, R. L.; Shaik, A. B.; Innis, R. B.; Newman, A. H.; Pike, V. W., *Molecules* **2018**, 23 (11), 2737.
- <sup>140</sup> Zeng, F.; Nye, J. A.; Voll, R. J.; Howell, L.; Goodman, M. M., *ACS Medicinal Chemistry Letters* **2018**, 9 (3), 188–192.
- <sup>141</sup> Wang, X.; Dong, F.; Miao, C.; Li, W.; Wang, M.; Gao, M.; Zheng, Q.-H.; Xu, Z., *Bioorganic & Medicinal Chemistry Letters*, **2018**, 28 (10), 1836–1841.
- <sup>142</sup> Fu, H.; Yu, L.; Cui, M.; Zhang, J.; Zhang, X.; Li, Z.; Wang, X.; Jia, J.; Yang, Y.; Yu, P.; Jia, H.; Liu, B., *Bioorganic & Medicinal Chemistry* **2013**, 21 (13), 3708–3714.
- <sup>143</sup> (a) Anpat, S.; Dabholkar, V. V.; Gulve, S.; Krishnan, K., *Journal of Chemistry and Chemical Sciences* **2018**, 8(4), 671–676; (b) Su, W.-Q.; Yang, C.; Xu, D.-Z., *Catalysis Communications* **2017**, 100, 38–42; (c) Yu, C. J.; Liu, C. J., *Molecules* **2009**, 14 (9), 3222–3228; (c) Khan, M. T. H., *Bioactive Heterocycles V, Topics in Heterocyclic Chemistry*, Vol. 11, Springer-Verlag Berlin Heidelberg, **2007**, Chapter 1, 1–61.
- <sup>144</sup> Damodiran, M.; Kumar, R. S.; Sivakumar, P. M.; Doble, M.; Perumal, P. T., *Journal of Chemical Sciences* **2009**, 121 (1), 65–73.
- <sup>145</sup> Murthy, Y. L. N.; Choppara, P.; Prasad, Y. V.; Ranjan, T. J. U., *Current Pharmaceutical Analysis* **2014**, 10 (4), 284–292.

- <sup>146</sup> (a) Patel, T.; Gaikwad, R.; Jain, K.; Ganesh, R.; Bobde, Y.; Ghosh, B.; Das, K.; Gayen, S., *Chemistry Select* **2019**, 4 (15), 4478–4482; (b) Siddappa, M. K.; Satyanarayan, N. D.; Yarbagi, K. M.; Jagadeesha, A. H., *Cogent Chemistry* **2016**, 2, Article ID: 1172542; (c) Masagalli, J. N.; Mahadevan, K. M.; Jayadevappa, H.; Harishkumar, H. N.; Ganalu, R.; Nagaraja, P., *Medicinal Chemistry Research* **2014**, 23, 2880–2889.
- <sup>147</sup> Manjunatha, K. S.; Manu, C. P.; Satyanarayan, N. D.; Vinay, K. N.; Vineetha, M. S.; Sunil More, S., *Asian Journal of Pharmaceutical and Clinical Research* **2017**, 10 (8), 83–86.
- <sup>148</sup> Canales, A., *Biophysical Techniques in Drug Discovery*, Royal Society of Chemistry, USA, **2017**, Chapter 11, 277–306.
- <sup>149</sup> Chen, X., *Molecular Imaging Probes for Cancer Research*, World Scientific, Singapore, **2012**, Chapter 14, 419–450.
- <sup>150</sup> Matarazzo, A.; Hudson, R. H. E., *Tetrahedron* **2015**, 71 (11), 1627–1657.
- <sup>151</sup> Protti, S.; Albin, A.; Viswanathan, R.; Greer, A., *Photochemistry and Photobiology* **2017**, 93 (5), 1139–1153.
- <sup>152</sup> Holt, D.; Singhal, S.; Selmic, L. E., *Veterinary Surgery* **2020**, 49 (1), 33–43.
- <sup>153</sup> Owens, E. A.; Henary, M.; El Fakhri, G.; Choi, H. S., *Accounts of Chemical Research* **2016**, 49 (9), 1731–1740.
- <sup>154</sup> Sajedi, S.; Sabet, H.; Choi, H. S., *Nanophotonics* **2019**, 8 (1), 99–116.
- <sup>155</sup> Tipirneni, K. E.; Rosenthal, E. L.; Moore, L. S.; Haskins, A. D.; Udayakumar, N.; Jani, A. H.; Carroll, W. R.; Morlandt, A. B.; Bogoyo, M.; Rao, J.; Warram, J. M., *Molecular Imaging and Biology* **2017**, 19 (5), 645–655.
- <sup>156</sup> Hong, G.; Antaris, A.; Dai, H., *Nature Biomedical Engineering* **2017**, 1, 0010.
- <sup>157</sup> (a) Dong, H.; Du, S.-R.; Zheng, X.-Y.; Lyu, G.-M.; Sun, L.-D.; Li, L.-D.; Zhang, P.-Z.; Zhang, C.; Yan, C.-H., *Chemical Reviews* **2015**, 115 (19), 10725–10815; (b) Cheng, L.; Wang, C.; Feng, L.; Yang, K.; Liu, Z., *Chemical Reviews* **2014**, 114 (21), 10869–10939.
- <sup>158</sup> (a) Gibbs, S. L., *Quantitative Imaging in Medicine and Surgery* **2012**, 2 (3), 177–187; (b) Kobayashi, H.; Ogawa, M.; Alford, R.; Choyke, P. L.; Urano, Y., *Chemical Reviews* **2010**, 110 (5), 2620–2640.
- <sup>159</sup> Jo, D.; Hyun, H., *Chonnam Medical Journal* **2017**, 53 (2), 95–102.
- <sup>160</sup> (a) van Manen, L.; Handgraaf, H. J. M.; Diana, M.; Dijkstra, J.; Ishizawa, T.; Vahrmeijer, A. L.; Mieog, J. S. D., *Journal of Surgical Oncology* **2018**, 118 (2), 283–300; (b) van der Vorst, J. R.; Schaafsma, B. E.; Verbeek, F. P.; Swijnenburg, R. J.; Tummers, Q. R.; Hutteman, M.; Hamming, J. F.; Kievit, J.; Frangioni, J. V.; van de Velde, C. J.; Vahrmeijer, A. L., *Head Neck* **2014**, 36 (6), 853–858; (c) Cousins, A.; Thompson, S. K.; Wedding, A. B.; Thierry, B., *Biotechnology Advances* **2014**, 32 (2), 269–279; (d) Morita, Y.; Sakaguchi, T.; Unno, N.; Shibasaki, Y.; Suzuki, A.; Fukumoto, K.; Inaba, K.; Baba, S.; Takehara, Y.; Suzuki, S.; Konno, H., *International Journal of Clinical Oncology* **2013**, 18 (2), 232–241; (e) Peloso, A.; Franchi, E.; Canepa, M. C.; Barbieri, L.; Briani, L.; Ferrario, J.; Bianco, C.; Quaretti, P.; Brugnattelli, S.; Dionigi, P.; Maestri, M., *HPB* **2013**, 15 (12),

- 928–934; (f) Winer, J. H.; Choi, H. S.; Gibbs-Strauss, S. L.; Ashitate, Y.; Colson, Y. L.; Frangioni, J. V., *Annals of Surgical Oncology* **2010**, 17, 1094–1100.
- <sup>161</sup> (a) Sajedi, S.; Sabet, H.; Choi, H. S., *Nanophotonics* **2019**, 8 (1), 99–116; (b) Schols, R. M.; Connell, N. J.; Stassen, L. P. S., *World Journal of Surgery* **2015**, 39, 1069–1079.
- <sup>162</sup> Bae, P. K.; Jung, J.; Chung, B. H., *Nano Convergence* **2014**, 1 (1), 6.
- <sup>163</sup> Kirchherr, A. K.; Briel, A.; Mäder, K., *Molecular Pharmaceutics* **2009**, 6 (2), 480–491.
- <sup>164</sup> Singh, N.; Kumar, P.; Riaz, U., *Spectrochimica Acta Part A: Molecular and Biomolecular Spectroscopy* **2019**, 222, 117279.
- <sup>165</sup> Zhang, R. R.; Schroeder, A. B.; Grudzinski, J. J.; Rosenthal, E. L.; Warram, J. M.; Pinchuk, A. N.; Eliceiri, K. W.; Kuo, J. S.; Weichert, J. P., *Nature Reviews Clinical Oncology* **2017**, 14 (6), 347–364.
- <sup>166</sup> Ashitate, Y.; Levitz, A.; Park, M. H.; Hyun, H.; Venugopal, V.; Park, G.; El Fakhri, G.; Henary, M.; Gioux, S.; Frangioni, J. V.; Choi, H. S., *Chemical Communications (Camb)* **2016**, 52 (67), 10305–10308.
- <sup>167</sup> Mantareva, V.; Petrova, D.; Avramov, L.; Angelov, I.; Borisova, E.; Peeva, M.; Wöhrle, D., *Journal of Porphyrins and Phthalocyanines* **2005**, 09 (01), 47–53.
- <sup>168</sup> Lv, F.; He, X.; Lu, L.; Wu, L.; Liu, T., *Journal of Porphyrins and Phthalocyanines* **2012**, 16 (01), 77–84.
- <sup>169</sup> Lv, F.; He, X.; Wu, L.; Liu, T., *Bioorganic & Medicinal Chemistry Letters* **2013**, 23 (6), 1878–1882.
- <sup>170</sup> Lu, L.; Lv, F.; Cao, B.; He, X.; Liu, T., *Molecules* **2014**, 19 (1), 525–537.
- <sup>171</sup> Li, K.; Dong, W.; Liu, Q.; Lv, G.; Xie, M.; Sun, X.; Qiu, L.; Lin, J., *Journal of Photochemistry & Photobiology, B: Biology* **2019**, 190, 1–7.
- <sup>172</sup> Yu, L.; Wang, Q.; Wong, R. C.-H.; Zhao, S.; Ng, D. K. P.; Lo, P.-C., *Dyes and Pigments* **2019**, 163, 197–203.
- <sup>173</sup> Topal, S. Z.; İşci, Ü.; Kumru, U.; Atilla, D.; Gürek, A. G.; Hirel, C.; Durmuş, M.; Tommasino, J. B.; Luneau, D.; Berber, S.; Dumoulin, F.; Ahsen, V., *Dalton Transactions* **2014**, 43 (18), 6897–6908.
- <sup>174</sup> (a) Sekkat, N.; van den Bergh, H.; Nyokong, T.; Lange, N., *Molecules* **2012**, 17 (1), 98–144; (b) Nyokong, T.; Isago, H., *Journal of Porphyrins and Phthalocyanines* **2004**, 08 (09), 1083–1090.
- <sup>175</sup> (a) Kim, S. H.; Namgoong, J. W.; Yuk, S. B.; Kim, J. Y.; Lee, W.; Yoon, C.; Kim, J. P., *Journal of Inclusion Phenomena and Macrocyclic Chemistry* **2015**, 82 (1-2), 195–202; (b) Bıyıklioğlu, Z.; Acar, I., *Synthetic Metals* **2012**, 162 (13–14), 1156–1163; (c) Yanık, H.; Aydın, D.; Durmuş, M.; Ahsen, V., *Journal of Photochemistry and Photobiology A: Chemistry* **2009**, 206 (1), 18–26.
- <sup>176</sup> (a) Köksoy, B.; Durmuş, M.; Bulut, M., *Journal of Luminescence* **2015**, 161, 95–102; (b) Durmuş, M.; Nyokong, T., *Polyhedron* **2007**, 26 (13), 3323–3335.
- <sup>177</sup> (a) Turkmen, A. T.; Zeng, L.; Cui, Y.; Fidan, İ.; Dumoulin, F.; Hirel, C.; Zorlu, Y.; Ahsen, V.; Chernonosov, A. A.; Chumakov, Y.; Kadish, K. M.; Gürek, A. G.; Öztürk, S. T., *Inorganic Chemistry* **2018**, 57 (11), 6456–6465; (b) Cidlina, A.; Pausimova, Z.; Miletin, Miroslav, M.;

---

Zimcik, P.; Novakova, V., *Journal of Porphyrins and Phthalocyanines* **2015**, 19 (10), 1095–1106; (c) Machacek, M.; Cidlina, A.; Novakova, V.; Svec, J.; Rudolf, E.; Miletin, M.; Kučera, R.; Simunek, T.; Zimcik, P., *Journal of Medicinal Chemistry* **2015**, 58 (4), 1736–1749; (d) Cook, M. J.; Chambrier, I., *Journal of Porphyrins and Phthalocyanines* **2011**, 15 (03), 149–173.

<sup>178</sup> (a) Safonova, E. A.; Meshkov, I. N.; Polovkova, M. A.; Volostnykh, M. V.; Tsivadzea, A. Y.; Gorbunova, Y. G., *Mendeleev Communications* **2018**, 28 (3), 275–277; (b) Zorlu, Y.; Dumoulin, F.; Durmus, M.; Ahsen, V., *Tetrahedron* **2010**, 66, 3248–3258; (c) Durmuş, M.; Ayhan, M. M.; Gürek, A. G.; Ahsen, V., *Dyes and Pigments* **2008**, 77 (3), 570–577.

<sup>179</sup> (a) Sakamoto, K.; Sakaguchi, Y.; Watabiki, S.; Igarashi, Y.; Komoriya, T.; Yoshino, S., *Journal of Medicinal Chemical Sciences* **2019**, 2, 64–70.

<sup>180</sup> (a) Tekdaş, D. A.; Kumru, U.; Gürek, A. G.; Durmuş, M.; Ahsen, V.; Dumoulin, F., *Tetrahedron Letters* **2012**, 53 (39), 5227–5230; (b) Burnham, P. M.; Cook, M. J.; Gerrard, L. A.; Heeney, M. J.; Hughes, D. L., *Chemical Communications* **2003**, 16, 2064–2065.

## CHAPTER 2

---

### *Development of $^{64}\text{Cu}$ -labelled phthalocyanines as potential probes for application in cancer PET imaging*

---

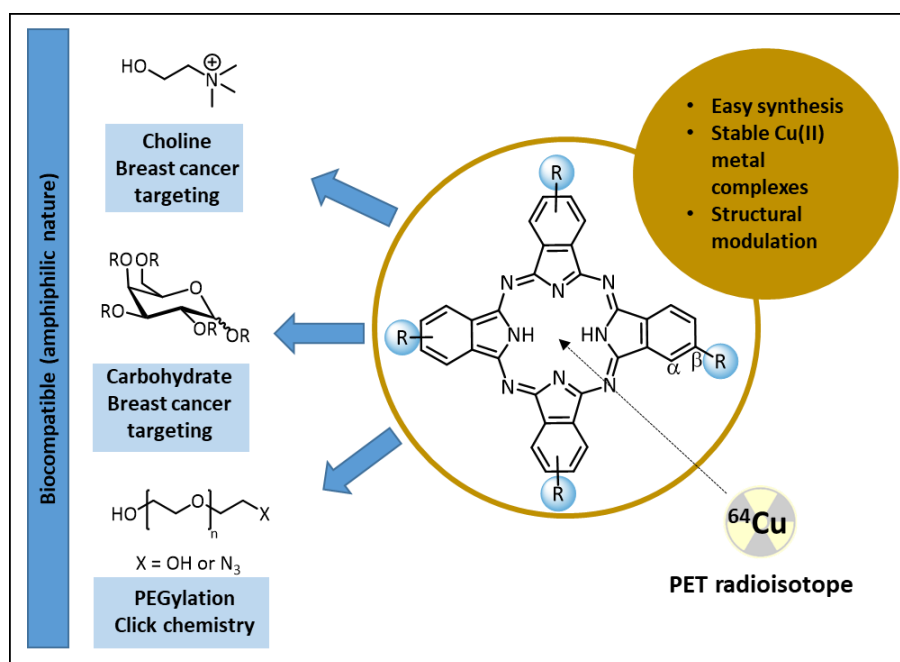
#### 2.1 Introduction

The main goal of the studies described in this chapter is centered on the synthesis and characterization of a family of biocompatible metal-free phthalocyanines, suitably functionalized with selected cancer-targeting moieties, for the development of  $^{64}\text{Cu}$ -labelled phthalocyanines as potential PET probes for early cancer diagnosis (**Scheme 2.1**).

As previously mentioned in Chapter 1, phthalocyanines are excellent coordination scaffolds for radiolabelling with copper-64 ( $^{64}\text{Cu}$ ), due to the straightforward formation of highly stable copper(II) metal complexes.<sup>1</sup> In addition, phthalocyanines are macrocycles that can be easily prepared and structurally modulated to provide the desired biological and targeting properties.<sup>2-6</sup>

Thus, aiming the development of new PET imaging probes with increased specificity for cancer cells, we envisaged the synthesis of biocompatible tetra-substituted phthalocyanine derivatives bearing choline or carbohydrate moieties at  $\beta$ -positions, since it is known that cancer cells have increased levels of carbohydrates (e.g. glucose and galactose)<sup>7,8</sup> and choline<sup>9,10</sup> uptake (**Scheme 2.1**). In addition, to modulate the PET imaging probes' amphiphilicity and prolong blood circulating lifetime, we also prepared PEGylated phthalocyanines (PEG = polyethylene glycol).<sup>11,12</sup> Particularly, the azido-polyethylene glycol phthalocyanines are potential synthons for

development of *in vitro/in vivo* PET imaging click-chemistry with valuable target molecules as specific cancer reporters (**Scheme 2.1**).<sup>13-16</sup>



**Scheme 2.1.** Design of  $^{64}\text{Cu}$ -labelled phthalocyanines suitably functionalized with biocompatible and/or cancer-targeting groups as potential PET probes.

As said before, since structural post-modulation of phthalocyanines is a challenging task, we started these studies by appropriately modulating phthalonitrile's structures. Then, we describe the reactions leading to the synthesis of the corresponding metal-free phthalocyanines, followed by the synthesis of the non-radioactive copper(II) phthalocyanine complexes reference standards. Finally, the studies were extended to the  $^{64}\text{Cu}$ -labelling experiments, along with the *in vivo* PET imaging and biodistribution studies of selected compounds.

## 2.2 Synthesis and structural modulation of phthalonitriles

As previously stated, aiming the preparation of tetra-substituted phthalocyanines containing the desired targeting groups at peripheral ( $\beta$ ) positions, these studies started with the synthesis of the corresponding mono-substituted



phthalonitriles. We selected 4-nitrophthalonitrile **2.1** as starting material due to its commercial availability and reactivity for the type of reaction chosen to structurally modulate the phthalonitriles (aromatic nucleophilic substitution). Four different alcohols have been used as *O*-nucleophiles, in order to obtain the desired 4-substituted phthalonitriles: *N,N*-dimethylaminoethanol **2.2a**, 1,2:3,4-di-*O*-isopropylidene- $\alpha$ -*D*-galactopyranose **2.2b**, polydisperse polyethylene glycol group **2.2c** (average molecular weight of 200 g.mol<sup>-1</sup>; 3.1 average repeating ethylene oxide subunits) and tetraethylene glycol **2.2d** (4 repeating ethylene oxide subunits) (**Table 2.1**).

In a typical experiment, 4-nitrophthalonitrile **2.1** was dissolved in *N,N*-dimethylformamide (DMF) and, after addition of an excess of potassium carbonate (K<sub>2</sub>CO<sub>3</sub>) and the selected nucleophiles **2.2a-d**, the reaction was kept at room temperature with magnetic stirring (**Table 2.1**). In each case, the reaction's progress was followed by TLC analysis of samples taken from the reaction mixture. After complete conversion of 4-nitrophthalonitrile **2.1** into to the corresponding 4-substituted phthalonitriles **2.3a-d** (lower R<sub>f</sub> values), the reaction was stopped. In order to isolate and characterize the products obtained, the reaction mixtures were subjected to work-up by standard procedures, including purification through column chromatography, using silica gel as stationary phase and mixtures of appropriated eluents (procedures described in detail in Chapter 5, section 5.3.1). After isolated and purified, the 4-substituted phthalonitriles **2.3a-d** were suitably characterized by <sup>1</sup>H and <sup>13</sup>C-NMR and mass spectrometry or Gas Chromatography-Mass Spectrometry (GC-MS). **Table 2.1** presents the reaction conditions and the isolated yields for each of the synthesized phthalonitriles.

**Table 2.1.** Reaction conditions and isolated yields of product obtained for each of the synthesized phthalonitrile **2.3a-d**.

Entry	Nucleophile	Time (h)	Product	Yield (%) <sup>a</sup>
1		96 <sup>b</sup>		83
2	<b>2.2a</b>	8 <sup>b,d</sup>	<b>2.3a</b>	81
3		72 <sup>b</sup>		77
4	<b>2.2b</b>	4 <sup>b,d</sup>	<b>2.3b</b>	79
5		24 <sup>b</sup>		39
6		10 <sup>c</sup>	<b>2.3c</b>	59
7	<b>2.2c</b>	1 <sup>c,d</sup>		61
8		24 <sup>b</sup>		42
9	<b>2.2d</b>	10 <sup>c</sup>	<b>2.3d</b>	62
10		1 <sup>c,d</sup>		60

<sup>a</sup> Isolated yield.<sup>b</sup> Reaction conditions: 5.78 mmol of 4-nitro-1,2-dicyanobenzene **2.1**, 1.2 equivalents of nucleophile, 5 equivalents of K<sub>2</sub>CO<sub>3</sub> and 30 mL of DMF.<sup>c</sup> Reaction conditions: 5.78 mmol of 4-nitro-1,2-dicyanobenzene **2.1**, 10 equivalents of nucleophile and 5 equivalents of K<sub>2</sub>CO<sub>3</sub> and 30 mL of DMF.<sup>d</sup> Reactions performed under ultrasound irradiation.

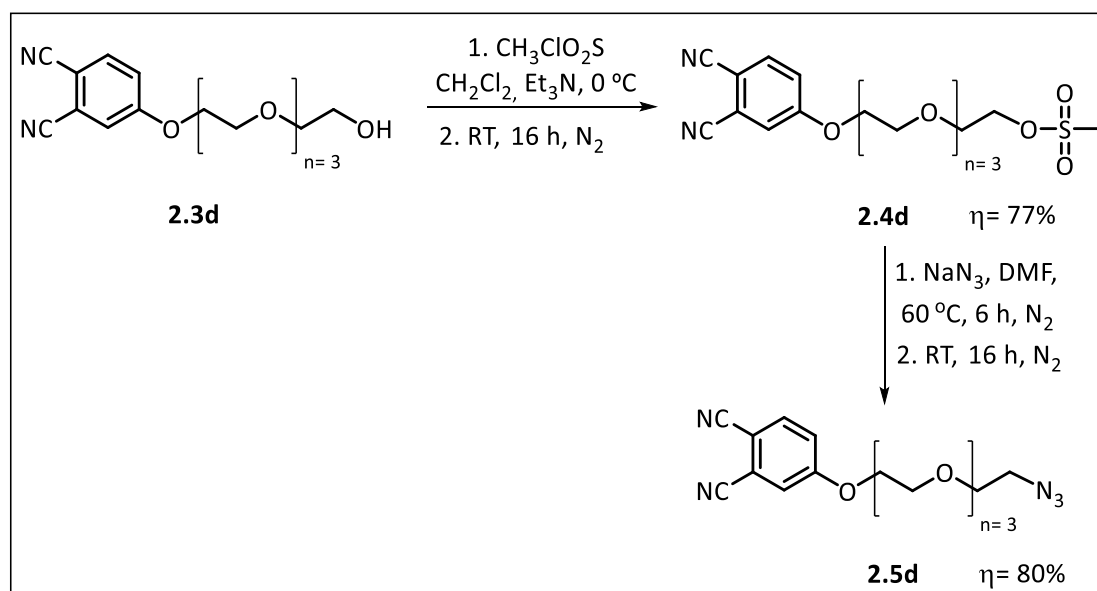
At first, *N,N*-dimethylaminoethanol **2.2a** and 1,2:3,4-di-*O*-isopropylidene- $\alpha$ -*D*-galactopyranose **2.2b** were used as nucleophiles for the synthesis of the corresponding phthalonitriles. Reaction times of 96 h and 72 h were required to obtain phthalonitriles **2.3a** and **2.3b**, in 83% and 77% isolated yields, respectively (entries 1 and 3, **Table 2.1**). Attempting to improve this classic phthalonitrile synthesis,<sup>17</sup> namely regarding the reaction time, we have replicated the reaction conditions for the preparation of phthalonitriles **2.3a** and **2.3b** but using ultrasonic irradiation.<sup>18</sup> From the results presented in **Table 2.1** (entries 2 and 4), we observed a significant reduction on the reactions times, shortened from more than 3 days to just hours, achieving similar high isolated yields ( $\approx$  80%, entries 1-4, **Table 2.1**).

The studies proceeded with the nucleophilic substitution reaction of 4-nitrophthalonitrile **2.1** using polyethylene glycol polydisperse group **2.2c** or tetraethylene glycol **2.2d** as nucleophiles. Under the reaction conditions described above, after 24 h, we obtained 39% and 42% isolated yields of the desired phthalonitriles **2.3c** and **2.3d**, respectively (entries 5 and 8, **Table 2.1**). These lower isolated yields, when compared with the ones obtained in the synthesis of phthalonitriles **2.3a** and **2.3b**, may be attributed to the formation of di-substituted product (dimer), since nucleophiles **2.2c** and **2.2d** have two reactive terminal hydroxyl groups. This was confirmed by <sup>1</sup>H-NMR spectroscopy, upon dimer isolation, by silica gel column chromatography.

Attempting to improve the yields of phthalonitriles **2.3c** and **2.3d**, we repeated the nucleophilic substitution reactions under the same reactions conditions, but using a large excess of nucleophiles **2.2c** and **2.2d** (10 equiv.). From **Table 2.1** we observe that, in both cases, reaction times decreased from 24 h to 10 h (followed by TLC), concomitantly with an increase in isolated yields (59% for **2.3c** and 62% for **2.3d**; entries 6 and 9, **Table 2.1**). This yield improvement is attributed to a significant reduction on the formation of the corresponding dimers, confirmed by TLC analysis against isolated samples. Furthermore, we also performed the same nucleophilic substitutions reactions under ultrasonic irradiation. As previously observed, a significant reduction of reaction times concomitantly with similar isolated yields were obtained ( $\approx$  60%, entries 6-7 and 9-10, **Table 2.1**). Given this results, we can conclude that this alternative sustainable phthalonitrile synthetic approach using ultrasonic irradiation is the best methodology to

prepare this type of mono-substituted phthalonitriles, allowing significant time saving which is a very important issue for potential industrial translation.

Aiming the synthesis of peripherally tetra-substituted phthalocyanine with azido-polyethylene glycol chains in their structure, the studies pursued with the synthesis of phthalonitriles bearing azido-polyethylene glycol groups, using the previously synthesized phthalonitrile **2.3d**. Therefore, we delineated the synthetic strategy presented in **Scheme 2.2**, encompassing two steps: a) introduction of a strong leaving group, such as the mesylate group and b) nucleophilic substitution of the mesylate group by sodium azide.



**Scheme 2.2** Synthetic procedure of phthalonitrile **2.5d**.

Experimentally, phthalonitrile **2.3d** was suspended in a mixture of dry dichloromethane and triethylamine and the reaction vessel was introduced in an ice cold bath, followed by slow dropwise addition of methanesulfonyl chloride, dissolved in dry dichloromethane. Once the addition was complete, the reaction mixture was allowed to warm up to room temperature and stirred for 16 h. Work-up and purification procedures were followed (described in detail in Chapter 5, section 5.3.1) and the desired compound **2.4d** was obtained in 77% isolated yield (**Scheme 2.2**). The structure of this intermediate was confirmed by  $^1\text{H}$ - and  $^{13}\text{C}$ -NMR spectroscopy (described in detail in Chapter 5, section 5.3.1). Finally, phthalonitrile **2.4d** was dissolved in dry DMF and sodium azide

(NaN<sub>3</sub>) was added, and the reaction was kept under inert atmosphere at 60 °C for 6 h, followed by room temperature for 16 h. After full conversion of the starting material **2.4d**, evaluated by TLC, the desired phthalonitrile bearing an azide moiety (**2.5d**) was purified by silica gel column chromatography, using dichloromethane first and then a mixture of dichloromethane: ethanol (100/1) as eluent. The phthalonitrile **2.5d** was obtained in 80% isolated yield (**Scheme 2.2**), and its structure was confirmed by <sup>1</sup>H-, <sup>13</sup>C-NMR and FTIR-ATR spectroscopy and MS spectrometry (described in detail in Chapter 5, section 5.3.1).

### **Phthalonitrile characterization**

All the 4-substituted phthalonitriles **2.3a-d**, **2.4d** and **2.5d** were fully characterized by suitable spectroscopic techniques, described with detail in Chapter 5, section 5.3.1. As an illustrative example, the spectroscopic characterization of phthalonitrile **2.3b** is presented and discussed. The <sup>1</sup>H-NMR spectrum of phthalonitrile **2.3b**, recorded in CDCl<sub>3</sub>, is presented in **Figure 2.1**. As expected, the three phthalonitrile's aromatic protons appear at a lower field, presenting their typical coupling patterns: at δ 7.70 ppm one doublet having a large coupling constant ( $J = 8.8$  Hz) appears, at δ 7.33 ppm there is a doublet with a smaller coupling constant ( $J = 2.6$  Hz) and at δ 7.25 ppm a doublet of doublets ( $J = 8.8$  and 2.6 Hz) appears. The signals at δ 7.70, 7.33 and 7.25 ppm are attributed to the resonances of H6, H3 and H5 protons, respectively. Among the protons of the isopropylidene protected *D*-galactose unit, the doublet at δ 5.56 ppm ( $J = 5.0$  Hz) is assigned to the resonance of the proton of the anomeric carbon H1', since this proton is connected to a carbon bearing two oxygen atoms. This signal is a doublet due to coupling to H2', which in turn appears as a doublet of doublets at δ 4.37 ppm, as confirmed by its coupling constant ( $J = 5.0$  and 2.5 Hz). This doublet of doublets shows two distinct coupling constants: one corresponds to the H1'–H2' coupling ( $J_{1',2'} = 5.0$  Hz), as previously assigned, and the other coupling constant is attributed to H2'–H3' coupling ( $J_{2',3'} = 2.5$  Hz). Proton H3', on the other hand, also displays a doublet of doublets at δ 4.67 ppm ( $J = 7.9$  and 2.5 Hz), since it couples with the signal at δ 4.31 ppm, which was assigned to H4' proton. The signal attributed to the H4' proton is a doublet of doublets ( $J = 7.9$  and 1.4 Hz) and couples with the H3' proton

( $J = 7.9$  Hz) and with the H5' proton ( $J = 1.4$  Hz). The multiplet at  $\delta$  4.25–4.16 ppm is attributed to the resonances of H5' and H6' protons. Finally, the  $^1\text{H-NMR}$  spectrum (**Figure 2.1**) shows three singlets at  $\delta$  1.54, 1.47 and 1.35 ppm, integrating for 3:3:6 protons, which correspond to the non-equivalent methyl groups of the two isopropylidene groups. The  $^1\text{H-NMR}$  spectrum of phthalonitrile **2.3b** was in agreement to that previously reported in the literature.<sup>19</sup>

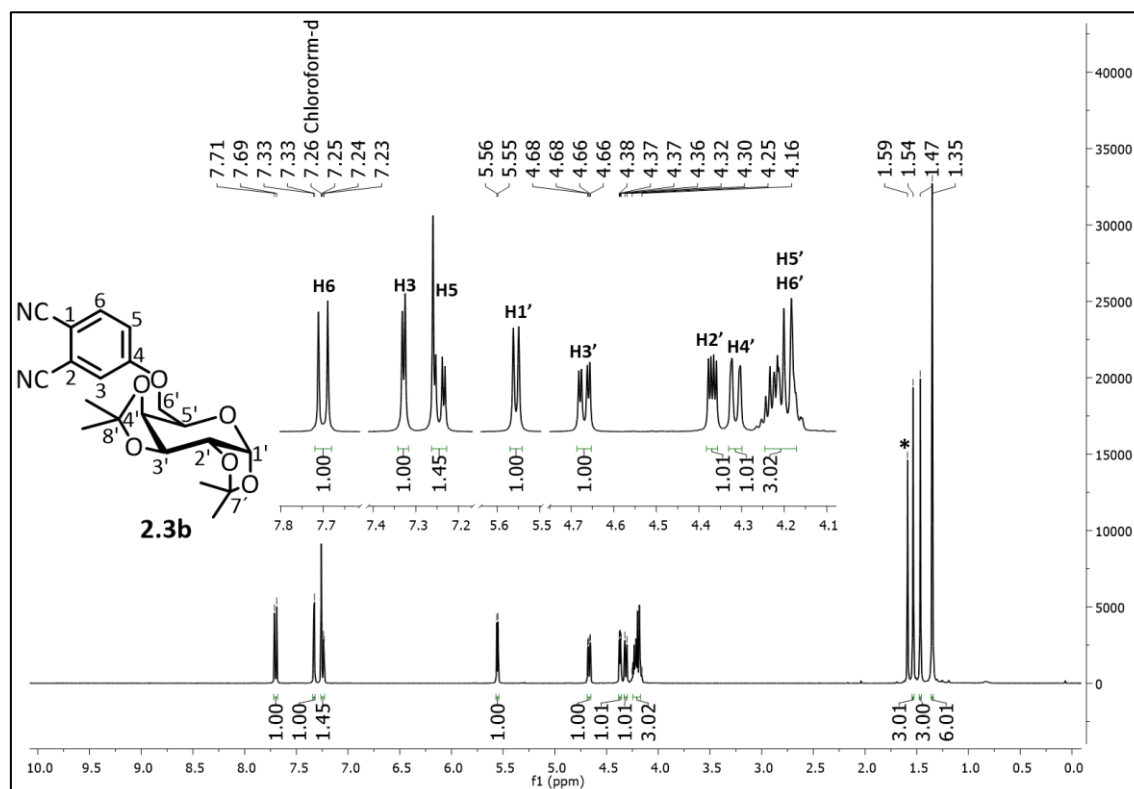


**Figure 2.1**  $^1\text{H-NMR}$  spectrum of phthalonitrile **2.3b** in  $\text{CDCl}_3$  (the residual signal marked with \* is due to the water in  $\text{CDCl}_3$  solvent). Inset: expansions of the  $^1\text{H-NMR}$  spectrum between  $\delta$  7.80 to 4.00 ppm.

The  $^{13}\text{C-NMR}$  spectrum of phthalonitrile **2.3b** in  $\text{CDCl}_3$  is presented in **Figure 2.2**. To perform the full assignment of its carbons, two-dimensional (2D) NMR experiments, namely,  $^1\text{H-}^{13}\text{C}$  HSQC (Heteronuclear Single Quantum Coherence) and  $^1\text{H-}^{13}\text{C}$  HMBC (Heteronuclear Single Quantum Coherence) NMR spectra were recorded and presented in **Figures 2.3** and **2.4**, respectively.

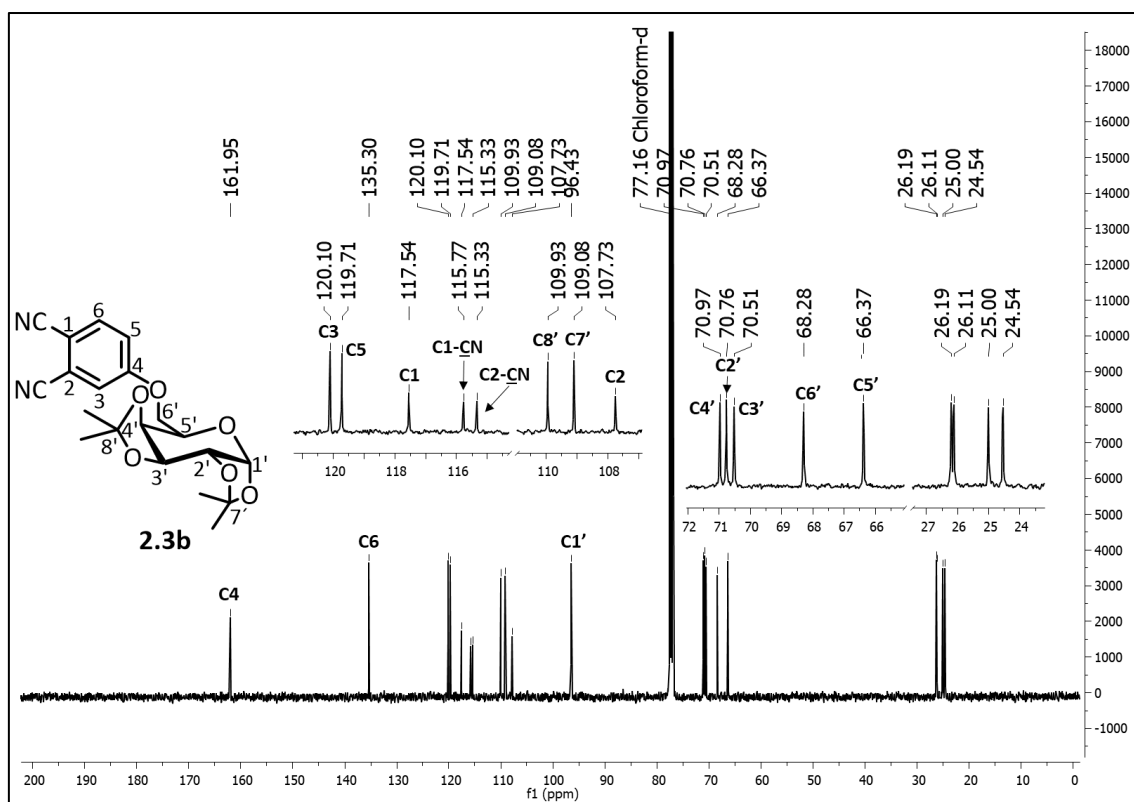


**Figure 2.2**  $^{13}\text{C}$ -NMR spectrum of phthalonitrile **2.3b** in  $\text{CDCl}_3$ .

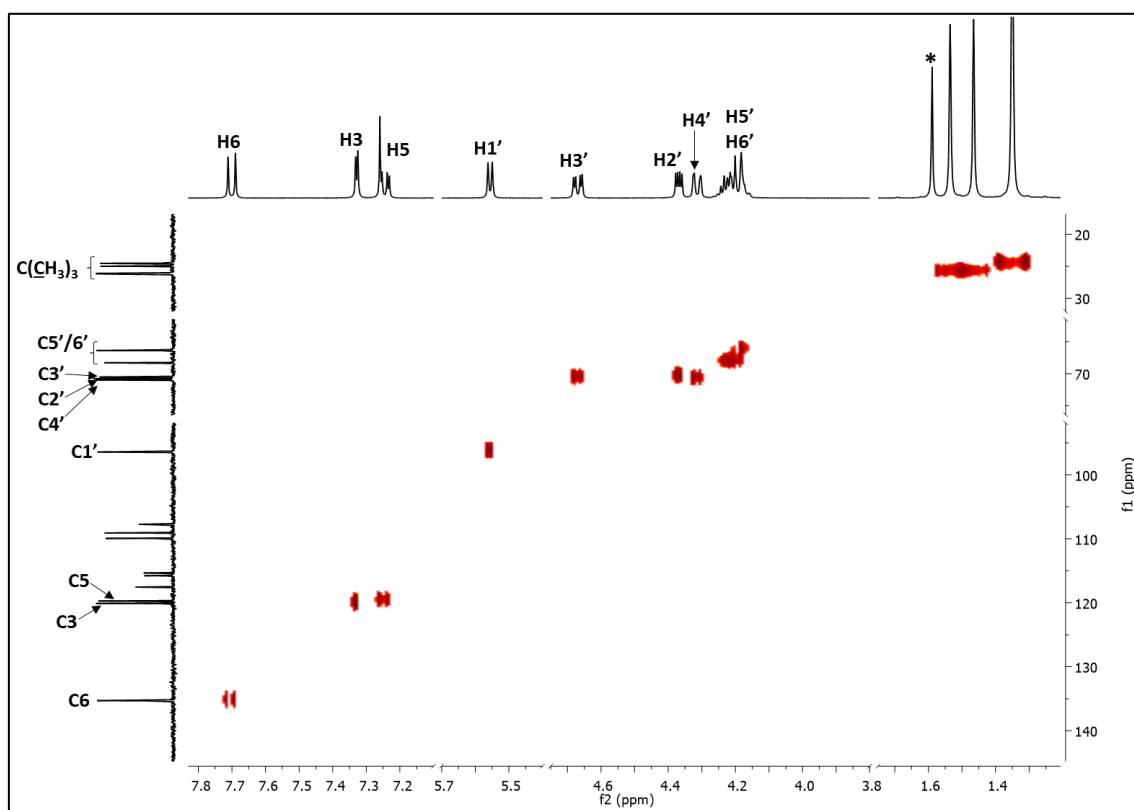


**Figure 2.3** Selected expansion of  $^1\text{H}$ - $^{13}\text{C}$  HSQC NMR spectrum of phthalonitrile **2.3b** in  $\text{CDCl}_3$  (the residual signal marked with \* is due to the water in  $\text{CDCl}_3$  solvent).

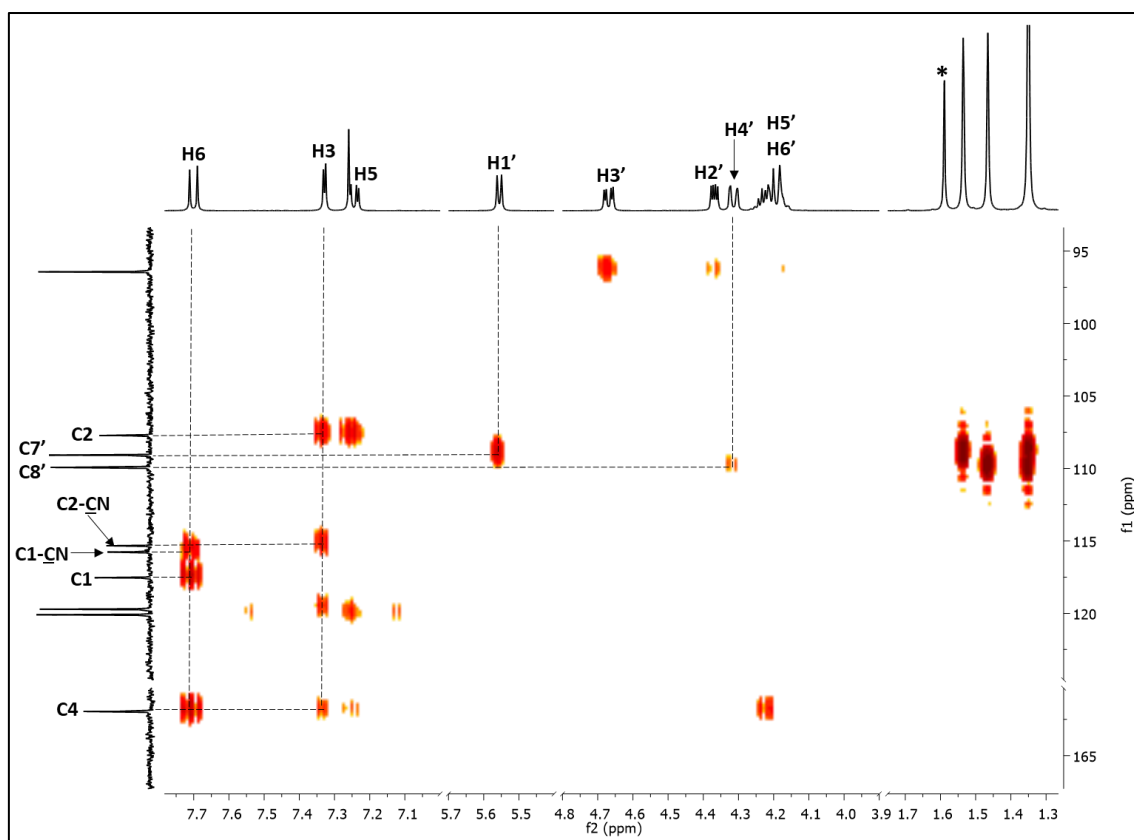


**Figure 2.4.** Selected expansion of  $^1\text{H}$ - $^{13}\text{C}$  HMBC NMR spectrum of phthalonitrile **2.3b** in  $\text{CDCl}_3$  (the residual signal marked with \* is due to the water in  $\text{CDCl}_3$  solvent). The most relevant correlations for the assignment of the quaternary carbons are presented.

The  $^{13}\text{C}$ -NMR spectrum shows one signal at  $\delta$  162.0 ppm which is characteristic of an aromatic ether and thus can be assigned to the alkyloxy substituted aromatic carbon in position C4 (also confirmed by the  $^1\text{H}$ - $^{13}\text{C}$  HMBC NMR spectrum). The aromatic carbons C6, C3 and C5 were assigned at  $\delta$  135.3, 120.1 and 119.7 ppm, respectively, as confirmed by the  $^1\text{H}$ - $^{13}\text{C}$  HSQC spectrum (**Figure 2.3**). The peaks with no correlation in the  $^{13}\text{C}$ - $^1\text{H}$  HSQC NMR spectrum at  $\delta$  117.5, 109.9, 109.1 and 107.7 ppm correspond to the quaternary carbons C1, C8', C7' and C2, respectively. These correlations were confirmed by the  $^1\text{H}$ - $^{13}\text{C}$  HMBC NMR spectrum (**Figure 2.4**). The two close peaks at  $\delta$  115.8 ppm and  $\delta$  115.3 ppm were assigned to the carbon atoms of each nitrile group (C1-CN and C2-CN, respectively). The C1', C4', C2' and C3' carbons belonging to the



isopropylidene protected *D*-galactose unit are shown at  $\delta$  96.4, 71.0, 70.8 and 70.5 ppm, respectively, as observed in the  $^1\text{H}$ - $^{13}\text{C}$  HSQC NMR spectrum. The C5' and C6' carbons can be assigned to the signals at  $\delta$  66.4 and 68.3 ppm, respectively. Finally, the four peaks between  $\delta$  26.2–24.5 ppm were assigned to the methyl carbons atoms of the isopropylidene groups.

The structure of the phthalonitrile **2.3b** was also confirmed by GC-MS spectrometry and it was observed an ion peak at  $m/z$  386.2, which corresponds to the mass of the molecular ion  $[\text{M}]^+$  of the phthalonitrile **2.3b**.

### 2.3 Synthesis of $\beta$ -tetra-substituted phthalocyanines

As mentioned before, one of the goals of this work was the synthesis of biocompatible metal-free phthalocyanines as precursors for the desired copper(II) metallophthalocyanines, aiming further application as potential  $^{64}\text{Cu}$ -labelled PET probes. To this purpose, we based our studies in two literature described methodologies: the first, based on the *Luedtke* method,<sup>20</sup> involves the demetallation of a previously synthesized zinc(II) phthalocyanine complex with pyridine hydrochloride; the second one is based on the method developed by *Calvete* and *Hanack*,<sup>21</sup> and comprises the demetallation of a previously synthesized magnesium(II) phthalocyanine complex using trifluoroacetic acid (TFA).

Thus, the synthesis of the  $\beta$ -tetra-substituted phthalocyanines was carried out by cyclotetramerization reaction of the previously synthesized phthalonitriles **2.3a-c** and **2.5d** in high boiling point solvents, using zinc(II) or magnesium(II) metal salts as templates (**Table 2.2**). The reaction conditions details and the isolated yields obtained for each of the synthesized metallophthalocyanine complexes (**2.6a-d** and **2.7a-c**) are presented in **Table 2.2**.



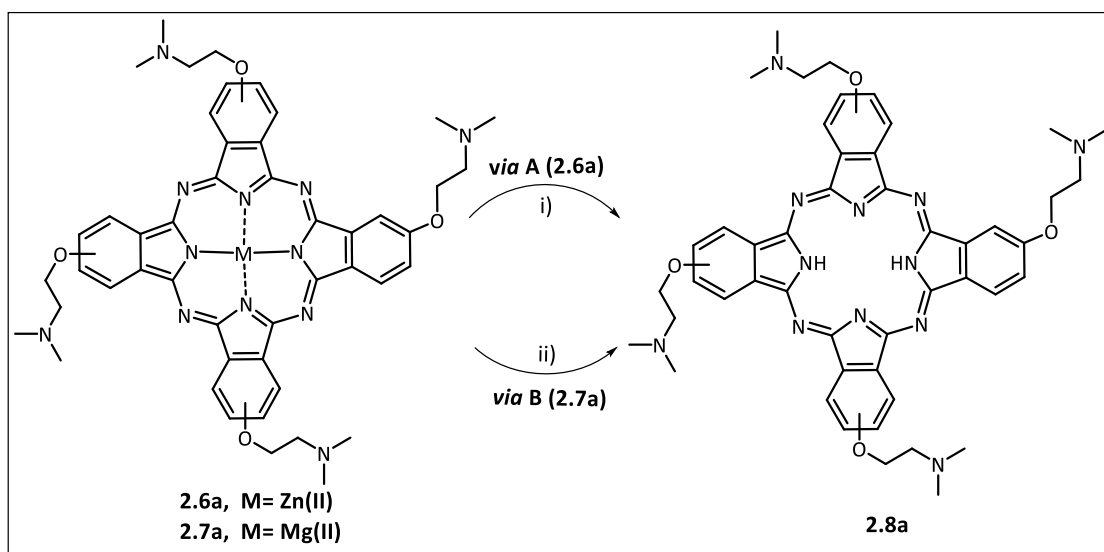
Regarding the preparation of zinc(II) metallophthalocyanine complexes **2.6a-d**, we adapted the synthetic strategy described in literature,<sup>26</sup> by promoting the cyclotetramerization reaction of the desired phthalonitriles **2.3a-c** and **2.5d** in presence of zinc acetate dihydrate ( $\text{Zn}(\text{OAc})_2 \cdot 2\text{H}_2\text{O}$ ), using *N,N*-dimethylaminoethanol/butan-1-ol (DMAE/BuOH; 2:1) mixture as solvent,<sup>26</sup> under nitrogen atmosphere, at 120 °C, for the corresponding optimized reaction times (entries 1-4, **Table 2.2**). After observing the complete conversion of phthalonitriles into the corresponding zinc(II) metallophthalocyanines products by TLC analysis (lower  $R_f$  values) and by the appearance of the typical metallophthalocyanine Q-band at around  $\approx 681\text{--}683$  nm in UV-Vis spectrum, the reactions were stopped. The crude mixtures were cooled to room temperature and, after subsequent work-up, the resulting residues were purified by column chromatography using silica gel or alumina oxide, as stationary phases, with mixtures of appropriated eluents (described in detail in Chapter 5, section 5.3.2.). Zinc(II) metallophthalocyanine complexes **2.6a**, **2.6b**, **2.6c** and **2.6d** were afforded in 60%, 63%, 65% and 52% isolated yields, respectively (**Table 2.2**). All compounds **2.6a-d** were fully characterized by  $^1\text{H-NMR}$ , UV-Vis spectroscopy and mass spectrometry, and the details are presented in Chapter 5, section 5.3.2.

This improved synthetic strategy allowed the preparation of zinc(II) metal complexes **2.6a** and **2.6b** in higher yields than those reported in literature (entries 1-2, **Table 2.2**).<sup>22-24</sup> Such high yields may be attributed to the use of a DMAE/butan-1-ol mixture as solvent, once DMAE improves reagent's solubilization while butan-1-ol induces the separation of the phthalocyanine directly from the reaction medium, facilitating the cyclotetramerization reaction and avoiding partial decomposition of the macrocycle.<sup>26</sup>

Then, the studies proceeded with the preparation of magnesium(II) phthalocyanine complexes **2.7a-c** (entries 5-7, **Table 2.2**). In a typical experiment, the magnesium bispentanoate, formed *in situ* by reaction of pentan-1-ol (PeOH) with magnesium turnings at 150 °C, was mixed with the desired phthalonitriles **2.3a-c**, using octan-1-ol (OcOH) as solvent, under nitrogen atmosphere, and heated at 160 °C (entries 5-7, **Table 2.2**). The reactions were conducted for the suitable time and, after observing the complete transformation of phthalonitriles **2.3a-c** into the corresponding magnesium(II) metallophthalocyanines complexes **2.7a-c** by TLC analysis and by the

appearance of the typical metallophthalocyanine Q-band at around  $\approx 680\text{--}682\text{ nm}$  in UV-Vis spectrum, the reactions were cooled to room temperature. In each experiment, the products were isolated by precipitation with an optimized mixture of solvents. The crude mixtures were then purified by column chromatography using silica gel or alumina oxide, as stationary phases, and mixtures of appropriate eluents (exact purification procedures are specified in Chapter 5, section 5.3.2.). The desired magnesium(II) phthalocyanine complexes **2.7a**, **2.7b** and **2.7c** were isolated in 44%, 42% and 37% yields, respectively (entries 5-7, **Table 2.2**), being fully characterized by  $^1\text{H-NMR}$ , UV-Vis spectroscopy and mass spectrometry (details are presented in Chapter 5, section 5.3.2.).

After the successful synthesis of the zinc(II) and magnesium(II) phthalocyanine complexes, we proceeded with their demetallation procedures, as described above. The zinc(II) and magnesium(II) phthalocyanines **2.6a** and **2.7a**, containing *N,N*-dimethylaminoethoxy groups in  $\beta$ -positions, were selected as model substrates (**Scheme 2.4**).



**Scheme 2.4** Demetallation procedures to obtain the metal-free phthalocyanine **2.8a**.

Reaction conditions: **via A**: i) pyridine, pyridine.HCl,  $110\text{ }^\circ\text{C}$ ,  $\text{N}_2$ , 17 h, 79%; **via B**: ii) dry THF, TFA,  $50\text{ }^\circ\text{C}$ ,  $\text{N}_2$ , 17 h, 45%.

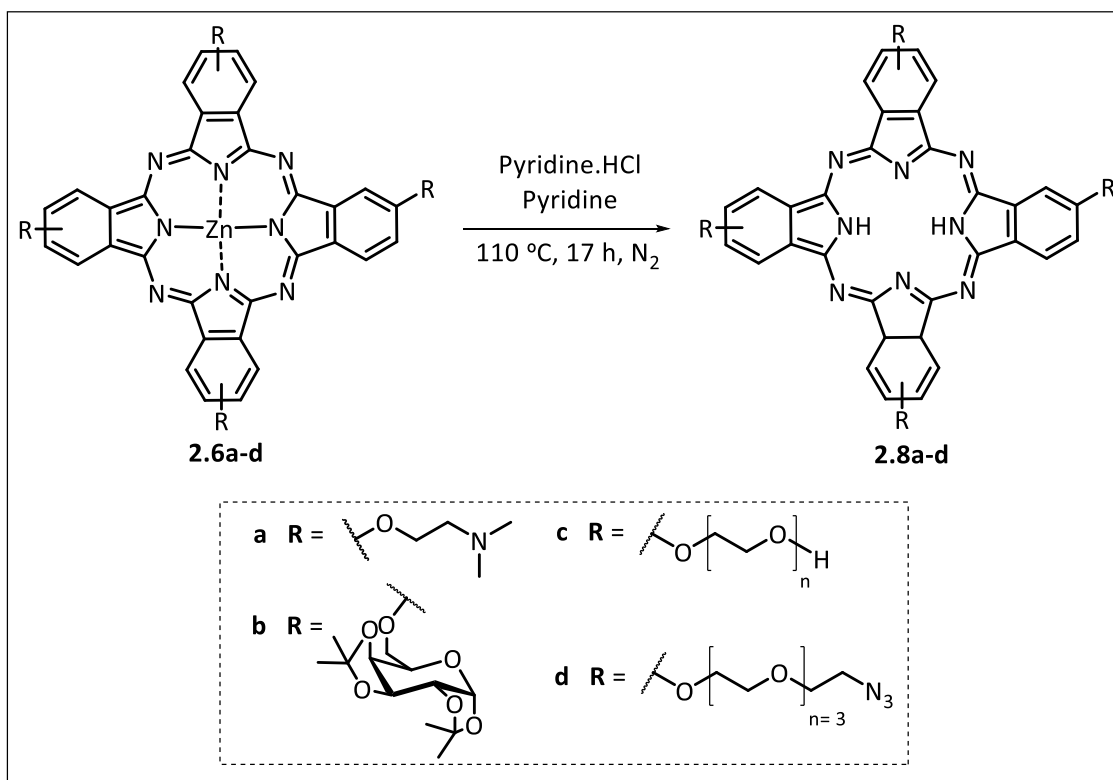
Using the first synthetic route (*via A*, **Scheme 2.4**), the zinc(II) phthalocyanine complex **2.6a** was dissolved in pyridine and pyridine hydrochloride was added. The evolution of the reaction was controlled by UV-Vis spectroscopy and, after 17 hours at

110 °C, the reaction was considered finished, after observing the appearance of the typical bands of the demetallated phthalocyanines ( $\lambda_{\text{max}} \approx 671$  and 703 nm), concomitantly with the disappearance of the single Q-band at 681 nm, typical of metallophthalocyanines. After purification procedures, the metal-free phthalocyanine **2.8a** was obtained in 79% isolated yield. Using the second synthetic approach (*via B*, **Scheme 2.4**), the magnesium(II) phthalocyanine **2.7a** was dissolved in dry THF, and TFA was slowly added. The reaction was stirred for 17 h at 50 °C and controlled by UV-Vis spectroscopy. After similar type of purification procedure as mentioned above, the demetallation reaction afforded product **2.8a** in 45% isolated yield.

The analysis of the two methods for the synthesis of metal-free phthalocyanine **2.8a** shows us that *via A* provided this phthalocyanine in 47% overall isolated yield (from the phthalonitrile), while *via B* only afforded **2.8a** in 20% overall isolated yield (from the phthalonitrile). Since the main goal of this work was the preparation of metal-free phthalocyanines for further  $^{64}\text{Cu}$ -labelling, we chose the synthetic pathway denoted as *via A*, which uses zinc metallation/demetallation route, given its suitability in obtaining significantly higher yields of metal-free phthalocyanines.

The demetallation reaction was further extended to the other previously synthesized zinc(II) metallophthalocyanines **2.6a-d**. So, in a typical experimental, zinc(II) phthalocyanine complexes **2.6a-d** were dissolved in pyridine, followed by addition of pyridine hydrochloride, and heated over a period of 17 h, at a temperature of 110 °C (entries 1-4, **Table 2.3**). When the complete demetallation was observed by UV-Vis spectroscopy, the UV-Vis spectrum showed a typical Q-band split into two intense bands corresponding to the metal-free phthalocyanines (671 and 703 nm for **2.8a**, 672 and 704 nm for **2.8b**, 672 and 704 nm for **2.8c** and 672 and 705 nm for **2.8d**). Then, each reaction mixture was subjected to the typical work-up, followed by purification through column chromatography or dialysis (in the case of PEGylated phthalocyanine **2.8c**), affording the desired metal-free phthalocyanines **2.8a-d** in isolated yields up to 85% (entries 1-4, **Table 2.3**). All compounds were suitably characterized by  $^1\text{H-NMR}$ , UV-Vis spectroscopy and mass spectrometry (details are presented in Chapter 5, section 5.3.2)

**Table 2.3.** Reactions conditions and isolated yield product for demetallation reactions and their corresponding metal-free phthalocyanines.



Entry	Metal-free phthalocyanine	Isolated yield (%)	Literature yield (%)
1	<b>2.8a</b>	79	12 <sup>22</sup>
2	<b>2.8b</b>	85	-----
3	<b>2.8c</b>	81	-----
4	<b>2.8d</b>	85	60 <sup>25</sup>

We can conclude that, independently of phthalocyanine's substituents, the use of pyridine hydrochloride method allowed us to obtain the target metal-free phthalocyanines **2.8a-d** in very high isolated yields (79–85%). Furthermore, it should be noted that the phthalocyanine **2.8a** was previously reported in 12% isolated yield (entry 1, **Table 2.3**), whose synthesis was accomplished by direct cyclotetramerization of phthalonitrile **2.3a**.<sup>22</sup> Our approach provided phthalocyanine **2.8a** in 47% overall isolated yield, in two steps (from phthalonitrile), representing a great improvement over the literature reported yield.

### Phthalocyanines characterization

All zinc(II) and magnesium(II) metallophthalocyanine complexes and their metal-free counterparts have been fully characterized by suitable spectroscopic techniques, described with detail in Chapter 5, section 5.3.2. As an illustrative example, the spectroscopic characterization of the new magnesium(II) phthalocyanine complex **2.7b** is presented and discussed. It is important to mention that the  $^1\text{H-NMR}$  spectra of the synthesized tetra-substituted phthalocyanines show, in general, complex patterns due to the presence of different positional isomers, resulting from possible combinations of the substituents on the  $\beta$ -positions of the four isoindole units of the macrocycle. The  $^1\text{H-NMR}$  spectrum of phthalocyanine **2.7b**, recorded in  $\text{DMSO-}d_6$  is presented in **Figure 2.5**.

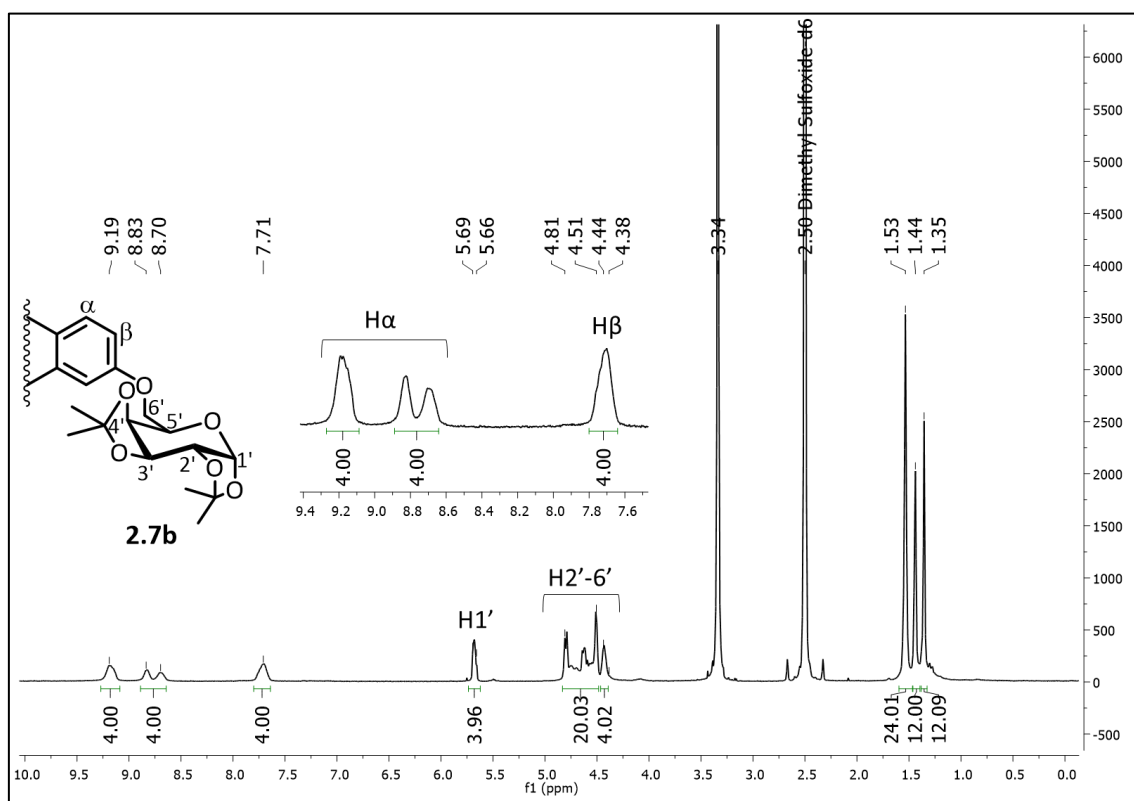


**Figure 2.5**  $^1\text{H-NMR}$  spectrum of magnesium(II) phthalocyanine complex **2.7b** in  $\text{DMSO-}d_6$  (the signal at  $\delta$  3.34 ppm is due to the presence of water in  $\text{DMSO-}d_6$  solvent).

The  $^1\text{H-NMR}$  spectrum (**Figure 2.5**) shows three singlets at  $\delta$  1.35, 1.44 and 1.53 ppm, integrating in a total of forty-eight protons, attributed to the resonances of the eight non-equivalent isopropylidene methyl groups (similarly to the  $^1\text{H-NMR}$  signals

observed in the corresponding phthalonitrile **2.3b** – section 2.2 of this chapter). The set of multiplets between  $\delta$  4.38 and 4.81 ppm can be attributed to H2'–6' *D*-galactose unit protons, integrating to twenty-four protons, while the broad signal at  $\delta$  5.68 ppm is attributed to the resonance of proton H1', integrating to four protons, due to the deshielding effect of the two electronegative oxygen atoms. Finally, the typical phthalocyanine aromatic protons appear at lower field, as broad signals at  $\delta$  7.71, 8.70–8.83 and 9.19 ppm, attributed to the resonances of the four Pc- $\beta$  protons, the four Pc- $\alpha$  protons and the other four Pc- $\alpha$  protons, respectively.

Regarding the mass spectrometry characterization, the MALDI-TOF spectrum obtained for the magnesium(II) phthalocyanine complex **2.7b** (Figure 2.6) shows an excellent agreement between the theoretical isotopic standard and the experimentally observed peak for the phthalocyanine's molecular ion  $[M]^+$ , with an isotopic distribution between 1568-1574 m/z. The peaks of higher intensities, with the values of 1568.57701 and 1569.58872 m/z correspond to the mass of the molecular ion  $[M]^+$  and  $[M+H]^+$ , respectively. The remaining peaks are related to the other isotopes. The MALDI-TOF spectrum corroborates the proposed structure for magnesium(II) phthalocyanine complex **2.7b**.

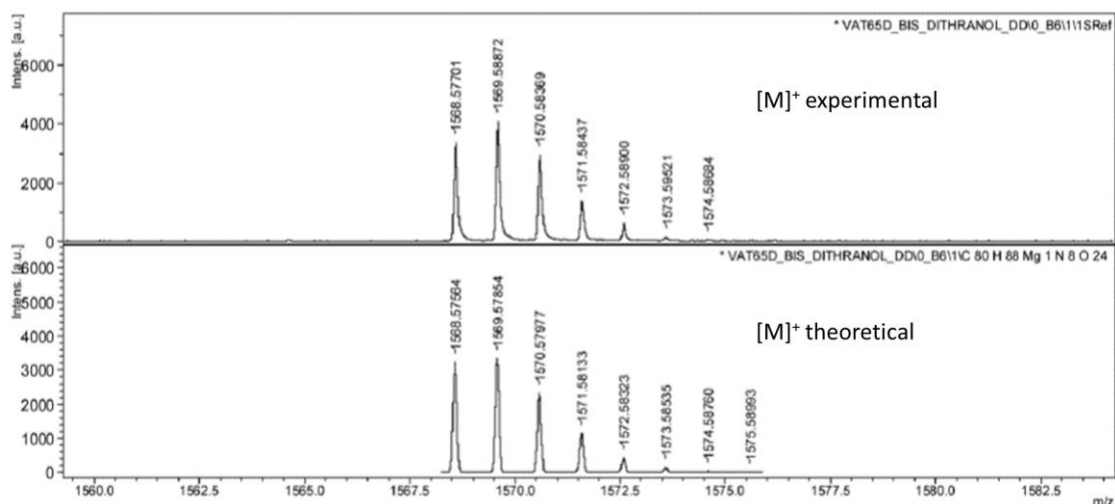
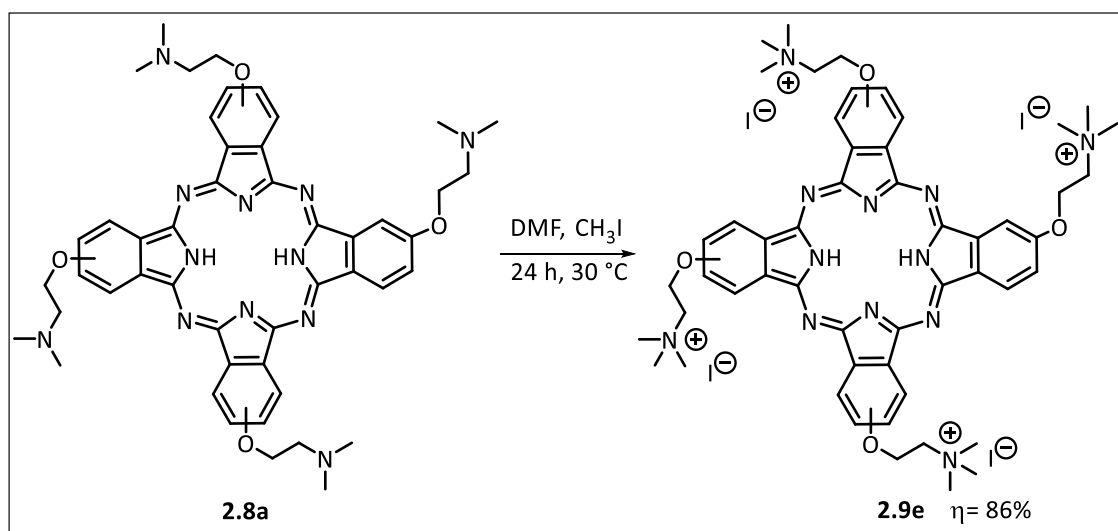


**Figure 2.6.** Observed experimentally and theoretical molecular ion  $[M]^+$ , obtained by high resolution MALDI-TOF of magnesium(II) phthalocyanine complex **2.7b**.



### 2.3.1 Synthesis of tetra-choline substituted phthalocyanine

As previously discussed, the presence of positively charged choline moieties is an important structural feature to enhance the selectivity of phthalocyanine derivatives for cancer cells.<sup>9,10</sup> Therefore, we proceeded the studies with the cationization of the *N,N*-dimethylaminoethoxy groups of phthalocyanine **2.8a** with iodomethane. Phthalocyanine **2.8a** was dissolved in DMF and a large excess of CH<sub>3</sub>I was added in portions to the reaction mixture, which remained at 30 °C for approximately 24 h, to ensure that all tertiary amino groups were methylated (**Scheme 2.5**). After reaction completion, the final product was isolated by precipitation from diethyl ether, to afford phthalocyanine **2.9e** in 86% isolated yield. The tetracationic phthalocyanine **2.9e** were fully characterized by spectroscopic means, described in experimental section (Chapter 5, section 5.3.2).



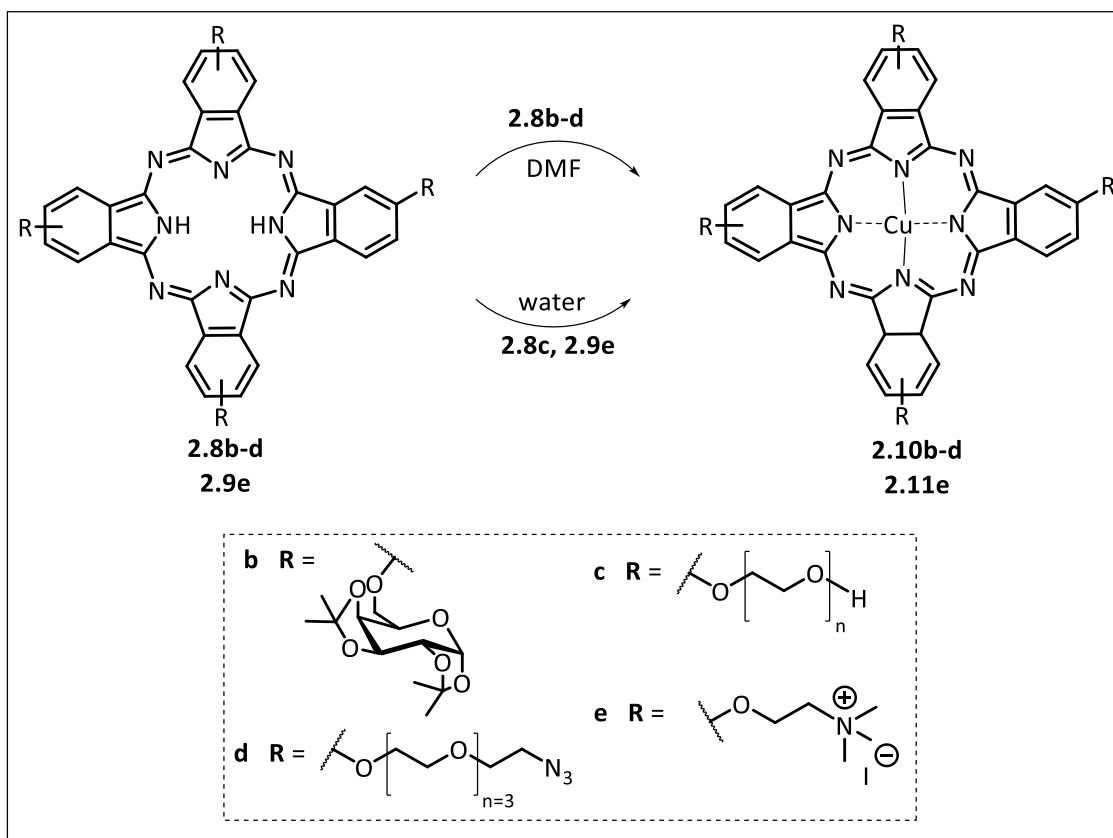
**Scheme 2.5.** Synthesis of tetra-choline substituted phthalocyanine **2.9e**.

## 2.4 Radiolabelling of phthalocyanines with copper-64

### 2.4.1 Synthesis of copper(II) metallophthalocyanines (non-radioactive synthesis)

Aiming the preparation of  $^{64}\text{Cu}$ -labelled phthalocyanines as potential probes for application in cancer PET imaging, the previously synthesized  $\beta$ -tetra-substituted metal-free phthalocyanines were complexated with non-radioactive copper(II), to serve as models for the  $^{64}\text{Cu}$ -labelling studies and also to be further used as analytical HPLC and/or Radioactive Thin Layer Chromatography (radio-TLC) non-radioactive reference standards.

In a typical experiment, the metal-free phthalocyanines **2.8b**, **2.8c**, **2.8d** and **2.9e** were dissolved in the appropriate solvent (DMF or water, according to the solubility of each phthalocyanine), and copper(II) chloride ( $\text{CuCl}_2$ ) was added (two-fold excess), leaving the reaction mixture under stirring, at 75 °C (**Table 2.4**). The reaction's progress was followed by UV-Vis spectroscopy analysis of samples taken from the reaction mixtures. After complete conversion of the metal-free phthalocyanines into to the corresponding copper(II) phthalocyanine complexes, corroborated by the appearance of the typical metallophthalocyanine Q-band at around  $\approx 678\text{--}680$  nm in UV-Vis spectrum, the reactions were stopped. The reaction conditions and the isolated yield for each synthesized copper(II) phthalocyanine complexes are presented in **Table 2.4**.

**Table 2.4.** Reaction conditions and isolated yields for metalation reaction and the corresponding copper(II) metallophthalocyanines.

Entry	Metal-free Pc	Reaction conditions	Cu(II) Pc	Yield (%) <sup>a</sup>
1	<b>2.8b</b>	CuCl <sub>2</sub> <sup>b</sup> , DMF, 75 °C, 15 min	<b>2.10b</b>	92
2	<b>2.8d</b>	CuCl <sub>2</sub> <sup>b</sup> , DMF, 75 °C, 15 min	<b>2.10d</b>	86
3	<b>2.8c</b>	CuCl <sub>2</sub> <sup>b</sup> , water, 75 °C, 15 min	<b>2.10c</b>	-----
4		CuCl <sub>2</sub> <sup>b</sup> , DMF, 75 °C, 15 min		87
5	<b>2.9e</b>	CuCl <sub>2</sub> <sup>b</sup> , water, 75 °C, 15 min	<b>2.11e</b>	94

<sup>a</sup> Isolated yield.<sup>b</sup> 2 equivalents of CuCl<sub>2</sub> were added to reaction mixture.

Regarding the preparation of copper(II) metallophthalocyanines **2.10b** and **2.10d**, we promoted the metalation reaction in DMF (entries 1-2, **Table 2.4**). The reactions were complete in just 15 min at 75 °C, as confirmed by UV-Vis spectroscopy. The reaction mixtures were subjected to standard purification procedures (details described in Chapter 5, section 5.3.2), affording the new copper(II) phthalocyanine complexes **2.10b** and **2.10d** in 92% and 86% isolated yields, respectively (entries 1-2, **Table 2.4**).

For copper(II) phthalocyanine complexes **2.10c** and **2.11e**, we performed the metalation reaction in water (entries 3 and 5, **Table 2.4**). After just 15 min of reaction at 75 °C, the new phthalocyanine complex **2.11e** was subjected to purification through dialysis, being obtained in 94% isolated yield (entry 5, **Table 2.4**). However, the rate of metalation of the metal-free phthalocyanine **2.8c**, using water as solvent, was negligible after 15 min (entry 3, **Table 2.4**). Using UV-Vis spectroscopy, we observed that the reaction proceeded very slowly (**Figure 2.6, A**), being incomplete after 1h 30 min. Even after 3 h of reaction, the presence of metal-free phthalocyanine could still be observed (**Figure 2.6, A**), reason why we stopped the reaction at this point. In view of this result, we then chose to carry out the reaction in DMF (entry 4, **Table 2.4**). After 15 min at 75 °C, we accomplished the desired copper(II) metallophthalocyanine **2.10c** (**Figure 2.6, B**) in 87% isolated yield (entry 4, **Table 2.4**), after purification through dialysis.

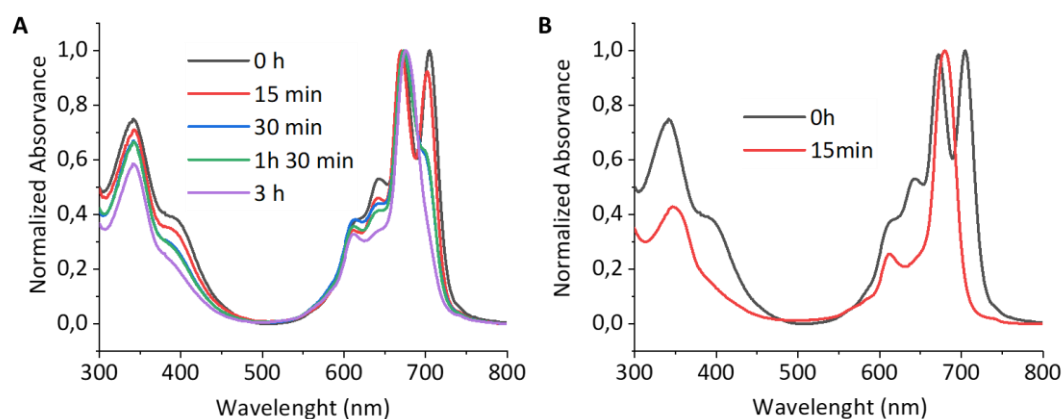


**Figure 2.6** UV-Vis spectrum, in DMF, of evolution of metalation reaction of phthalocyanine **2.8c** with  $\text{CuCl}_2$  at 75 °C in: **A** – water and **B** – DMF, as reaction solvent.

The copper(II) phthalocyanine complexes **2.10b-d** and **2.11e** were suitably characterized by mass spectrometry, elemental analysis and UV-Vis spectroscopy, with details described in Chapter 5, section 5.3.2.

In conclusion, these results suggest that the metal-free phthalocyanines developed in this work can be used as precursors for the formation of  $^{64}\text{Cu}$ -labelled phthalocyanine complexes, for further use as probes in cancer diagnosis using PET imaging.

## 2.4.2 Labelling methodology

Among the multiple nuclear reactions to produce copper-64 in a cyclotron (e.g.  $^{66}\text{Zn}(p, 2pn)^{64}\text{Cu}$ ,  $^{66}\text{Zn}(d, \alpha)^{64}\text{Cu}$ ,  $^{64}\text{Zn}(d, 2p)^{64}\text{Cu}$ ,  $^{68}\text{Zn}(p, \alpha)^{64}\text{Cu}$ ,  $^{64}\text{Ni}(d, x)^{64}\text{Cu}$  and  $^{64}\text{Ni}(p, n)^{64}\text{Cu}$ ), the  $^{64}\text{Ni}(p, n)^{64}\text{Cu}$  nuclear reaction is the usually preferred route, due to its higher production yield and easy synthesis in medical cyclotrons.<sup>27</sup> Therefore, the  $^{64}\text{Ni}(p, n)^{64}\text{Cu}$  was the selected method for copper-64 ( $^{64}\text{Cu}$ ) production for further  $^{64}\text{Cu}$ -labelling of the previously synthesized metal-free phthalocyanines. The production of copper-64 radioisotope was performed in collaboration with Radiochemistry and Cyclotron Laboratory of the Institute for Nuclear Sciences Applied to Health (ICNAS) by Dr. Vítor Alves (PhD), whose general production procedure is schematically represented in **Figure 2.7**.

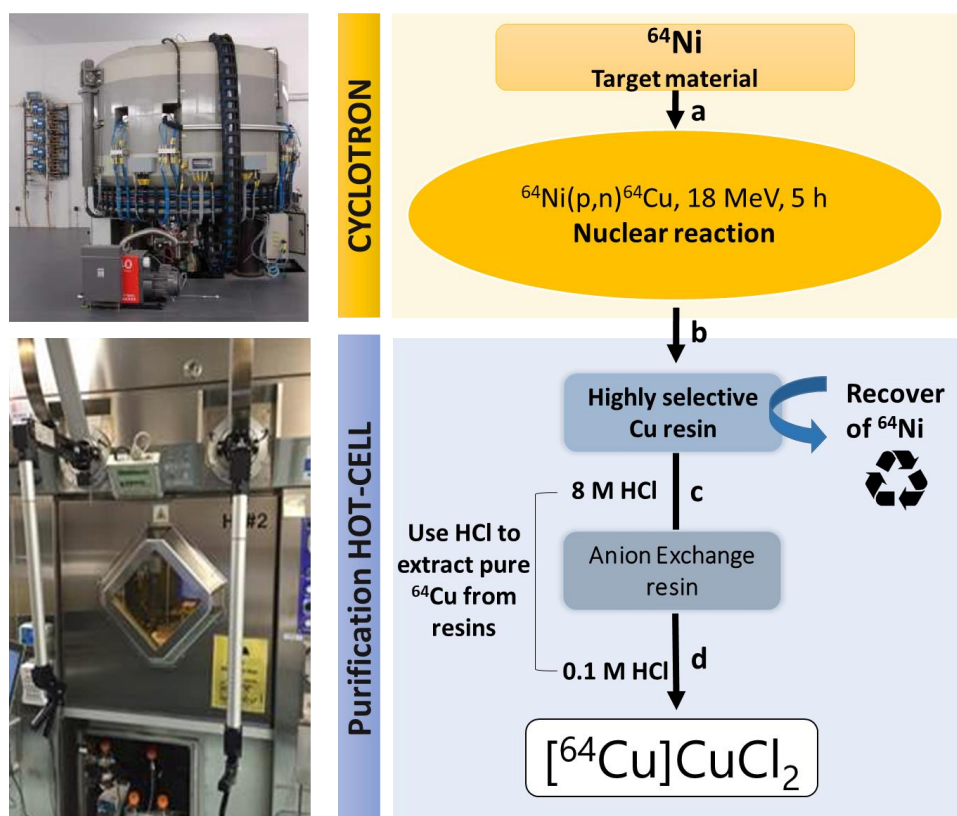


**Figure 2.7.** Schematic diagram of  $[^{64}\text{Cu}]\text{CuCl}_2$  production.<sup>27</sup>

Copper-64 production is initiated in an IBA Cyclone 18/9<sup>®</sup> cyclotron (IBA, Louvain-la-Neuve, Belgium), where an electroplated enriched nickel-64 ( $^{64}\text{Ni}$ ) target is

irradiated with a beam of protons of 18 MeV for 5 h (**Figure 2.7, a**). After the radioisotope production is finished, the  $^{64}\text{Cu}$  is transferred from the cyclotron to a so-called hot-cell (lead-shielded fume hood with thick glass windows) with remote control, to be purified (**Figure 2.7, b**). The  $^{64}\text{Cu}$  is purified using an automated Synthra® Extension module system (IBA, Louvain-la-Neuve, Belgium), housed inside the hot-cell, and it is obtained in a small volume of  $[^{64}\text{Cu}]\text{CuCl}_2$  solution. Due to the high cost of enriched  $^{64}\text{Ni}$ , recycling of this target material is a key issue for lowering the cost of  $^{64}\text{Cu}$  production. So, in the first step of  $^{64}\text{Cu}$  purification, the  $^{64}\text{Ni}$  target solution is diluted and loaded into a high selective copper resin to separate the  $^{64}\text{Cu}$  from  $^{64}\text{Ni}$ . The  $^{64}\text{Ni}$  is eluted from the resin with a 0.01 M nitric acid solution and collected for recycling (**Figure 2.7, b**). Subsequently, in the second step, the  $^{64}\text{Cu}$  is eluted from copper resin, with an 8 M HCl solution and transferred onto a strong anion exchange resin (**Figure 2.7, c**). In the last step, the anion exchange resin is eluted using a small volume of 0.1 M HCl solution in order to achieve the final  $[^{64}\text{Cu}]\text{CuCl}_2$  solution (**Figure 2.7, d**). This purification process takes about 1 h to complete. The final solution is then evaporated to dryness before starting the further  $^{64}\text{Cu}$ -labelling reaction with the desired metal-free phthalocyanines.

All labelling studies followed the required radiation protection rules and proceeded through manual technique using laboratory lead castles, since these  $^{64}\text{Cu}$ -labelling studies using phthalocyanine chelate units were in initial optimization phase and the produced  $[^{64}\text{Cu}]\text{CuCl}_2$  solution was expected to display low activity. In the  $^{64}\text{Cu}$ -labelling studies, careful optimization of the pH, temperature and reaction time parameters is essential to achieve high radiochemical yields (radiochemical yield, denoted as RCY, is defined as the amount of activity in the product expressed as the percentage (%) of related starting activity used in the corresponding process;<sup>28</sup> all RCYs presented in this thesis are non-decay corrected). Regarding the pH, the  $^{64}\text{Cu}$ -labelling of phthalocyanines was performed under pH control, using ammonium acetate buffer solutions with pH value of approximately 5.5,<sup>29</sup> in order to avoid the formation of insoluble radiochemical species such as  $[^{64}\text{Cu}]\text{Cu}(\text{OH})_2$ . Moreover, it should be noted that the selection of this buffer solution is relevant since it is considered safe for further *in vivo* injections.<sup>29</sup>

In this context, the  $^{64}\text{Cu}$ -labelling studies started with the optimization of reaction conditions regarding temperature and reaction time, being the results

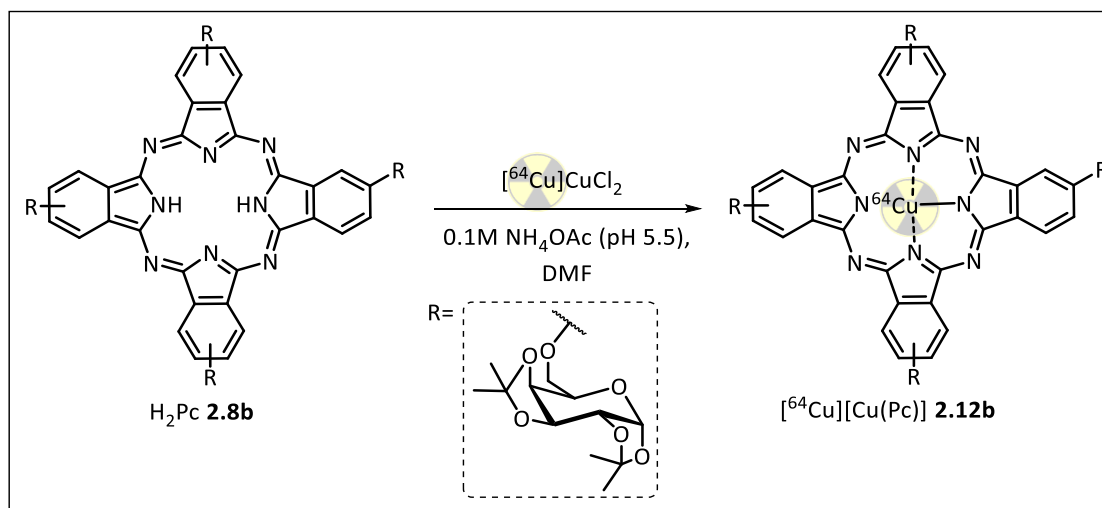
presented and discussed in the following section. Nevertheless, it is important to state that this optimization of the reaction conditions had to be performed in radioactive conditions, since the reaction kinetics differ between the radioactive labelling and the conventional organic chemistry reactions (non-radioactive synthesis).<sup>30</sup> Moreover, the [<sup>64</sup>Cu]CuCl<sub>2</sub> is only provided in picomolar quantities, whereas the chelate unit (*i.e.* metal-free phthalocyanine) is generally provided in micromolar amounts. Thus, in the <sup>64</sup>Cu-labelling reaction studies it was expected to have non-radiolabelled phthalocyanine (*i.e.* metal-free phthalocyanine) in all the <sup>64</sup>Cu-labelled phthalocyanine complexes final solution.

### 2.4.3 Labelling of phthalocyanines with [<sup>64</sup>Cu]copper dichloride (radioactive synthesis)

The <sup>64</sup>Cu-labelling studies were performed with selected  $\beta$ -tetra-substituted metal-free phthalocyanines, namely the phthalocyanines containing isopropylidene protected *D*-galactose (**2.8b**), polyethylene glycol (**2.8c**) and choline (**2.9e**) substituents. The studies were initiated with the optimization of the reaction conditions (temperature and reaction time) using the metal-free phthalocyanine **2.8b** as model. In a typical experiment, 1.8 nmol of phthalocyanine **2.8b** was added to the [<sup>64</sup>Cu]CuCl<sub>2</sub> in ammonium acetate buffer (pH $\approx$  5.5) solution, followed by the addition of DMF to prevent aggregation during the reaction, adjusting the phthalocyanine concentration in all labelling reactions to  $3.8 \times 10^{-5}$  M. The evaluation of the temperature (between 25 °C and 95 °C) and reaction time (5–60 min) effect on the radiochemical conversion (*i.e.* expressed as the percentage of the <sup>64</sup>Cu-incorporation into phthalocyanine; denoted as RCC)<sup>30</sup> was carried out and the results are presented in **Table 2.5**. The RCC was assessed by radio-TLC standard method.<sup>30</sup> At the different time points for each temperature, aliquots taken from the reaction mixtures were mixed with ethylenediaminetetraacetic acid (EDTA) solution and applied onto silica gel TLC plates (free [<sup>64</sup>Cu]CuCl<sub>2</sub> was complexed by supplementing with 10 mM EDTA for easier analysis). The TLC plates were briefly dried and developed using the conventional 10% NH<sub>4</sub>OAc/methanol (1:1) mixture as eluent.<sup>31</sup> In this chromatographic system, the <sup>64</sup>Cu-labelled phthalocyanine **2.12b**

shows a  $R_f \approx 0$  (green colored), while the “free”  $[^{64}\text{Cu}]\text{CuCl}_2$  ( $[^{64}\text{Cu}][\text{Cu}(\text{EDTA})]$ ) complex displays  $R_f \approx 1$  (pink colored), as shown in **Figure 2.6**.

**Table 2.5.** Optimization of reaction conditions for the radiosynthesis of complex  $^{64}\text{Cu}$ -labelled phthalocyanine **2.12b** (phthalocyanine concentration =  $3.8 \times 10^{-5}$  M).



Entry	Temperature (°C)	Time (min)	RCC (%) <sup>a</sup>
1	25	5	4
		10	5
		15	6
		30	6
		60	6
2	50	5	62
		10	76
		15	86
		30	90
		60	90
3	75	5	90
		10	93
		15	93
4	95	5	>99

<sup>a</sup> RCC: radiochemical conversion, estimated by radio-TLC analysis (was calculated by dividing the activity of the product spots by the total activity deposited on the silica gel TLC plate).

Setting the temperature at 25 °C and varying the reaction time (5–60 min), the reaction proceeded quite slowly, affording only 6% RCC, even after 60 min (entry 1, **Table 2.5** and **Figure 2.6**, A). Then, the temperature was raised up to 50 °C and, after 30 min 90% RCC was obtained. Attempting to obtain near-quantitative RCC the reaction



was extended to 60 min, but no RCC increase was observed (entry 2, **Table 2.5** and **Figure 2.6**, B). Further temperature increase to 75 °C resulted in a significant enhancement of RCC in shorter reaction times (reaching to 93% RCC after 10 min). Once again, when the reaction time was extended to 15 min no RCC improvement was observed (entry 3, **Table 2.5** and **Figure 2.6**, C). Finally, the  $^{64}\text{Cu}$ -labelling reaction was carried out at temperature of 95 °C, and in 5 min, a near-quantitative RCC was obtained (>99%, entry 4, **Table 2.5** and **Figure 2.6**, D).

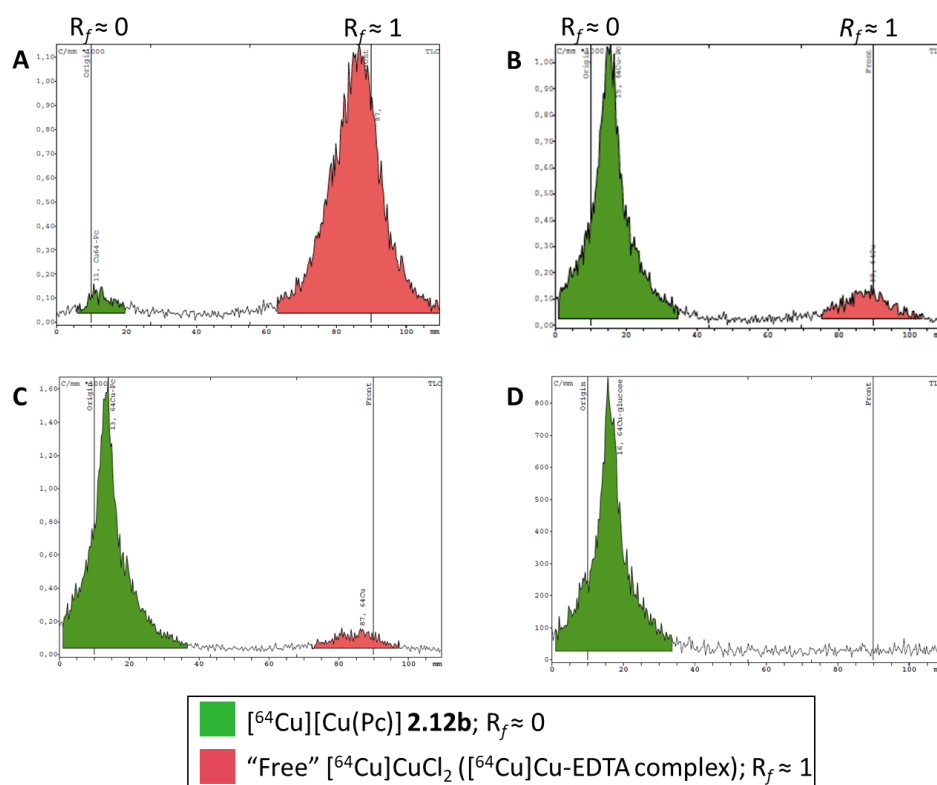


**Figure 2.6.** Radio-TLC chromatograms of the labelling reactions of phthalocyanine **2.8b** with  $^{64}\text{Cu}$   $\text{CuCl}_2$  at (A) 25 °C in 60 min, (B) 50 °C in 60 min, (C) 75 °C in 10 min e (D) 95 °C in 5 min. Vertical lines represent  $R_f$  values:  $R_f \approx 0$  (left) and  $R_f \approx 1$  (right).  $^{64}\text{Cu}$   $[\text{Cu}(\text{Pc})]$  **2.12b** displays a  $R_f \approx 0$  (green colored) and “free”  $^{64}\text{Cu}$   $\text{CuCl}_2$  (*i.e.*  $^{64}\text{Cu}$   $[\text{Cu}(\text{EDTA})]$ ) displays a  $R_f \approx 1$  (pink colored).

As shown in **Table 2.5**, it is observed that the  $^{64}\text{Cu}$ -labelling reaction proceeded at higher rates with increasing reaction temperatures. Thus, in order to achieve the maximum (near-quantitative) RCC, higher temperature (95 °C) was required in the  $^{64}\text{Cu}$ -labelling phthalocyanine reaction. This could be attributed to the well known rigidity of the phthalocyanine macrocycle, which could result in a slow kinetics

complexation with  $[^{64}\text{Cu}]\text{CuCl}_2$ , also in agreement with the results previously observed for the non-radioactive synthesis conditions for the complexation of phthalocyanine **2.8b** with  $\text{CuCl}_2$  (section 2.4.1).

Regarding the purification procedure, the  $^{64}\text{Cu}$ -labelled phthalocyanine **2.12b** was purified by solid phase extraction (SPE) using a reversed phase C18 cartridge. After placing the reaction mixture on the top of the C18 SPE cartridge, the cartridge was washed with water to remove the DMF solvent, followed by elution with methanol/THF (1:1) mixture to collect the  $^{64}\text{Cu}$ -labelled phthalocyanine **2.12b**. The radiochemical yield (*i.e.* the ratio of activity of the  $^{64}\text{Cu}$ -labelled product after its purification and its activity originally present in the corresponding purification process; non-decay corrected) was 37%. This evident difference between the RCC (>99%, entry 4, **Table 2.4**) and the non-decay corrected RCY (37%) may be attributed to a significant loss of  $^{64}\text{Cu}$ -labelled phthalocyanine **2.12b** in the transfer process between the labelling reaction vessel and C18 SPE cartridge, caused by a strong adsorption of the  $^{64}\text{Cu}$ -labelled phthalocyanine **2.12b** to the reaction vessel.

Furthermore, the radiochemical purity of the resulting  $^{64}\text{Cu}$ -labelled phthalocyanine **2.12b** was assessed by radio-TLC using the method described above (**Figure 2.7**, A and B). In **Figure 2.7**, A) just one spot ( $R_f \approx 0$ ), typical of  $^{64}\text{Cu}$ -labelled phthalocyanine **2.12b**, is shown, without evidence of the presence of “free”  $[^{64}\text{Cu}]\text{CuCl}_2$  ( $R_f \approx 1$ ), as shown in **Figure 2.7**, B). This is indicative of the high radiochemical purity in which compound **2.12b** was obtained (>98%), being on the range required for clinical human transposition.<sup>32</sup>

To assign the radiochemical identity of  $^{64}\text{Cu}$ -labelled phthalocyanine **2.12b** we used High-Performance Liquid Chromatography (HPLC), through comparison of the non-radioactive copper(II) reference standard (phthalocyanine **2.10b**) with the radioactive sample (**2.12b**). We observed that compound **2.12b** revealed extremely high affinity to the silica-based reverse-phase (RP) (C18) stationary phase (single available analytical HPLC column) when using common HPLC solvents (acetonitrile, water (buffer) and methanol). So it was not possible to elute the samples tested. Since this methodology did not allow a qualitative radiochemical identity of  $^{64}\text{Cu}$ -labelled phthalocyanine **2.12b** we then compared, by radio-TLC, the  $R_f$  value of the non-radioactive copper(II) phthalocyanine reference standard **2.10b** (**Figure 2.7**, C,

right-2) with the corresponding  $^{64}\text{Cu}$ -labelled phthalocyanine **2.12b** (Figure 2.7, C, left-1), and both chromatograms show an intense blue color in the baseline of the radio-TLC ( $R_f \approx 0$ ). This observation allowed us to indirectly assume the same radiochemical identity for both “spots” on the radio-TLC and qualitatively confirm the radiochemical identity of phthalocyanine **2.12b**.

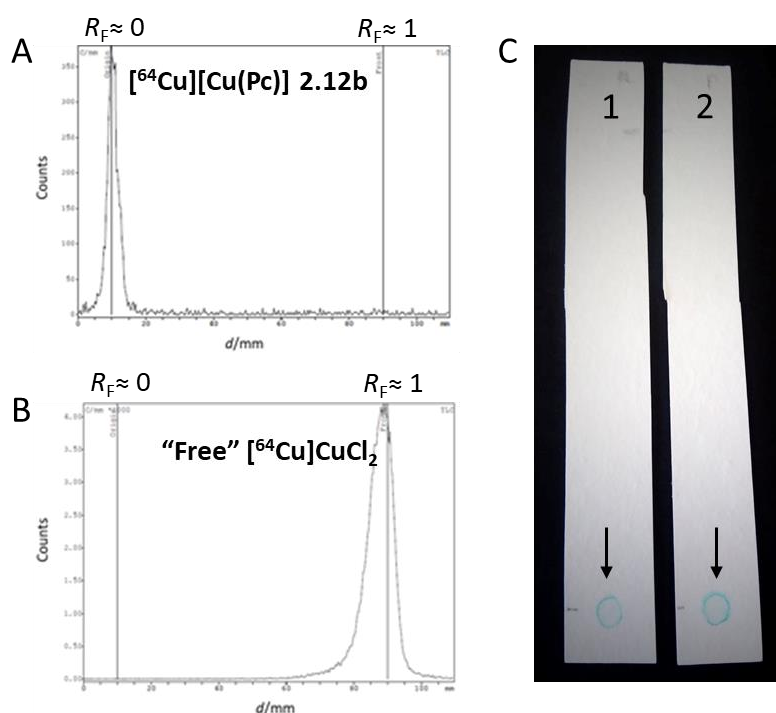


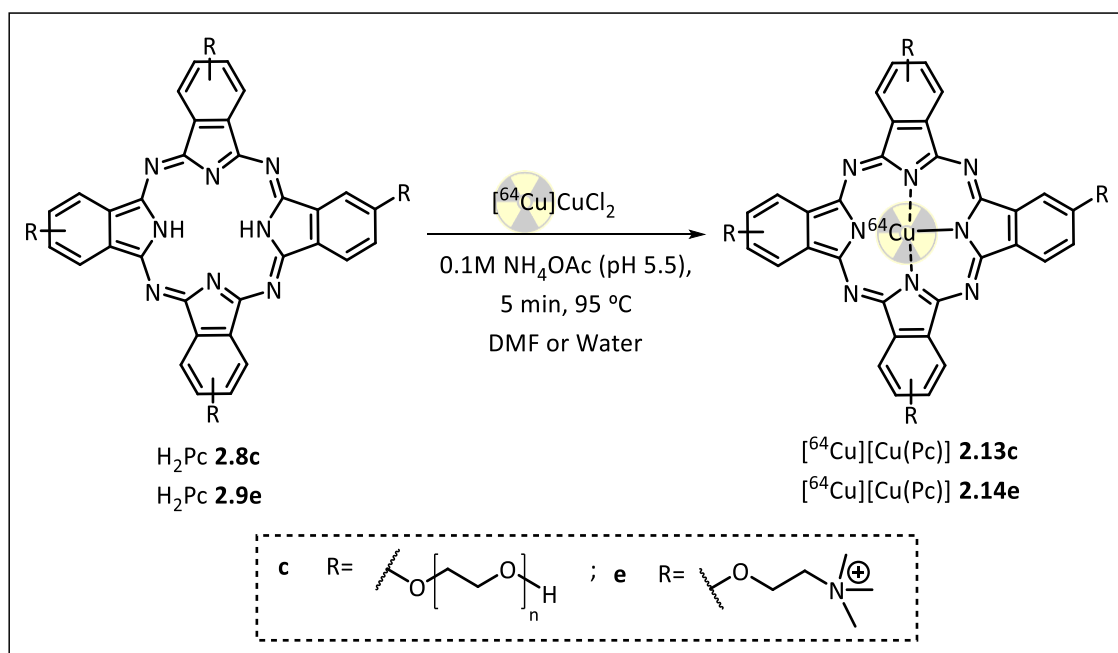
**Figure 2.7.** Radio-TLC chromatograms of **A)**  $^{64}\text{Cu}$ -labelled phthalocyanine **2.12b** ( $R_f \approx 0$ ) and **B)** “free”  $^{64}\text{Cu}$   $\text{CuCl}_2$  (*i.e.*  $^{64}\text{Cu}$   $[\text{Cu}(\text{EDTA})]$ ;  $R_f \approx 1$ ). Vertical lines represent  $R_f$  values:  $R_f \approx 0$  (left) and  $R_f \approx 1$  (right). **C)** Radio-TLC plates showing 1)  $^{64}\text{Cu}$ -labelled phthalocyanine **2.12b** at  $R_f \approx 0$  under white light and 2) non-radioactive copper(II) phthalocyanine **2.10b** reference standard at  $R_f \approx 0$  under white light. All radio-TLC plates were made of silica gel and developed with 10%  $\text{NH}_4\text{OAc}/\text{MeOH}$  (1:1).

Conclusively, we can assume that the optimal reaction conditions for preparing  $^{64}\text{Cu}$ -labelled phthalocyanine complexes from their corresponding metal-free phthalocyanines, with  $^{64}\text{Cu}$   $\text{CuCl}_2$  in 0.1M ammonium acetate buffer ( $\text{pH} \approx 5.5$ ) is using a phthalocyanine concentration =  $3.8 \times 10^{-5}$  M, a temperature of  $95^\circ\text{C}$  and 5 min of reaction. Hence, these were the selected reaction conditions to proceed with the remaining phthalocyanine  $^{64}\text{Cu}$ -labelling reaction studies.

The studies proceeded with the  $^{64}\text{Cu}$ -labelling of the remaining metal-free phthalocyanines **2.8c** and **2.9e**, under the above optimized reaction conditions, in

DMF/ammonium acetate buffer or water/ ammonium acetate buffer and the RCC results are presented in **Table 2.7**. The  $^{64}\text{Cu}$ -incorporation into phthalocyanine was again assessed by radio-TLC, using the same chromatographic method described above for the  $^{64}\text{Cu}$ -labelled phthalocyanine **2.12b**.

**Table 2.7.** Synthesis of  $^{64}\text{Cu}$ -labelled phthalocyanines **2.13c** and **2.14e** with a metal-free phthalocyanine concentration of  $3.8 \times 10^{-5}$  M, at 95 °C.



Entry	Metal-free Pc	Solvent	Time (min)	$^{64}\text{Cu}$ -labelled Pc	RCC (%) <sup>a</sup>
1	<b>2.8c</b>	DMF	5	<b>2.13c</b>	96
2		Water	5		2
			10		3
			15		30
3	<b>2.9e</b>	Water	5	<b>2.14e</b>	>99

<sup>a</sup> RCC: radiochemical conversion, estimated by radio-TLC analysis (was calculated by dividing the activity of the product spots by the total activity deposited on the TLC plate).

Regarding the  $^{64}\text{Cu}$ -labelling reaction of PEGylated phthalocyanine **2.8c**, we first carried out the reaction under optimized conditions, using DMF as reaction medium and the  $^{64}\text{Cu}$ -labelled phthalocyanine **2.13c** was obtained in a RCC of 96% (entry 1, **Table 2.7**). Given the great advantage in performing the radiolabelling reaction in water, which allows simple water evaporation after labelling in case of near quantitative RCC, the  $^{64}\text{Cu}$ -labelling reaction of **2.8c** was also performed, under the same reaction conditions,

using water (buffer) as solvent (entry 2, **Table 2.7**). This was possible because PEG substitution pattern usually confers water solubility to phthalocyanines<sup>33</sup> but, to our dismay, only 30% RCC was achieved, after 15 min of reaction (entry 2, **Table 2.7**). Nevertheless, these results are in agreement with the observations made for the non-radioactive metalation of metal-free phthalocyanine **2.8c** with CuCl<sub>2</sub> (see section 2.4.1), where the full copper(II) complexation in water was not achieved, regardless of longer reaction times.

Since the labelling reaction carried out in DMF showed a much higher RCC, in a much shorter time, we chose to use the <sup>64</sup>Cu-labelled phthalocyanine **2.13c** reaction mixture to continue the purification steps. The <sup>64</sup>Cu-labelled phthalocyanine **2.13c** was then purified using a reversed phase C18 SPE cartridge. The column was washed with water to remove the unreacted [<sup>64</sup>Cu]CuCl<sub>2</sub> and the DMF solvent, followed by elution with methanol to collect the <sup>64</sup>Cu-labelled phthalocyanine **2.13c**. The non-decay corrected RCY was 50%. Once again, the noticeable difference between the RCC (96%, entry 1, **Table 2.5**) and the non-decay-corrected RCY (50%) could be attributed to the strong adsorption of the <sup>64</sup>Cu-labelled phthalocyanine **2.13c** to the radiolabelling reaction vessel. Finally, the radiochemical purity of the resulting <sup>64</sup>Cu-labelled phthalocyanine **2.13c** was assessed by the radio-TLC method described above (**Figure 2.8**). From the results presented in **Figure 2.8**, the <sup>64</sup>Cu-labelled compound **2.13c** was obtained with radiochemical purity above 98%, again being in the acceptable range for clinical human transposition.<sup>32</sup>

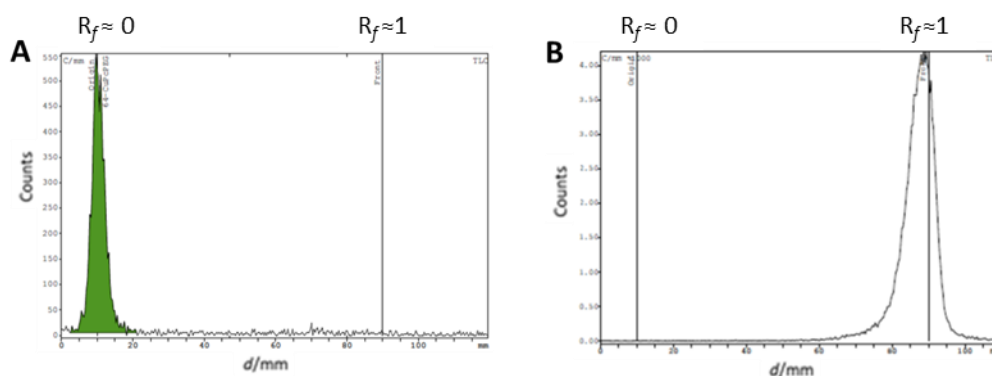


**Figure 2.8.** Radio-TLC chromatograms of **A**) <sup>64</sup>Cu-labelled phthalocyanine **2.13c** ( $R_f \approx 0$ ) and **B**) “free” [<sup>64</sup>Cu]CuCl<sub>2</sub> (*i.e.* [<sup>64</sup>Cu][Cu(EDTA)]);  $R_f \approx 1$ ). Vertical lines represent  $R_f$  values:  $R_f \approx 0$  (left, green colored) and  $R_f \approx 1$  (right). All radio-TLC plates were made of silica gel and developed in 10% NH<sub>4</sub>OAc/MeOH (1:1).

Once again, to qualitatively verify the radiochemical identity of  $^{64}\text{Cu}$ -labelled phthalocyanine **2.13c**, the non-radioactive reference standard compound **2.10c** was analyzed using the radio-TLC method, following the similar methodology as above. The same  $R_f$  was again observed for the non-radioactive reference standard and the radioactive analogue, corroborating the structure of the  $^{64}\text{Cu}$ -labelled phthalocyanine **2.13c**.

Given the previous indication of the non-radioactive copper(II) complexation reaction feasibility for metal-free phthalocyanine **2.9e** in water (see section 2.4.1), and again knowing the advantage in using water as solvent, the  $^{64}\text{Cu}$ -labelling of the metal-free phthalocyanine **2.9e** using water as reaction medium was carried out. Full  $^{64}\text{Cu}$ -complexation (near-quantitative RCC - ca 99%) was achieved for  $^{64}\text{Cu}$ -labelled phthalocyanine **2.14e**, at 95 °C in 5 min (entry 3, **Table 2.7**). This high RCC value allowed to simply evaporate the water-buffer solution used as reaction medium.

The non-decay corrected RCY was then calculated, reaching 98%. The radiochemical purity of  $^{64}\text{Cu}$ -labelled phthalocyanine **2.14e** was also assessed by radio-TLC, using the method described above (**Figure 2.9**).

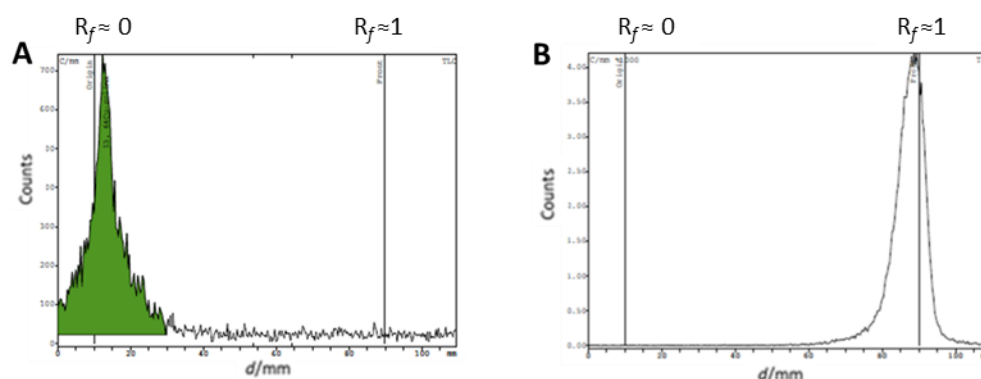


**Figure 2.9.** Radio-TLC chromatogram of **A)**  $^{64}\text{Cu}$ -labelled Pc **2.14e** ( $R_f \approx 0$ ) and **B)** “free”  $^{64}\text{Cu}$   $[\text{CuCl}_2]$  (*i.e.*  $^{64}\text{Cu}$   $[\text{Cu}(\text{EDTA})]$ ;  $R_f \approx 1$ ). Vertical lines represent  $R_f$  values:  $R_f \approx 0$  (left, green colored) and  $R_f \approx 1$  (right). All radio-TLC plates were made of silica gel and developed in 10%  $\text{NH}_4\text{OAc}/\text{MeOH}$  (1:1).

The  $^{64}\text{Cu}$ -labelled compound **2.14e** was obtained with a radiochemical purity >98%, being in the acceptable range for clinical application.<sup>32</sup> Once again, to qualitatively attest the radiochemical identity of  $^{64}\text{Cu}$ -labelled Pc **2.14e**, the non-radioactive reference standard compound **2.11e** was analyzed using the same radio-TLC method, as

previously described for the other  $^{64}\text{Cu}$ -labelled phthalocyanines, again corroborating the structure of the  $^{64}\text{Cu}$ -labelled phthalocyanine **2.14e**.

Summing up,  $^{64}\text{Cu}$ -labelled phthalocyanines **2.12b**, **2.13c** and **2.14e** were synthesized in RCCs of 96-99%. The purified  $^{64}\text{Cu}$ -labelled were isolated in non-decay corrected RCYs of 37-98%, all in excellent radiochemical purity (> 98%).

#### **2.4.4 *In vitro* radiochemical stability studies of $^{64}\text{Cu}$ -labelled phthalocyanines**

A crucial property for the development of new metal-based complexes as probes with potential PET clinical application is their *in vitro/in vivo* radiochemical stability. This is due to the possible formation of radiochemical impurities that may affect blood and tissue/organ clearance, as well as, the biological distribution and excretion pathways of the PET probe. Thus, we also performed *in vitro* radiochemical stability studies for the  $^{64}\text{Cu}$ -labelled phthalocyanine complexes **2.12b**, **2.13c** and **2.14e**, in media mimicking physiological conditions. First, each  $^{64}\text{Cu}$ -labelled phthalocyanine complex was incubated in NaCl 0.9%, PBS (0.1 M, pH 7.4), and cell medium (DMEM - Dulbecco's Modified Eagle Medium), at 37 °C. In the order to evaluate the possible presence of “free”  $^{64}\text{Cu}$  (*i.e.*  $^{64}\text{Cu}[\text{Cu}(\text{EDTA})]$ ) resulting from phthalocyanine decomplexation, aliquots were taken at different time points (0, 1, 18 and 24 h) and analyzed by the radio-TLC method described above, whose results are present in **Figure 2.10**.

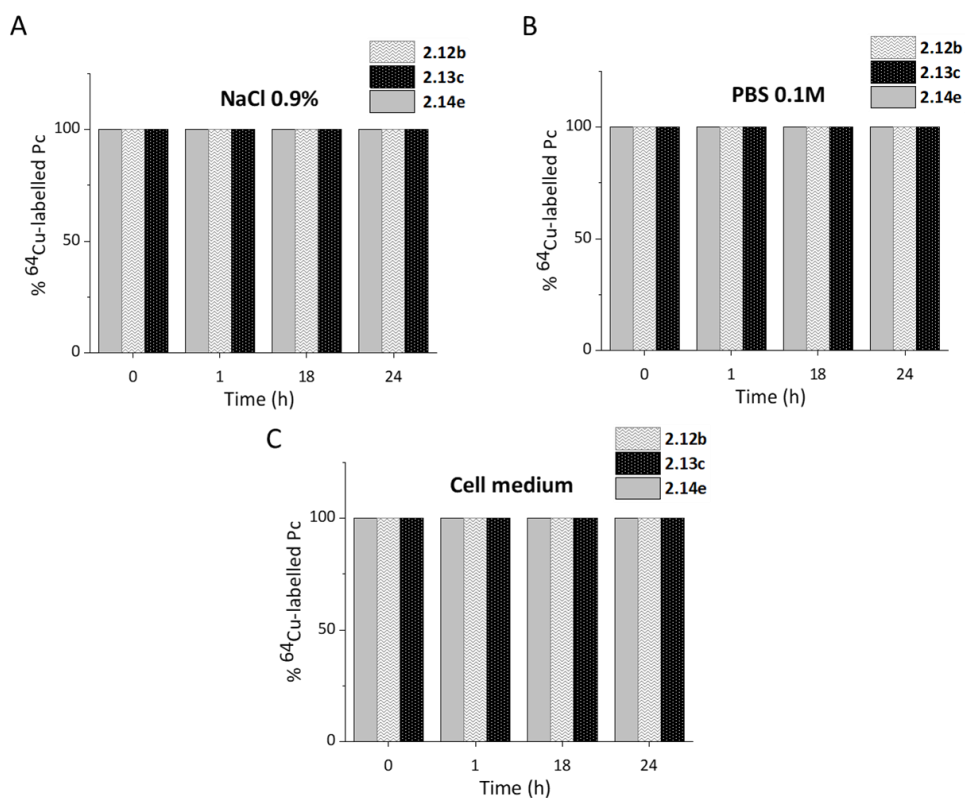


**Figure 2.10.** *In vitro* radiochemical stability of  $^{64}\text{Cu}$ -labelled phthalocyanines **2.12b**, **2.13c** and **2.14e** in the presence of: **A)** NaCl 0.9%, **B)** PBS (0.1M, pH 7.4) and **C)** DMEM cell medium.

From the results presented in **Figure 2.10**, we can see that all radiolabelled phthalocyanines display remarkable stability in all selected media, since no “free”  $^{64}\text{Cu}$  (*i.e.*  $^{64}\text{Cu}[\text{Cu}(\text{EDTA})]$ ) was observed in the corresponding radio-TLC chromatogram till 24 hours.

Summing the available data, we have selected the  $^{64}\text{Cu}$ -labelled tetra-choline phthalocyanine **2.14e** as the lead compound to pursue the *in vivo* PET imaging biodistribution studies, particularly for its easier  $^{64}\text{Cu}$ -labelling, purification and high biocompatibility.



## 2.5 *In vivo* PET imaging and biodistribution studies of tetra-choline $^{64}\text{Cu}$ -labelled phthalocyanine

The studies described in this section was performed in collaboration with ICNAS Pre-Clinical Imaging Facility, where Dr. José Sereno (PhD) executed the imaging experiments described below, using normal BALB/c mice (C57BL6 mice). These studies were expected to provide a first insight in the biodistribution profile of  $^{64}\text{Cu}$ -labelled tetra-choline phthalocyanine **2.14e**, in terms of blood clearance and excretion pathways. Each animal ( $n=3$ , males BALB/c) was injected in the tail vein with 100  $\mu\text{L}$  of tetra-choline  $^{64}\text{Cu}$ -labelled phthalocyanine **2.14e** saline solution ( $21.8 \pm 0.2 \mu\text{Ci/g}$ ,  $n=3$ ). The mice were placed on a high resolution micro-PET imaging system and the PET images were acquired during 1h 30 min post-injection time (p.i.). The MRI imaging was performed after the PET acquisition, aiming the identification of the mice's organs in the PET images, and therefore allowing the identification of phthalocyanine **2.14e** accumulation in each mice organ (**Figure 2.11**).

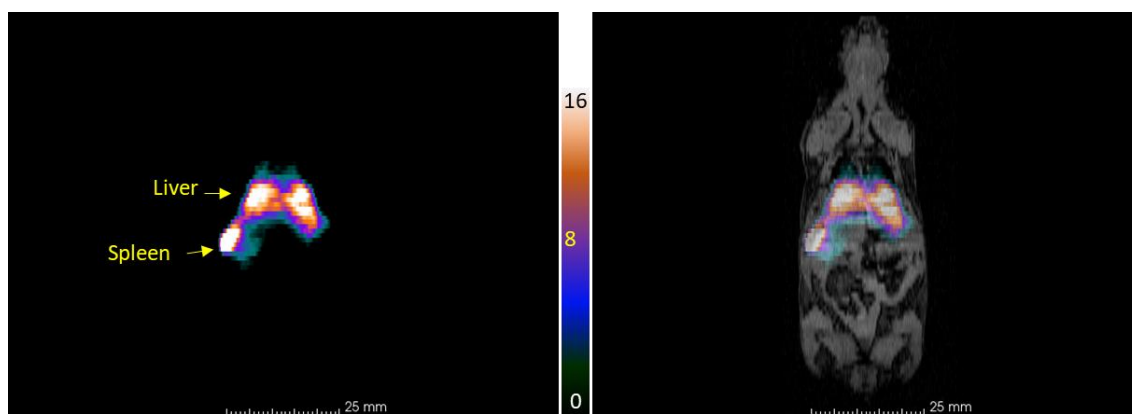


**Figure 2.11.** Micro-PET imaging studies of  $^{64}\text{Cu}$ -labelled phthalocyanine **2.14e** after 1h 30 min post-injection time. Color scale: counts per min/ $(\text{mm}^3 \cdot \text{I.D.}/\text{g})$ .

The quantification of activity content in each organ are expressed as percentage of injected dose per gram of organ ( $\% \text{I.D.}/\text{g}$ ), being the results presented in **Table 2.8**. After 3 h post-injection, the animals were sacrificed by cervical dislocation. Tissue samples of the main organs were removed and weighed, and the activity was measured in a gamma

counter corrected for background activity and copper-64 decay. The results of activity content (% I.D./g) are also presented in **Table 2.8**.

**Table 2.8.** Biodistribution results (mean  $\pm$  SD,  $n=3$ ; expressed as %I.D./g of organ) for tetra-choline  $^{64}\text{Cu}$ -labelled phthalocyanine **2.14e** after intravenous administration post-injection (p.i.) in BALB/c mice.

Organ	% I.D./g	
	1h 30 min p.i. ( <i>in vivo</i> )	3 h p.i. ( <i>ex vivo</i> )
Lung	2.7 $\pm$ 0.2	5.5 $\pm$ 0.6
Liver	7.0 $\pm$ 1.9	2.5 $\pm$ 0.5
Spleen	7.9 $\pm$ 1.2	31.2 $\pm$ 5.1
Kidney	3.4 $\pm$ 0.5	4.6 $\pm$ 0.2
Bladder	0.38 $\pm$ 0.03	0.24 $\pm$ 0.02
Muscle	0.17 $\pm$ 0.1	0.12 $\pm$ 0.02
Bone	0.2 $\pm$ 0.1	0.5 $\pm$ 0.02
Blood	3.6 $\pm$ 0.5	2.2 $\pm$ 0.2
Heart	-----	4.2 $\pm$ 0.5
Intestine	-----	0.6 $\pm$ 0.07
Stomach	-----	0.5 $\pm$ 0.1
Brain	-----	0.05 $\pm$ 0.01

At 1h 30 min p.i. the *in vivo* biodistribution profile of  $^{64}\text{Cu}$ -labelled phthalocyanine **2.14e** (**Table 2.8**) indicated a very fast uptake by the reticuloendothelial system (RES) organs, as shown by the high uptake values of 7.0  $\pm$  1.9 and 7.9  $\pm$  2.7% I.D./g, in the liver and spleen, respectively. There is also a significant accumulation of compound **2.14e** in the kidneys (3.4  $\pm$  0.5% I.D./g), as well as in the blood stream (3.6  $\pm$  0.5% I.D./g) after 1h 30 min p.i. Moreover, there is a negligible bladder, muscle and bone uptake (0.38  $\pm$  0.03, 0.17  $\pm$  0.1 and 0.2  $\pm$  0.1% I.D./g at 1h 30 min p.i., respectively).

After 3 h p.i., the *ex vivo* biodistribution results showed an increased accumulation of tetra-choline  $^{64}\text{Cu}$ -labelled phthalocyanine **2.14e** when compared with 1h 30 min p.i., namely in the spleen (7.9  $\pm$  1.2% I.D./g and 31.2  $\pm$  5.1% I.D./g at 1h 30

min and 3 h p.i., respectively), as well as in the lungs ( $2.7 \pm 0.2\%$  I.D./g and  $5.5 \pm 0.6\%$  I.D./g at 1h 30 min and 3 h p.i., respectively) and in the kidneys ( $3.4 \pm 0.5\%$  I.D./g and  $4.6 \pm 0.2\%$  I.D./g at 1h 30 min and 3 h p.i., respectively). A slightly accumulation decrease of compound **2.14e** in blood stream ( $3.6 \pm 0.5\%$  I.D./g and  $2.2 \pm 0.2\%$  I.D./g at 1h 30 min and 3 h p.i., respectively) was also observed. On the other hand, a considerable decrease of compound **2.14e** accumulation in liver ( $7.0 \pm 1.9\%$  I.D./g and  $2.5 \pm 0.5\%$  I.D./g at 1h 30 min and 3 h p.i., respectively) was detected. Moreover, a negligible bladder, muscle, bone, intestine, stomach and brain uptake, after 3 h p.i. was observed. Nevertheless, it is noteworthy the increased heart uptake ( $4.2 \pm 0.5\%$  I.D./g) after 3 h p.i.

The results presented in **Table 2.8** reveal that the tetra-choline  $^{64}\text{Cu}$ -labelled phthalocyanine **2.14e** manages to circulate inside the body for a long time period (*i.e.* reduced blood clearance), before starting to be eliminated ( $3.6 \pm 0.5\%$  I.D./g and  $2.2 \pm 0.2\%$  I.D./g at 1h 30 min and 3 h p.i., respectively). This indicates that, during circulation, the organ/tissue distribution of phthalocyanine **2.14e** is slow and the binding with plasma proteins should be high. This is corroborated by the literature, since it is known that the positively charged  $\beta$ -tetra substituted phthalocyanines have a tendency to bind plasma blood proteins.<sup>34</sup> Subsequently, the retention of activity in deeply irrigated organs such as lungs, heart, kidneys and spleen ( $5.5 \pm 1.9$ ,  $4.2 \pm 0.5$ ,  $4.6 \pm 0.2$  and  $31.2 \pm 5.1\%$  I.D./g at 3 h p.i., respectively) could be a consequence of the reduced blood clearance.

Despite of the tetra-choline  $^{64}\text{Cu}$ -labelled phthalocyanine **2.14e** kidneys uptake ( $3.4 \pm 0.5\%$  I.D./g and  $4.6 \pm 0.2\%$  I.D./g at 1h 30 min and 3 h p.i., respectively), the elimination process of compound **2.14e** did not pass through the kidneys, as indicated by the residual bladder uptake ( $0.38 \pm 0.03\%$  I.D./g and  $0.24 \pm 0.02\%$  I.D./g at 1h 30 min and 3 h p.i., respectively). Thus, we can conclude that the elimination of compound **2.14e** did not follow the renal excretion pathway. For compound **2.14e**, excretion is predominantly done through hepatobiliary pathway, as seen by the high liver uptake ( $7.0 \pm 1.9\%$  I.D./g and  $2.5 \pm 0.5\%$  I.D./g at 1h 30 min and 3 h p.i., respectively).

## 2.6 Conclusion

The main goal of the work discussed in this chapter was to the design and synthesis of a new family metal-free phthalocyanines suitably functionalized with biocompatible and/or cancer-targeting groups for the development of potential copper-64 labelled radiopharmaceuticals, as PET probes for cancer diagnosis. Hence, four different topics were explored in this chapter:

i) the first topic involved the structural modulation of several phthalonitriles, as precursors for the desired phthalocyanine synthesis. In this study, an environmentally benign, time and cost effective approach was developed using the ultrasonic irradiation for the phthalonitrile synthesis, via *ipso* substitution, achieving quite high isolated yields (61–83%), comparable to those obtained in conventional heating;

ii) in the second topic, an efficient method for the synthesis of zinc(II) and magnesium(II) metallophthalocyanine complexes was described, along with their corresponding metal-free counterparts, incorporating choline, isopropylidene protected *D*-galactose and also polyethylene glycol groups as substituents, all selected for their biocompatibility and/or cancer cells specificity. It has been concluded that the synthesis of the metal-free *via* zinc(II) phthalocyanine complex (in alternative to magnesium(II)), followed by demetallation, is the most viable and reproducible method to obtain the desired metal-free phthalocyanines, with very high isolated yields (79-85%);

iii) the third topic discussed the optimization of <sup>64</sup>Cu-labelling procedure for the previously synthesized phthalocyanines. Before radiolabelling, all copper(II) phthalocyanine reference standards were synthesized in excellent isolated yields (86-94%), allowing us to confirm the high potentiality of these compounds. <sup>64</sup>Cu-labelled phthalocyanines **2.12b**, **2.13c** and **2.14e** were successfully synthesized in RCCs of 96-99%, using just 1.8 nmol of each  $\beta$ -tetra-substituted metal-free phthalocyanine. Furthermore, the purified <sup>64</sup>Cu-labelled compounds were isolated in satisfactory non-decay corrected RCYs (37-98%) and in excellent radiochemical purity (> 98%). The *in vitro* radiochemical stability studies demonstrated that in all physiological media (*e.g.* NaCl, PBS and cell culture medium) the <sup>64</sup>Cu-labelled phthalocyanines **2.12b**, **2.13c** and **2.14e** show an outstanding stability;

iv) the fourth and last topic was focused on the evaluation of the biodistribution profile of  $^{64}\text{Cu}$ -labelled tetra-choline phthalocyanine **2.14e** in BALB/c mice. These studies allowed us to conclude that compound **2.14e** accumulates in highly irrigated organs such as liver, spleen, kidneys, heart and lungs, being the most activity retained in the spleen, which could be attributed to its prolonged circulation time in blood. Moreover, the compound **2.14e** is eliminated by the hepatobiliary pathway.

Altogether, these preliminary results are encouraging for the development of phthalocyanine-based probes labelled with copper-64 radioisotope for PET imaging. As a future step it is crucial to determine their specific/molar activity (measurement of the fraction of  $^{64}\text{Cu}$ -labelled compound compared with non-radiolabelled compound), since it is plausible to say that the mechanism of action of the synthesized  $^{64}\text{Cu}$ -labelled phthalocyanines involves a specific receptor binding. This is very important because the *in vivo* density of the receptors in cancer cells is very low, and subsequently the use of  $^{64}\text{Cu}$ -labelled phthalocyanines with low specific/molar activity can easily lead to saturation of these receptors in cancer cells. It is also important to perform *in vivo* PET imaging and biodistribution studies in tumor-bearing mice to infer the specificity of the  $^{64}\text{Cu}$ -labelled compound for cancer cells.

Furthermore, we also highlight the  $\beta$ -tetra-substituted phthalocyanine functionalized azido-polyethylene glycol chains groups **2.8c**, which can open the way for future *in vivo* PET click-chemistry approaches, giving a relevant contribution for *in vivo* pre-targeting strategies purposing cancer diagnosis, or further SPAAC (strain-promoted alkyne-azide cycloaddition) reactions for conjugation with valuable target molecules as specific cancer reporters.<sup>13-16</sup>

## 2.7 References

- 
- <sup>1</sup> Watt, G. W.; Dawes, J. W., *Journal of Inorganic and Nuclear Chemistry* **1960**, 14 (1-2), 32–34.
- <sup>2</sup> (a) Okoth, E. A.; Zhou, Z.; Ongarora, B.; Stutes, A.; Mathis J. M.; Vicente, M. G. H., *Journal of Porphyrins and Phthalocyanines* **2019**, 23, 125–135; (b) Li, K.; Dong, W.; Liu, Q.; Lv, G.; Xie, M.; Sun, X.; Qiu, L.; Lin, J., *Journal of Photochemistry and Photobiology B: Biology* **2019**, 190, 1–7.
- <sup>3</sup> Matlou, G. G.; Oluwole, D. O.; Prinsloo, E.; Nyokong, T., *Journal of Photochemistry and Photobiology B: Biology* **2018**, 186, 216–224.
- <sup>4</sup> (a) Li, F.; Liu, Q.; Liang, Z.; Wang, J.; Pang, M.; Huang, W.; Wu, W.; Hong, Z., *Organic & Biomolecular Chemistry* **2016**, 14 (13), 3409–3422.
- <sup>5</sup> Hanack, M.; Crucius, G.; Calvete, M. J. F.; Ziegler, T., *Current Organic Synthesis* **2014**, 11 (1), 59–66.
- <sup>6</sup> Dumoulin, F.; Durmuş, M.; Ahsen, V.; Nyokong, T., *Coordination Chemistry Reviews* **2010**, 254 (23–24), 2792–2847.
- <sup>7</sup> Barrona, C. C.; Bilan, P. J.; Tsakiridis, T.; Tsiani, E., *Metabolism Clinical and Experimental* **2016**, 65, 124–139.
- <sup>8</sup> (a) Calvo, M. B.; Figueroa, A.; Pulido, E. G.; Campelo, R. G.; Aparicio, L. A., *International Journal of Endocrinology* **2010**, 205357; (b) Airley, R. E.; Mobasheri, A., *Chemotherapy* **2007**, 53 (4), 233–256.
- <sup>9</sup> Cheng, M.; Bhujwalla, Z. M.; Glunde, K., *Frontiers in Oncology* **2016**, 6, 266.
- <sup>10</sup> Glunde, K.; Penet, M. F.; Jiang, L.; Jacobs, M. A.; Bhujwalla, Z. M., *Expert Review of Molecular Diagnostics* **2015**, 15 (6), 735–747.
- <sup>11</sup> van Vlerken, L. E.; Vyas, T. K.; Amiji, M. M., *Pharmaceutical Research* **2007**, 24 (8), 1405–1414
- <sup>12</sup> Liu, J.-Y.; Jiang, X.-J.; Fong, W.-P.; Ng, D. K. P., *Organic & Biomolecular Chemistry* **2008**, 6 (24), 4560–4566.
- <sup>13</sup> Kim, E.; Koo, H., *Chemical Science*, **2019**, 10, 7835–7851.
- <sup>14</sup> Mushtaq, S.; Yun, S. J.; Jeon, J., *Molecules* **2019**, 24 (19), E3567.
- <sup>15</sup> Meyer, J. P.; Adumeau, P.; Lewis, J. S.; Zeglis, B. M., *Bioconjugate Chemistry* **2016**, 27 (12), 2791–2807.
- <sup>16</sup> Zeng, D.; Zeglis, B. M.; Lewis, J. S.; Anderson, C. J., *Journal of Nuclear Medicine* **2013**, 54 (6), 829–832.
- <sup>17</sup> Nemykin, V. N.; Luk'yanets, E. A., *Reviews and Accounts* **2010**, 1, 136–208.
- <sup>18</sup> (a) Puri, S.; Kaur, B.; Parmar, A.; Kumar, H., *Current Organic Chemistry* **2013**, 17 (16), 1790–1828; (b) Meciárová, M.; Toma, S.; Magdolen, P., *Ultrasonics Sonochemistry* **2003**, 10 (4-5), 265–270.
- <sup>19</sup> Choi, C. F.; Huang, J. D.; Lo, P. C.; Fong, W. P.; Ng, D. K., *Organic & Biomolecular Chemistry* **2008**, 6 (12), 2173–2181.

- <sup>20</sup> Alzeer, J.; Roth, P. J. C.; Luedtke, N. W., *Chemical Communications* **2009**, 15, 1970–1971.
- <sup>21</sup> Calvete, M. J. F.; Dini, D.; Flom, S. R.; Hanack, M.; Pong, R. G. S.; Shirk, J. S., *European Journal of Organic Chemistry* **2005**, 16, 3499–3509.
- <sup>22</sup> Zhang, L.; Huang, J.; Ren, L.; Bai, M.; Wu, L.; Zhai, B.; Zhou, X., *Bioorganic & Medicinal Chemistry* **2008**, 16 (1), 303–312.
- <sup>23</sup> Soares, A. R. M.; Tomé, J. P. C.; Neves, M. G. P. M. S.; Tomé, A. C.; Cavaleiro J. A. S., Torres, T., *Carbohydrate Research* **2009**, 344 (4), 507–510.
- <sup>24</sup> Kimani, S. G.; Shmigol, T. A.; Hammond, S.; Phillips, J. B.; Bruce, J. I.; MacRobert, A. J.; Malakhov, M. V.; Golding, J. P., *Photochemistry and Photobiology* **2013**, 89 (1), 139–149.
- <sup>25</sup> Koç, V.; Topal, S. Z.; Aydın Tekda, D.; Ate, Ö. D.; Önal, E.; Dumoulin, F.; Gurek, A. G.; Ahsen, V., *New Journal of Chemistry* **2017**, 41 (18), 10027–10036.
- <sup>26</sup> Alvarez-Mico, X.; Calvete, M. J. F.; Hanack, M.; Ziegler, T., *Tetrahedron Letters* **2006**, 47 (19), 3283–3286.
- <sup>27</sup> Alves, F.; Alves, V. H. P.; Do Carmo, S. J. C.; Neves, A. C. B.; Silva, M.; Abrunhosa, A. J., *Modern Physics Letters A* **2017**, 32 (17), 1740013–1740021.
- <sup>28</sup> (a) de Blois, E.; de Zanger, R. M. S.; Chan, H. S.; Konijnenberg, M.; Breeman, W. A. P., *EJNMMI Radiopharmacy and Chemistry* **2019**, 4 (3). DOI: 10.1186/s41181-018-0052-1; (b) Coenen, H. H.; Gee, A. D.; Adam, M.; Antoni, G.; Cutler, C. S.; Fujibayashi, Y.; Jeong, J. M.; Mach, R. H.; Mindt, T. L.; Pike, V. W.; Windhorst, A. D., *Nuclear Medicine and Biology* **2017**, 55, v–xi.
- <sup>29</sup> McInnes, L. E.; Rudd, S. E.; Donnelly, P. S., *Chemistry Reviews* **2017**, 352, 499–516.
- <sup>30</sup> Postigo, A., *Late-Stage Fluorination of Bioactive Molecules and Biologically-Relevant Substrates*, Elsevier, **2019**, Chapter 2, 29–103.
- <sup>31</sup> Torres Martin de Rosales, R.; Tavaré, R.; Paul, R. L.; Jauregui-Osoro, M.; Protti, A.; Glaria, A.; Varma, G.; Szanda, I.; Blower, P. J., *Angewandte Chemie International Edition* **2011**, 50 (24), 5509–5513.
- <sup>32</sup> (a) European Pharmacopoeia, *Guide for the elaboration of monographs on radiopharmaceutical preparations*, Edition 2018, **2018**; (b) European Pharmacopoeia, 9<sup>th</sup> Edition, Vol. 1, **2017**, Chapter 2.2.66 – Detection and measurement of radioactivity, 01/2017; (c) European Pharmacopoeia, 9<sup>th</sup> Edition, Vol. 1, **2017**, Chapter 5 – Radiopharmaceutical preparations, 01/2017.
- <sup>33</sup> Pinto, S. M. A.; Tomé, V. A.; Calvete, M. J. F.; Pereira, M. M.; Burrows, H. D.; Cardoso, A. M. S.; Pallier, A.; Castro, M. M. C. A.; Tóth, E. M.; Geraldès, C. F. G. C., *Journal of Inorganic Biochemistry* **2016**, 154, 50–59.
- <sup>34</sup> (a) Li, X.; Jeong, K.; Lee, Y.; Guo, T.; Lee, D.; Park, J.; Kwon, N.; Na, J. H.; Hong, S. K.; Cha, S. S.; Huang, J. D.; Choi, S.; Kim, S.; Yoon, J., *Theranostics* **2019**, 9 (22), 6412–6423; (b) Çolak, S.; Durmus, M.; Yildiz, S. Z., *Polyhedron* **2016**, 113, 115–122; (c) Durmus, M.; Yaman, H.; Göl, C.; Ahsen, V.; Nyokong, T., *Dyes and Pigments* **2011**, 91 (2), 153–163.

## CHAPTER 3

---

### *Development of $^{11}\text{C}$ -labelled $\beta$ -indolyketones as potential probes for application in brain PET imaging*

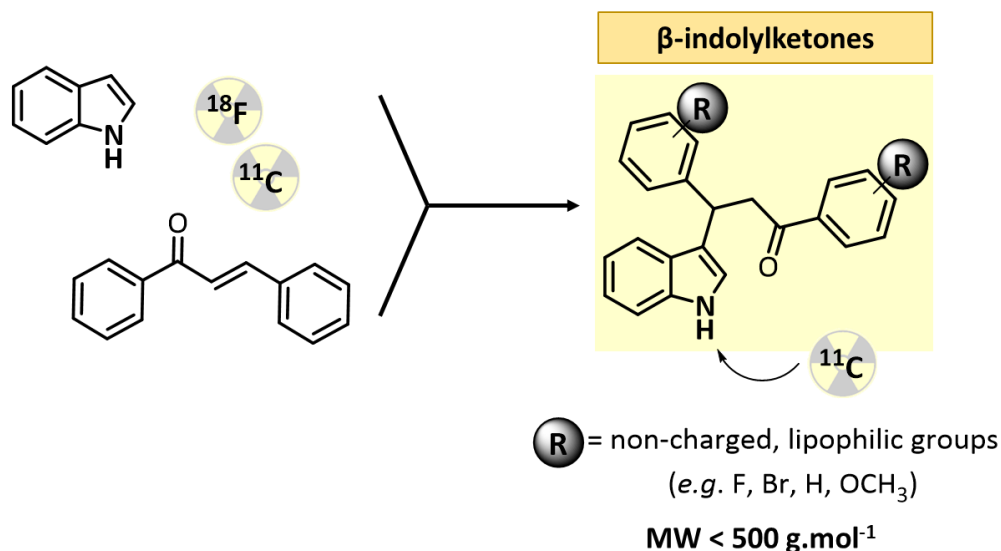
---

#### 3.1 Introduction

Understanding the neurobiological basis of the human brain and to investigate the pathophysiology underlying and treatment of human brain disorders have become some of the great scientific challenges in recent decades. We consider that the non-invasive *in vivo* PET imaging technique is a valuable tool to clarify such pertinent issues and, subsequently, the development of new small molecules as potential PET radiopharmaceuticals for *in vivo* brain imaging is a hot topic for chemistry and radiochemistry scientific communities.<sup>1,2</sup>

As previously described in Chapter 1 of this thesis, chalcone- and indole-type radiolabelled derivatives (*e.g.* with  $^{11}\text{C}$  or  $^{18}\text{F}$ ) possess relevant properties to be used as potential brain PET imaging probes. Therefore, we hypothesized that the synthesis of a new small molecules of the  $\beta$ -indolyketone-type (scaffold based on conjugate addition reaction of indoles with chalcones), containing a structural moiety amenable for  $^{11}\text{C}$ -labelling and suitable physiochemical properties to successfully penetrate the BBB (structural modulation with non-charged and lipophilic groups taking into account the low molecular weight pre-requisite),<sup>3-5</sup> would allow the preparation of new promising probes for potential application in brain PET imaging (**Scheme 3.1**).





**Scheme 3.1.** Design of <sup>11</sup>C-labelled  $\beta$ -indolylketones as potential PET probes for brain imaging.

In this chapter we describe the synthesis and structural modulation of a set of  $\beta$ -indolylketones, and report the *in vitro* cytotoxicity and theoretical octan-1-ol/water partition coefficient values (ClogP) of the resulting *N*-methylated  $\beta$ -indolylketone products. Moreover, in this chapter the optimization of HPLC purification and control quality method for the further <sup>11</sup>C-labelled  $\beta$ -indolylketones will be described, followed by the pioneering synthesis of the corresponding <sup>11</sup>C-labelled  $\beta$ -indolylketones, in fully automated radiosynthesis module of Radiochemistry and Cyclotron Laboratory at ICNAS. Finally, preliminary data regarding the *in vivo* biodistribution studies of these new <sup>11</sup>C-labelled  $\beta$ -indolylketones, using PET imaging, is also presented and discussed.

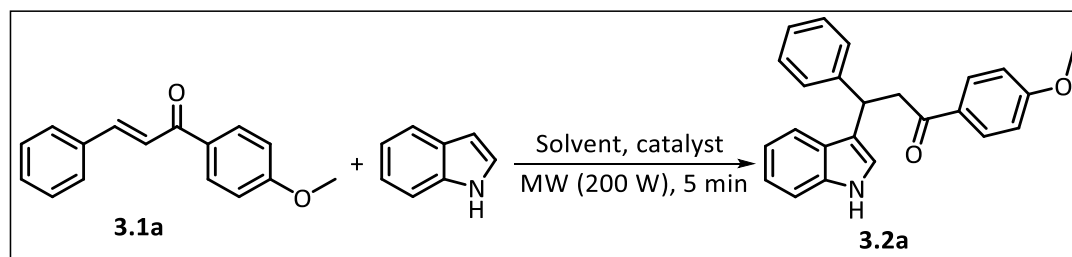
### 3.2 Synthesis of $\beta$ -indolylketones

Over the past few years, a variety of methods have been reported for the preparation of  $\beta$ -indolylketones. A simple and direct one involves the Michael addition reaction of indoles with chalcones through C-3 alkylation of indole, commonly in the presence of Brønsted (e.g. ionic liquids, silica sulfuric acid, TFA, *p*-toluenesulfonic acid, polyvinylsulfonic acid, triflic acid, *D*-camphorsulfonic acid) or Lewis acid catalysts (e.g.

InBr<sub>3</sub>, Bi(OTf)<sub>3</sub>, SbCl<sub>3</sub>, GaI<sub>3</sub>, GaCl<sub>3</sub>, Zr(OTf)<sub>4</sub>, NbCl<sub>5</sub>, SmI<sub>3</sub>) using either conventional heating<sup>6-18</sup> or ultrasonic irradiation<sup>19-22</sup> or even microwave irradiation.<sup>23-28</sup>

After a critical literature review and aiming the development of sustainable and eco-friendly synthetic processes, we selected the microwave irradiation approach<sup>29</sup> to promote the synthesis of this class of compounds. So, studies initiated with the Michael addition reaction between chalcone **3.1a** and indole, which was selected as model reaction. In a general experiment, chalcone **3.1a**, indole and acid catalyst were dissolved in an appropriated solvent, and the reaction was conducted under microwave irradiation (200 W of power) for 5 min, upon stirring at the selected temperature (**Table 3.1**). The reaction's evolution and product identification was performed by TLC analysis of samples taken from the reaction mixture. The reaction mixture was then concentrated and evaporated to dryness. After work-up procedures, the reaction mixture were then purified by column chromatography, using silica gel as stationary phase and dichloromethane as eluent. The optimization of the reaction conditions on the final isolated yield of  $\beta$ -indolyketone **3.2a** are presented in **Table 3.1**.

**Table 3.1.** Optimization of  $\beta$ -indolyketone **3.2a** synthesis under microwave irradiation.<sup>a</sup>



Entry	Solvent	Catayst	Temperature (°C)	Yield (%) <sup>b</sup>
1	EtOH	BF <sub>3</sub> .OEt <sub>2</sub>	90	N. R. <sup>c</sup>
2	EtOH	InCl <sub>3</sub>	90	N. R. <sup>c</sup>
3	EtOH	<i>p</i> -TSOH	90	66
4	<i>i</i> PrOH	<i>p</i> -TSOH	90	84
5	<i>i</i> PrOH	<i>p</i> -TSOH	110	88

<sup>a</sup> Reaction conditions: chalcone (1 mmol), indole (1.2 mmol), solvent (1 mL), 10 mol% of catalyst.

<sup>b</sup> Isolated yield.

<sup>c</sup> N. R.: No product was obtained.

First, we selected ethanol as solvent and studied the effect of several catalysts such as  $\text{BF}_3 \cdot \text{OEt}_2$ ,  $\text{InCl}_3$  and *para*-toluenesulfonic acid (*p*-TSA) at a temperature of 90 °C (entries 1-3, **Table 3.1**). We conclude that the best reaction conditions to promote the classic Michael addition reaction, between compound **3.1a** and indole, involves the use of *p*-TSA as Brønsted acid catalyst: the reaction using this catalyst produced the desired product in 66% isolated yield (entry 3, **Table 3.1**), conversely to the use of Lewis acid catalysts  $\text{BF}_3 \cdot \text{OEt}_2$  and  $\text{InCl}_3$  (entries 1-2, **Table 3.1**), which did not produce the desired  $\beta$ -indolyketone **3.2a** (*i.e.*, no conversion of starting materials **3.1a** and indole were observed after 5 min of reaction at 90 °C, checked by TLC). Based on these optimized conditions, and keeping *p*-TSA as acid catalyst, we then evaluated the effect of solvent and temperature. Regarding the solvent, the substitution of ethanol (EtOH) by isopropanol (*i*PrOH) was found to give the best results: 84% isolated yield of  $\beta$ -indolyketone **3.2a**, after 5 min at 90 °C (entry 4, **Table 3.1**). Furthermore, when the temperature was raised to 110 °C, a slight increase in the isolated yield of **3.2a** was observed (88%), after 5 min (entry 5, **Table 3.1**). From a sustainability point of view, this synthetic process denotes a significant enhancement, regarding energy and solvent consumption (5 min; 1 mL *i*PrOH), when compared with previous results reported in the literature using ultrasound irradiation (1.7 h; 2 mL of EtOH), while maintaining similar isolated yields (88% vs. 93%).<sup>20</sup>

Aiming to explore the effect of different substituents in the  $\beta$ -indolyketone scaffold on the BBB penetration, we extended the scope of the Michael addition reaction of indole or 1-methylindole to a range of substituted chalcones (**3.1a-c**), bearing different substituents in **A** or **B** rings (**Figure 3.1**; **Table 3.2**).

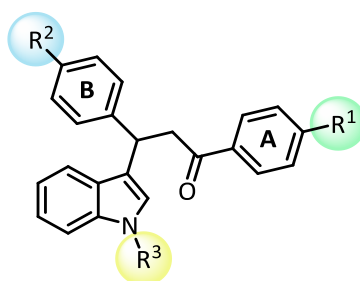
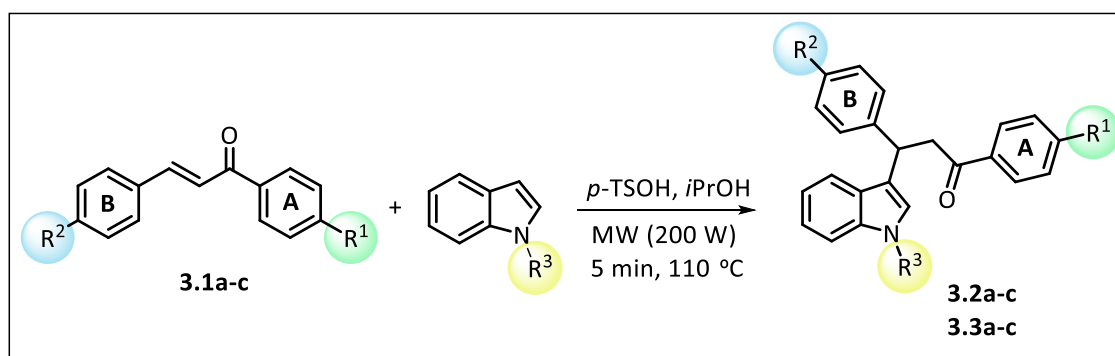


**Figure 3.1.** Structural modulation of  $\beta$ -indolyketone scaffold.

Therefore, the work proceed with the use of previously optimized reaction conditions for the synthesis of  $\beta$ -indolylyketone **3.2a** (isopropanol as solvent, *p*-TSOH as catalyst, 5 min MW irradiation at 110 °C). In order to isolate and characterize the obtained products, reaction mixtures were subjected to work-up and purification standard procedures (exact procedures for each compound are specified in Chapter 5, section 5.4.1), and the  $\beta$ -indolylyketones **3.2a-c** and **3.3a-c** were suitably characterized by  $^1\text{H}$ - and  $^{13}\text{C}$ -NMR and GC-MS, with **Table 3.2** showing the yields of isolated product for each of the synthesized  $\beta$ -indolylyketones.

**Table 3.2.**  $\beta$ -indolylyketones microwave-assisted synthesis at optimized conditions.<sup>a</sup>



Entry	Chalcone	Indole		$\beta$ -Indolylyketone	Yield (%) <sup>b</sup>	
		R <sup>1</sup>	R <sup>2</sup>			R <sup>3</sup>
1	<b>3.1a</b>	OMe	H	H	<b>3.2a</b>	88
2	<b>3.1b</b>	OMe	Br	H	<b>3.2b</b>	90
3	<b>3.1c</b>	F	OMe	H	<b>3.2c</b>	87
4	<b>3.1a</b>	OMe	H	Me	<b>3.3a</b>	90
5	<b>3.1b</b>	OMe	Br	Me	<b>3.3b</b>	88
6	<b>3.1c</b>	F	OMe	Me	<b>3.3c</b>	85

<sup>a</sup> Reaction conditions: chalcone (1 mmol), indole (1.2 mmol), 1 mL *i*PrOH, 10 mol% of *p*-TSOH.

<sup>b</sup> Isolated yield.

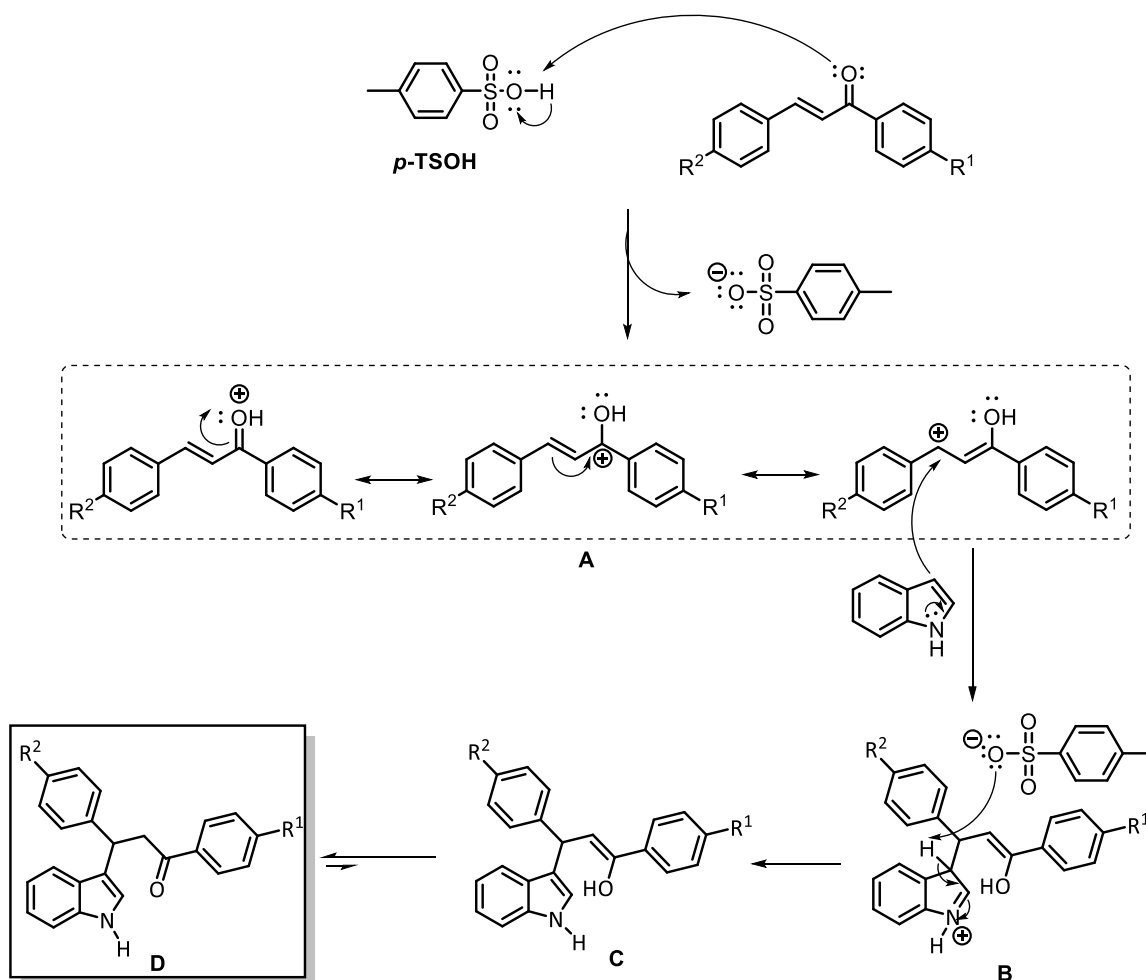
The analysis of the results presented in **Table 3.2** led us to conclude that, under the optimized conditions described above, the yield of the Michael addition reaction between indole and chalcones **3.1a-c** (entries 1-3, **Table 3.2**) was not significantly

affected by the presence of different substituents on the *para* position of **A** or **B** chalcone ring (e.g. H, F, Br or OCH<sub>3</sub>) (isolated yields up to 90%).

In addition, we also evaluated the Michael addition reaction between chalcones **3.1a-c** with 1-methyl indole (entries 4-6, **Table 3.2**). From the data in **Table 3.2** we observed that the substitution of indole (entries 1-3, **Table 3.2**) by 1-methyl indole (entries 4-6, **Table 3.2**) did not substantially influence the overall yield of the Michael addition reaction, being the isolated yields of  $\beta$ -indolylketones **3.3a-c**, once again, up to 90%. It is worth mentioning that, the resulting non-radioactive *N*-methylated  $\beta$ -indolylketone reference standards **3.3a-c** were synthesized for the dual purpose of confirming the radiochemical identity of their further <sup>11</sup>C-labelled radioactive congeners (*via* analytical column HPLC analysis) and determining the *in vitro* cytotoxicity in healthy cell lines, whose results are presented in the following section.

In sum, the use of microwave irradiation in the synthesis of  $\beta$ -indolylketones **3.2a-c** and **3.3a-c** revealed to be an efficient and energy-cost-saving method, opening the way for future  $\beta$ -indolylketone preparation with a broad range of substituents.

A mechanism for the conjugate addition of indole to chalcones is proposed in **Scheme 3.2**. The acid catalysis promoted by the addition of *p*-TSOH results in the activation of the chalcone's ketone group by protonation of the oxygen atom and consequent formation of intermediate **A**. This intermediate is composed by three main resonance structures, which show two possible electrophilic carbon centers that can bond with the indole ring. Thus, the nucleophilic attack to an  $\alpha,\beta$ -unsaturated ketone can be performed through a 1,4-addition (Michael addition) or a 1,2-addition (direct attack to the carbonyl group) and selectivity is dependent on the hardness of softness of the nucleophile. Indeed, due to the fact that the indole ring is a soft nucleophile, addition to the softer electrophilic center (*i.e.*  $\beta$ -carbon of the ketone group) is favored.<sup>30</sup> Due to a higher electronic density, this attack will proceed through the 3-position of the 1*H*-indole ring, yielding intermediate **B**, which then undergoes the thermodynamically favored regeneration of the aromaticity of the indole ring, yielding  $\beta$ -indolylketone **C**. Due to the keto-enol tautomerism favoring the conversion of the enol group into the more stable ketone group, the equilibrium is shifted towards the formation of the  $\beta$ -indolylketone **D**.



**Scheme 3.2.** Proposed mechanism for *p*-TSOH acid catalyzed Michael addition reaction of indoles to chalcones.

### *β*-indolyketones characterization

As mentioned in this chapter, all the *β*-indolyketones have been fully characterized by suitable spectroscopic techniques, described with detail in Chapter 5, section 5.4.1. As an illustrative example, the new *β*-indolyketone **3.3c** was selected for its spectroscopic characterization, resulting from the Michael addition between chalcone **3.1c** and 1-methylindole.

The **Figures 3.2** and **3.3** show the <sup>1</sup>H- and <sup>13</sup>C-NMR spectra of *N*-methylated *β*-indolyketone **3.3c**, both recorded in CDCl<sub>3</sub>. Additionally, to elucidate the structure of this compound, the full assignment of its proton and carbon signals was performed based on two-dimensional (2D) NMR experiments, namely, <sup>1</sup>H-<sup>1</sup>H COSY (Correlated spectroscopy), <sup>1</sup>H-<sup>13</sup>C HSQC (Heteronuclear Single Quantum Coherence) and <sup>1</sup>H-<sup>13</sup>C

HMBC (Heteronuclear Single Quantum Coherence), whose spectra are presented in **Figures 3.4, 3.5** and **3.6**, respectively.

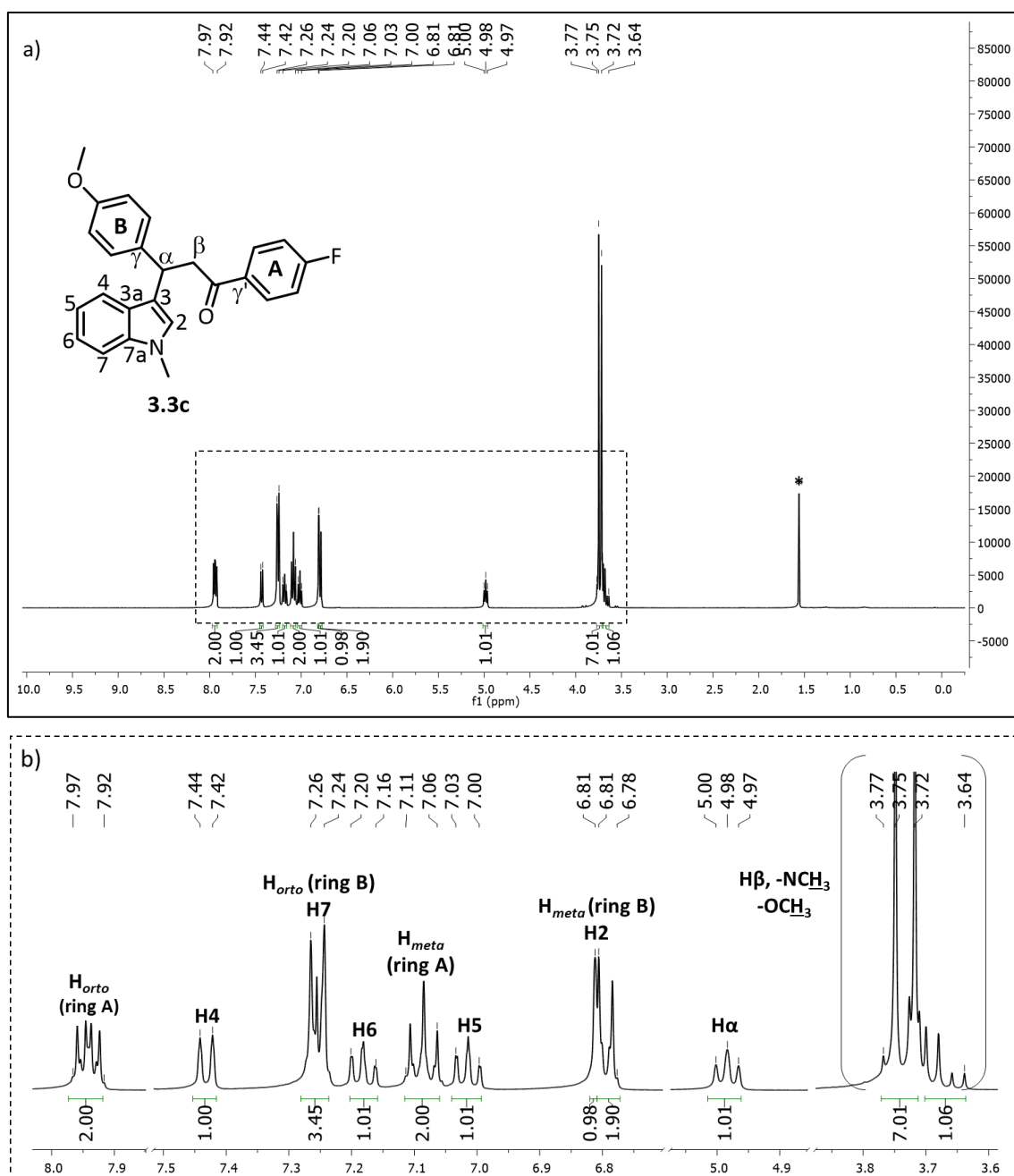


**Figure 3.2.** a) Total  $^1\text{H-NMR}$  spectrum of  $\beta$ -indolylyketone **3.3c** in  $\text{CDCl}_3$  (the residual signal marked with \* is due to the water in  $\text{CDCl}_3$  deuterated solvent); b) Selected expansion of the  $^1\text{H-NMR}$  spectrum of **3.3c** in  $\text{CDCl}_3$ .

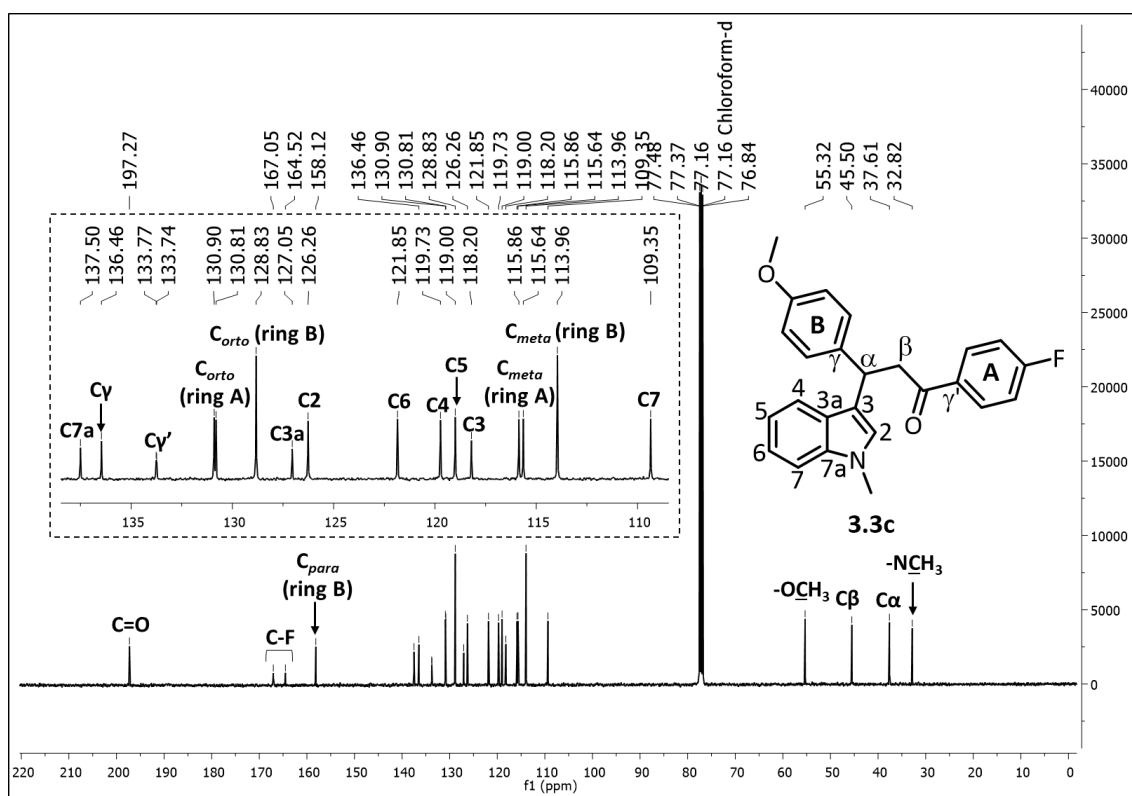


**Figure 3.3.**  $^{13}\text{C}$ -NMR spectrum of  $\beta$ -indolyketone **3.3c** in  $\text{CDCl}_3$ . Inset: expansion of  $^{13}\text{C}$ -NMR spectrum between  $\delta$  138 to 108 ppm.

In the  $^1\text{H}$ -NMR spectrum of  $\beta$ -indolyketone **3.3c** (**Figure 3.2**), the protons of the *ortho* position of the aromatic ring **A** show their resonance as multiplet at  $\delta$  7.97–7.92 ppm, integrating a total of 2 protons. Since these protons are *ortho* located to the electron-withdrawing carbonyl group, the corresponding resonance appears as the most deshielded among the signals assigned to compound **3.3c**. In the  $^1\text{H}$ - $^1\text{H}$  COSY NMR spectrum (**Figure 3.4**) a correlation was observed between this signal with the multiplet at  $\delta$  7.11–7.06 ppm, which can be attributed to the resonances of the protons of the *meta* position of the aromatic ring **A**.



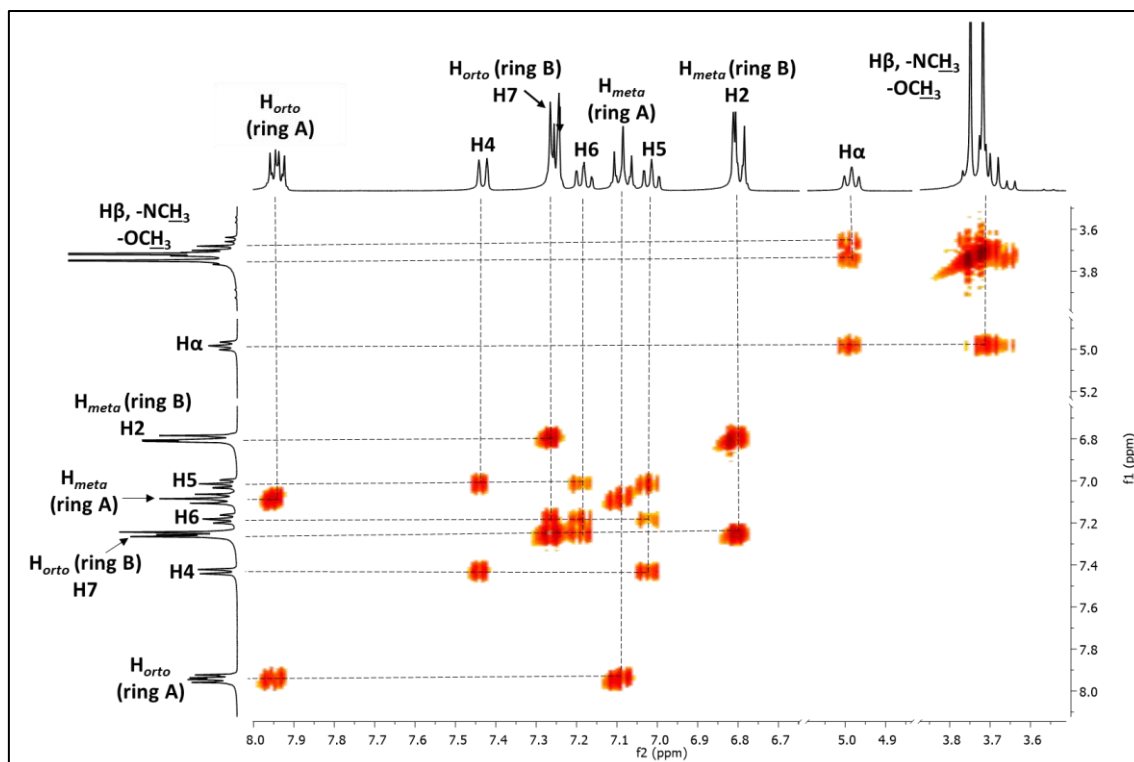


**Figure 3.4.** Selected expansion of  $^1\text{H}$ - $^1\text{H}$  COSY NMR spectrum of  $\beta$ -indolylyketone **3.3c**, recorded in  $\text{CDCl}_3$ . The relevant correlations are presented.

Once identified these signals of the  $^1\text{H}$ -NMR spectrum of **3.3c**, it was possible to assign the signals of the  $^{13}\text{C}$ -NMR spectrum by  $^1\text{H}$ - $^{13}\text{C}$  HSQC NMR spectroscopy (**Figure 3.5**). The  $^{13}\text{C}$ -NMR spectrum shows one splitting signal at  $\delta$  130.9/130.8 ppm, assigned to the carbons in *ortho* position, and the other split signal at  $\delta$  115.9/115.6 ppm was assigned to the carbons in *meta* position, both belonging to aromatic ring **A**. The remaining carbon atoms belonging to aromatic ring **A** system that show no correlation in the  $^1\text{H}$ - $^{13}\text{C}$  HSQC NMR spectrum were assigned by the observed correlations in  $^1\text{H}$ - $^{13}\text{C}$  HMBC NMR spectrum (**Figure 3.6**). From the  $^1\text{H}$ - $^{13}\text{C}$  HMBC spectrum, it is possible to confirm that the splitting signals relative to the resonances of the quaternary carbons  $\text{C}_{\gamma'}$  and  $\text{C-F}$  appear at  $\delta$  133.8/133.7 and 167.1/164.5 ppm, respectively. The observed signal splitting is due to the fact the fluorine-19 possessed a  $\frac{1}{2}$  nuclear spin, which makes it NMR active and

therefore can couple with  $^1\text{H}$  and  $^{13}\text{C}$  nuclei. This translates into an increased multiplicity of the observed  $^1\text{H}$ -NMR signals in ring **A** system and the appearance of doublets in the  $^{13}\text{C}$ -NMR signals with decreasing coupling constants as the number of bonds between  $^{19}\text{F}$  and  $^{13}\text{C}$  nuclei increases, as would be expected. Indeed, the  $^1J$  constant for C-F is 254.6 Hz, the  $^2J$  constant for the carbons in the *meta* position is 21.8 Hz, the  $^3J$  constant for the carbons in *ortho* position is 9.3 Hz, and the  $^4J$  constant for carbon  $\text{C}_{\gamma'}$  is 2.9 Hz, which clearly illustrates this effect. Also evident in the  $^{13}\text{C}$ -NMR spectrum is the signal at  $\delta = 197.3$  ppm, which is characteristic of an aromatic ketone and thus can be safely assigned to the carbonyl carbon atom ( $\text{C}=\text{O}$ ).

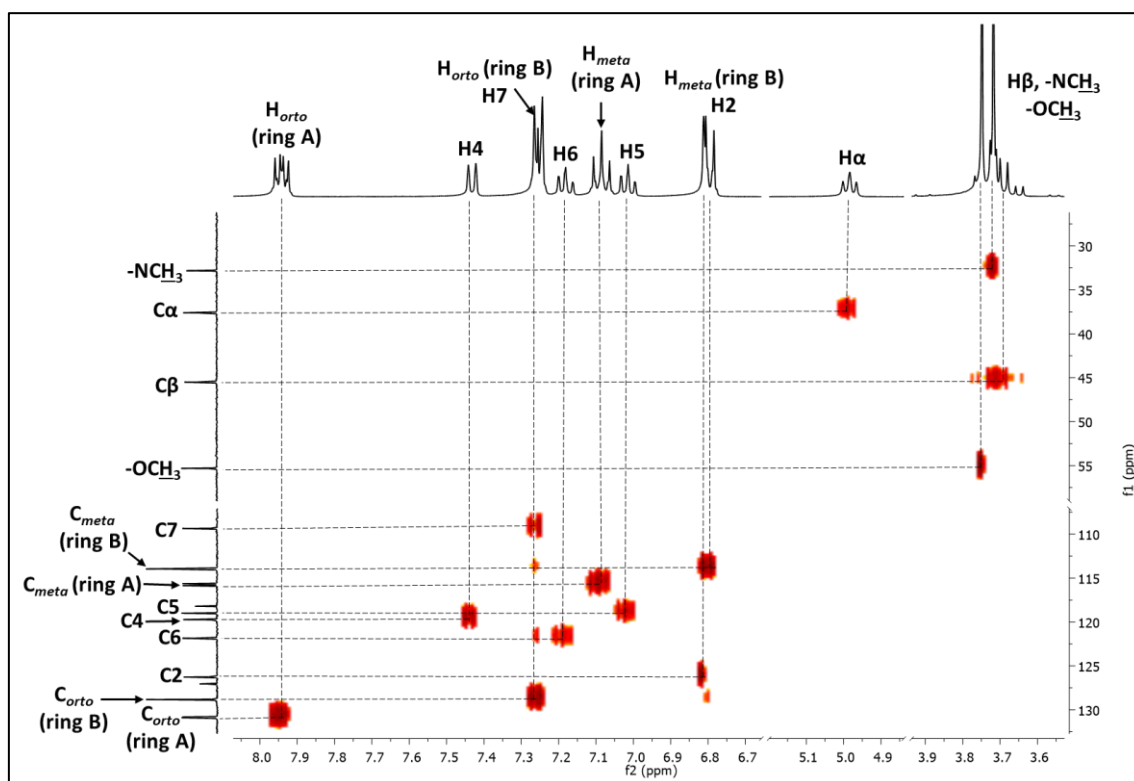


**Figure 3.5.** Selected expansion of  $^1\text{H}$ - $^{13}\text{C}$  HSQC NMR spectrum of  $\beta$ -indolyketone **3.3c**, recorded in  $\text{CDCl}_3$ .

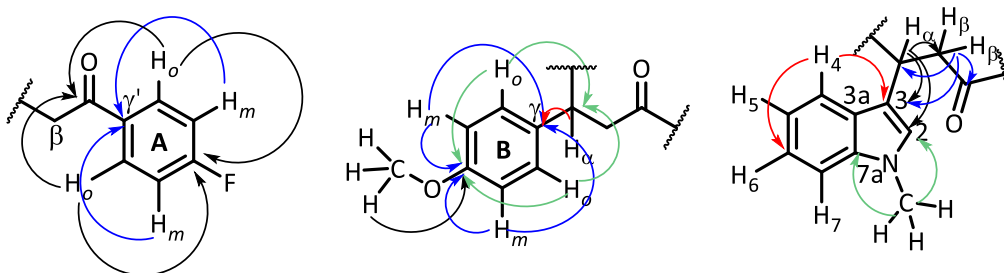
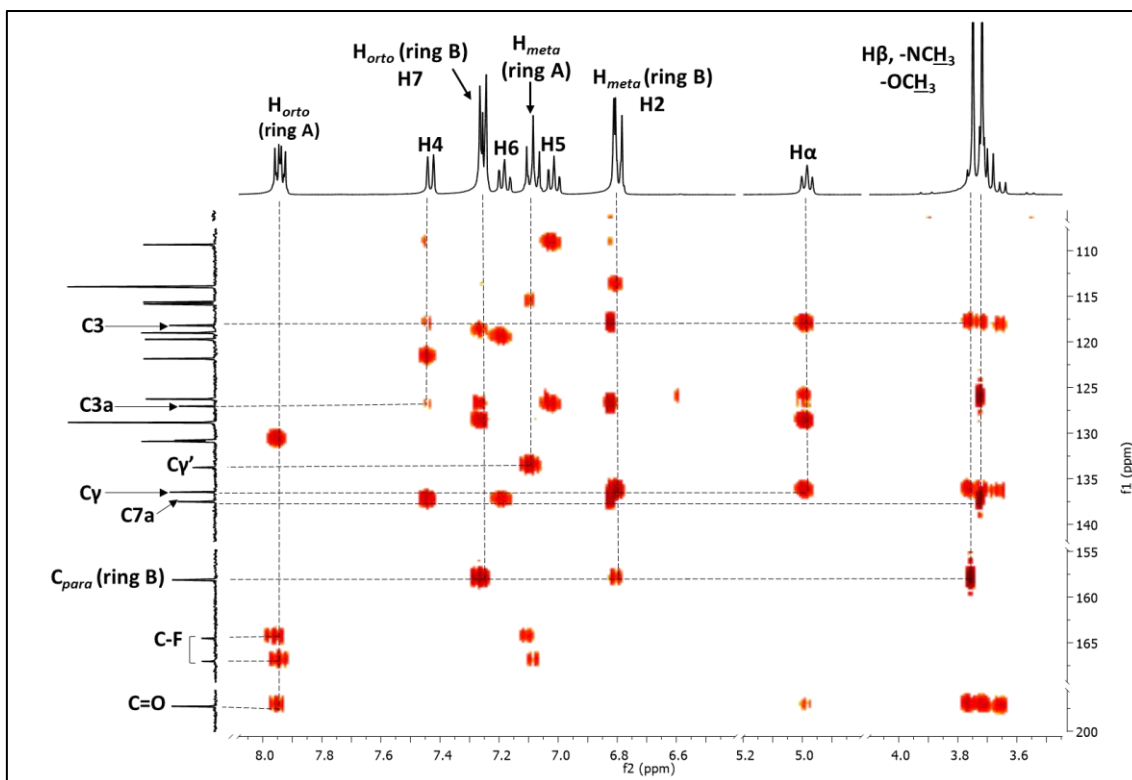


**Figure 3.6.** Selected expansion of  $^1\text{H}$ - $^{13}\text{C}$  HMBC NMR spectrum of  $\beta$ -indolyllketone **3.3c**, recorded in  $\text{CDCl}_3$ . The most relevant correlations for the assignment of the quaternary carbons are presented.

Analyzing the aliphatic region of the  $^1\text{H}$ -NMR spectrum of  $\beta$ -indolyllketone **3.3c** (Figure 3.2), the triplet at  $\delta$  4.98 ppm ( $J = 7.2$  Hz) was assigned to the CH proton ( $\text{H}_\alpha$ ). The remaining resonances of the aliphatic protons were assigned to the region of  $\delta$  3.77–3.64 ppm. In this region, two singlets are superimposed with one pair of double doublets. Despite the superimposed signals, the two close singlets at  $\delta$  3.72 and 3.75 ppm were attributed to the resonances of nitrogen-bonded methyl proton atoms ( $-\text{NCH}_3$ ) and oxygen-bonded methyl protons atoms ( $-\text{OCH}_3$ ), respectively, being the latter in a lower field due to the close proximity to the more electronegative oxygen atom. Thus, the two superimposed double doublets in the region of  $\delta$  3.77–3.64 ppm were assigned to the  $\text{CH}_2$  protons ( $\text{H}_\beta$ ). Given their close proximity to a chiral center,

these diastereotopic protons are expected to have different chemical shifts and possess a geminal and a vicinal coupling. In the  $^{13}\text{C}$ -NMR spectrum of  $\beta$ -indolylketone **3.3c** (Figure 3.3) the signals at  $\delta$  55.3, 45.5, 37.6 and 32.8 ppm were assigned to oxygen-bonded methyl carbon atom ( $-\text{O}\underline{\text{C}}\text{H}_3$ ), secondary carbon atom  $\text{C}\beta$ , tertiary carbon atom  $\text{C}\alpha$  and nitrogen-bonded methyl carbon atom ( $-\text{N}\underline{\text{C}}\text{H}_3$ ), respectively. These correlations were confirmed by  $^1\text{H}$ - $^1\text{H}$  COSY and  $^1\text{H}$ - $^{13}\text{C}$  HSQC NMR spectra (Figure 3.4 and Figure 3.5).

Based on the  $^1\text{H}$ - $^1\text{H}$  COSY and  $^1\text{H}$ - $^{13}\text{C}$  HMBC NMR studies, it was possible to assign all the remaining signals corresponding to the dihydrochalcone moiety. The protons of the *ortho* and *meta* position of the aromatic ring **B** show their proton resonances as multiplets (due to superimposition with resonances from the indole ring) at  $\delta$  7.26–7.24 and 6.81–6.78 ppm, respectively. In the  $^{13}\text{C}$ -NMR spectrum of  $\beta$ -indolylketone **3.3c**, the signals at  $\delta$  158.1, 136.5, 128.8 and 114.0 ppm were assigned to carbons atoms *para* position,  $\text{C}_\gamma$ , *ortho* and *meta* position of the aromatic ring **B**, respectively, as deduced by  $^1\text{H}$ - $^{13}\text{C}$  HMBC and  $^1\text{H}$ - $^{13}\text{C}$  HSQC NMR spectra (Figure 3.5 and Figure 3.6).

Among the signals of the indole unit in the  $^1\text{H}$ -NMR spectrum (Figure 3.2), the H-5 appears as a triplet at  $\delta$  7.01 ppm ( $J = 7.9$  Hz). This resonance (later confirmed by  $^1\text{H}$ - $^{13}\text{C}$  HMBC NMR spectrum) can be easily attributed because it is well-known that the electronic density in this position of the benzene portion of the indole ring is higher. Based on the coupling patterns observed in the  $^1\text{H}$ - $^1\text{H}$  COSY NMR spectrum (Figure 3.4), we can only identify two correlations with H5, which corresponding to the two protons in *ortho* positions: i) a doublet at  $\delta$  7.43 ppm ( $J = 8$  Hz), which corresponds to H4 and ii) a triplet at  $\delta$  7.18 ppm ( $J = 8$  Hz), which can only be attributed to H6, due to its coupling with protons H5 and H7. The proton H7 appears as a doublet overlapped in the multiplet at  $\delta$  7.26–7.24 ppm (due to superimposition with the deuterated solvent and the resonances from aromatic ring **B**). As deduced by the  $^1\text{H}$ - $^{13}\text{C}$  HSQC spectrum (Figure 3.5), the carbons atoms C4, C5, C6 and C7 were assigned to the signals at  $\delta$  119.7, 119.0, 121.9 and 109.4 ppm. The remaining proton H2 appears as singlet overlapped in the multiplet (due to superimposition with the resonances from aromatic ring **B**) at  $\delta$  6.81–6.78 ppm, and its corresponding carbon was assigned to the signal at  $\delta$  126.3 ppm. From the  $^1\text{H}$ - $^{13}\text{C}$  HMBC spectrum (Figure 3.6) it is possible to assign the signals relative to the

resonances of the quaternary carbons C3, C3a and C7a, which appear at  $\delta$  118.2, 127.1 and 137.5 ppm, respectively.

The structure of the  $\beta$ -indolyketone **3.3c** was also confirmed by GC-MS spectrometry, and it was observed an ion peak at  $m/z$  387.2, which corresponds to the mass of the molecular ion  $[M]^+$  of the  $\beta$ -indolyketone **3.3c**.

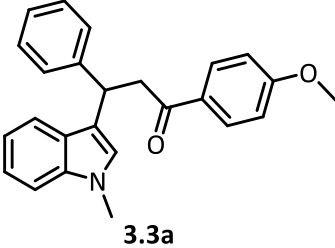
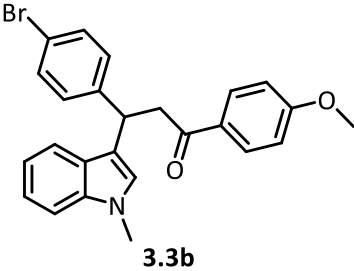
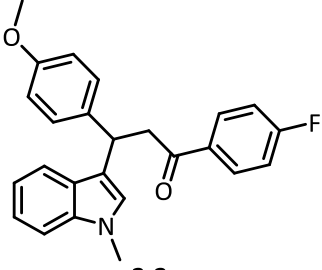
### **3.3 *In vitro* cytotoxicity studies and computational determination of octan-1-ol/water partition coefficient values of *N*-methylated $\beta$ -indolyketones**

The studies described in this section were performed in collaboration with Photonics and Reactivity Laboratory of Coimbra Chemistry Center, where MSc Hélder Soares executed the experiments described below.

The absence of toxicity in healthy cells, at suitable *in vivo* PET imaging concentrations, is one of the main requirements in the development of new potential PET radiopharmaceuticals. In this context, the *in vitro* cytotoxicity of the synthesized *N*-methylated  $\beta$ -indolyketones **3.3a-c** against 3T3 (mouse embryo fibroblasts) cell line was carried out. The compounds **3.3a-c** were dissolved in a small amount of DMSO (<2 % v/v DMSO of total final solution volume) in cell culture medium (DMEM - Dulbecco's modified Eagle's medium), and the 3T3 cells were incubated with a solution containing various concentrations of each  $\beta$ -indolyketone compound (ranging 10  $\mu$ M to 400  $\mu$ M) in PBS medium for a period of 20 h. Control cells, without addition of  $\beta$ -indolyketone compounds, were incubated under the same conditions. After the incubation period, the 3T3 cells were washed with PBS (phosphate buffered saline) and the resazurin reduction assay was used to quantify the cell viability. This assay is based on the conversion of the resazurin dye (blue non-fluorescent dye) into pink-colored, highly fluorescent resorufin, by mitochondrial and other enzymes in viable cells. Essentially, the viable cells convert continuously resazurin to resorufin, increasing the overall fluorescence and color of the cell culture medium. Thus, the amount of produced resorufin is proportional to the number of viable cells, which is quantified by using a

microplate reader fluorometer. The half-maximal inhibitory concentration ( $IC_{50}$ ) values were achieved by nonlinear regression of dose response curves and the values are present in **Table 3.3**.

**Table 3.3.** Cytotoxicity ( $IC_{50}$ ) against healthy cell line and the calculated LogP (ClogP) values of *N*-methylated  $\beta$ -indolyketones **3.3a-c**.

Entry	$\beta$ -indolyketones	$IC_{50}$ ( $\mu$ M)	ClogP
1	 <p><b>3.3a</b></p>	96.5	2.73
2	 <p><b>3.3b</b></p>	121.8	3.13
3	 <p><b>3.3c</b></p>	658.1	2.80

From data presented in **Table 3.3**, the  $\beta$ -indolyketones **3.3a**, **3.3b** and **3.3c** presented an  $IC_{50}$  values of 96.5, 121.8 and 658.1  $\mu$ M, respectively. These results point out that there are significant influences of the substituents on  $\beta$ -indolyketone scaffold in the *in vitro* cytotoxicity, being the fluorinated  $\beta$ -indolyketone **3.3c** the less cytotoxic compound ( $IC_{50}$  = 658.1  $\mu$ M) (entry 3, **Table 3.3**) and the  $\beta$ -indolyketone **3.3a**, bearing a methoxy group, the one with highest cytotoxicity ( $IC_{50}$  = 96.5  $\mu$ M) (entry 1, **Table 3.3**).

Nevertheless, it is important to recall that PET is an exquisitely sensitive technique, able to measure *in vivo* radiopharmaceutical concentration in the nanomolar to picomolar range and, consequently, the radiopharmaceutical is not expected to have any pharmacological effect.<sup>31</sup> Therefore, these *in vitro* studies in 3T3 cells indicated that the compounds **3.3a-c** show no cell toxicity in the concentration range used for the *in vivo* PET imaging, allowing for the safe administration of these compounds.

Furthermore, the determination of LogP values is also key parameter to infer the BBB permeability, and subsequently the radiopharmaceutical's brain uptake. In this context, we also evaluated the relative lipophilicity of each  $\beta$ -indolylketone *via* theoretical determination of octan-1-ol/water partition coefficient values (ClogP), using a computational approach (program Marvin Sketch 14.10.6.0). The results are summarized in **Table 3.3**. The  $\beta$ -indolylketones have a ClogP values ranging 2.73 to 3.13, which fulfill the LogD<sub>7.4</sub> recommendations for the development of ideal radiopharmaceutical to successfully penetrate in BBB (2–3.5).<sup>3b,5</sup> However, in this work, we only determined the ClogP values, not the experimental LogD<sub>7.4</sub> values. This is worth mentioning, since computational approaches have been frequently employed by several authors to predict the LogD<sub>7.4</sub>, where a report by Wagner *et al.*<sup>32</sup> states that the mean value for ClogP for 119 marketed central nervous system (CNS) drugs is 2.8. In this work, the ClogP mean value for the *N*-methylated  $\beta$ -indolylketones **3.3a-c** is 2.9, a value that is in good agreement with the suitable range. The trend observed for ClogP values is: **3.3a** < **3.3c** < **3.3b**; where the most lipophilic compound (higher ClogP) is bromine  $\beta$ -indolylketone **3.3b** (entry 2, **Table 3.3**) and the less lipophilic compound (lower ClogP) is the  $\beta$ -indolylketone substituted bearing a methoxy group **3.3a** (entry 1, **Table 3.3**).

We can conclude that the *N*-methylated  $\beta$ -indolylketones **3.3a-c**, synthesized in this work, combine an interesting low *in vitro* cytotoxicity with suitable ClogP values, encouraging us to pursue the <sup>11</sup>C-labelling studies of this  $\beta$ -indolylketones as potential brain PET imaging probes. Due to time constraints, we only performed the <sup>11</sup>C-labelling studies of one  $\beta$ -indolylketone compound. We selected the fluorinated  $\beta$ -indolylketone **3.3c** to proceed to the further <sup>11</sup>C-labelling reaction, considering its good balance between low cellular cytotoxicity (IC<sub>50</sub> = 658.1  $\mu$ M) and suitable ClogP value (2.80).

### 3.4 Radiolabelling of $\beta$ -indolyketones with carbon-11

#### 3.4.1 Labelling methodology

One of the most commonly used strategies for the production of  $^{11}\text{C}$ -labelled compounds involves the use of [ $^{11}\text{C}$ ]iodomethane ([ $^{11}\text{C}$ ]CH<sub>3</sub>I), as  $^{11}\text{C}$ -methylating agent to promote the labelling of non-methylated compounds with N-, O- and S-heteroatoms, through a simple nucleophilic substitution reaction.<sup>33</sup> As an example, the routinely used  $^{11}\text{C}$ -labelled PET radiopharmaceuticals, [ $^{11}\text{C}$ ]PiB, [ $^{11}\text{C}$ ]Flumazenil and [ $^{11}\text{C}$ ]Choline are prepared via *N*- $^{11}\text{C}$ -methylation (**Figure 3.7**).<sup>34</sup> These standard reactions are usually carried out in solvents such as DMF, DMSO, acetone or acetonitrile depending on the temperature and/or polarity required for reaction. Essentially, [ $^{11}\text{C}$ ]CH<sub>3</sub>I is directly driven into the solution which contains the non-methylated precursor (typically in large excess) and usually a base (such as sodium hydroxide, sodium hydride, potassium carbonate or tetrabutylammonium hydroxide), which is used to deprotonate the functional group (amines, hydroxyl and thiol groups). These methylation reactions, occurs within a short period of time (1-10 minutes) and reaction temperatures vary in a range from room temperature to 100 °C.<sup>35</sup>

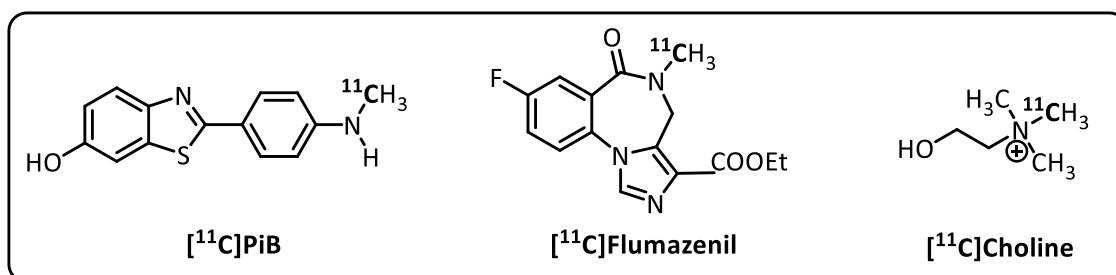


**Figure 3.7.** Illustrative  $^{11}\text{C}$ -labelled radiopharmaceuticals by *N*- $^{11}\text{C}$ -methylation.<sup>34</sup>

Since [ $^{11}\text{C}$ ]CH<sub>3</sub>I is a volatile intermediate and larger quantities of activity is expected in the carbon-11 radiochemistry process due to the short carbon-11 half-life, the traditional manual manipulation using lead castles for radiochemist's radiation protection are not feasible. Therefore, to minimize the radiation exposure, the production of  $^{11}\text{C}$ -labelled radiopharmaceuticals is carried out in semi-automated or fully automated radiosynthesis modules, housed inside the so called hot-cells.<sup>36,37</sup> These automated modules are a unit remotely controlled by computers with software



programs, which allows sequentially carrying out the different steps of the carbon-11 synthesis and its labelling reaction with a strict control of the flow, pressure, temperature and activity. Obviously, these computer-controlled automation modules are desirable for the routine commercial production of PET radiopharmaceuticals. The **Figure 3.8** shows the carbon-11 automated radiosynthesis module housed inside the hot-cell in the Radiochemistry and Cyclotron Laboratory at ICNAS, where the  $^{11}\text{C}$ -labelling experiments were performed.

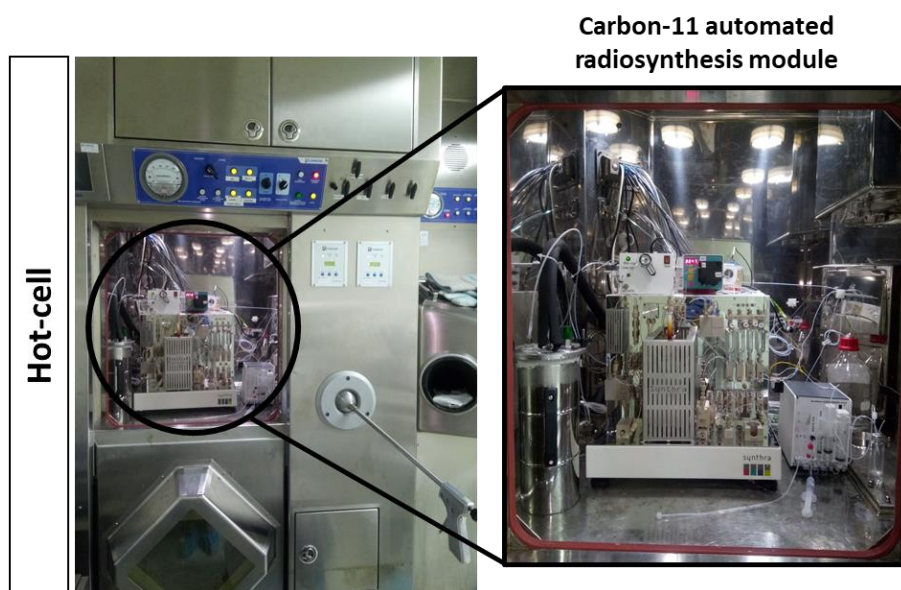


**Figure 3.8.** Carbon-11 automated radiosynthesis module housed inside the hot-cell in the Radiochemistry and Cyclotron Laboratory at ICNAS.

To better understand the operation settings of the above pictured carbon-11 automated radiosynthesis module a schematics is displayed in **Figure 3.9**. All the parts of the automated module are connected via tubes and externally controllable valves, being all gaseous or liquids, precursors, intermediates, and products transferred with a helium flow.

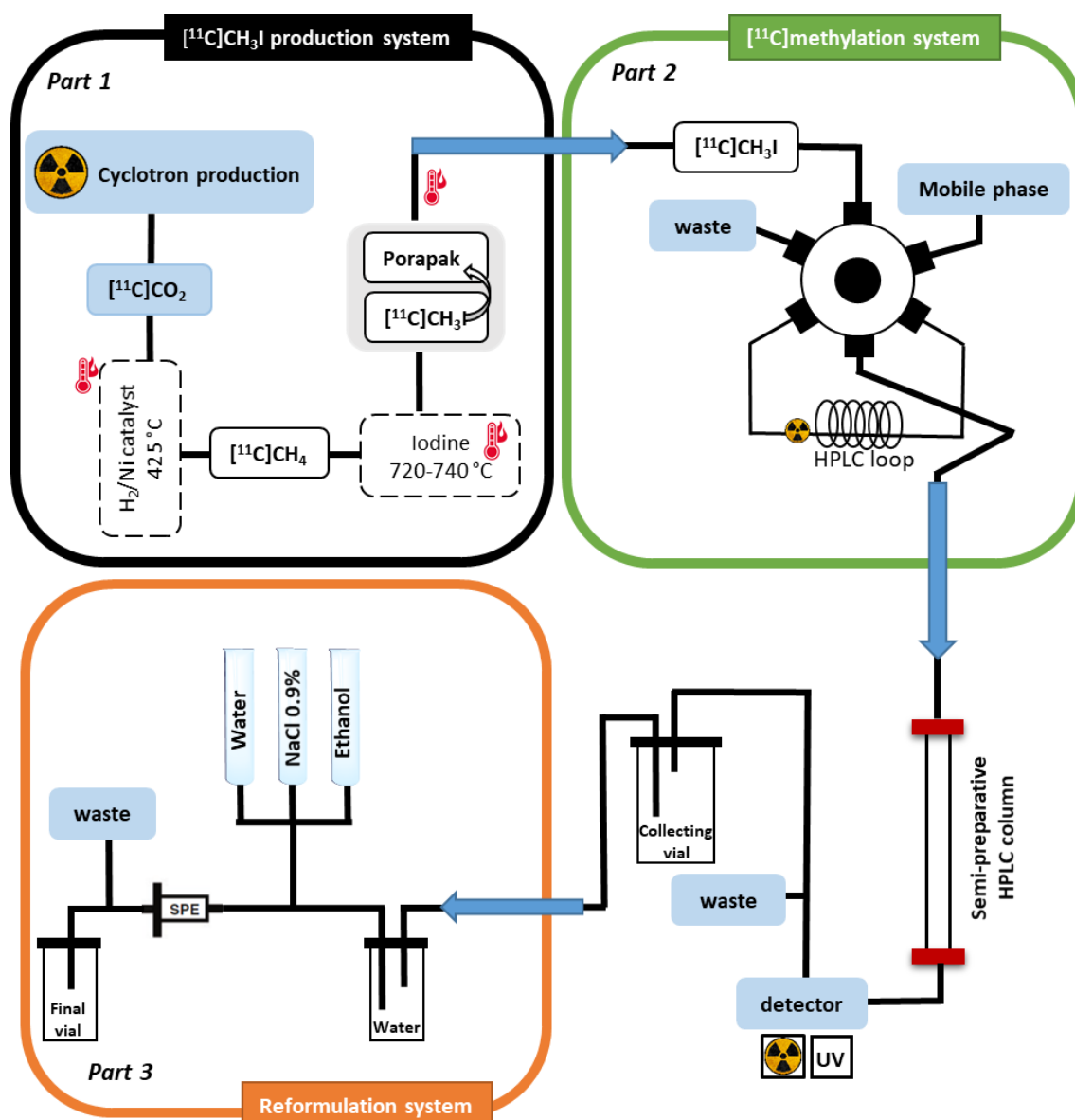


**Figure 3.9.** Schematic diagram of the carbon-11 automated radiosynthesis module used in this work at ICNAS (captive solvent “loop” method for  $^{11}\text{C}$ -methylation).

The first part of the automated radiosynthesis module is the  $^{11}\text{C}$ CH<sub>3</sub>I production system, aiming the production of the  $^{11}\text{C}$ -methylating agent  $^{11}\text{C}$ CH<sub>3</sub>I (Part 1, **Figure 3.9**). Carbon-11 can be produced by several nuclear reactions in the cyclotron.<sup>38</sup> Among them,  $^{14}\text{N}(p,\alpha)^{11}\text{C}$  reaction is by far the most commonly used in the radiochemistry field,<sup>34,39</sup> being also the one used for this work. The  $^{14}\text{N}(p,\alpha)^{11}\text{C}$  reaction uses nitrogen gas with 0.5% of oxygen as a target material, which is irradiated with a 16.5 MeV proton beam yielding  $^{11}\text{C}$ carbon dioxide ( $^{11}\text{C}$ CO<sub>2</sub>). Starting from  $^{11}\text{C}$ CO<sub>2</sub>, the synthesis of the radioactive precursor  $^{11}\text{C}$ CH<sub>3</sub>I is accomplished by the so called “gas method”.<sup>35,40</sup> Essentially, the  $^{11}\text{C}$ CO<sub>2</sub> produced is further converted in  $^{11}\text{C}$ methane ( $^{11}\text{C}$ CH<sub>4</sub>)

through a hydrogen reduction in presence of a nickel catalyst, at 425 °C. In a second step, the  $[^{11}\text{C}]\text{CH}_4$  reacts with iodine vapor, at  $\approx 720\text{--}740$  °C, to produce the desired  $[^{11}\text{C}]\text{CH}_3\text{I}$ . The product  $[^{11}\text{C}]\text{CH}_3\text{I}$  is trapped on a Porapak® cartridge and, upon heat induced releasing, is transferred by a helium stream to the  $^{11}\text{C}$ -methylation system (Part 2, **Figure 3.9**). In this system, based on the captive solvent “loop” method,<sup>41</sup> the  $^{11}\text{C}$ -methylation labelling reaction takes place in a HPLC loop previously prepared. Thus, before the synthesis, the precursor solution, in the presence of base, is slowly injected into the stainless steel loop (100  $\mu\text{l}$ ). Then, the produced  $[^{11}\text{C}]\text{CH}_3\text{I}$  is led into the loop with the precursor solution and it becomes efficiently trapped. Therein, the  $^{11}\text{C}$ -methylation labelling of the precursor occurs, yielding the desired radiolabelled product, which is directly injected into a semi-preparative HPLC column for purification. The separation of different chemical and radiochemical species (*e.g.* precursor separation from the radiolabelled product and possible by-products) is achieved by an UV and radioactivity detector, which are positioned at the end of the semi-preparative HPLC column. After collect the desired radiolabelled product and aiming the reformulation of the radiolabelled product from the HPLC mobile phase into a suitable intravenous injection, the collected radiolabelled product is diluted with water, and then trapped into a reversed phase C18 solid-phase extraction (SPE) cartridge (Part 3, **Figure 3.9**). The C18 SPE cartridge is rinsed with sufficient water to effectively remove any residual organic solvents from HPLC mobile phase. The product is eluted of the C18 SPE cartridge to the final product vial with small volume of ethanol (<10 % v/v ethanol of total final product volume) and diluted with a sodium chloride (NaCl) solution (0.9% w/v). Additionally, this automated synthesis module also includes a solvent delivery module, which controls the introduction of cleaning solvents and the nitrogen gas into the systems, as well as a waste recovery module, which is the recipient of the waste gas and solvents during the synthesis and cleaning processes.

The considerably short half-life of carbon-11 (20.4 min) requires that the synthesis time for any  $^{11}\text{C}$ -labelled radiopharmaceuticals should be performed as quickly as possible. It should be noticed that the synthesis, purification, reformulation and quality control of PET radiopharmaceuticals and its delivery to the clinical PET facility should not exceed two to three half-lives of the radioisotope in use, which for carbon-11 this is about 40 to 60 minutes.<sup>36,42</sup>

### 3.4.2 Optimization of HPLC conditions

As mentioned before, the total production time for  $^{11}\text{C}$ -labelled radiopharmaceuticals must be kept as short as possible. Besides short methylation reaction times, the main approach to accomplish this purpose is to ensure the selection of the best chromatographic system since a long separation time, either during the purification or during quality parameters checking previous to *in vivo* administration, will obviously limit the total activity of the final  $^{11}\text{C}$ -labelled product. Keeping this in mind, after the selection of *N*-methylated  $\beta$ -indolylketone **3.3c** as lead compound, we proceeded to the optimization of the HPLC conditions, which was equipped with: i) a semi-preparative column, for further  $^{11}\text{C}$ -labelled product purification and ii) an analytical column, for radiolabelled compound purity check and radiochemical identity confirmation. Since the  $^{11}\text{C}$ -labelling experiments were carried out in the ICNAS facility, the optimization process was carried out using the therein available equipment, namely the semi-preparative and analytical reversed phase C18 HPLC columns, ensuring exactly the same chromatographic conditions.

So, we began the studies with the optimization of the separation conditions of the precursor  $\beta$ -indolylketone **3.2c** and *N*-methylated product **3.3c** in the analytical HPLC column, by injecting 20  $\mu\text{L}$  of the respective  $\beta$ -indolylketone dissolved in acetonitrile. In this study, mixtures of ammonium formate buffer solution (0.1M, pH = 7.2) and acetonitrile were used as mobile phase and the results are presented in **Table 3.4**.

**Table 3.4** Optimization of separation conditions in analytical HPLC column of the previously isolated pure products. Buffer: 0.1 M Ammonium Formate (pH=7.2).

Entry	Mobile phase (v/v)	Flow (mL.min <sup>-1</sup> )	Product	t <sub>R</sub> (min)
1	50% acetonitrile 50% buffer	1	3.2c	12.78
			3.3c	23.17
2		3.2c	6.26	
		3.3c	11.68	
3		3	3.2c	4.28
			3.3c	8.08
4	65% acetonitrile 35% buffer	1	3.2c	3.34
			3.3c	5.12
5		2	3.2c	1.51
			3.3c	2.42
6		3	3.2c	1.20
			3.3c	1.55

We started these studies by using an eluent mixture with 50% acetonitrile: 50% ammonium formate buffer, in a 1 mL.min<sup>-1</sup> flow rate (entry 1, **Table 3.4**). Under these conditions, the  $\beta$ -indolyketone **3.2c** showed a retention time (t<sub>R</sub>) 12.78 minutes, while the *N*-methylated product **3.3c** had a retention time of 23.17 minutes. Since our goal was the synthesis of <sup>11</sup>C-labelled compounds, these retention times were considered too long, and therefore we needed to increase the flow rate for 2 and 3 mL.min<sup>-1</sup> (entries 2-3, **Table 3.4**). Even with 3 mL.min<sup>-1</sup> flow rate, the  $\beta$ -indolyketone **3.2c** showed a retention time of 4.28 minutes, while the *N*-methylated product **3.3c** had a retention time of 8.08 minutes. These reduced retention times, although improved, were not considered optimal. In order to reduce the affinity of the products **3.2c** and **3.3c** for the stationary phase, we then increased the polarity of the mobile phase, by increasing the acetonitrile fraction to 65%, again changing the flow rates (entries 4-6, **Table 3.4**). With a 1 mL.min<sup>-1</sup> flow, the  $\beta$ -indolyketone **3.2c** showed a retention time of 3.34 minutes, while the *N*-methylated product **3.3c** had a retention time of 5.21 minutes. Using a 2 mL.min<sup>-1</sup> flow, the retention times for both compounds decreased to half, while in case of a 3 mL.min<sup>-1</sup> flow rate the retention times for both products were very similar, which could compromise the efficient separation of compounds **3.2c** and **3.3c**.

In conclusion, we selected as best chromatographic conditions the mixture 65% acetonitrile:35% buffer (0.1M ammonium formate; pH = 7.2) at a 2 mL.min<sup>-1</sup> flow rate. Under these conditions, the precursor  $\beta$ -indolyketone **3.2c** exhibits a retention of 1.51 minutes and the *N*-methylated product **3.3c** a retention time of 2.42 minutes (**Figure 3.9**), where the isolated peaks shown in the chromatograms (A and B, **Figure 3.9**) were assigned by injection of the pure products, previously isolated and characterized.

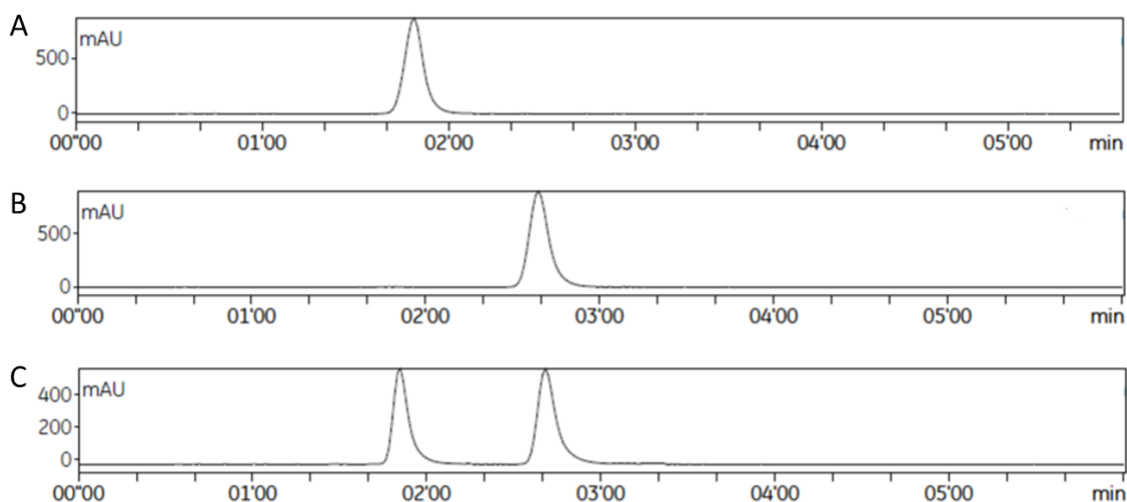


**Figure 3.9.** Analytical HPLC chromatograms with the mobile phase acetonitrile/buffer (65:35, v:v) at a flow of 2 mL.min<sup>-1</sup> of: **A** –  $\beta$ -indolyketone **3.2c** ( $t_R \approx 1.51$  min); **B** – *N*-methylated  $\beta$ -indolyketone **3.3c** ( $t_R \approx 2.42$  min) and **C** – co-injection of both  $\beta$ -indolyketones **3.2c** and **3.3c**. (UV detector = 254 nm).

After optimization of the HPLC conditions for the analytical control of the final <sup>11</sup>C-labelled product, we needed to similarly proceed for the semi-preparative system. In this step, it is crucial to have an adequate HPLC resolution between the peak corresponding to <sup>11</sup>C-labelled product from the peak corresponding to the precursor. In the radiosynthesis process the precursor is generally used in large excess, thus it will be expected a considerable amount of this precursor at the final crude mixture. Therefore, in order to prevent an expectable tailing effect of precursor's peak in the HPLC chromatogram, capable to contaminate or even mask the peak corresponding to <sup>11</sup>C-labelled product, which is intended to separate and collect, it is fundamental to ensure a satisfactory difference between each peak to ensure the chemical purity of the final product.

To accomplish this purpose, we began our studies in the semi-preparative HPLC system by injecting 100  $\mu\text{L}$  of the respective  $\beta$ -indolyketone dissolved in DMF, and the results are presented in **Table 3.5**.

**Table 3.5.** Optimization of the separation conditions in semi-preparative HPLC column of the previously isolated pure products. Buffer: 0.1 M Ammonium Format (pH = 7.2)

Entry	Mobile phase (v/v)	Flow ( $\text{mL}\cdot\text{min}^{-1}$ )	Product	$t_R$ (min)
1	65% acetonitrile 35% buffer	6	3.2c	9-10
			3.3c	13-14
		7	3.2c	8-9
			3.3c	11.3-12.3
		9	3.2c	6.5-7.5
			3.3c	9.5-10.7
2	70% acetonitrile 30% buffer	9	3.2c	4.5-6
			3.3c	6.3-7.3
3	80% acetonitrile 20% buffer	4	3.2c	5.7-6.7
			3.3c	7.3-8.7
		5	3.2c	4.7-5.3
			3.3c	6-7

Based on previous results for the analytical HPLC column, we initiated the studies using the mixture 65% acetonitrile: 35% ammonium formate buffer (0.1 M, pH = 7.2), as mobile phase, at a 6  $\text{mL}\cdot\text{min}^{-1}$  flow rate (entry 1, **Table 3.5**). Under these conditions, a good separation was obtained; however, retention times were much too high for our needs (9-10 min and 13-14 min for **3.2c** and **3.3c**, respectively). Maintaining the eluent ratio and increasing the flow to 7  $\text{mL}\cdot\text{min}^{-1}$ , we observed a decrease in retention times, but still not sufficient for our purposes ( $\approx$ 8-9 min and  $\approx$ 11-12 min for **3.2c** and **3.3c**, respectively). We could only find more adequate retention times when a 9  $\text{mL}\cdot\text{min}^{-1}$  flow rate was used (entry 1, **Table 3.5**). We then carried on additional chromatographic test runs, using eluents with higher acetonitrile fractions at several flow rates (entries 2-3, **Table 3.5**). However, the retention times for **3.2c** and **3.3c** were very similar in all

experiments, which could compromise the efficient separation of the  $^{11}\text{C}$ -labelled product from the precursor **3.2c**.

In conclusion, the best conditions available were when a  $9\text{ mL}\cdot\text{min}^{-1}$  flow rate with 65% acetonitrile: 35% ammonium formate buffer (0.1 M, pH = 7.2) as mobile phase were used. Under these conditions, the  $\beta$ -indolylketone **3.2c** showed a retention time between  $\approx 6.5$ -7.5 minutes (390-450 seconds) and *N*-methylated product **3.3c** between  $\approx 9.7$ -10.7 minutes (580-640 seconds) (**Figure 3.10**).

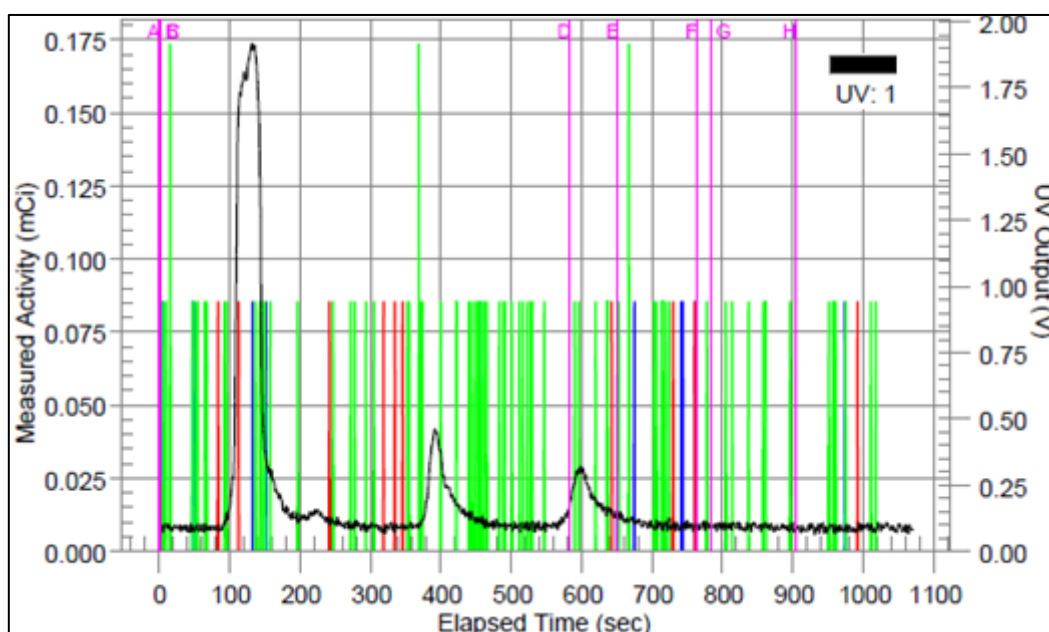


**Figure 3.10.** Semi-preparative HPLC chromatogram of co-injection of **3.2c** ( $t_R \approx 390$ -450 seconds) and product **3.3c** ( $t_R \approx 580$ -640 seconds) with eluent acetonitrile/buffer (65:35, v:v) at flow of  $9\text{ mL}\cdot\text{min}^{-1}$ . The first peak corresponds to DMF solvent. (UV: 1 = 254 nm)

Summarizing, the best and used chromatographic conditions during all purification and quality control processes were an isocratic acetonitrile/ammonium formate buffer (0.1 M, pH = 7.2) (65:35, v:v) mobile phase with a flow rate of  $9\text{ mL}\cdot\text{min}^{-1}$ , for the semi-preparative HPLC system, and with flow rate of  $2\text{ mL}\cdot\text{min}^{-1}$ , for the analytical HPLC system. Additionally, in order to determine the concentration of the final  $^{11}\text{C}$ -labelled product solution for the *in vivo* administration, an additional experiment was performed in the analytical HPLC system. By injecting 3 replicates of 5 different known concentrations of the *N*-methylated  $\beta$ -indolylketone reference standard **3.3c** in the analytical HPLC column we constructed a reference calibration curve, which allowed



us to precisely estimate the concentration of compound **3.3c** using UV-Vis spectroscopy (Figure 3.11).

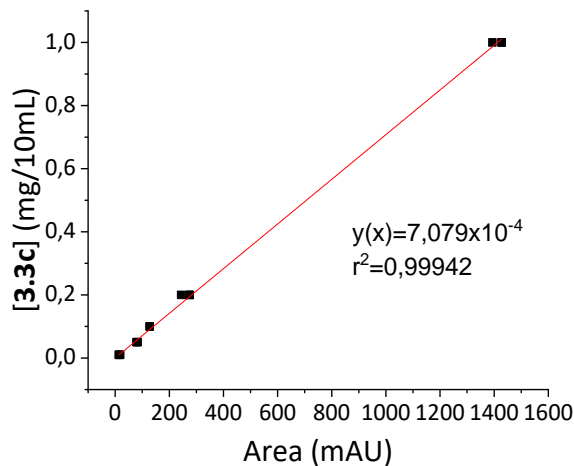
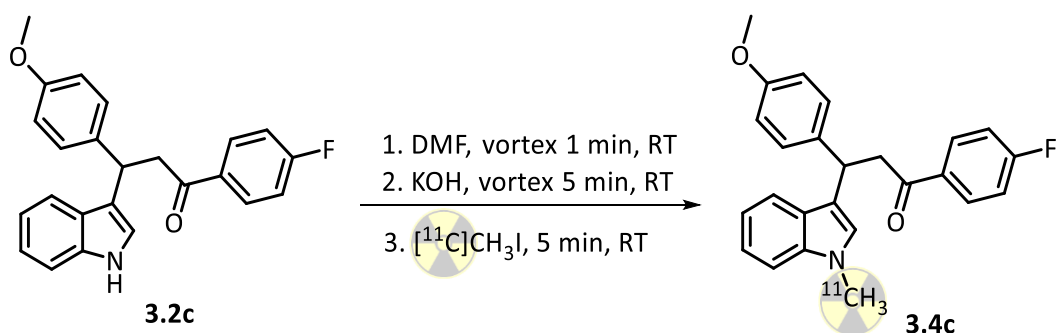


**Figure 3.11.** Reference curve for the calculation of  $\beta$ -indolyketone **3.3c** concentration.

### 3.4.3 Labelling of $\beta$ -indolyketones with [ $^{11}\text{C}$ ]iodomethane

After optimization of the HPLC conditions, we proceeded with the radiolabelling of  $\beta$ -indolyketone **3.2c** in the carbon-11 automated radiosynthesis module, following the procedure described above. As DMF is a commonly used solvent in methylation reactions using [ $^{11}\text{C}$ ]CH<sub>3</sub>I,<sup>43</sup> and possesses the ability to dissolve the precursor **3.2c**, we selected it as the reaction solvent. The process started with the production of the carbon-11 in the cyclotron in the form of [ $^{11}\text{C}$ ]CO<sub>2</sub>. The produced [ $^{11}\text{C}$ ]CO<sub>2</sub> was then converted to [ $^{11}\text{C}$ ]CH<sub>4</sub> which, by reaction with gaseous iodine, giving the desired [ $^{11}\text{C}$ ]CH<sub>3</sub>I methylation agent. In parallel, the non-methylated  $\beta$ -indolyketone **3.2c** was stirred in DMF in presence of KOH (for deprotonation). This solution was injected into the HPLC stainless loop of the carbon-11 automated radiosynthesis module. Then, the produced [ $^{11}\text{C}$ ]CH<sub>3</sub>I was driven through the loop, pre-filled with the solution of the non-methylated precursor **3.2c**, and allowed to react for 5 min, at room temperature (Scheme 3.3).



**Scheme 3.3.** Radiosynthesis of  $^{11}\text{C}$ -labelled  $\beta$ -indolyketone **3.4c**.

After 5 min reaction in the loop, the final crude mixture was immediately injected into the semi-preparative HPLC column of the carbon-11 automated radiosynthesis module for purification, where the analysis was performed through the UV (254 nm) and radioactivity detectors. The semi-preparative HPLC chromatogram obtained is shown in **Figure 3.12**.

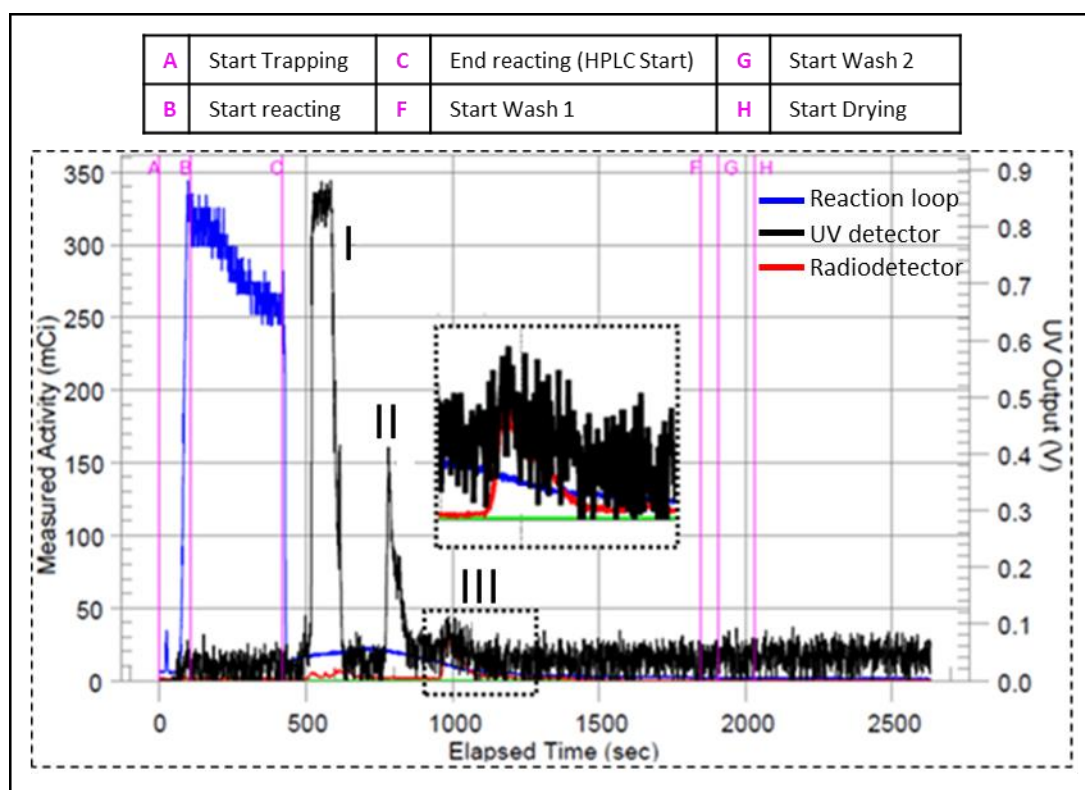


**Figure 3.12.** Control of the reaction by UV at 254 nm (black line) and radioactivity (red line) associated with semi-preparative HPLC apparatus. Conditions: acetonitrile/0.1M ammonium formate buffer (65:35, v:v) and  $9 \text{ mL}\cdot\text{min}^{-1}$  flow rate. Consider time 0 seconds after 419 seconds for HPLC chromatogram analysis purposes (identified as C point).

From the HPLC chromatogram analysis (**Figure 3.12**), two distinctive peaks, related to UV absorption, were observed. The first one, identified as peak **I**, located at 100-190 seconds, was attributed to the DMF solvent, while the second (peak **II**), with a retention time of  $\approx$  390-450 seconds, was assigned to the precursor  $\beta$ -indolyllketone **3.2c**, as expected, given the large excess used in the reaction. Another peak (identified as peak **III**), between  $\approx$  580-640 seconds, was also observed, corresponding to the desired  $^{11}\text{C}$ -labelled product **3.4c**. A slight overlap of peaks **II** and **III** in the chromatogram was observed, an aspect that can compromise the purity of the final  $^{11}\text{C}$ -labelled product. Then, the compound related to peak **III** was collected from the semi-preparative HPLC system and subsequently driven into the SEP system for reformulation, as follows: the collected HPLC fraction was first diluted in a vial (by adding ca 5-10 mL of water), and then slowly passed through a C18 SPE cartridge. As the  $^{11}\text{C}$ -labelled product **3.4c** was retained in the C18 SPE cartridge, elution with additional 15 mL of water followed, to ensure complete removal of the acetonitrile:buffer solution. Finally,  $^{11}\text{C}$ -labelled product **3.4c** was recovered by elution with additional 1 mL of ethanol, and again diluted by addition of 9 mL of 0.9% NaCl (also passed through the C18 SPE cartridge), affording the reformulated  $^{11}\text{C}$ -labelled product **3.4c**. The radiochemical yield (*i.e.* the ratio of the activity of the  $^{11}\text{C}$ -labelled product after its reformulation and the starting  $[^{11}\text{C}]\text{CO}_2$  activity obtained from the cyclotron; non-decay corrected) was  $21.2 \pm 0.90\%$  ( $n=3$ ).

The reformulated product **3.4c** was subsequently submitted to quality control using the analytical HPLC system, using an UV (254 nm) and radioactivity detectors (**Figure 3.13**), under the previously optimized conditions.

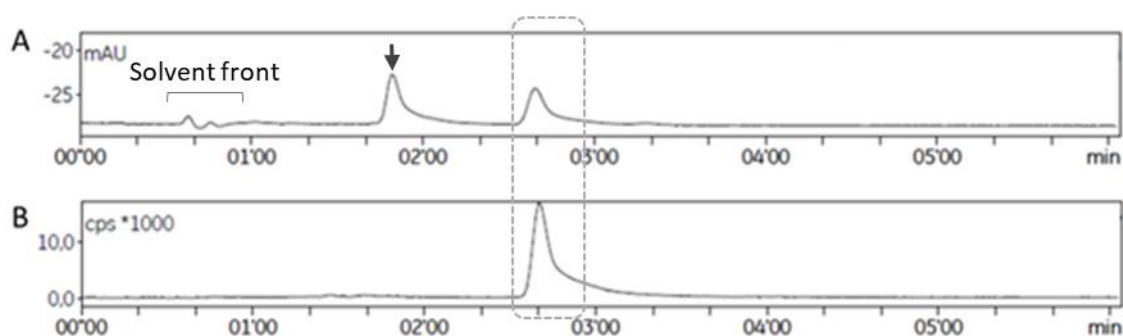


**Figure 3.13.** Radio-chromatogram of  $^{11}\text{C}$ -labelled product **3.4c** ( $t_{\text{R}} = 2.42$  min). **A:** UV (254 nm) and **B:**  $\gamma$ -detection, recorded simultaneously. Conditions: acetonitrile/0.1 M ammonium formate buffer solution (65:35, v:v) as a mobile phase with flow of  $2 \text{ mL}\cdot\text{min}^{-1}$ .

Both UV (A) and radioactivity detection (B) chromatograms in **Figure 3.13** displayed a peak with a retention time at 2.42 minutes, attributed to  $^{11}\text{C}$ -labelled product **3.4c**, corroborating its efficient synthesis. Additionally, using the UV (A) detector, a peak at around 1.51 minutes, attributed to the unreacted precursor **3.2c**, was also observed. **Figure 3.3** demonstrates that the labelling of **3.2c** with radioactive  $[^{11}\text{C}]\text{CH}_3\text{I}$  was successfully accomplished, and  $^{11}\text{C}$ -labelled  $\beta$ -indolylketone **3.4c** was obtained in a radiochemical purity of  $> 98\%$ . However, the chemical purity was obtained in just  $\approx 50\%$ , which can be attributed to the tailing effect of the precursor's peak in the semi-preparative HPLC chromatogram (peak II, **Figure 3.12**), which partially overlaps with the peak related to the target compound (peak III, **Figure 3.12**). This issue is attributed to the use of a large excess (increased concentration) of the precursor (peak II, **Figure 3.12**). Nevertheless, we are able to determinate the concentration of the final  $^{11}\text{C}$ -labelled product **3.4c** solution for potential *in vivo* administration, according to **Figure 3.11**, which was found to be  $3.13 \pm 0.12 \mu\text{M}$  ( $n=3$ ), a value much lower than its  $\text{IC}_{50}$  value ( $658.1 \mu\text{M}$ ).

Aiming to accomplish the maximum chemical purity possible, a new  $^{11}\text{C}$ -labelling experiment was performed, with some adjustments in the conditions used in the semi-preparative HPLC system. So, an isocratic acetonitrile/0.1M ammonium formate buffer (0.1 M, pH = 7.2) (65:35, v:v) mobile phase with a flow rate of  $6 \text{ mL}\cdot\text{min}^{-1}$  (entry 1, **Table 3.5**) was used in the semi-preparative purification, performed after the radiolabelling process, using the same reaction conditions described above (**Scheme**

3.3). Again, the semi-preparative HPLC chromatogram analysis was performed using the UV (254 nm) and radioactivity detectors (**Figure 3.14**).

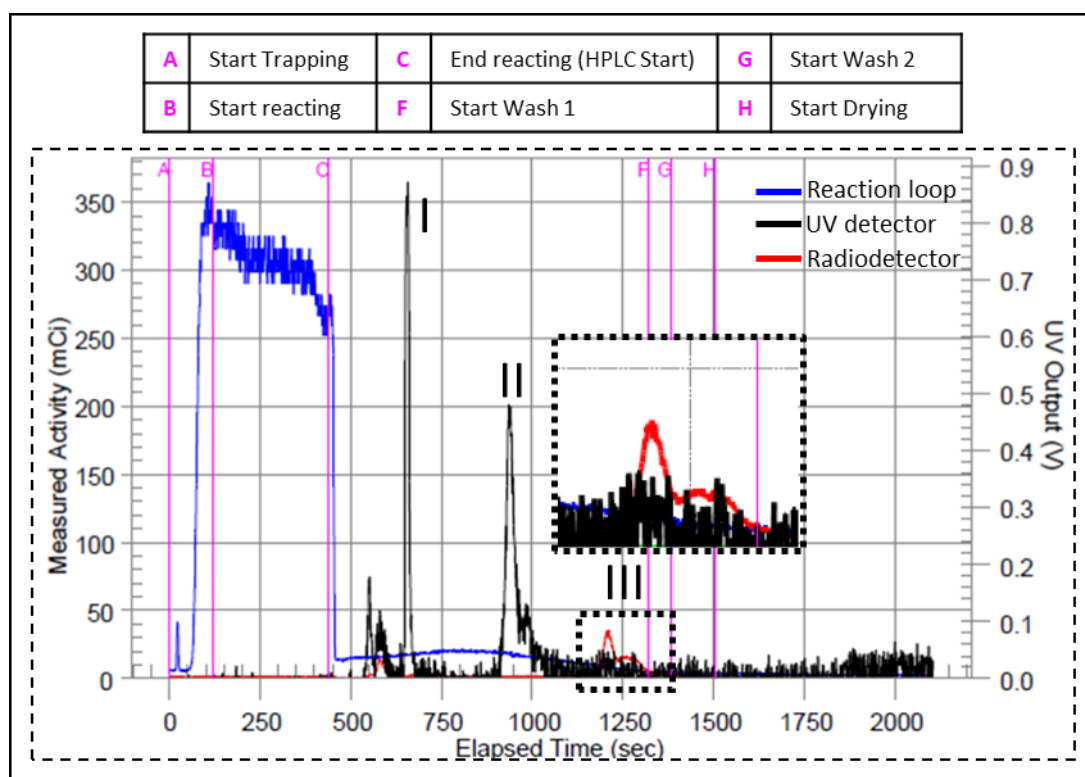


**Figure 3.14.** Control of the reaction by UV at 254 nm (black line) and radioactivity (red line) associated with semi-preparative HPLC apparatus. Conditions: acetonitrile/ 0.1M ammonium formate buffer (65:35, v:v) and 6 mL.min<sup>-1</sup> flow rate. Considering time 0 seconds after 419 seconds for HPLC chromatogram analysis purposes (identified as C point).

**Figure 3.14** displays, once again, two distinctive peaks in the chromatogram related to UV absorption. The first, identified as peak I, was attributed to DMF solvent, while the second peak, identified as peak II, with a retention time of  $\approx$  540-600 seconds, was assigned to the precursor  $\beta$ -indolyketone **3.2c**. In the chromatogram related to radioactivity, the <sup>11</sup>C-labelled product **3.4c**, identified as peak III, was collected, showing activity between  $\approx$ 780-840 seconds. According to **Figure 3.14**, negligible or no overlap of peak II (precursor) and peak III (<sup>11</sup>C-labelled product **3.4c**) was found, as desired. As described before, the compound related to peak III was collected, the solvent was removed by the SPE system, after which the product was reformulated in 0.9% NaCl/ EtOH (9:1, v/v), to produce an intravenous injection solution. The non-decay corrected

radiochemical yield was  $9.5 \pm 0.8\%$  ( $n=3$ ). The reformulated  $^{11}\text{C}$ -labelled product **3.4c** was subsequently re-submitted to previously optimized quality control using the analytical HPLC system, as depicted in **Figure 3.15**.

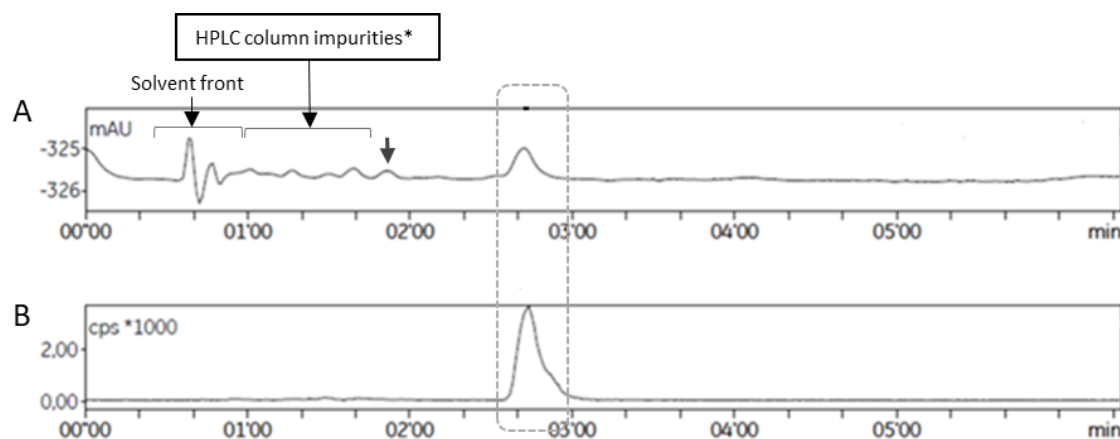


**Figure 3.15.** Radio-chromatogram of  $^{11}\text{C}$ -labelled product **3.4c** ( $t_R = 2.42$  min). **A:** UV (254 nm) and **B:**  $\gamma$ -detection, recorded simultaneously. Conditions: acetonitrile/0.1 M ammonium formate buffer solution (65:35, v:v) as a mobile phase with flow of  $2 \text{ mL}\cdot\text{min}^{-1}$ . (\*a “blank” was previously carried out in HPLC apparatus before the  $^{11}\text{C}$ -labelled product **3.4c** solution injection).

From the analysis of **Figure 3.15**, a peak at 2.42 min could be observed both in UV (A) and radioactivity (B) detection, as previously observed in the non-radioactive conditions (**Figure 3.9**). This corroborates, once again, the efficient synthesis of  $^{11}\text{C}$ -labelled product **3.4c**. As observed before for the UV (A) detector, a peak at  $\approx 1.51$  minutes, attributed to the unreacted precursor **3.2c** was also found. The substantially lower quantity observed ( $< 10\%$ ), when compared to the previous  $^{11}\text{C}$ -labelling reaction (50%, **Figure 3.13**), allowed us to nearly accomplish the maximum chemical purity ( $\geq 95\%$ ). Therefore, it should be emphasized that both labelling of  $\beta$ -indolyketone **3.2c** with carbon-11 and its purification processes were quite successfully accomplished, since the  $^{11}\text{C}$ -labelled  $\beta$ -indolyketone **3.4c** was obtained in a radiochemical purity  $> 98\%$  and with a chemical purity  $\approx 90\%$ .

To unequivocally confirm the radiochemical identity of the  $^{11}\text{C}$ -labelled product **3.4c**, we further performed the co-injection and co-elution on HPLC of both radiolabelled product **3.4c** and the corresponding non-radioactive reference standard **3.3c** (**Figure 3.16**). This allowed us to corroborate the radiochemical identity of

$^{11}\text{C}$ -labelled product **3.4c** as, both by UV (A) and radioactivity detection (B), just one peak with a retention time between 2.42 min was found.

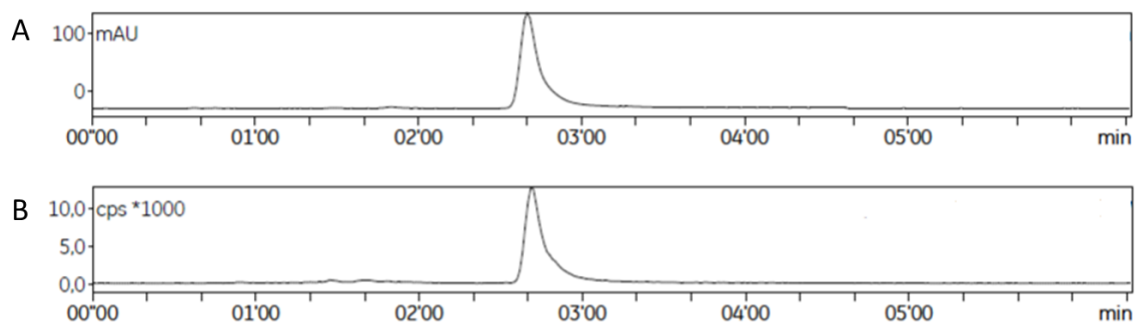


**Figure 3.16.** Radio-chromatogram of co-injection of  $^{11}\text{C}$ -labelled product **3.4c** and non-radioactive reference standard **3.3c**. **A:** UV (254 nm) and **B:**  $\gamma$ -detection, recorded simultaneously. Conditions: acetonitrile/0.1 M ammonium formate buffer solution (65:35, v:v) as a mobile phase with flow of  $2 \text{ mL}\cdot\text{min}^{-1}$ .

From **Figures 3.15** and **3.11**, we determined that the concentration of the final  $^{11}\text{C}$ -labelled product **3.4c** solution for the *in vivo* administration was  $1.2 \pm 0.3 \mu\text{M}$  ( $n=3$ ) which is much below its  $\text{IC}_{50}$  value ( $658.1 \mu\text{M}$ ). To ensure the safety of the reformulated  $^{11}\text{C}$ -labelled compound **3.4c** for *in vivo* experiments, some parameters were quantified using analytical techniques according to the general radiopharmaceutical preparations monograph prescribed by the European Pharmacopoeia (Ph. Eur.).<sup>44</sup> Levels of residual solvents in final injection solution were quantified by GC/FID (see **Figure 3.17**). Since the  $^{11}\text{C}$ -labelled compound **3.4c** injection solution was a solution 0.9% NaCl/EtOH (9:1, v/v) and acetonitrile belongs of the mobile phase, these were the two possible organic volatile impurities that could be present in the final injection solution within the limits described at Ph. Eur. (acetonitrile  $\leq 4.1 \text{ mg}/10 \text{ mL}$  and ethanol  $\leq 2500 \text{ mg}/10 \text{ mL}$ ).<sup>44,45</sup> Both acetonitrile and ethanol amounts detected –  $2.9 \pm 0.8$  ( $n=3$ ) and  $445.2 \pm 51.6$  ( $n=3$ ), respectively – in the reformulated  $^{11}\text{C}$ -labelled product **3.4c** were below the limit allowed for *in vivo* intravenous administration.

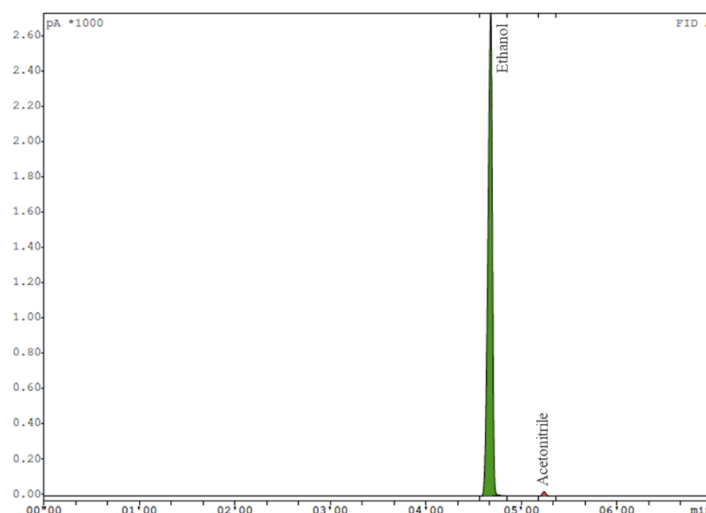


**Figure 3.17.** Gas chromatography of the  $^{11}\text{C}$ -labelled product **3.4c** injection solution.  $t_R$  (ethanol): 04'41'' min and  $t_R$  (acetonitrile): 05'14'' min.

Concerning the pH testing, the value obtained was  $5.8 \pm 0.7$  ( $n=3$ ) which is in agreement with the Ph. Eur. referenced range for radiopharmaceutical injection solutions (pH = 4.5-8.5).<sup>44</sup>

Other relevant parameter concern the radioisotope purity and its identity, and both were assessed by the radioisotope half-life ( $t_{1/2}$ ). We obtained a half-life value of  $20.4 \pm 0.1$  ( $n=3$ ) for the  $^{11}\text{C}$ -labelled compound **3.4c**, clearly indicating the absence of other radioisotopes, which may be present when a deviation of more than 5% of the expected value (20.4 minutes for carbon-11) occurs.<sup>44</sup>

Regarding the time necessary to obtain the  $^{11}\text{C}$ -labelled compound **3.4c**, the total preparation time, including radiosynthesis, HPLC purification, product reformulation and quality control (analytical HPLC analysis, pH, GC and half-life) was 53 minutes, which is within the acceptable time frame for radiopharmaceutical viability (less than 60 minutes for carbon-11).

### 3.5 Exploratory *in vivo* PET imaging and biodistribution studies of $^{11}\text{C}$ -labelled $\beta$ -indolyketones

The studies described in this section were performed in collaboration with ICNAS Pre-Clinical Imaging Facility, where Dr. José Sereno (PhD) executed the imaging



experiments described below. Due to time constraints, we only performed the radiosynthesis of the  $^{11}\text{C}$ -labelled  $\beta$ -indolyketone **3.4c** (Figure 3.18). However, aiming the *in vivo* biodistribution evaluation of all synthesized  $\beta$ -indolyketones as potential brain PET probes, the remaining  $^{11}\text{C}$ -labelled  $\beta$ -indolyketones **3.4a-b** (Figure 3.18) were kindly provided by Prof. Gilberto L. B. Aquino (Faculty of Pharmacy, State University of Goiás, Brazil), as part of a post-Doc project developed in Coimbra Chemistry Centre.

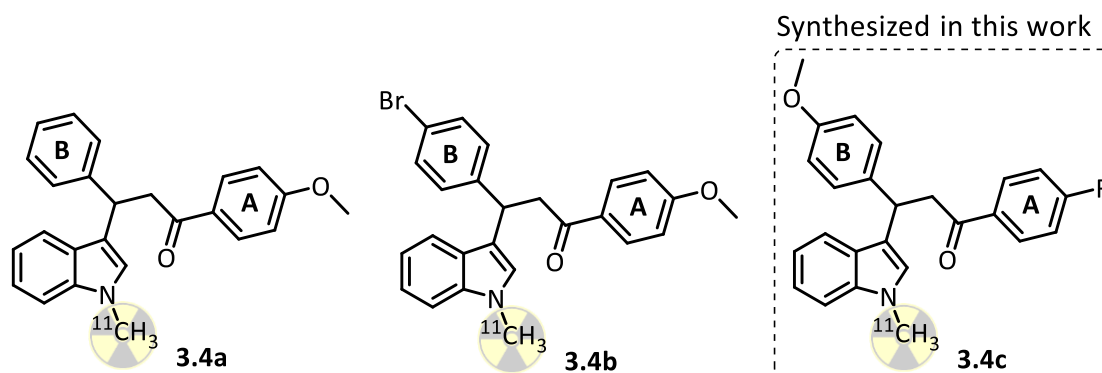


**Figure 3.18** Structures of  $^{11}\text{C}$ -labelled  $\beta$ -indolyketones **3.4a-c** subjected to *in vivo* biodistribution PET studies.

*In vivo* biodistribution studies were carried out using normal BALB/c mice. The animals were injected in the tail vein with 100  $\mu\text{L}$  of each  $^{11}\text{C}$ -labelled  $\beta$ -indolyketone in 0.9% NaCl/EtOH (9:1, v/v) solution. Then, the mice were placed on a high resolution micro-PET imaging system. For compounds **3.4a-b** evaluation, the PET acquisition lasted for 73 min post injection (p.i.) in total, but was acquired in three parts, since one mouse body cannot fit completely in the PET scanner's field of view (FOV). Thus, in the first section, from 0 to 20 min, the mouse's head was placed in the center of the FOV; in the second, from 21 to 41 min, the liver was placed in the center of the FOV; and in the third, from 42 to 73 min, the bladder was placed in the center of the FOV. The results are expressed as percentage of injected dose per gram of organ (% I.D./g) after p.i. and are presented in **Table 3.6**.

**Table 3.6.** Biodistribution results ( $n=1$ ; expressed as % I.D./g of organ) for  $^{11}\text{C}$ -labelled  $\beta$ -indolylketones **3.4a** and **3.4b** after intravenous administration (p.i) in BALB/c mice.

Organ	% I.D./g					
	20 min		41 min		73 min	
	3.4a	3.4b	3.4a	3.4b	3.4a	3.4b
Brain	5.7	7.9	-	-	-	-
Liver	-	-	40.5	25.1	-	-
Spleen	-	-	9.1	8.6	10.2	- <sup>a</sup>
Bladder	-	-	7.1	10.9	13.6	27.2
Kidneys	-	-	15.6	20.5	36.8	- <sup>a</sup>
Muscle	-	-	8.0	6.3	16.5	5.5
Heart	-	-	11.0	8.8	-	-

<sup>a</sup> Due to an instrumentation problem in the micro-PET imaging system, it was not possible to calculate the % I.D./g of the organ.

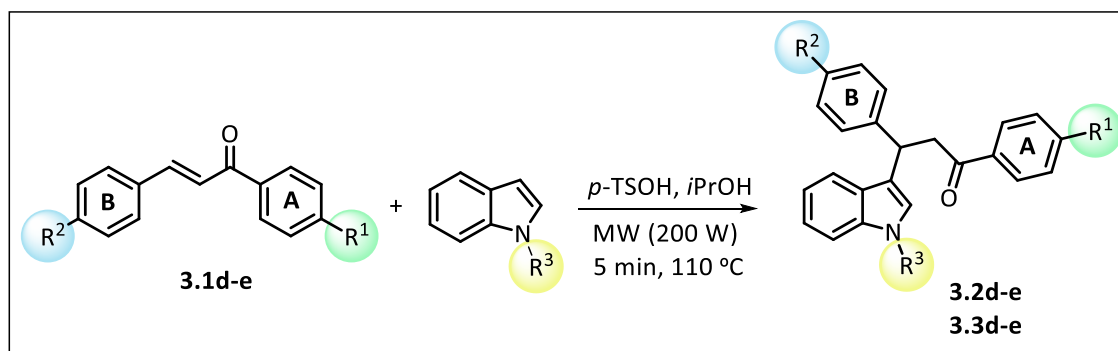
Aiming to achieve a proof of concept regarding the suitability of the  $\beta$ -indolylketones scaffold to successfully penetrate the BBB, the *in vivo* biodistribution profile of  $^{11}\text{C}$ -labelled  $\beta$ -indolylketone **3.4a** (Table 3.6) indicated a quite good brain uptake (5.7% I.D./g at 20 min p.i.) and also a significant liver (40.5% I.D./g at 40 min p.i.), as well as, kidney uptake (15.6% I.D./g and 36.8% I.D./g at 41 min and 73 min p.i., respectively). The liver uptake was clearly visible, demonstrating that this is the main pathway for excretion of the  $\beta$ -indolylketone **3.4a**.

Regarding the  $^{11}\text{C}$ -labelled  $\beta$ -indolylketone **3.4b** (Table 3.6), the *in vivo* biodistribution profile shows a very good brain uptake (7.9% I.D./g at 20 min p.i.), which is slightly higher than that of compound **3.4a**. At 41 min p.i., the liver uptake of  $^{11}\text{C}$ -labelled  $\beta$ -indolylketone **3.4b** (25.1% I.D./g at 41 min p.i.), is significantly lower than that showed by  $\beta$ -indolylketone **3.4a** (40.5% I.D./g at 41 min p.i.). On the other hand, there is a more significant renal excretion component for the compound **3.4b**, as evidenced by its highest kidneys uptake (20.5% I.D./g at 41 min p.i) and moderate bladder uptake (10.5% I.D./g and 27.2% I.D./g at 41 and 73 min p.i., respectively). The data demonstrated that the main pathway for excretion of the  $\beta$ -indolylketone **3.4b** was through the liver and kidneys.

In the case of compound **3.4c**, the PET acquisition lasted for 60 minutes p.i. in total, but only the mouse's head was placed in the center of the FOV. Subsequently, we only obtained information about the brain's uptake, which is the main purpose of this work. Unfortunately, the *in vivo* PET images of  $^{11}\text{C}$ -labelled  $\beta$ -indolyketone **3.4c** showed a quite low uptake into the brain ( $0.958 \pm 0.074\%$  ID/g at 20 min p.i.), being insufficient for a clear brain PET image acquisition.

We can conclude that the  $\beta$ -indolyketones **3.4a** and **3.4b** show high uptake into the brain, while compound **3.4c** displays insufficient brain uptake. A plausible explanation for the differences could be related to the  $\beta$ -indolyketone structure, where the presence of methoxy group in **A** ring of  $\beta$ -indolyketones may play an important role, while the substitution pattern in **B** ring may not be as important in the brain uptake process. Apparently, the presence of methoxy group at *para* position of **A** ring of  $\beta$ -indolyketones **3.4a-b** allows successful  $^{11}\text{C}$ -labelled  $\beta$ -indolyketones **3.4a-b** uptake into the brain. On the other hand, the *para*-methoxy group's replacement on **A** ring by a fluorine atom in **3.4c** may have caused a significant decrease in brain uptake. Furthermore, it seems that having a methoxy group (**3.4c**) or a bromine (**3.4a**) or even its absence (**3.4b**) on the *para*-position on **B** ring in  $\beta$ -indolyketone structure does not improve the brain uptake capacity of the  $^{11}\text{C}$ -labelled  $\beta$ -indolyketone.

Based on these assumptions, we may establish a preliminary structure–activity correlation for the development of new *in vivo* brain PET probes based on  $\beta$ -indolyketone molecular platform. However, more studies are required to unequivocally infer a structure–activity correlation, pursuing a superior understanding of the structural requirements for the  $\beta$ -indolyketone scaffold, aiming successful BBB penetration. Nevertheless, these preliminary results of the present *in vivo* biodistribution study may pave the way to new horizons for the  $\beta$ -indolyketone molecular platform, as potential brain PET probe, extending the scientific importance of these compounds. Driven by the idea that the substitution pattern on **A** ring of  $\beta$ -indolyketones could be a key point to BBB penetration, we decided to preliminary extend our synthetic studies to a series of other  $\beta$ -indolyketones (**Table 3.7**).

**Table 3.7.**  $\beta$ -indolyllketones synthesis at optimized conditions.<sup>a</sup>

Entry	Chalcone	Indole		$\beta$ -Indolyllketone	Yield (%) <sup>b</sup>	
		R <sup>1</sup>	R <sup>2</sup>			R <sup>3</sup>
1	3.1d	H	H	H	3.2d	82
2	3.1e	H	OMe	H	3.2e	85
3	3.1d	H	H	Me	3.3d	91
4	3.1e	H	OMe	Me	3.3e	86

<sup>a</sup> Reaction conditions: chalcone (1 mmol), indole (1.2 mmol), 1 mL *i*PrOH, 10 mol% of *p*-TSOH.

<sup>b</sup> Isolated yield.

Using the optimal reaction conditions described above, we enlarged the reaction scope by reacting indole or 1-methyl indole with a range of substituted chalcones (3.1d-e) to obtain the corresponding  $\beta$ -indolyllketones 3.2d-e and 3.3d-e (Table 3.7). After work-up and purification procedures through column chromatography (silica gel),  $\beta$ -indolyllketones 3.2d-e and 3.3d-e were isolated in good to excellent yields (up to 91 %). All  $\beta$ -indolyllketones were characterized by <sup>1</sup>H-, <sup>13</sup>C-NMR spectroscopy and GC-MS spectrometry, and their structures confirmed (characterization for each compound are specified in Chapter 5, section 5.4.1).

### 3.6 Conclusion

In this chapter, a family of  $\beta$ -indolyllketones and their corresponding *N*-methylated compounds have been efficiently synthesized *via* a Michael addition

reaction, using microwave irradiation as an eco-friendly and sustainable approach, which provided the  $\beta$ -indolyketones in high to excellent isolated yields (up to 91%).

*In vitro* cytotoxicity (3T3 cell line) and computational determination of CLogP studies were carried out for all synthesized *N*-methylated  $\beta$ -indolyketones, showing a low *in vitro* cytotoxicity ( $IC_{50} = 96.5\text{--}658.1 \mu\text{M}$ ) with suitable CLogP values (2.73–3.13) for potential application as brain PET imaging probes. Since the fluorinated  $\beta$ -indolyketone **3.3c** showed a good balance between low cellular cytotoxicity ( $IC_{50} = 658.1 \mu\text{M}$ ) and suitable CLogP value (2.80), this compound was selected to proceed to the further  $^{11}\text{C}$ -labelling reaction.

After optimization of the chromatographic separation conditions in the semi-preparative and analytical HPLC systems, for the purification and checking the quality control parameters, respectively, the  $^{11}\text{C}$ -labelling reaction was performed using a carbon-11 automated radiosynthesis module in the Radiochemistry and Cyclotron Laboratory at ICNAS. Through the automated module, it was possible to accomplish a nearly efficient and reproducible process for the radiolabelling, further purification and reformulation of  $^{11}\text{C}$ -labelled  $\beta$ -indolyketone **3.4c** into a suitable physiological solution for *in vivo* studies. The  $^{11}\text{C}$ -labelled  $\beta$ -indolyketone **3.4c** was obtained in a satisfactory radiochemical yield ( $9.5 \pm 0.8\%$ , non decay-corrected RCY), radiochemical purity greater than 98% and a chemical purity  $\approx 90\%$  (calculated by analytical HPLC system). Moreover, the  $^{11}\text{C}$ -labelled  $\beta$ -indolyketone **3.4c** injection solution complied with the parameters of quality assurance (pH, radioisotope identity and levels of residual solvents in the final solution) to ensure the safe intravenous administration in further *in vivo* studies.

The  $^{11}\text{C}$ -labelled  $\beta$ -indolyketone **3.4c** and the kindly provided  $^{11}\text{C}$ -labelled  $\beta$ -indolyketones **3.4a-b** were used in *in vivo* PET imaging biodistribution studies. An high brain uptake for  $^{11}\text{C}$ -labelled  $\beta$ -indolyketones **3.4a-b** were observed, namely for **3.4b** (7.9% I.D./g at 20 min p.i.), while the  $\beta$ -indolyketone **3.4c** revealed an insufficient brain uptake ( $0.958 \pm 0.074\%$  ID/g at 20 min p.i.). These differences could be associated to the different  $\beta$ -indolyketone structure, in particular, to the substitution pattern on **A** ring of the  $\beta$ -indolyketone scaffold. Nevertheless, these *in vivo* results are very promising but additional studies are needed to confirm unequivocally a structure–activity correlation in  $\beta$ -indolyketone scaffold aiming the successful BBB penetration and subsequently

brain uptake. This theme is ongoing in a collaboration project between ICNAS and the Catalysis & Fine Chemistry group of the Department of Chemistry of Coimbra University.

### 3.7 References

- <sup>1</sup> McCluskey, S. P.; Plisson, C.; Rabiner, E. A.; Howes, O., *European Journal of Nuclear Medicine and Molecular Imaging* **2020**, 47, 451–489.
- <sup>2</sup> Danon, J. J.; Reekie, T. A.; Kassiou, M., *Trends in Chemistry*, **2019**, 1 (6), 612–624.
- <sup>3</sup> (a) McCluskey, S. P.; Plisson, C.; Rabiner, E. A.; Howes, O., *European Journal of Nuclear Medicine and Molecular Imaging* **2020**, 46, 451–489; (b) Lewis, J.; Windhorst, A.; Zeglis, B., *Radiopharmaceutical Chemistry*, Springer, Cham, Switzerland, **2019**, Chapter 34, 583–606.
- <sup>4</sup> Fong, C. W., *Journal of Membrane Biology* **2015**, 248, 651–669.
- <sup>5</sup> Pike, W. P., *Trends in Pharmacological Sciences* **2009**, 30 (8), 431–440.
- <sup>6</sup> Yu, C.-J.; Liu, C.-J., *Molecules* **2009**, 14 (9), 3222–3228.
- <sup>7</sup> Zhang, H.-B.; Liu, L.; Liu, Y.-L.; Chen, Y.-J.; Wang, J.; Wang, D., *Synthetic Communications* **2007**, 37 (2), 173–181.
- <sup>8</sup> Zhou, W.; Xu, L.-W.; Li, L.; Yang, L.; Xia, C.-G., *European Journal of Organic Chemistry* **2006**, 2006 (23), 5225–5227.
- <sup>9</sup> Ekbote, S. S.; Panda, A. G.; Bhor, M. D.; Bhanage, B. M., *Catalysis Communications* **2009**, 10 (12), 1569–1573.
- <sup>10</sup> Bandini, M.; Cozzi, P. G.; Giacomini, M.; Melchiorre, P.; Selva, S.; Umani-Ronchi, A., *Journal of Organic Chemistry* **2002**, 67 (11), 3700–3704.
- <sup>11</sup> Reddy, A. V.; Ravinder, K.; Goud, T. V.; Krishnaiah, P.; Raju, T. V.; Venkateswarlu, Y., *Tetrahedron Letters* **2003**, 44 (33), 6257–6260.
- <sup>12</sup> Maiti, G.; Kundu, P., *Synthetic Communications* **2007**, 37, 2309–2316.
- <sup>13</sup> Von Der Heiden, D.; Bozkus, S.; Klussmann, M.; Breugst, M., *Journal of Organic Chemistry* **2017**, 82 (8), 4037–4043.
- <sup>14</sup> Huang, Z.-H.; Zou, J.-P.; Jiang, W.-Q., *Tetrahedron Letters* **2006**, 47 (45), 7965–7968.
- <sup>15</sup> Xu, R.; Ding, J. C.; An Chen, X.; Liu, M. C.; Wu, H. Y., *Chinese Chemical Letters* **2009**, 20 (6), 676–679.
- <sup>16</sup> Shi, M.; Cui, S. C.; Li, Q. J., *Tetrahedron* **2004**, 60 (31), 6679–6684.
- <sup>17</sup> Yaragorla, S.; Gangam, S., *Indian Journal of Chemistry Section B* **2015**, 54 (2), 240–244.
- <sup>18</sup> Zhan, Z.-P.; Yang, R.-F.; Lang, K., *Tetrahedron Letters* **2005**, 46 (22), 3859–3862.
- <sup>19</sup> Li, J.-T.; Dai, H.-G.; Xu, W.-Z.; Li, T.-S., *Journal of Chemical Research* **2006**, 2006 (1), 41–42.
- <sup>20</sup> Ji, S.-J.; Wang, S.-Y., *Ultrasonics Sonochemistry* **2005**, 12 (5), 339–343.
- <sup>21</sup> (a) Mahmoudi, H.; Jafari, A. A.; Saeedi, S.; Firouzabadi, H., *RSC Advances* **2015**, 5 (4), 3023–3030; (b) Ji, S.-J.; Wang, S.-Y., *Synlett* **2003**, 13, 2074–2076.
- <sup>22</sup> Zeng, X.; Ji, S.; Shen, S., *Chinese Journal of Chemistry* **2007**, 25 (12), 1777–1780.
- <sup>23</sup> Zhan, Z.-P.; Lang, K., *Synlett* **2005**, 10, 1551–1554.
- <sup>24</sup> Kathing, C.; Tumtin, S.; Singh, N. G.; Rani, J. W.; Phucho, I. T.; Nongpiur, A.; Nongrum, R.; Nongkhaw, R. L., *Organic Chemistry: an Indian Journal* **2013**, 9 (7), 257–266.
- <sup>25</sup> Xie, Y.; Mao, L.; Li, L., *Journal of Chemical Research* **2013**, 37 (8), 476–479.

- <sup>26</sup> Tumtin, S.; Kathing, C.; Phucho, I. T.; Nongrum, R.; Myrboh, B.; Nongkhlaw, R., *Journal of the Chinese Chemistry Society* **2015**, 62 (4), 321–327.
- <sup>27</sup> Gohain, M.; Jacobs, J.; Marais, C.; Bezuidenhout, B. C. B., *Australian Journal of Chemistry* **2013**, 66 (12), 1594–1599.
- <sup>28</sup> Patel, T.; Gaikwad, R.; Jain, K.; Ganesh, R.; Bobde, Y.; Ghosh, B.; Das, K.; Gayen, S., *Chemistry Select* **2019**, 4 (15), 4478–4482.
- <sup>29</sup> (a) Berrino, E.; Supuran, C. T., *Expert Opinion on Drug Discovery* **2018**, 13 (9), 861–873; (b) Kappe, C. O.; Dallinger, D., *Nature Reviews Drug Discovery* **2006**, 5, 51–63.
- <sup>30</sup> Pearson, R. G., *Coordination Chemistry Reviews* **1990**, 100, 403–425.
- <sup>31</sup> Lu, F. M.; Yuan, Z., *Quantitative Imaging in Medicine and Surgery* **2015**, 5 (3), 433–447.
- <sup>32</sup> (a) Wager, T. T.; Chandrasekaran, R. Y.; Hou, X.; Troutman, M. D.; Verhoest, P. R.; Villalobos, A.; Will, Y., *ACS Chemical Neuroscience* **2010**, 1 (6), 420–434; (b) Wager, T. T.; Hou, X.; Verhoest, P. R.; Villalobos, A., *ACS Chemical Neuroscience* **2010**, 1 (6), 435–449.
- <sup>33</sup> Khalil, M. M., *Basic Science of PET Imaging*, Springer, Cham, Switzerland, **2017**, Chapter 4, 79–103.
- <sup>34</sup> Karamé, I.; Shaya, J.; Srouf, H., *Carbon Dioxide Chemistry, Capture and Oil Recovery*, IntechOpen, London, UK, **2017**, Chapter 7, 123–138.
- <sup>35</sup> Lewis, J.; Windhorst, A.; Zeglis, B., *Radiopharmaceutical Chemistry*, Springer, Cham, Switzerland, **2019**, Chapter 12, 221–236.
- <sup>36</sup> Dahl, K.; Halldin, C.; Schou, M., *Clinical and Translational Imaging* **2017**, 5 (3), 275–289.
- <sup>37</sup> Welch, M. J.; Redvanly, C. S., *Handbook of Radiopharmaceuticals: Radiochemistry and Applications*, John Wiley & Sons, **2003**, Chapter 8, 283–305.
- <sup>38</sup> Welch, M. J.; Redvanly, C. S., *Handbook of Radiopharmaceuticals: Radiochemistry and Applications*, John Wiley & Sons, **2003**, Chapter 1, 1–70.
- <sup>39</sup> Ametamey, S. M.; Honer, M.; Schubiger P. A., *Chemical Reviews* **2008**, 108 (5), 1501–1516.
- <sup>40</sup> (a) Larsen, P.; Ulin, J.; Dahlstrom, K.; Jensen, M., *Applied Radiation and Isotopes* **1997**, 48 (2), 153–157; (b) Link, J. M.; Krohn, K. A.; Clark, J. C., *Nuclear Medicine and Biology* **1997**, 24 (1), 93–97.
- <sup>41</sup> (a) Wilson, A. A.; Garcia, A.; Houle, S.; Vasdev, N., *Journal of Labelled Compounds and Radiopharmaceuticals* **2009**, 52, 490–492; (b) Wilson, A. A.; Garcia, A.; Jin, L.; Houle, S., *Nuclear Medicine and Biology* **2000**, 27 (6), 529–532.
- <sup>42</sup> Lewis, J.; Windhorst, A.; Zeglis, B., *Radiopharmaceutical Chemistry*, Springer, Cham, Switzerland, **2019**, Chapter 11, 207–220.
- <sup>43</sup> (a) Huang, H.; Ning, Y.; Zhang, B.; Lou, C., *Hellenic Journal of Nuclear Medicine* **2015**, 18 (3), 189–192; (b) Wuest, F.; Berndt, M.; Kniess, T., *Ernst Schering Research Foundation Workshop* **2007**, 62, 183–213.
- <sup>44</sup> European Pharmacopoeia, *Guide for the elaboration of monographs on radiopharmaceutical preparations*, Edition 2018, **2018**.



---

<sup>45</sup> European Pharmacopoeia, 9<sup>th</sup> Edition, Vol. 1, **2017**, chapter 5.4 – Residual Solvents, 07/2016:50400, 665–672.

## CHAPTER 4

---

### *Structural modulation of glyco-phthalocyanines for the development of potential fluorophores for Fluorescence Imaging*

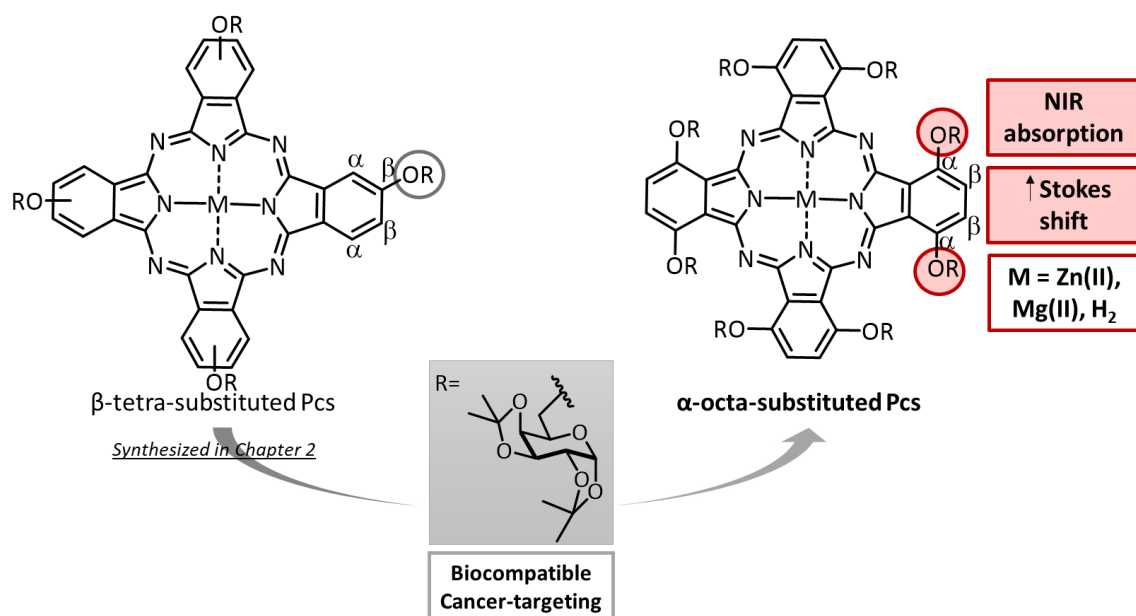
---

#### 4.1 Introduction

As previously mentioned in Chapter 1, the progress in Fluorescence Imaging (FI) technique as a diagnostic tool depends on the availability of biocompatible NIR fluorophores with optimized properties. An ideal fluorophore should have the following properties: i) absorb light in the “phototherapeutic window” (700–900 nm), as well exhibit high molar extinction coefficients; ii) have high fluorescence quantum yields and large Stokes shifts between absorption and fluorescence and iii) have capability of accumulating in tumors.<sup>1</sup>

It is well established that the absorption of phthalocyanines bearing electron donating substituents at the non-peripheral ( $\alpha$ ) positions of the macrocycle causes a strong shift in light absorption into NIR region, when compared to the corresponding peripheral ( $\beta$ ) substituted ones.<sup>2,3</sup> Particularly, strong shifts have been found for  $\alpha$ -octa-substituted phthalocyanines bearing eight alkoxy groups with typical Q-bands absorption values beyond 730 nm and Stokes shifts up to 35 nm.<sup>4,5</sup> Therefore, we hypothesized that the synthesis of  $\alpha$ -octa-substituted phthalocyanines with 1,2:3,4-di-*O*-isopropylidene- $\alpha$ -*D*-galactopyranose biocompatible groups, as electron donor moieties, would give rise to non-planar phthalocyanines with intense absorption in the “phototherapeutic window” and large Stokes shifts (**Scheme 4.1**). The

incorporation of these isopropylidene protected *D*-galactose biocompatible moieties is expected to play a major role in improving tumor selectivity, which is an useful feature for the potential application of such compounds as NIR fluorophores for cancer diagnosis using FI technique.



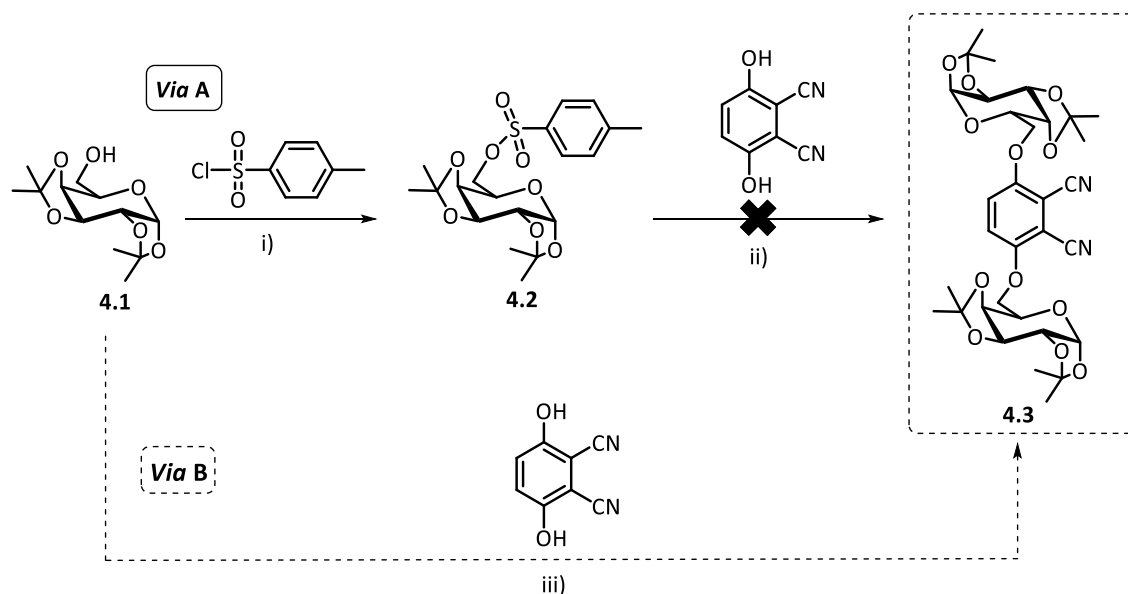
**Scheme 4.1.** Design of phthalocyanines as potential NIR fluorophores.

Since Hanack and co-workers<sup>6</sup> pioneering work regarding the synthesis of a zinc(II) phthalocyanine complex, a  $\beta$ -octa-functionalized with *D*-galactose units, other examples of glycosylated octa-functionalized have been described in the literature<sup>7-11</sup> but, so far to the best of our knowledge, there are no examples of the corresponding  $\alpha$ -octa-substituted ones. Therefore, pursuing our goal regarding the development of potential NIR fluorophores, in this chapter we describe the synthesis of new  $\alpha$ -octa-substituted phthalocyanines containing isopropylidene protected *D*-galactose units.

In the first part of this chapter, we will describe the optimization of the reaction conditions for the synthesis of the desired  $\alpha$ -octa-substituted phthalocyanine and its corresponding zinc(II) and magnesium(II) metal complexes. In the second part, in order to evaluate the application of these phthalocyanines as potential NIR fluorophores, the UV-Vis absorption and fluorescence emission properties for both  $\beta$ -tetra-substituted (synthesized in Chapter 2) and  $\alpha$ -octa-substituted phthalocyanines sets incorporating isopropylidene protected *D*-galactose moieties are presented and discussed.

## 4.2 Synthesis of $\alpha$ -octa-substituted phthalocyanines

The  $\alpha$ -octa-substituted phthalocyanines were synthesized from the appropriate 3,6-disubstituted phthalonitrile bearing isopropylidene protected *D*-galactose groups. Therefore, this study started with the synthesis of the desired 3,6-disubstituted phthalonitrile **4.3** using the synthetic approaches presented in **Scheme 4.2**.



**Scheme 4.2.** Synthesis of 3,6-disubstituted phthalonitrile **4.3**. Reaction conditions: **Via A** – i) Pyridine, room temperature, 1 h, N<sub>2</sub> and then 0-5 °C, 16 h, 80%; ii) K<sub>2</sub>CO<sub>3</sub>, DMF, N<sub>2</sub>, 25-50 °C, 120 h; **Via B** – DEAD, PPh<sub>3</sub>, toluene, 110 °C, N<sub>2</sub>, 24 h, 39%.

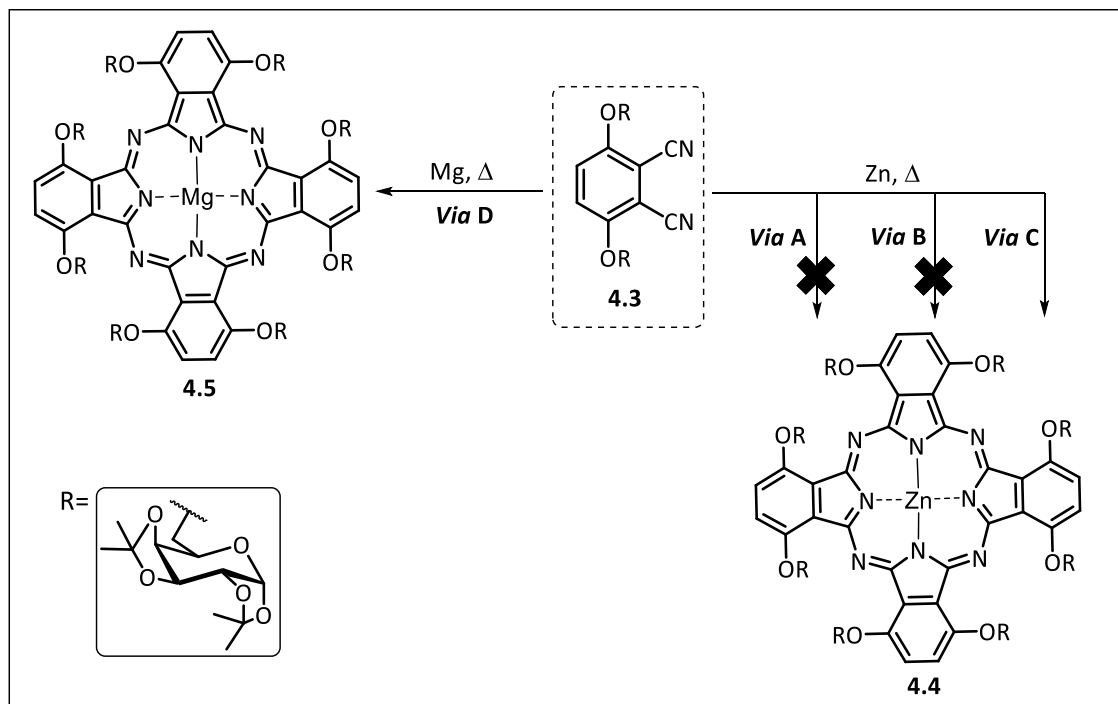
The first synthetic approach adopted to prepare 3,6-disubstituted phthalonitrile **4.3** comprises a two-step process (*via A*, **Scheme 4.2**). First, *p*-toluenesulfonyl chloride and 1,2:3,4-di-*O*-isopropylidene- $\alpha$ -*D*-galactopyranose **4.1** were stirred, in dry pyridine at room temperature, under nitrogen atmosphere, for 1 h. Subsequently, the mixture was cooled down to 0-5 °C and stirred for 16 h. After work-up and purification procedures, the desired compound **4.2** was obtained in 80% isolated yield (*via A*, **Scheme 4.2**). The structure of this intermediate was confirmed by <sup>1</sup>H- and <sup>13</sup>C-NMR and the data is in agreement with those previously reported in literature.<sup>12</sup> In the second step, compound **4.2**, 2,3-dicyanohydroquinone and potassium carbonate (K<sub>2</sub>CO<sub>3</sub>), were dissolved in dry DMF and stirred, under nitrogen atmosphere, at room temperature. The evolution of

the reaction was followed by TLC and no conversion of the starting material 2,3-dicyanohydroquinone was observed, after 24 h of reaction. The reaction temperature was then increased to 50 °C, and further portions of K<sub>2</sub>CO<sub>3</sub> were added to the reaction mixture over a period of 96 h. Nevertheless, besides the starting material 2,3-dicyanohydroquinone and decomposed material, no products were detected even after such long reaction time. Other experimental conditions, such as using sodium hydride (NaH) as base was also studied. However, once again, no product was detected. Unfortunately, the 3,6-disubstituted phthalonitrile **4.3** was not obtained using these reaction conditions, probably due to the fact that the alkoxide ion originated from 2,3-dicyanohydroquinone, maybe less reactive for the studied nucleophilic substitution reaction.

After this unsuccessful attempt to achieve the 3,6-disubstituted phthalonitrile **4.3**, we turned then our attention to the use of the *Mitsunobu* reaction method (*via B*, **Scheme 4.2**). In a typical reaction, to a stirring solution of 2,3-dicyanohydroquinone and triphenylphosphine (PPh<sub>3</sub>) in dry toluene, diethyl azodicarboxylate (DEAD) was slowly added dropwise, at room temperature. Once the addition was complete, the 1,2:3,4-di-*O*-isopropylidene- $\alpha$ -*D*-galactopyranose alcohol was added in dry toluene, and the reaction mixture was allowed to heat up to 110 °C, under nitrogen atmosphere, with magnetic stirring. The reaction's progress was controlled by TLC analysis of samples taken from the reaction mixture. After 24 h, the complete conversion of reactants into product was observed, and the reaction was subsequently treated by standard work-up procedures. The target phthalonitrile **4.3** was then purified by column chromatography on silica gel, using a mixture of CH<sub>2</sub>Cl<sub>2</sub>/methanol (200:1, respectively) as eluent, and it was obtained in 39% isolated yield (*via B*, **Scheme 4.2**). The spectroscopic data are in agreement with the literature<sup>13</sup> and are presented in the experimental section (Chapter 5, section 5.5).

Afterwards, we proceeded with the synthesis of the desired  $\alpha$ -octa-substituted phthalocyanines. The studies were initiated with the optimization of the cyclotetramerization reaction of the previous synthesized phthalonitrile **4.3** using high boiling point solvents and zinc(II) or magnesium(II) metal salts, as templates (**Table 4.1**). The synthetic approaches details and the isolated yields for each of the synthesized phthalocyanines are presented in **Table 4.1**.

**Table 4.1.** Reactions conditions and isolated yields for the cyclotetramerization reactions and respective  $\alpha$ -octa-metallophthalocyanine complexes **4.4** and **4.5**. [PeOH: pentan-1-ol; BuOH: butan-1-ol; OcOH: octan-1-ol]



Entry	Via	Reaction conditions	MPc	Yield <sup>a</sup>
1	A	Zn(OAc) <sub>2</sub> ·2H <sub>2</sub> O, DMAE/BuOH <sup>b</sup> , 120 °C, 24 h, N <sub>2</sub>	<b>4.4</b>	0
2		Zn(OAc) <sub>2</sub> ·2H <sub>2</sub> O, DMAE/BuOH <sup>b</sup> , MW <sup>c</sup> , 120 °C, 2-32 min		
3	B	Zn(OAc) <sub>2</sub> ·2H <sub>2</sub> O, DMAE/BuOH <sup>b</sup> , MW <sup>c</sup> , 160 °C, 2-32 min	<b>4.4</b>	0
4		Zn(OAc) <sub>2</sub> ·2H <sub>2</sub> O, DMAE/BuOH <sup>b</sup> , MW <sup>c</sup> , 200 °C, 2-32 min		
5	C	Zn(OAc) <sub>2</sub> ·2H <sub>2</sub> O, PeOH, DBU (10 mol%), 150 °C, 6 h, N <sub>2</sub>	<b>4.4</b>	25
6	D	1. Mg, PeOH, 150 °C, 1 h; 2. <b>4.3</b> , OcOH, 160 °C, 3 h, N <sub>2</sub>	<b>4.5</b>	15

<sup>a</sup> Isolated yield.

<sup>b</sup> DMAE/BuOH (2:1).

<sup>c</sup> Microwave-assisted synthesis (200 W of power).

Regarding the synthesis of  $\alpha$ -octa-substituted zinc(II) phthalocyanine complex **4.4**, the studies started with the cyclotetramerization reaction of the phthalonitrile **4.3** in the presence of zinc(II) acetate dihydrate (Zn(OAc)<sub>2</sub>·2H<sub>2</sub>O), using DMAE/butan-1-ol (2:1) mixture as solvent, under nitrogen atmosphere, at 120 °C (entry 1, *via A*, **Table 4.1**). The reaction's progress was followed by TLC analysis and UV-Vis spectroscopy, and after 24 h no product was observed. Knowing the benefits of using microwave irradiation in a great number of chemical processes,<sup>14,15</sup> we then attempted the microwave-assisted

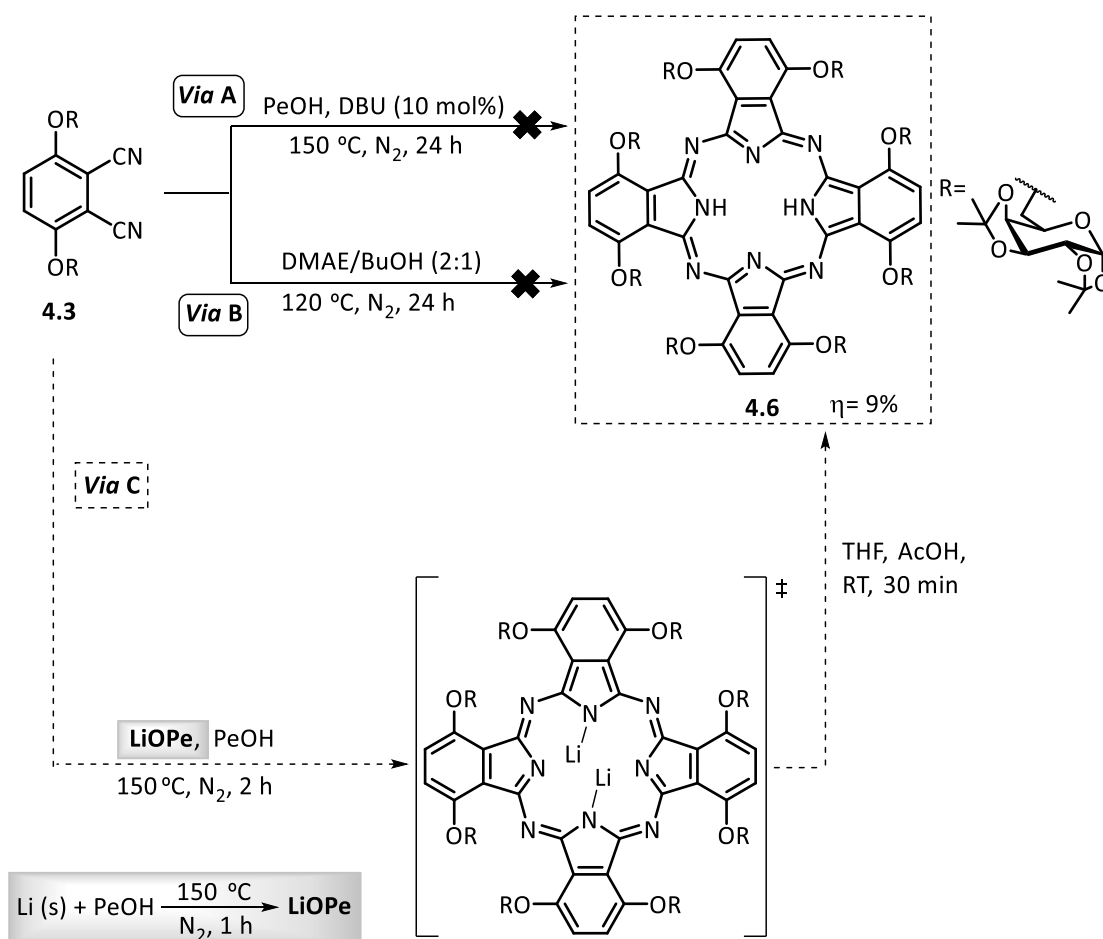
synthesis of phthalocyanine **4.4** (*via* B, **Table 4.1**). In a typical experiment, the phthalonitrile **4.3** and zinc(II) acetate dihydrate were dissolved in a mixture of DMAE/butan-1-ol (2:1, respectively). This solution was submitted to microwave irradiation (200 W), at 120 °C, for 2 min (entry 2, *via* B, **Table 4.1**). After 2 min, the TLC revealed absence of reaction. The reaction time was further increased to 10 and 20 additional min; however, TLC analysis revealed the presence the starting material **4.3**, some degradation products and the absence of phthalocyanine, as confirmed by UV-Vis spectroscopy. Several attempts to optimize this microwave-assisted synthesis were carried out by varying the temperature (160–200 °C) and time (2–32 min), but only starting material **4.3** and degradation products were observed on TLC (entries 3–4, *via* B, **Table 4.1**).

These results led us to choose another synthetic approach which uses pentan-1-ol, as solvent, and 1,8-diazabicyclo[5.4.0]undec-7-e (DBU), as hindered non-nucleophilic strong base (entry 5, *via* C, **Table 4.1**). It should be noted that the amount of DBU employed in the reaction must be strickly controled to avoid the formation of zinc(II) phthalocyanine-DBU complexes, as previously observed by Melle and collaborators.<sup>16</sup> Thus, the synthesis of the desired zinc(II) phthalocyanine complex **4.4** was performed by stirring the 3,6-disubstituted phthalonitrile **4.3** with zinc(II) acetate dihydrate, in pentan-1-ol and a catalytic amount of DBU (10% mol), under nitrogen atmosphere, at 150 °C. After 6 h, the complete disappearance of the starting material **4.3** was observed, by TLC, and the reaction was subsequently treated by standard work-up procedures. The crude product was then purified by column chromatography (silica gel), providing the desired new phthalocyanine **4.4** in 25% isolated yield (entry 5, **Table 4.1**). Its structure was confirmed by UV-Vis and <sup>1</sup>H-NMR spectroscopy, and mass spectrometry (described in detail in Chapter 5, section 5.5).

Aiming the modulation of the photophysical properties of these compounds the studies proceeded with the synthesis of the  $\alpha$ -octa-substituted magnesium(II) phthalocyanine complex **4.5**. The synthesis involved the *in situ* formation of magnesium bis-pentanolate by reaction of pentan-1-ol with magnesium turnings, followed by condensation of the phthalonitrile **4.3** with the previous synthesized magnesium bis-pentanolate, using octan-1-ol as solvent, at temperature of 160 °C (entry 6, *via* D, **Table 4.1**). The reaction's progress was followed by TLC, and after the complete

consumption of the starting material **4.3** in 3 h, the solvent was removed and the resulting brown solid was suspended in dichloromethane/hexane (1:1). After work-up standard procedures, the crude mixture was purified by silica gel column chromatography and the desired new magnesium(II) phthalocyanine complex **4.5** was isolated in 15% yield (entry 6, via D, **Table 4.1**). The structure of magnesium(II) complex **4.5** was characterized by suitable spectroscopic techniques, and the details are presented in Chapter 5, section 5.5.

Moving forward, the studies proceeded with the optimization of the reaction conditions for the synthesis of the  $\alpha$ -octa-substituted metal-free phthalocyanine **4.6**, as depicted in **Scheme 4.3**.



**Scheme 4.3.** Synthetic approaches for the synthesis of the  $\alpha$ -octa-substituted metal-free phthalocyanine **4.6**. LiOPe: lithium pentanolate; PeOH: pentan-1-ol; BuOH: butan-1-ol.



The studies of the synthesis of the  $\alpha$ -octa-substituted metal-free phthalocyanine **4.6** were initiated with the conventional synthetic approaches based on the cyclotetramerization reaction of phthalonitrile **4.3** in high-boiling point solvents, such as the DMAE/butan-1-ol mixture (*via A*, **Scheme 4.3**) or pentan-1-ol in the presence of DBU as base (*via B*, **Scheme 4.3**). However, both synthetic approaches did not allow the formation of the desired phthalocyanine **4.6**. These results may be attributed to the steric hindrance caused by the presence of eight bulky substituents at  $\alpha$  positions of the macrocycle, which in the absence of a metal as template, hamper the cyclotetramerization of its corresponding phthalonitrile.

Finally, we attempted the preparation of the  $\alpha$ -octa-substituted metal-free phthalocyanine **4.6** based on cyclotetramerization reaction of the 3,6-disubstituted phthalonitrile **4.3**, in the presence of lithium alcoholate, which acts as the metal template, followed by demetallation with dilute acid (*via C*, **Scheme 4.3**).<sup>17</sup> However, in order to avoid the formation of metal-free triazaporphyrin by-product on the cyclotetramerization reaction, phthalonitrile **4.3** must be added to a solution of preformed lithium alcoholate in the appropriated alcohol, either at reflux or at room temperature, followed by heating to reflux, as previously described by Cook and collaborators.<sup>18,19</sup> For this reason, we promoted, in the first step, the synthesis of the lithium pentanolate (PeOH) by refluxing the lithium metal with pentan-1-ol for 1 h, followed by the cyclotetramerization reaction of 3,6-disubstituted phthalonitrile **4.3** in a solution of the preformed lithium pentanolate (LiOPe) in pentan-1-ol (PeOH), at reflux temperature (*via C*, **Scheme 4.3**). The reaction's progress was followed by TLC and UV-Vis spectroscopy analysis of samples taken from the reaction mixture. After complete conversion of phthalonitrile **4.3** into the product ( $\approx 2$  h), the reaction was quenched by THF, and subsequent slow acetic acid (AcOH) addition, over 30 min, at room temperature, provided the desired  $\alpha$ -octa-substituted metal-free phthalocyanine **4.6**. The crude mixture was then subjected to the usual work-up procedures and purified by column chromatography (silica gel), providing the compound **4.6** in 9% isolated yield (*via C*, **Scheme 4.3**). The characterization of this new metal-free phthalocyanine **4.6** was performed by <sup>1</sup>H-NMR and UV-Vis spectroscopy, as well as, mass spectrometry (described in detail in Chapter 5, section 5.5).

Summing up, the combination of theoretical synthetic knowledge with the systematic experimental work, allowed us to obtain the  $\alpha$ -octa-substituted zinc(II), magnesium(II) and metal-free phthalocyanines in 25%, 15% and 9% isolated yields, respectively, which can be potentially used as NIR fluorophores in FI experiments.

### Phthalocyanine characterization

As aforementioned in this chapter, all new  $\alpha$ -octa-substituted metal and metal-free phthalocyanines have been fully characterized by suitable spectroscopic techniques, described with detail in Chapter 5, section 5.5. As an illustrative example, the  $^1\text{H-NMR}$  spectrum of the new  $\alpha$ -octa-substituted zinc(II) phthalocyanine complex **4.4** is depicted in **Figure 4.1**. In order to minimize the typical aggregation of the macrocycle, the  $^1\text{H-NMR}$  spectrum of phthalocyanine **4.4** was recorded in a mixture of  $\text{CDCl}_3$  and pyridine- $d_5$ .

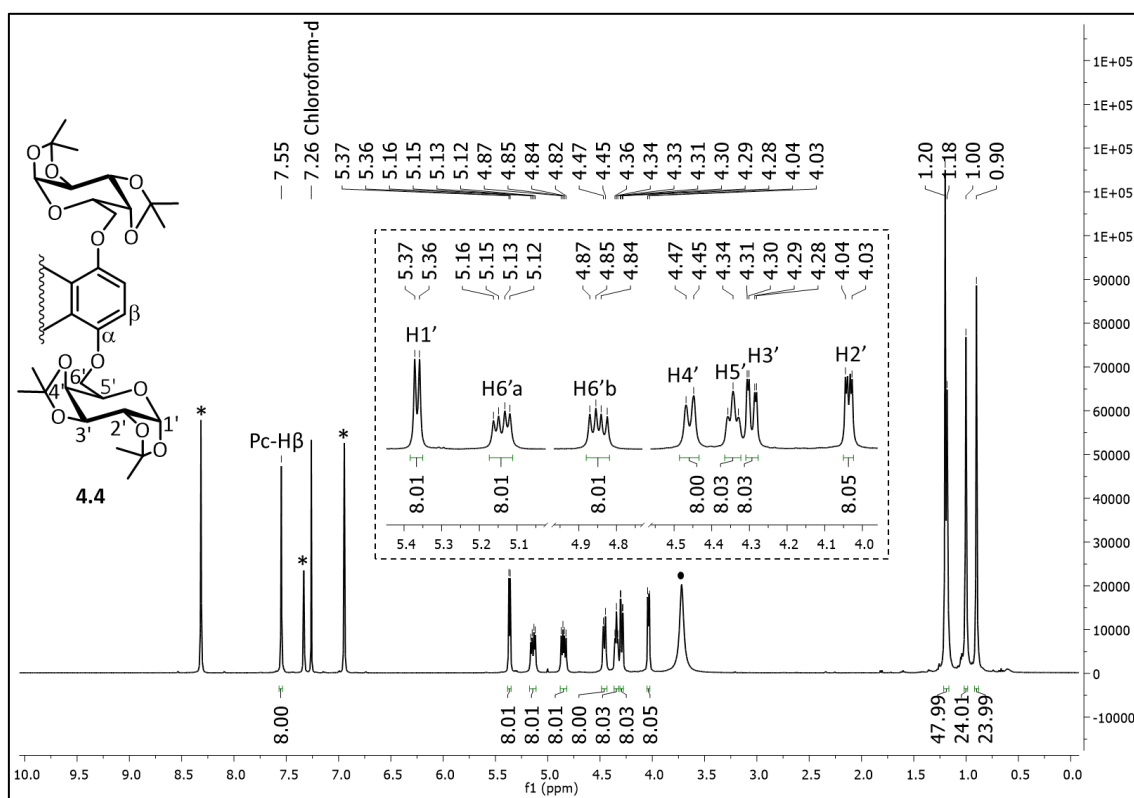


**Figure 4.1.**  $^1\text{H-NMR}$  spectrum of zinc(II) phthalocyanine complex **4.4** in  $\text{CDCl}_3$  and pyridine- $d_5$  (pyridine- $d_5$  signals marked with \*). Inset: expansion of the  $^1\text{H-NMR}$  spectrum between  $\delta$  5.40 to 4.00 ppm. The large signal at  $\delta$  3.72 ppm is due to the water in deuterated solvents.

The well-defined  $^1\text{H}$ -NMR spectrum showed resonances that are attributed to the isopropylidene methyl groups, appearing as several singlets at  $\delta$  0.90–1.20 ppm and integrating a total of 96 protons. The signals between  $\delta$  4.00 and 5.40 ppm are attributed to the resonances of the protons of the *D*-galactose unit. To assign the protons of the *D*-galactose unit, a two-dimensional  $^1\text{H}$ - $^1\text{H}$  COSY NMR was performed (Figure 4.2).

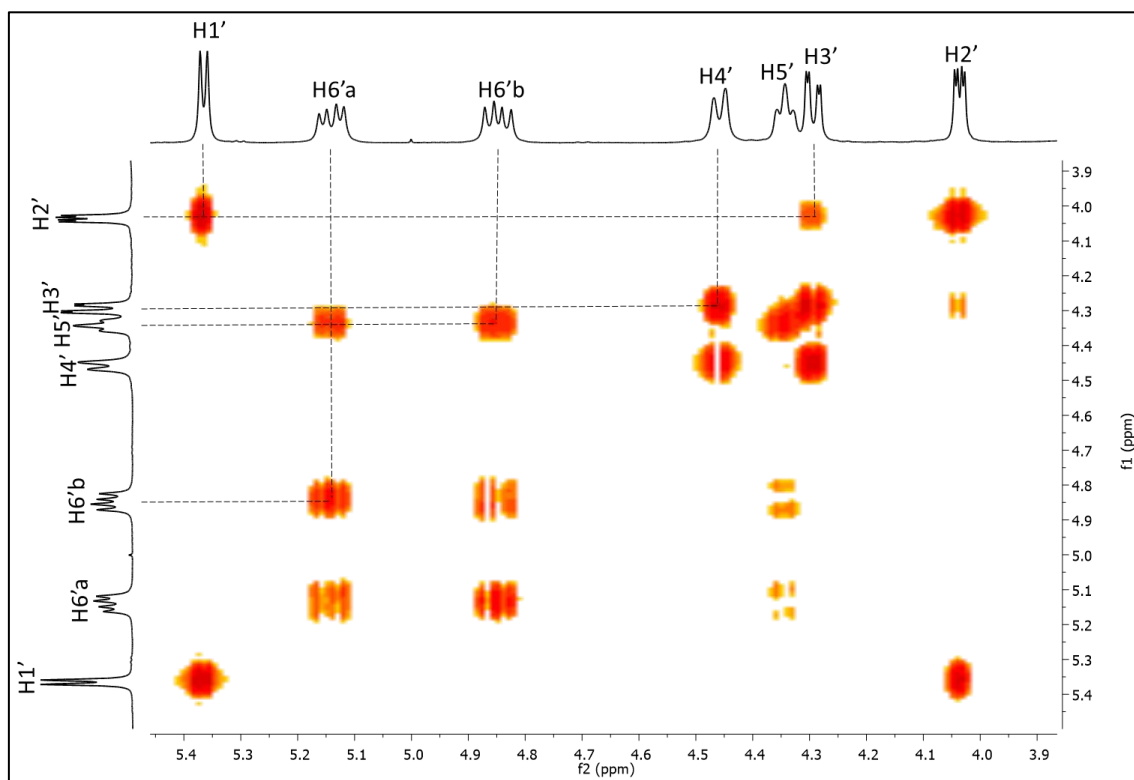


**Figure 4.2.** Selected expansion of  $^1\text{H}$ - $^1\text{H}$  COSY NMR spectrum of zinc(II) phthalocyanine 4.4, signals of the *D*-galactose unit, in  $\text{CDCl}_3$  and pyridine- $d_5$ .

Among the signals of the *D*-galactose unit, the resonance of the proton of the anomeric carbon H1' appears as the most deshielded signal at  $\delta$  5.37 ppm ( $J = 5.0$  Hz), since it is the only proton connected to a carbon bearing two oxygen atoms (Figure 4.1). This signal is a doublet due to coupling to H2', which appears as a double doublet at  $\delta$  4.04 ppm ( $J = 5.0$  and 2.1 Hz), as deduced by  $^1\text{H}$ - $^1\text{H}$  COSY NMR spectrum (Figure 4.2). This double doublet shows two distinct coupling constants. One corresponds to the H1'–H2' coupling ( $J_{1',2'} = 5.0$  Hz), as previously assigned. The other coupling constant is attributed to H2'–H3' coupling ( $J_{2',3'} = 2.1$  Hz), whose correlations were confirmed by the  $^1\text{H}$ - $^1\text{H}$  COSY NMR spectrum (Figure 4.2). Proton H3', on the other hand, displays also a

double doublet at  $\delta$  4.29 ppm ( $J = 8.0$  and  $2.1$  Hz), since it has also a correlation with the signal at  $\delta$  4.47 ppm, which was assigned to H4' proton. On the other hand, the signal attributed to the H4' proton signal is a doublet and only couples with the H3' proton, as confirmed by its coupling constant ( $J = 8.1$  Hz) and the  $^1\text{H}$ - $^1\text{H}$  COSY NMR spectrum (**Figure 4.2**). The lack of H4'–H5' coupling could probably arise from their geometrical disposition, as they could form a dihedral angle close to  $90^\circ$ , and therefore exhibiting a very low  $J_{4',5'}$ , according to the Karplus equation. Taking all this into consideration, the remaining resonances of H5' and H6' protons were assigned by comparison of their coupling constants. The two double doublets, one at  $\delta$  4.85 ppm ( $J = 12.0$  and  $6.5$  Hz) and the other one at  $\delta$  5.14 ppm ( $J = 12.0$  and  $5.4$  Hz), integrating each one for eight protons, have a typical coupling constant for geminal ( $^2J$ ) diastereotopic protons ( $^2J_{\text{H,H}} = 10$ – $16$  Hz). Thus, the two double doublets can be assigned to both H6'a and H6'b protons, which are magnetically non-equivalent protons due to their proximity to a chiral center, and thus they have different resonances in the  $^1\text{H}$ -NMR spectrum (**Figure 4.1**). The correlations given by  $^1\text{H}$ - $^1\text{H}$  COSY NMR allowed to confirm that the signal at  $\delta$  4.34 ppm corresponded to H5', integrating for eight protons. Finally, at a lower field, the signal attributed to the phthalocyanine  $\beta$ -protons (Pc-H $\beta$ ), appears as a singlet at  $\delta$  7.55 ppm, integrating for 8 protons.

To corroborate the structure of  $\alpha$ -octa-substituted zinc(II) phthalocyanine **4.4**, we also performed mass spectroscopy measurements, as depicted in **Figure 4.3**. In the MALDI-TOF spectrum, obtained for the zinc(II) phthalocyanine **4.4** (**Figure 4.3**), an intense molecular ion peak at  $m/z$  2642.44 Da was obtained, which corresponds to the mass of the molecular ion  $[\text{M}+2\text{H}]^+$  of the phthalocyanine **4.4**, corroborating the structure of the expected metallophthalocyanine.

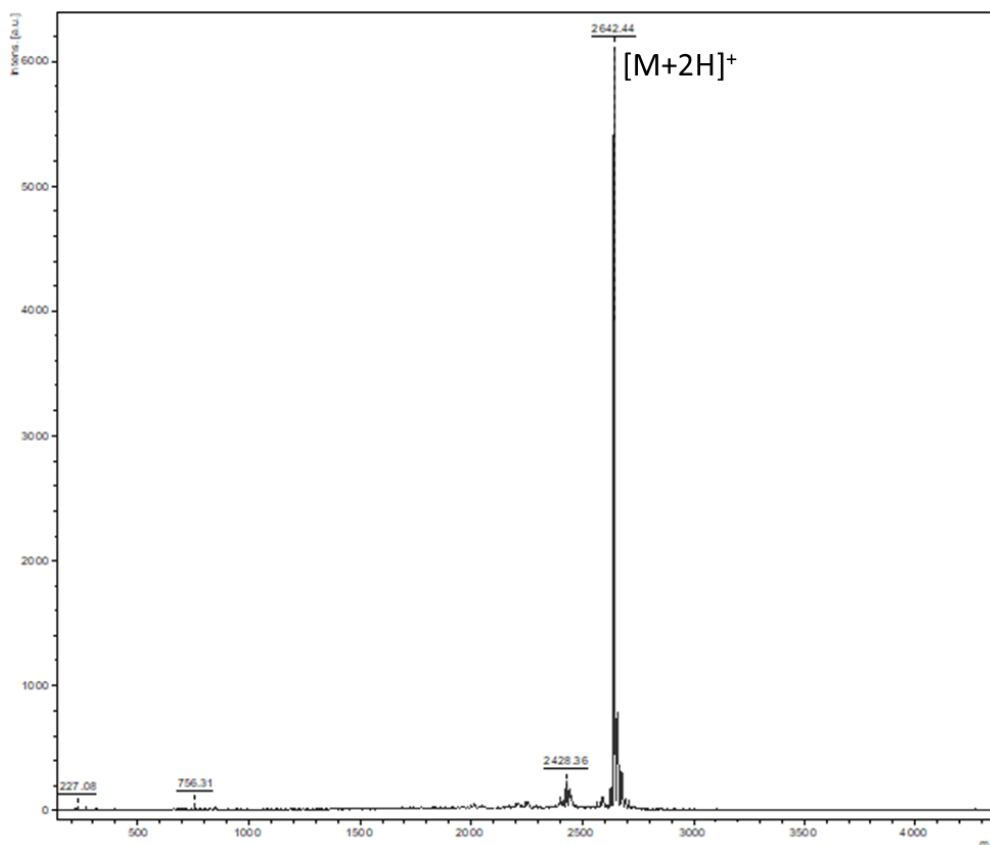


**Figure 4.3.** Observed experimentally molecular ion  $[M+2H]^+$ , obtained by MALDI-TOF of zinc(II) phthalocyanine complex **4.4**.

### 4.3. UV-Visible absorption and fluorescence emission spectroscopy of synthesized glycophthalocyanines

One of the main goals of this thesis is the development of new biocompatible molecular targeted phthalocyanines as potential NIR fluorophores, for cancer diagnosis using FI technique. In order to evaluate the application of the synthesized  $\alpha$ -octa-substituted phthalocyanines **4.4**, **4.5** and **4.6** (Figure 4.4) as potential NIR fluorophores, some photophysical properties concerning the electronic absorption and fluorescence emission are presented and discussed in this section. Also, since isopropylidene protected *D*-galactose  $\beta$ -tetra-substituted phthalocyanines related compounds **2.6b**, **2.7b** and **2.8b** (previously synthesized in Chapter 2; Figure 4.4) could also exhibit promising characteristics as NIR fluorophores, a comparative study was

performed in order to evaluate the effect of the number and position of the substituents in the macrocycle on the photophysical features.

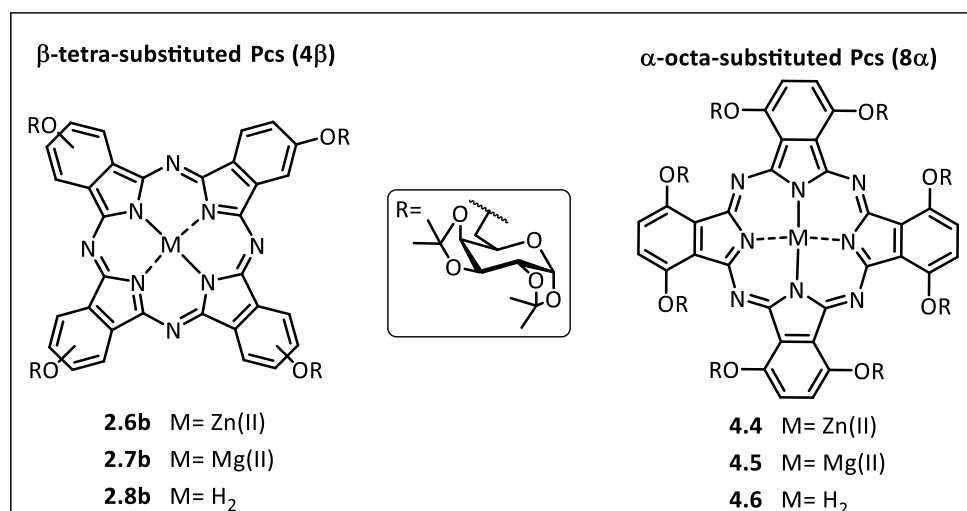


**Figure 4.4.** Phthalocyanines for photophysical properties evaluation in this section.

For all the photophysical characterizations described in further sections, DMSO was chosen as solvent to perform all the studies, since it is the only solvent able to confer the required solubility for all the synthesized phthalocyanines. The UV-Vis spectra obtained for the  $\alpha$ -octa-substituted zinc(II) and magnesium(II) phthalocyanine complexes **4.4** and **4.5** and their metal-free counterpart **4.6** are presented in **Figure 4.5**, as well as, the spectra of the related  $\beta$ -tetra-substituted compounds **2.6b**, **2.7b** and **2.8b**, which are plotted on the same axis for comparison. The values of Q and Soret band absorption maxima and molar extinction coefficients ( $\epsilon$ ), for both  $\beta$ -tetra and  $\alpha$ -octa-substituted phthalocyanines bearing isopropylidene protected *D*-galactose groups are summarized in **Table 4.2**.

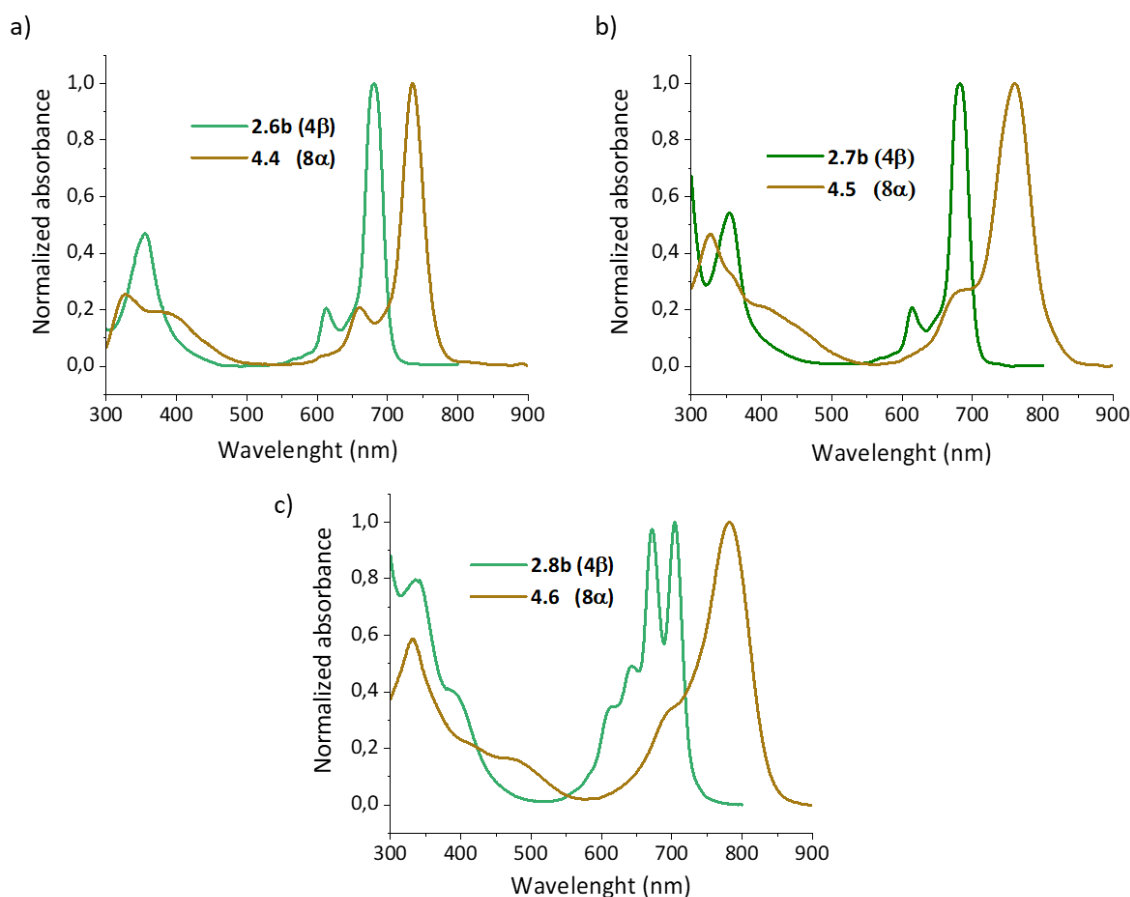


**Figure 4.5.** UV-Vis spectra of the  $\beta$ -tetra-substituted phthalocyanines ( $4\beta$ ) and  $\alpha$ -octa-substituted compounds ( $8\alpha$ ) in DMSO: (a) zinc(II) Pc complexes **2.6b** and **4.4**; (b) magnesium(II) Pc complexes **2.7b** and **4.5**; (c) metal-free Pcs **2.8b** and **4.6**.

**Table 4.2.** UV-Vis absorption data for  $\beta$ -tetra-substituted ( $4\beta$ ) and  $\alpha$ -octa-substituted ( $8\alpha$ ) Pcs bearing isopropylidene protected *D*-galactose groups in DMSO.

Phthalocyanine	Soret band, $\lambda/\text{nm}$ ( $\epsilon/\text{M}^{-1} \text{cm}^{-1}$ )	Q-band, $\lambda/\text{nm}$ ( $\epsilon/\text{M}^{-1} \text{cm}^{-1}$ )
<b><math>\beta</math>-tetra-substituted phthalocyanines</b>		
Zinc(II) complex <b>2.6b</b>	355 ( $7.4 \times 10^4$ )	682 ( $1.6 \times 10^5$ )
Magnesium(II) complex <b>2.7b</b>	355 ( $9.3 \times 10^4$ )	682 ( $1.8 \times 10^5$ )
Metal-free <b>2.8b</b>	342 ( $6.3 \times 10^4$ )	672 ( $8.3 \times 10^4$ ), 704 ( $8.5 \times 10^4$ )
<b><math>\alpha</math>-octa-substituted phthalocyanines</b>		
Zinc(II) complex <b>4.4</b>	326 ( $4.5 \times 10^4$ )	736 ( $1.1 \times 10^5$ )
Magnesium(II) complex <b>4.5</b>	327 ( $4.6 \times 10^4$ )	760 ( $9.7 \times 10^4$ )
Metal-free <b>4.6</b>	332 ( $5.7 \times 10^4$ )	782 ( $9.4 \times 10^4$ )

As shown in **Figure 4.5**, all  $\beta$ -tetra-substituted phthalocyanines showed typical UV-Vis spectra for non-aggregated phthalocyanines, displaying an intense and narrow Q-band in the red visible region of the spectrum. For  $\beta$ -tetra-substituted metallophthalocyanine complexes **2.6b** and **2.7b** (**Figure 4.5a-b**; **Table 4.2**), the Q-bands were observed at 682 nm, as typical of metallophthalocyanines with  $D_{4h}$  symmetry,<sup>20</sup> and the Soret bands were observed at 355 nm. The UV-Vis spectrum of the metal-free phthalocyanine **2.8b** (**Figure 4.5c**; **Table 4.2**), exhibits a split Q-band at 672 and 704 nm, typical of metal-free phthalocyanines with  $D_{2h}$  symmetry,<sup>20</sup> and a Soret band in the ultraviolet region at 342 nm. Comparing the Q-band maximum absorption wavelengths with those of the corresponding unsubstituted zinc(II) (672 nm)<sup>21</sup>, magnesium(II) (670 nm)<sup>22</sup> and metal-free (664 and 698 nm)<sup>23</sup> phthalocyanines in DMSO, the UV-Vis spectra showed a Q-band bathochromic shift of 10 nm, 12 nm and 8 nm, respectively. This bathochromic (red) shift can be ascribed to the introduction of electron-donating  $\beta$ -substituents groups in the periphery of macrocycle, as the electron donor effect decreases the energy level difference between the HOMO and the LUMO orbitals.

Regarding  $\alpha$ -octa-substituted metallophthalocyanine complexes **4.4** and **4.5**, the UV-Vis spectra are also typical of non-aggregated phthalocyanines, exhibiting an intense and sharp Q-band into NIR region at 736 nm and 760 nm, respectively. The Soret bands were observed around  $\approx$  326 nm (**Figure 4.5a-b**; **Table 4.2**). For the  $\alpha$ -octa-substituted metal-free phthalocyanine **4.6** a single broad Q-band was observed at 782 nm, when compared to the parent  $\beta$ -substituted compound **2.8b**, which exhibits a pair of sharp Q-bands in the same region (672 and 704 nm, **Figure 4.5c**). This observation is in agreement with previous reports in the literature.<sup>4a-b,5a,24,25</sup>

From **Figure 4.5** and **Table 4.2** it is clearly observed that the absorption wavelength of the Q-band is strongly red-shifted, in 54–78 nm for the  $\alpha$ -octa-substituted phthalocyanines when compared to the  $\beta$ -tetra-substituted counterparts (682 nm vs. 736 nm for **2.6b** vs. **4.4**; 682 nm vs. 760 nm for **2.7b** vs. **4.5**; 704 nm vs. 782 nm for **2.8b** vs. **4.6**). This observed bathochromic (red) shift is consistent with previous reports for this type of substituted phthalocyanines, and has been attributed to the respective  $\alpha$ -alkoxy substitution pattern. According to literature, the HOMO level is more destabilized by the non-peripheral  $\alpha$ -position than it is by the peripheral  $\beta$ -position, resulting in a decrease of the HOMO–LUMO energy gap, thereby shifting the Q-band



into NIR region.<sup>5a,26-28</sup> In all  $\alpha$ -octa-substituted phthalocyanines, the Soret bands were blue-shifted by 10–29 nm, when compared to the  $\beta$ -tetra-substituted counterparts (355 nm vs. 326 nm for **2.6b** vs. **4.4**; 355 nm vs. 327 nm for **2.7b** vs. **4.5**; 342 nm vs. 332 nm for **2.8b** vs. **4.6**), being in agreement with the literature data.<sup>5a</sup>

Additionally, all synthesized  $\beta$ - and  $\alpha$ -substituted phthalocyanines exhibit a  $\epsilon$  value on the order or closely to  $10^5 \text{ M}^{-1} \text{ cm}^{-1}$  for the Q-band, which is also in agreement with the literature values for this type of substituted phthalocyanines.<sup>4,29,30</sup>

Briefly, the red-shift absorbance with characteristic  $\epsilon$  values of  $\approx 10^5 \text{ M}^{-1} \text{ cm}^{-1}$  in all  $\alpha$ -octa-substituted phthalocyanines makes them attractive as potential NIR fluorophores for FI as the Q-band (736–782 nm) lies in the range of the “phototherapeutic window” (700–900 nm). Hence, this may allow the use of light with longer wavelengths that can penetrate further into the tissue, thereby enabling more effective diagnosis of deep-seated tumor tissues.

After obtaining the UV-Vis absorption spectra, the studies proceeded by measuring the fluorescence emission and excitation spectra of the synthesized compounds, as well their fluorescence quantum yields ( $\Phi_f$ ). The excitation spectrum are particularly relevant for the control of other fluorescent impurities. Thus, if there is only one fluorophore in solution, the excitation spectrum will have a similar shape to its corresponding UV-Vis absorption spectra.<sup>31</sup>

**Figure 4.6** shows the overlap of the UV-Vis absorption, fluorescence emission and excitation spectra of  $\beta$ -tetra-substituted zinc(II) phthalocyanine **2.6b** (**Figure 4.6a**), magnesium(II) phthalocyanine **2.7b** (**Figure 4.6b**), metal-free phthalocyanine **2.8b** (**Figure 4.6c**) and the  $\alpha$ -octa-substituted zinc(II) phthalocyanine **4.4** (**Figure 4.6d**), magnesium(II) phthalocyanine **4.5** (**Figure 4.6e**) and metal-free phthalocyanine **4.6** (**Figure 4.6f**).

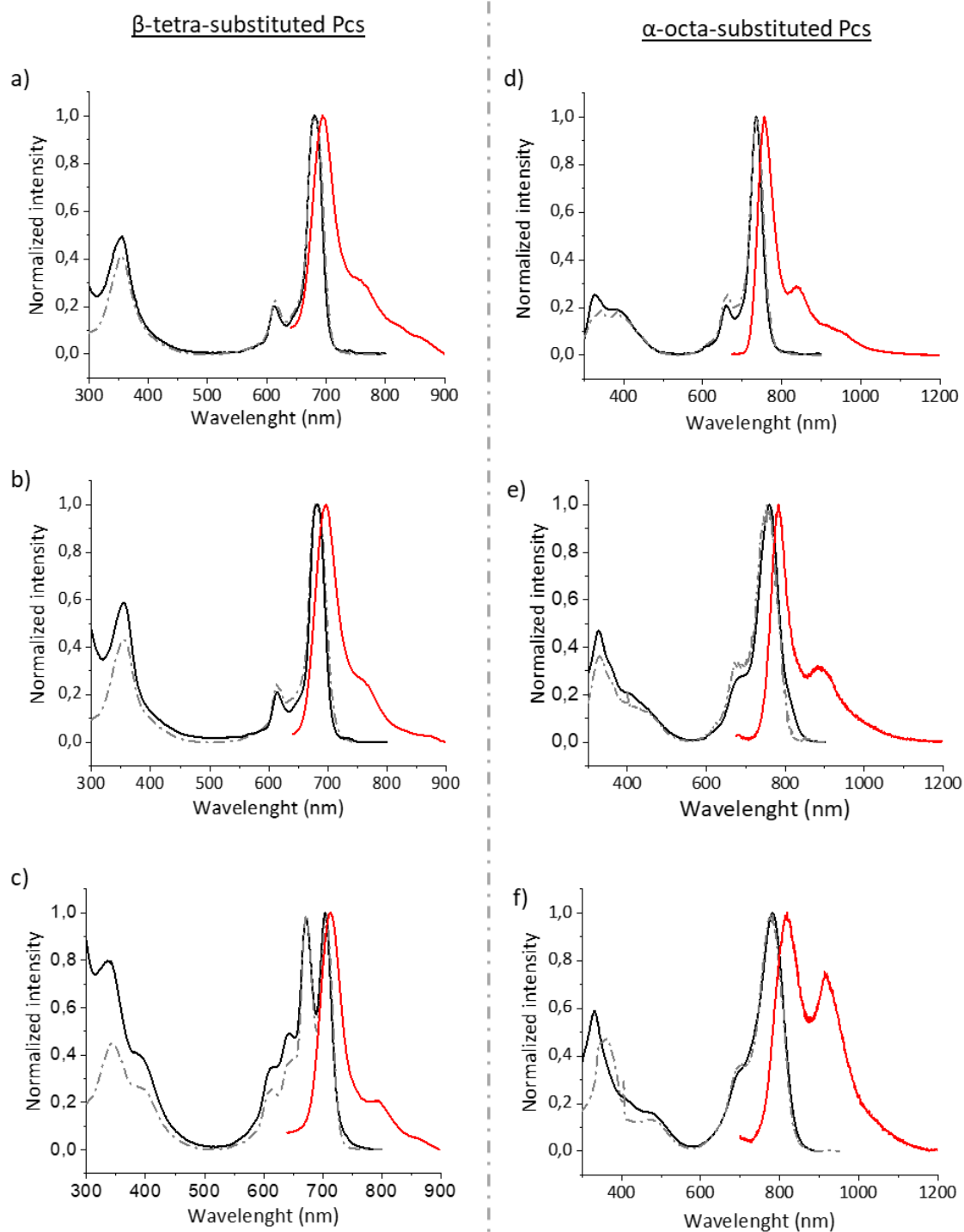


**Figure 4.6.** UV-Vis absorption (black line), fluorescence emission (red line) and excitation (dashed line) spectra overlapping in DMSO of phthalocyanines (a) ZnPc **2.6b** ( $4\beta$ ), (b) MgPc **2.7b** ( $4\beta$ ), (c) H<sub>2</sub>Pc **2.8b** ( $4\beta$ ), (d) ZnPc **4.4** ( $8\alpha$ ), (e) MgPc **4.5** ( $8\alpha$ ) and (f) H<sub>2</sub>Pc **4.6** ( $8\alpha$ ).

From analysis of **Figure 4.6** we can observe that the shape of the excitation spectra is similar to the corresponding UV-Vis absorption spectra shape for all  $\beta$ -tetra- and  $\alpha$ -octa-substituted phthalocyanines, corroborating the presence of a single

fluorophore. The fluorescence emission spectrum of these phthalocyanines is characterized by intense bands with maxima at 694 nm for **2.6b**, 696 nm for **2.7b**, 714 nm for **2.8b**, 753 nm for **4.4**, 782 nm for **4.5** and 812 nm for **4.6**. Furthermore, the fluorescence emission spectra was found to be a good mirror image of the UV-Vis absorption spectra, but shifted to longer wavelengths, which is characteristic of this type of macrocycles.<sup>32</sup>

As previous described, the UV-Vis spectrum of  $\beta$ -tetra-substituted metal-free phthalocyanine **2.8b** showed a pair of Q-bands in the same region (**Figure 4.6c**). However, the emission spectrum of the same compound in the same solvent shows a single peak (not split; **Figure 4.6c**) at a slightly longer wavelength than the absorption peak at 704 nm. This observation is in agreement with Kasha's rule.<sup>33,34</sup>

The fluorescence quantum yields ( $\Phi_F$ ) were calculated based on the comparative method, according to the following equation (1).<sup>35</sup>

$$\Phi_F = \Phi_F^{Std} \frac{F A_{Std} \eta^2}{F_{Std} A \eta_{Std}^2} \quad (1)$$

Where F and  $F_{Std}$  correspond to the fluorescence emission integral of the sample and standard respectively; A and  $A_{Std}$  to the absorption at the wavelength used in the excitation of the sample and standard, respectively;  $\eta$  and  $\eta_{Std}$  correspond to the refractive indices of solvents used for the sample and standard, respectively. Unsubstituted zinc(II) phthalocyanine (ZnPc) was used as the standard ( $\Phi_{FStd}$  (DMSO) = 0.18)<sup>36</sup> to determine the fluorescence quantum yield of  $\beta$ -tetra-substituted phthalocyanines. Regarding  $\alpha$ -octa-substituted phthalocyanines, 1,1',3,3,3',3'-hexamethylindotricarbocyanine iodide (HITIC) was used as standard ( $\Phi_{FStd}$  (Ethanol) = 0.28).<sup>37</sup>

The maximum emission wavelengths and the fluorescence quantum yields for each of synthesized  $\beta$ -tetra- and  $\alpha$ -octa-substituted phthalocyanines are presented in **Table 4.3**.

**Table 4.3.** Fluorescence data obtained for each of synthesized phthalocyanines in DMSO.

Phthalocyanine	$\lambda_{\max}$ emission (nm)	Stokes shift (nm)	$\Phi_F$
<b><math>\beta</math>-tetra-substituted phthalocyanines</b>			
Zinc(II) complex <b>2.6b</b>	694	12	0.19 <sup>a</sup>
Magnesium(II) complex <b>2.7b</b>	696	12	0.34 <sup>a</sup>
Metal-free <b>2.8b</b>	714	10	0.22 <sup>a</sup>
<b><math>\alpha</math>-octa-substituted phthalocyanines</b>			
Zinc(II) complex <b>4.4</b>	753	17	0.17 <sup>b</sup>
Magnesium(II) complex <b>4.5</b>	782	22	0.03 <sup>b</sup>
Metal-free <b>4.6</b>	812	30	0.02 <sup>b</sup>

<sup>a</sup> Ref.  $\Phi_F$  (ZnPc) = 0.18 (DMSO)

<sup>b</sup> Ref.  $\Phi_F$  (HITIC) = 0.28 (Ethanol)

Regarding  $\beta$ -tetra-substituted phthalocyanines **2.6b**, **2.7b** and **2.8b**, we observed a small Stokes shifts within the range  $\approx$  10-12 nm (**Table 4.3**), being typical of tetra-substituted phthalocyanines having peripheral  $\beta$ -substituents,<sup>38,39</sup> due to the macrocyclic ligand rigidity.

The fluorescence quantum yields values obtained for the  $\beta$ -tetra-substituted phthalocyanines ranged from 0.19 to 0.34 (**Table 4.3**), which is in accordance to the values reported in literature.<sup>38,40</sup> Among them, the magnesium(II) phthalocyanine **2.7b** showed an higher fluorescence quantum yield ( $\Phi_F=0.34$ ) than the metal-free **2.8b** ( $\Phi_F=0.22$ ) and zinc(II) **2.6b** ( $\Phi_F=0.19$ ) phthalocyanines, in a trend similar to previously reported in literature.<sup>38,40</sup> The zinc(II) phthalocyanine complex **2.6b** has the lowest fluorescence quantum yield, probably due to heavy atom effect of the central metal atom,<sup>41</sup> which leads to higher intersystem crossing quantum yield from the first excited singlet ( $S_1$ ) state to the first excited triplet ( $T_1$ ) state, resulting in a decrease of its fluorescence. The higher value of fluorescence quantum yield of magnesium(II) phthalocyanine complex **2.7b** has been ascribed by other authors to the the small size of the magnesium(II) central atom,<sup>40b,42</sup> which would result in less intersystem crossing from the  $S_1$  to  $T_1$  state, when compared to zinc(II) phthalocyanine complex **2.6b**.

Although magnesium(II) phthalocyanine complex **2.7b** exhibits promising photophysical characteristics to be applied in FI, as it displays a moderate to high fluorescence quantum yield value ( $\Phi_F = 0.34$ ) and an emission wavelength very closely to NIR region of the electromagnetic spectrum ( $\lambda_{\max} = 696$  nm), it possesses a small Stokes shift (12 nm). This small Stokes shift could significantly limit its application in FI, as it would result in reabsorption of the emitted photons leading to undesired background interferences.

Regarding the  $\alpha$ -octa-substituted phthalocyanines **4.4**, **4.5** and **4.6**, the observed Stokes shifts were within the range  $\approx 17$ -30 nm (**Table 4.3**), being in agreement with the values reported by other authors in literature.<sup>4a-c</sup> These values are much higher in comparison to the corresponding  $\beta$ -tetra substituted compounds (10-12 nm; **Table 4.3**), and it could be attributed to the planarity distortion of the macrocycle caused by the steric repulsion between the eight  $\alpha$ -substituents.<sup>43</sup> Concerning the obtained fluorescence quantum yields (**Table 4.3**), the zinc(II) phthalocyanine **4.4** showed a higher fluorescence quantum yield ( $\Phi_F = 0.17$ ) than the magnesium(II) **4.5** ( $\Phi_F = 0.03$ ) and metal-free **4.6** ( $\Phi_F = 0.02$ ) phthalocyanines. The general trend observed in fluorescence quantum yields values (metal-free **4.6** < magnesium(II) **4.5** < zinc(II) **4.4** phthalocyanines), is opposite to what would be expected based on heavy atom effect, where zinc(II) is expected to show low  $\Phi_F$  values, given its ability to induce intersystem crossing from  $S_1$  to  $T_1$  state. Nevertheless, this positive effect of zinc(II) central metal was also reported by other authors.<sup>4a-b,5a</sup> A possible explanation for this phenomenon could be based on the previous studies reported by Kobayashi and collaborators,<sup>5a</sup> who found that (i) the phthalocyanines showing emission peaks at shorter wavelengths have higher fluorescence quantum yields and (ii) the phthalocyanines showing an emission maximum at wavelengths longer than 740 nm generally have fluorescence quantum yields lower than 0.1. So, apparently, a decrease in  $\Phi_F$  is complemented by an increase in emission wavelengths, which is in agreement with the obtained values for the  $\alpha$ -octa-substituted phthalocyanines presented in **Table 4.3**.

Although  $\alpha$ -octa-substituted magnesium(II) and metal-free phthalocyanines may find interesting applications in NIR FI, due to its large Stokes shifts (22–30 nm) and fluorescence emission wavelength (782–812 nm), its  $\Phi_F$  is too low for FI experiments (**Table 4.3**). However, a good balance between intense absorption and emission in the

“phototherapeutic window” (736 and 753 nm, respectively), reasonable Stokes shift (17 nm) and fluorescence ( $\Phi_F = 0.17$ ) was found for the sterically distorted zinc(II) phthalocyanine complex **4.4**. According to previous studies reported by Arnaut and collaborators<sup>4b</sup> regarding the use of a silicon(IV)  $\alpha$ -octa-butoxy Pc as potential NIR fluorophore, a Stokes shift of 16 nm was appropriate to separate incident and fluorescent light in *in vivo* FI experiments. Overall, the previous results of Arnaut’s study and the satisfactory photophysical properties of  $\alpha$ -octa-substituted zinc(II) phthalocyanine **4.4** enable it to be a promising NIR fluorophore for FI application.

#### 4.4 Conclusion

In summary, in this chapter, we describe the development of alternative synthetic methods for a new family of non-planar octa-substituted metallophthalocyanines and their metal-free counterparts, containing eight isopropylidene protected *D*-galactose units with a  $\alpha$ -substitution pattern, *via* cyclotetramerization reaction of 3,6-disubstituted phthalonitrile precursor **4.3**. We have successfully synthesized the corresponding zinc(II), magnesium(II) and metal-free phthalocyanines in 25%, 15% and 9% isolated yields, respectively. All compounds have been fully characterized by <sup>1</sup>H-NMR, MS and UV-Vis techniques. Furthermore, we present the photophysical characterization of the new  $\alpha$ -octa-substituted phthalocyanines family, along with the related  $\beta$ -tetra-substituted compounds (whose synthesis is described in Chapter 2).

Concerning their potential application as NIR fluorophores, we concluded that some of these new biocompatible compounds present a strong absorption, having high molar absorption coefficients in the “phototherapeutic window” (700–900 nm). Moreover, some of them present large fluorescence quantum yields ( $\Phi_F$ ) and large Stokes shifts, which fulfill the main prerequisites for an ideal NIR fluorophore.

Among the  $\beta$ -tetra-substituted phthalocyanines, the magnesium(II) complex **2.7b** displays a high fluorescence quantum yield ( $\Phi_F = 0.34$ ), concomitantly with a strong absorption (682 nm) and emission (696 nm), close to the “phototherapeutic window”, but shows a relatively small Stokes shift (12 nm).

Regarding the  $\alpha$ -octa-substituted phthalocyanines, the fine-tuning of NIR absorbance of every synthesized metal and metal-free phthalocyanines is evident, as they all exhibit a strong red-shift absorption (736–782 nm), lying in the “phototherapeutic window”. Particularly, the  $\alpha$ -octa-substituted zinc(II) phthalocyanine complex **4.4** has a strong NIR absorption and emission (736 and 753 nm, respectively), a moderate fluorescence quantum yield ( $\Phi_F = 0.17$ ) and presents a Stokes shift of 17 nm. Overall, these photophysical characteristics match with the required features for development of ideal new NIR fluorophores. We further conclude that the zinc(II) phthalocyanine complex **4.4** is the most promising NIR fluorophore and that the presence of eight isopropylidene protected *D*-galactose substituent groups may contribute to the specific targeting of the cancer cells, thereby enabling cancer early detection. However, future *in vitro* and *in vivo* studies must be performed to demonstrate its suitability as an effective NIR fluorophore for early cancer diagnosis, through FI technique.

## 4.5 References

- <sup>1</sup> Gibbs, S. L., *Quantitative Imaging in Medicine and Surgery* **2012**, 2 (3), 177–187.
- <sup>2</sup> (a) Turkmen, A.T.; Zeng, L.; Cui, Y.; Fidan, İ.; Dumoulin, F.; Hirel, C.; Zorlu, Y.; Ahsen, V.; Chernonosov, A. A.; Chumakov, Y.; Kadish, K. M.; Gürek, A. G.; Öztürk, S. T., *Inorganic Chemistry* **2018**, 57 (11), 6456–6465; (b) Cidlina, A.; Pausimova, Z.; Miletin, Miroslav, M.; Zimcik, P.; Novakova, V., *Journal of Porphyrins and Phthalocyanines* **2015**, 19 (10), 1095–1106; (c) Cook, M. J.; Chambrier, I., *Journal of Porphyrins and Phthalocyanines* **2011**, 15 (03), 149–173.
- <sup>3</sup> (a) Köksoy, B.; Durmuş, M.; Bulut, M., *Journal of Luminescence* **2015**, 161, 95–102; (b) Durmuş, M.; Nyokong, T., *Polyhedron* **2007**, 26 (13), 3323–3335.
- <sup>4</sup> (a) Safonova, E. A.; Meshkov, I. N.; Polovkova, M. A.; Volostnykh, M. V.; Yu, A.; Yulia, T.; Gorbunova, G., *Mendeleev Communications* **2018**, 28 (3), 275–277; (b) Lobo, A. C.; Silva, A. D.; Tomé, V. A.; Pinto, S. M.; Silva, E. F.; Calvete, M. J. F.; Gomes, C. M.; Pereira, M. M.; Arnaut, L. G., *Journal of Medicinal Chemistry* **2016**, 59 (10), 4688–4696; (c) Zorlu, Y.; Dumoulin, F.; Durmuş, M.; Ahsen, V., *Tetrahedron* **2010**, 66, 3248–3258; (d) Durmuş, M.; Ayhan, M. M.; Gürek, A. G.; Ahsen, V., *Dyes and Pigments* **2008**, 77 (3), 570–577.
- <sup>5</sup> (a) Kobayashi, N.; Ogata, H.; Nonaka, N.; Luk'yanets, E. A., *Chemical European Journal* **2003**, 9 (20), 5123–5134; (b) Wróbel, D.; Boguta, A., *Journal of Photochemical and Photobiology A: Chemistry* **2002**, 150 (1–3), 67–76; (c) Cook, M. J.; Dunn, A. J.; Howe, S. D.; Thomson, A. J., *Journal of the Chemical Society Perkin transactions I* **1988**, 8, 2453–2458.
- <sup>6</sup> Iqbal, Z.; Hanack, M.; Ziegler, T., *Tetrahedron Letters* **2009**, 50 (8), 873–875.
- <sup>7</sup> Soares, A. R. M.; Tomé, J. P. C.; Neves, M. G. P. M. S.; Tomé, A. C.; Cavaleiro, J. A. S.; Torres, T., *Carbohydrate Research* **2009**, 344 (4), 507–510.
- <sup>8</sup> Iqbal, Z.; Lyubimtsev, A.; Herrmann, T.; Hanack, M.; Ziegler, T., *Synthesis* **2010**, 18, 3097–3104.
- <sup>9</sup> Berthold, H. J.; Franke, S.; Thiem, J.; Schotten, T., *Journal of Organic Chemistry* **2010**, 75 (11), 3859–3862.
- <sup>10</sup> Aggarwal, A.; Singh, S.; Zhang, Y.; Anthes, M.; Samaroo, D.; Gao, R.; Drain, C. M., *Tetrahedron Letters* **2011**, 52 (42), 5456–5459.
- <sup>11</sup> Silva, S.; Pereira, P. M. R.; Silva, P.; Almeida Paz, F. A.; Faustino, M. A. F.; Cavaleiro, J. A. S.; Tomé, J. P. C., *Chemical Communications* **2012**, 48 (30), 3608–3610.
- <sup>12</sup> (a) May Jr., J. A.; Sartorelli, A. C., *Journal of Medicinal Chemistry* **1979**, 22 (8), 971–976; (b) Benati, L.; Leardini, R.; Minozzi, M.; Nanni, D.; Scialpi, R.; Spagnolo, P.; Strazzari, S.; Zanardi, G., *Angewandte Chemie International Edition* **2004**, 43 (27), 3598–3601.
- <sup>13</sup> Crucius, G.; Hanack, M.; Ziegler, T., *Journal of Porphyrins and Phthalocyanines* **2013**, 17 (08), 807–813.
- <sup>14</sup> de la Hoz, A.; Loupy, A., *Microwaves in Organic Synthesis*, 3<sup>rd</sup> edition, volume 1, Wiley-VCH Verlag GmbH & Co. KGaA, Germany, **2012**, Chapter 4, 127–208.



- <sup>15</sup> (a) Karaoğlu, H. R. P.; Yenilmez, H. Y.; Koçak, M. B., *Journal of Coordination Chemistry* **2018**, 71 (15), 2340–2357; (b) Acar, I.; Kantekin, H.; Biyikliouglu, Z., *Journal of Organometallic Chemistry* **2010**, 695 (2), 151–155; (c) Loupy, A.; Bogdal, D.; Petit, A., *Tetrahedron* **2005**, 61 (1), 179–188.
- <sup>16</sup> Del Sole, R.; De Luca, A.; Mele, G.; Vasapollo, G., *Journal of Porphyrins and Phthalocyanines* **2005**, 9 (7), 519–527.
- <sup>17</sup> (a) Fukuda, T.; Ishiguro, T.; Kobayashi, N., *Tetrahedron Letters* **2005**, 46 (16), 2907–2909; (b) McKeown, N. B.; Chambrier, I.; Cook, M. J., *Journal of the Chemical Society Perkin transactions I* **1990**, 4, 1169–1177; (c) Cook, M. J.; Daniel, M. F.; Harrison, K. J.; McKeown, N. B.; Thomson, A. J., *Journal of the Chemical Society-Chemical Communications* **1987**, 14, 1086–1088.
- <sup>18</sup> Cammidge, A. N.; Cook, M. J.; Hughes, D. L.; Nekelson, F.; Rahman, M., *Chemical Communications* **2005**, 930–932.
- <sup>19</sup> Khene, S.; Cammidge, A. N.; Cook, M. J.; Nyokong, T., *Journal of Porphyrins and Phthalocyanines* **2007**, 11 (10), 761–770.
- <sup>20</sup> Isago, H., *Optical Spectra of Phthalocyanines and Related Compounds*, Springer, Tsukuba, Japan, **2015**, Chapter 2, 21–40.
- <sup>21</sup> Gürol, I.; Durmuş, M.; Ahsen, V.; Nyokong, T., *Dalton Transactions* **2007**, 34, 3782–3791.
- <sup>22</sup> Ghani, F.; Kristen, J.; Riegler, H., *Journal of Chemical and Engineering Data* **2012**, 57 (2), 439–449.
- <sup>23</sup> Edwards, L.; Gouterman, M., *Journal of Molecular Spectroscopy*, **1970**, 33 (2), 292–310.
- <sup>24</sup> (a) Martynov, A. G.; Mack, J.; May, Aviwe K.; Nyokong, T.; Gorbunova, Y. G.; Tsivadze, A. Y., *ACS Omega* **2019**, 4 (4), 7265–7284; (b) Furuyama, T.; Maeda, K.; Maeda, H.; Segi, M., *Journal of Organic Chemistry* **2019**, 84 (21), 14306–14312.
- <sup>25</sup> Fukuda, T.; Ishiguro, T.; Kobayashi, N., *Tetrahedron Letters* **2005**, 46 (16), 2907–2909.
- <sup>26</sup> Iqbal, Z.; Masilela, N.; Nyokong, T.; Lyubimtsev, A.; Hanack, M.; Ziegler, T., *Photochemical & Photobiological Sciences* **2012**, 11 (4), 679–686.
- <sup>27</sup> Kobayashi, N.; Furuyama, T.; Satoh, K., *Journal of the American Chemical Society* **2011**, 133, 19642–19645.
- <sup>28</sup> (a) Mack, J.; Kobayashi, N., *Chemical Reviews* **2011**, 111 (2), 281–321; (b) Cheng, G.; Peng, X.; Hao, G.; Kennedy, V. O.; Ivanov, I. N.; Knappenberger, K.; Hill, T. J.; Rodgers, M. A. J.; Kenney, M. E., *Journal of Physical Chemistry A* **2003**, 107, 3503–3514.
- <sup>29</sup> (a) Lv, F.; Li, Y.; Cao, B.; Liu, T., *Journal of Materials Science: Materials in Medicine* **2013**, 24 (3), 811–819; (b) Saka, E. T.; Durmuş, M.; Kantekin, H., *Journal of Organometallic Chemistry* **2011**, 696 (4), 913–924.
- <sup>30</sup> Gürel, E.; Pişkin, M.; Altun, S.; Odabaş, Z.; Durmuş, M., *Dalton Transactions* **2015**, 44 (13), 6202–6211.
- <sup>31</sup> Lakowicz, J. R., *Principles of Fluorescence Spectroscopy*, 3<sup>rd</sup> edition, Springer Science and Business Media, Singapore, **2006**, Chapters 1-2, 1–62.
- <sup>32</sup> Colak, S.; Durmuş, M.; Yıldız, S. Z., *Dalton Transactions* **2016**, 45, 10402–10410.

- 
- <sup>33</sup> Kasha, M., *Discussions of the Faraday Society* **1950**, 9, 14–19.
- <sup>34</sup> Freyer, W.; Mueller, S.; Teuchner, K., *Journal of Photochemistry and Photobiology A: Chemistry* **2004**, 163 (1-2), 231–240.
- <sup>35</sup> Fery-Forgues, S.; Lavabre, D., *Journal of Chemical Education* **1999**, 76 (9), 1260–1264.
- <sup>36</sup> Gurol, I.; Durmuş, M.; Ahsen, V.; Nyokong, T., *Dalton Transactions* **2007**, 34, 3782–3791.
- <sup>37</sup> Rurack, K.; Spieler, M., *Analytical Chemistry* **2011**, 83, 1232–1242.
- <sup>38</sup> Ömer, T.; Kılıçarslan, F. A.; Atmaca, G. Y.; Erdoğan, A., *Journal of Porphyrins and Phthalocyanines* **2018**, 22 (01-03), 250–265.
- <sup>39</sup> (a) Saka, E. T.; Göl, C.; Durmuş, M.; Kantekin, H.; Bıyıklıoğlu, Z., *Journal of Photochemistry and Photobiology A: Chemistry* **2012**, 241, 67–78; (b) Arslanoğlu, Y.; Idowu, M.; Nyokong, T., *Spectrochimica Acta Part A: Molecular and Biomolecular Spectroscopy* **2012**, 95, 407–413.
- <sup>40</sup> (a) Nombona, N.; Chidawanyika, W.; Nyokong, T., *Journal of Molecular Structure* **2012**, 1012, 31–36; (b) Canlica, M.; Nyokong, T., *Inorganica Chimica Acta* **2010**, 363 (13), 3384–3389.
- <sup>41</sup> Alberto, M. E.; De Simone, B. C.; Mazzone, G.; Sicilia, E.; Russo, N., *Physical Chemistry Chemical Physics* **2015**, 17, 23595–23601.
- <sup>42</sup> (a) Erdoğan, A.; Uğur, A. L.; Memişoğlu, A.; Erden, İ., *Journal of Luminescence* **2013**, 134, 483–490; (b) Nombona, N.; Chidawanyika, W.; Nyokong, T., *Polyhedron* **2011**, 30, 654–659.
- <sup>43</sup> Isago, H., *Optical Spectra of Phthalocyanines and Related Compounds*, Springer, Japan **2015**, Chapter 4, 107–132.

## CHAPTER 5

---

### *Experimental*

---

In this section, general information is provided, regarding materials, reagents and solvents, as well as the techniques and instruments used during the experimental work of this thesis. Briefly, this chapter is divided into five experimental sections:

- In section 5.1 is presented the instrumentation and methodology;
- In section 5.2 is described the reagents and solvents;
- In sections 5.3, 5.4 and 5.5 are presented the synthesis and the full characterization of the compounds previously synthesized in Chapter 2, Chapter 3 and Chapter 4, respectively.

### **5.1 Instrumentation and methodology**

#### **i) Organic chemistry**

##### **Thin Layer Chromatography (TLC)**

The reaction control, when necessary, was performed using thin layer chromatography (TLC) using aluminum plates coated with silica 60 (Sigma-Aldrich), with fluorescence indicator UV<sub>254</sub>, developed with appropriated mobile phases.

### **Column Chromatography**

The reaction products, when necessary, were purified by column chromatography using silica gel 60 (particles of size 0.06-0.20 mm) or neutral aluminum oxide as stationary phases and the appropriate eluents.

### **Dialysis**

The reaction products, when necessary, were purified by dialysis using an Amicon® stirred cells system (Milipore Corporation) with molecular weight cut-off membrane's of 1000 Da or a Pur-A-Lyzer™ Mega Dialysis Kit (Sigma-Aldrich Co. LLC, Portugal).

### **Ultrasound**

To facilitate the dissolution of some of the compounds studied, a Bandelin Sonorex TK52 device was used as the ultrasound system. Moreover, some organic reactions were performed using this system as an alternative source to conventional heating.

### **Microwave synthesis**

The microwave-assisted reactions were performed using a CEM Discover® SP microwave system. Appropriate glass tubes with a capacity of 10 mL were used.

### **Nuclear Magnetic Resonance Spectroscopy (NMR)**

NMR spectra were recorded on Bruker Advance 400 spectrometer (Department of Chemistry, University of Coimbra), using the appropriated deuterated solvent. The  $^1\text{H}$  and  $^{13}\text{C}$  chemical shifts ( $\delta$ ), expressed in ppm, are generally relative to a TMS internal standard ( $\delta = 0.00$  ppm). The data obtained are indicated in the following order: Nucleus (apparatus, solvent): chemical shift ( $\delta$ , ppm) [multiplicity (s – singlet, sl – large singlet, d - doublet, dd – double doublet, t – triplet, q – quartet, m – multiplet, br – broad signal), coupling constant ( $J$ , in Hertz), relative intensity (nH as number of protons), assignment in the structure].

### **Gas Chromatography coupled with Mass Spectrometry (GC-MS)**

GC-MS analysis was performed using an Hewlett-Packard Agilent 6890 chromatographer with HP-5 MS capillary column (30 m  $\times$  0.25 mm  $\times$  0.25  $\mu\text{m}$ ) coupled to Hewlett-Packard

5973 MSD spectrometer, belonging to Department of Chemistry of University of Coimbra.

### **Mass Spectrometry (MS)**

High-resolution mass spectrometry was carried out on a Bruker Microtof apparatus, equipped with selective ESI or MALDI detector, belonging to Unidade de Masas e Proteómica from the University of Santiago de Compostela (Spain) or on MALDI Ultraflex extreme Bruker Daltonics, belonging to Centro Analítico de Instrumentação from the University of São Paulo (Brazil).

### **Infrared Spectroscopy (IR)**

The FT-IR spectra were taken in a Thermo Scientific Nicolet 380 spectrometer, belonging to Department of Chemistry from the University of Coimbra.

### **Elemental analysis**

Elemental analysis for carbon, hydrogen and nitrogen were measured on LECO model (CHNS 932) Instruments apparatus, belonging to Unidade de Masas e Proteómica from University of Santiago de Compostela (Spain).

### **UV-Visible spectroscopy (UV-Vis)**

UV-Vis absorption spectra were obtained in a Hitachi U-2010 and Shimadzu UV-1700 spectrophotometers with 1 cm double-stranded quartz cells with 1 cm optical path and using the respective solvent as reference. The molar extinction coefficient ( $\epsilon$ ) of phthalocyanine compounds were determined according to Beer-Lambert's law,  $A = \epsilon bc$ , where  $A$  is the absorbance,  $\epsilon$  is the molar extinction coefficient,  $b$  is the light's path and  $c$  is the concentration of the solution. For each compound, a minimum of 6 solutions (by dilution of a stock solution) were prepared in concentrations ranging from  $10^{-6}$  to  $10^{-5}$  M in DMSO corresponding to absorbance values between 0.1 and 1.0. The absorption for the maximum band's considered as a function of the concentration of the different solutions was represented graphically, obtaining a line whose slope value corresponds to the value of the molar extinction coefficient. **Figure 5.1** exemplifies this methodology by showing the UV-Vis spectra obtained from the several dilutions in the case of the

$\beta$ -tetra-substituted zinc(II) phthalocyanine **2.6b** and its linear adjustment to the relation between concentration and absorbance at their respective maximum absorption (682 nm).

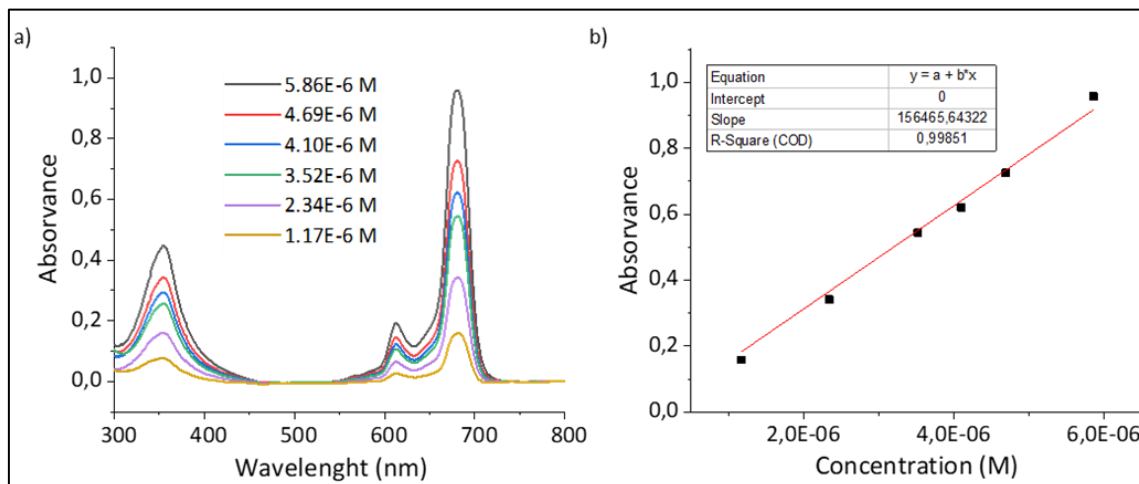


**Figure 5.1.** Determination of the molar extinction coefficient of  $\beta$ -tetra-substituted zinc(II) phthalocyanine **2.6b**: (a) UV-Vis spectra of all solutions in DMSO (b) Ratio obtained between concentration and absorbance at 682 nm and its corresponding linear adjustment.

### Fluorescence spectroscopy

The fluorescence emission spectra were obtained in Horiba Jobin Yvon e Spex Fluorolog 3.22 spectrophotometer equipped with a Hamamatsu R5509–42 photomultiplier, cooled to 193 K, and a fiber optic USB2000FL Ocean Optics fluorescence (350–1000 nm). The fluorescence quantum yields ( $\Phi_F$ ) of the phthalocyanines were determined in DMSO using a comparative method, according to Equation (1).<sup>1</sup>

$$\Phi_F = \Phi_F^{Std} \frac{F A_{Std} \eta^2}{F_{Std} A \eta_{Std}^2} \quad (1)$$

where  $F$  and  $F_{Std}$  are the integrals of the fluorescence emission curves of phthalocyanine sample and the standard, respectively.  $A$  and  $A_{Std}$  are the respective absorbances of the phthalocyanine sample and the standard at the excitation wavelength and  $\eta$  and  $\eta_{Std}$  are the refractive indices of the solvents used for the phthalocyanine sample and standard, respectively. In case of  $\beta$ -tetra-substituted phthalocyanines, unsubstituted zinc(II) phthalocyanine (ZnPc) in DMSO ( $\Phi_F = 0.18$ )<sup>2</sup> was used as standard. The absorbance of

tested solutions at the excitation wavelength (610-630 nm) ranged between 0.04 and 0.06. In the case of  $\alpha$ -octa-substituted phthalocyanines, 1,1',3,3',3',3'-hexamethylindotricarbocyanine iodide (HITIC) in ethanol ( $\Phi_F = 0.28$ )<sup>3</sup> was used as standard. The absorbance of tested solutions at the excitation wavelength (640-670 nm) ranged between 0.04 and 0.08.

## ii) Radiochemistry

### General considerations

All procedures were performed at Radiochemistry and Cyclotron Laboratory at ICNAS - Produção Unipessoal, Lda (ICNAS-P), following the required radiation protection rules. Manipulations of radioactive solutions were done using a lead protection barrier with a lead glass shield visor. The vials that contained radioactive solutions were placed inside lead containers with adequate thickness. The radiochemical yield (RCY) is defined as the amount of activity in the product expressed as the percentage (%) of starting activity used in the corresponding process; all RCYs presented in this thesis are non-decay corrected. The radiochemical purity is defined as the absence of other radiochemical compounds/species.

### Radio-Thin Layer Chromatography (Radio-TLC)

TLC analysis of <sup>64</sup>Cu-labelled phthalocyanine samples was done using an iTLC-SG (Instant Thin Layer Chromatography Medium (iTLC) is a binderless, glass microfiber chromatography paper impregnated with a silica gel (SG)) (Agilent Technologies). The samples were quenched with EDTA (10 mM) prior to analysis to chelate free copper-64 ions for ease of analysis. 1  $\mu$ l sample was spotted on a TLC strip and developed in mobile phase mixture 10% NH<sub>4</sub>OAc/MeOH (1:1). Radioactive distribution on the radio-TLC strips was detected using a miniGITA Star Gamma TLC Scanner with a V-BGO-Detector (Elysia-Raytest, Germany). Radiochemical conversions (RCCs) and radiochemical purities were calculated by dividing the radioactivity of the products spots by the total radioactivity deposited on the radio-TLC strip. All <sup>64</sup>Cu-labelled phthalocyanines displayed a  $R_f \approx 0$  and the "free" copper-64 (<sup>64</sup>Cu)[Cu(EDTA)] complex) exhibited a  $R_f \approx 1$ .

### **Solid Phase Extraction (SPE)**

The  $^{11}\text{C}$ - or  $^{64}\text{Cu}$ -labelled products, when necessary, were purified by solid phase extraction using a reversed-phase C18 cartridge (Sep-Pak<sup>®</sup> Light C18 cartridge, Waters, Ireland). Previously to purification process, the C18 SEP cartridge was activated with 5 mL of ethanol and then 5 mL of water.

### **High Performance Liquid Chromatography (HPLC)**

Analytical HPLC analysis was performed using Agilent 1260 Infinity II LC System with a Quaternary Pump G7111B coupled to an UV-Vis (variable wavelength detector G7114A) and radioactivity (Raytest, model Gabi Star T1, 0A) detector and a Rheodyne (IDEX H&S, Wertheim-Mondfeld, Germany) model 7125i syringe-loading sample injector valve with a 20  $\mu\text{l}$  loop. HPLC was performed using a mixture of ammonium formate buffer (0.1 M, pH= 7.2) and acetonitrile as the eluent with the selected flow rate by means of analytical reverse-phase Agilent Zorbax Eclipse XDB-C18 column (5  $\mu\text{m}$ , 4.5 x 150 mm, Agilent Technologies, USA).

### **Radioactivity measure**

The radioactivity of the solutions was measured using a dose calibrator (Ned Isomed 2010, version 5.4.66, MED Nuklear-Medizintechnik Dresden GmbH, Dresden, Deutschland).

### **Carbon-11 automated radiosynthesis module**

$[^{11}\text{C}]\text{CO}_2$  was generated in an IBA Cyclone 18/9 cyclotron (IBA, Louvain-la-Neuve, Belgium) *via* the nuclear reaction  $^{14}\text{N}(p,\alpha)^{11}\text{C}$ . The target gas [ $\text{N}_2$  with 0.5%  $\text{O}_2$ ] was irradiated with 16.5 MeV protons and the beam current was maintained at 21  $\mu\text{Ah}$  (pressure in the range 18-19 bar) during the bombardement to produce the  $[^{11}\text{C}]\text{CO}_2$ . The  $[^{11}\text{C}]\text{CH}_3\text{I}$  was produced by the so called "gas method"<sup>4</sup> in a Synthra C-11 Choline (Synthra GmbH, Hamburg, Germany) starting from  $[^{11}\text{C}]\text{CO}_2$ . The  $^{11}\text{C}$ -methylation reaction occurred in a specially designed HPLC loop (Autoloop system, Bioscan Inc., Washington DC, USA). The  $^{11}\text{C}$ -labelled product were purified using a semi-preparative HPLC system composed by a HPLC K-501 pump (Knauer, Berlin, Germany), a Phenomenex Luna C18 reverse-phase (RP) HPLC column (5  $\mu\text{m}$ , 250 x 10 mm,



Phenomenex, Le Pecq Cedex, France), a UV K-200 detector set at 254 nm (Knauer, Berlin, Germany), and a radioactivity detector. On the last step of the synthesis, the desired fraction was collected and reformulated using a C-11 reformulation kit Extension (Fluidomica, Coimbra, Portugal) using the IBA Synthera® Extension automated module (IBA, Louvain-la-Neuve, Belgium) and the flow of the solutions involved (water, ethanol and 0.9% NaCl) were remotely controlled by pressurization and/or vacuum of the desired compartments.

### **Quality control of carbon-11 labelled product**

Quality control of  $^{11}\text{C}$ -labelled product was performed to verify their purity and safety for *in vivo* injection. An Agilent 1260 Infinity II LC Series HPLC system with a UV (254 nm) and radioactivity detector was used. The chromatographic separation was performed using an analytical reverse-phase Agilent Zorbax Eclipse XDB-C18 column (5  $\mu\text{m}$ , 150x 4.5 mm) using a flow of 2  $\text{mL}\cdot\text{min}^{-1}$  and as eluent a mixture of acetonitrile and ammonium formate buffer (0.1 M, pH= 7.2) (65:35, respectively). The carbon-11 radioisotope identity was confirmed by measuring its half-life in a dose calibrator. To monitor the residual solvents concentration in the final  $^{11}\text{C}$ -labelled product solution it was used a gas chromatography (GC) system (GC Agilent 6850; RaytestGmbH, Straubenhardt, Germany). The pH was measured using a pH meter (JENWAY 3510 pH; Bibby Scientific Limited, Staffordshire, UK).

## **5.2 Solvents and reagents**

All solvents and chemicals were commercially obtained from Merck (Portugal), Sigma-Aldrich (Portugal) or FluoroChem (United Kingdom). The chalcone compounds were kindly provided by Professor Gilberto Aquino (Faculty of Pharmacy, State University of Goiás, Brazil). Air and moisture sensitive reagents or solutions were handled under nitrogen or argon atmosphere, in a vacuum system, using Schlenk techniques.<sup>5</sup> All the glassware was dried by heating. The solvents were purified by simple

distillation or, when necessary, properly dried and distilled by the standard procedures reported by literature,<sup>6</sup> described below.

#### **Dichloromethane, chloroform, ethyl acetate, hexane, acetone, ethanol**

These solvents were purified by simple distillation. Each one was placed in a round-bottom flask, with anhydrous calcium sulfate and pumice stone. The mixture was kept under reflux, for two hours. After distillation, the solvent was collected and passed through a column of basic alumina (grade I) and stored in a flask containing activated molecular sieves (3Å).

#### **Dichloromethane**

For experiments, which were highly water sensitive, dichloromethane was dried with calcium hydride, under reflux, for 5 h. After distillation, the solvent was collected and stored, under nitrogen atmosphere, in a vessel containing activated molecular sieves (3Å).

#### **Triethylamine, toluene and pyridine**

The solvents were dried with sodium flakes and benzophenone. The mixture was kept under reflux, at the boiling temperature for each solvent, until a strong blue color was observed. After distillation, the solvent was collected and stored, under nitrogen atmosphere, in a vessel containing activated molecular sieves (3Å).

#### **N,N-Dimethylformamide (DMF)**

DMF was placed in a round-bottom flask for 24 h with calcium oxide, previously activated in a muffle furnace at 500 °C. After this time NaOH pellets were added and the mixture was stirred for 1 h. After distillation under reduced pressure, the solvent was collected and stored in a vessel containing activated molecular sieves (3Å).

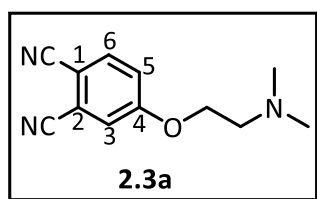
### 5.3 Experimental (referring to Chapter 2)

In this section, the synthetic procedures of 4-substituted phthalonitriles and  $\beta$ -tetra-substituted phthalocyanines are provided, as well as, their full characterization. Moreover, the  $^{64}\text{Cu}$ -labelling protocol of  $\beta$ -tetra-substituted phthalocyanines were also described. All  $^{64}\text{Cu}$ -labelling experiments were performed in Radiochemistry and Cyclotron Laboratory at ICNAS-P. The production and purification of  $^{64}\text{Cu}$  was carried out by Vítor Alves (PhD) from ICNAS-P. The *in vivo* PET imaging and biodistribution studies in mice were performed by José Sereno (PhD) from ICNAS Pre-Clinical Imaging Facility.

#### 5.3.1 Synthesis of 4-substituted phthalonitriles

##### 4-(dimethylaminoethoxy)phthalonitrile (**2.3a**)

In a round bottom flask, 1,2-(dimethylamino)-ethanol **2.2a** (0.70 mL, 6.93 mmol, 1.2 equiv.) and anhydrous  $\text{K}_2\text{CO}_3$  (4 g, 28.9 mmol, 5 equiv.) were mixed in anhydrous DMF (30 mL). Then, 4-nitrophthalonitrile (**2.1**) (1 g, 5.78 mmol) was added and the mixture was stirred for 96 h at room temperature (or 8 h in ultrasounds). The reaction mixture was filtered off, then diluted with dichloromethane (100 mL) and washed with distilled water (10x 50 mL). The organic phase was dried with anhydrous sodium sulfate, filtered and solvent was evaporated under reduced pressure. After purification by column chromatography on silica gel, using as eluent a mixture of dichloromethane/methanol (20:1), the target compound **2.3a** was obtained as a yellowish orange oil, in 83% isolated yield (1.03 g, 4.79 mmol) (81% in the case of ultrasonic irradiation). Spectroscopic data is in agreement with literature.<sup>7,8</sup>

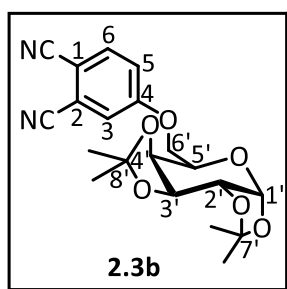


**$^1\text{H-NMR}$  (400 MHz,  $\text{CDCl}_3$ ),  $\delta/\text{ppm}$ :** 7.70 (d,  $J = 8.8$  Hz, 1H, H-6), 7.28 (d,  $J = 2.4$  Hz, 1H, H-3), 7.21 (dd,  $J = 8.8, 2.4$  Hz, 1H, H-5), 4.13 (t,  $J = 5.5$  Hz, 2H,  $\text{OCH}_2$ ), 2.76 (t,  $J = 5.4$  Hz, 2H,  $\text{OCH}_2\text{CH}_2$ ), 2.33 (s, 6H,  $\text{N}(\text{CH}_3)_2$ ).  **$^{13}\text{C-NMR}$  (100.1 MHz,  $\text{CDCl}_3$ ),  $\delta/\text{ppm}$ :** 161.8 ( $\text{C}_{\text{Ar}}\text{-O}$ ), 135.0 ( $\text{C}_{\text{Ar}}$ ), 119.5 ( $\text{C}_{\text{Ar}}$ ), 119.3 ( $\text{C}_{\text{Ar}}$ ), 117.2 ( $\text{C}_{\text{Ar}}$ ), 115.5 (CN),

115.1 (CN), 107.2 (C<sub>Ar</sub>), 67.1 (OCH<sub>2</sub>), 57.6 (OCH<sub>2</sub>CH<sub>2</sub>), 45.7 (N(CH<sub>3</sub>)<sub>2</sub>). **GC/MS (EI)**: m/z = 214.1 [M-H]<sup>+</sup>.

#### 4-(1,2:3,4-Di-*O*-isopropylidene- $\alpha$ -D-galactopyranos-6-*O*-yl)phthalonitrile (**2.3b**)

In a round bottom flask, 1,2:3,4-di-*O*-isopropylidene- $\alpha$ -D-galactopyranose **2.2b** (1.80 g, 6.93 mmol, 1.2 equiv.) and anhydrous K<sub>2</sub>CO<sub>3</sub> (4 g, 28.9 mmol, 5 equiv.) were mixed in anhydrous DMF (30 mL). Then, 4-nitrophthalonitrile (**2.1**) (1 g, 5.78 mmol) was added and the mixture was stirred for 72 h at room temperature (or 4 h in ultrasounds). The reaction mixture was filtered off, and suspended in 250 mL of cold water. The resulting precipitate was filtered, washed with water and dried under reduced pressure. After purification by column chromatography on silica gel, using dichloromethane as eluent, the target compound **2.3b** was obtained as a white solid, in 77% isolated yield (1.72 g, 4.45 mmol) (79% in the case of ultrasonic irradiation), after being precipitated from dichloromethane/petroleum ether. Spectroscopic data is in agreement with literature.<sup>9-11</sup>



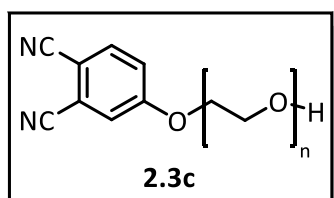
**<sup>1</sup>H-NMR (400 MHz, CDCl<sub>3</sub>),  $\delta$ /ppm:** 7.70 (d, *J* = 8.8 Hz, 1H, H-6), 7.33 (d, *J* = 2.6 Hz, 1H, H-3), 7.25 (dd, *J* = 8.8, 2.6 Hz, 1H, H-5), 5.56 (d, *J* = 5.0 Hz, 1H, H-1'), 4.67 (dd, *J* = 7.9, 2.5 Hz, 1H, H-3'), 4.37 (dd, *J* = 5.0, 2.5 Hz, 1H, H-2'), 4.31 (dd, *J* = 7.9, 1.4 Hz, 1H, H-4'), 4.25–4.16 (m, 3H, H-5',6'), 1.54 (s, 3H, CH<sub>3</sub>), 1.47 (s, 3H, CH<sub>3</sub>), 1.35 (s, 6H, 2 x CH<sub>3</sub>). **<sup>13</sup>C-NMR (100.1 MHz, CDCl<sub>3</sub>),**

**$\delta$ /ppm:** 162.0 (C-4), 135.3 (C-6), 120.1 (C3), 119.7 (C5), 117.5 (C1), 115.8 (C1-CN), 115.3 (C2-CN), 109.9 (C8'), 109.1 (C7'), 107.7 (C-2), 96.4 (C-1'), 71.0 (C-4'), 70.8 (C-2'), 70.5 (C-3'), 68.3 (C-6'), 66.4 (C-5'), 26.2 (CH<sub>3</sub>), 26.1 (CH<sub>3</sub>), 25.0 (CH<sub>3</sub>), 24.5 (CH<sub>3</sub>). **GC/MS (EI)**: m/z = 386.2 [M]<sup>+</sup>.

#### 4-(Polyethyleneglycoxy) phthalonitrile (**2.3c**)

In a round bottom flask, 4-nitrophthalonitrile (**2.1**) (1 g, 5.78 mmol) and polyethylene glycol (average molecular weight of 200 g.mol<sup>-1</sup>, 11.56 g, 57.8 mmol, 10 equiv.) were mixed in anhydrous DMF (30 mL), then anhydrous K<sub>2</sub>CO<sub>3</sub> (4 g, 28.9 mmol, 5 equiv.) was added portion wise over 2 h (30 min in case of ultrasounds). After 10 h mixing at room temperature (or 1 h under ultrasounds), the reaction mixture was filtered off, then

diluted with dichloromethane (100 mL) and washed with distilled water (6 x 50 mL). The organic phase was dried with anhydrous sodium sulfate, filtered and solvent was evaporated under reduced pressure. After purification by column chromatography on silica gel, using ethyl acetate as eluent, the target compound **2.3c** was obtained as a pale yellow oil, in 59% isolated yield (1.1 g, 3.39 mmol) (61% in the case of ultrasonic irradiation).

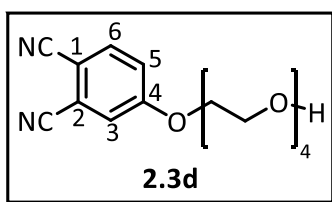


**$^1\text{H-NMR}$  (400 MHz,  $\text{CDCl}_3$ ),  $\delta/\text{ppm}$ :** 7.73–7.68 (m, 1H, H-Ar), 7.35–7.30 (m, 1H, H-Ar), 7.24–7.21 (m, 1H, H-Ar), 4.25–4.21 (m,  $\text{CH}_2\text{-PEG}$ ), 3.91–3.86 (m,  $\text{CH}_2\text{-PEG}$ ), 3.79–3.58 (m,  $\text{CH}_2\text{-PEG}$ ), 1.80 (s, 1H,  $\text{OH}$ ).  **$^{13}\text{C-NMR}$  (100.61 MHz,  $\text{CDCl}_3$ ),**

**$\delta/\text{ppm}$ :** 162.1 ( $\text{C}_{\text{Ar-O}}$ ), 135.3 ( $\text{C}_{\text{Ar}}$ ), 120.0 ( $\text{C}_{\text{Ar}}$ ), 119.8 ( $\text{C}_{\text{Ar}}$ ), 117.5 ( $\text{C}_{\text{Ar}}$ ), 115.8 (CN), 115.4 (CN), 107.7 ( $\text{C}_{\text{Ar}}$ ), 72.6 ( $\text{CH}_2$ ), 71.0 ( $\text{CH}_2$ ), 70.8 ( $\text{CH}_2$ ), 70.7 ( $\text{CH}_2$ ), 70.4 ( $\text{CH}_2$ ), 69.4 ( $\text{CH}_2$ ), 69.3 ( $\text{CH}_2$ ), 68.7 ( $\text{CH}_2$ ), 61.8 ( $\text{CH}_2$ ). **HRMS (ESI-TOF-INFUSION) (polydisperse distribution):**  $m/z$  calcd. for  $\text{C}_{12}\text{H}_{13}\text{N}_2\text{O}_3$  [ $\text{M}+\text{H}$ ] $^+$ : 233.0800, found: 233.0925 ( $n=2$ );  $m/z$  calcd. for  $\text{C}_{14}\text{H}_{17}\text{N}_2\text{O}_4$  [ $\text{M}+\text{H}$ ] $^+$ : 277.1100, found: 277.1181 ( $n=3$ );  $m/z$  calcd. for  $\text{C}_{16}\text{H}_{21}\text{N}_2\text{O}_5$  [ $\text{M}+\text{H}$ ] $^+$ : 321.1400, found: 321.1444 ( $n=4$ );  $m/z$  calcd. for  $\text{C}_{18}\text{H}_{25}\text{N}_2\text{O}_6$  [ $\text{M}+\text{H}$ ] $^+$ : 365.1600, found: 365.1709 ( $n=5$ ).

### 3-(2-{2-[2-(2-Hydroxyethoxy)ethoxy]ethoxy}ethoxy)phthalonitrile (**2.3d**)

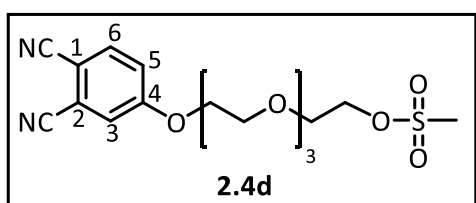
In a round bottom flask, 4-nitrophthalonitrile (**2.1**) (1 g, 5.78 mmol) and tetraethylene glycol (11.23 g, 57.8 mmol, 10 equiv.) were mixed in anhydrous DMF (30 mL), then anhydrous  $\text{K}_2\text{CO}_3$  (4 g, 28.9 mmol, 5 equiv.) was added portion wise over 2 h (30 min in case of ultrasounds). After 10 h mixing at room temperature (or 1 h under ultrasounds), the reaction mixture was filtered off, then diluted with dichloromethane (100 mL) and extracted with distilled water (10x 50 mL). The organic phase was dried with anhydrous sodium sulfate, filtered and solvent was evaporated under reduced pressure. After purification by column chromatography on silica gel, using ethyl acetate as eluent, the target compound **2.3d** was obtained as pale yellow oil, in 62% isolated yield (1.15 g, 3.6 mmol) (60% in the case of ultrasonic irradiation). Spectroscopic data is in agreement with literature.<sup>12</sup>



**<sup>1</sup>H-NMR (400 MHz, CDCl<sub>3</sub>), δ/ppm:** 7.69 (d, *J* = 8.8 Hz, 1H, H-6), 7.31 (d, *J* = 2.6 Hz, 1H, H-3), 7.22 (dd, *J* = 8.8, 2.6 Hz, 1H, H-5), 4.24–4.20 (m, 2H, CH<sub>2</sub>), 3.88–3.84 (m, 2H, CH<sub>2</sub>), 3.71–3.61 (m, 10H, CH<sub>2</sub>), 3.59–3.56 (m, 2H, CH<sub>2</sub>), 2.76 (s, 1H, OH). **<sup>13</sup>C-NMR (100.61 MHz, CDCl<sub>3</sub>), δ/ppm:** 161.8 (C<sub>Ar</sub>-O), 134.9 (C<sub>Ar</sub>), 119.6 (C<sub>Ar</sub>), 119.4 (C<sub>Ar</sub>), 117.0 (C<sub>Ar</sub>), 115.5 (CN), 115.0 (CN), 107.1 (C<sub>Ar</sub>), 72.3 (CH<sub>2</sub>), 70.6 (CH<sub>2</sub>), 70.3 (CH<sub>2</sub>), 70.2 (CH<sub>2</sub>), 69.9 (CH<sub>2</sub>), 68.9 (CH<sub>2</sub>), 68.3 (CH<sub>2</sub>), 61.4 (CH<sub>2</sub>). **FT-IR [(ATR), ν<sub>max</sub>/cm<sup>-1</sup>]:** 3428 (OH stretching vibration – broad band), 3073 (aromatic C-H stretching vibration), 2875 (aliphatic C-H stretching vibration), 2227 (CN stretching vibration), 1594 (C=C stretching vibration), 1041–1130 (C-O-C stretching vibration).

### 3-(2-{2-[2-(2-Methylsulfonyl-ethoxy)ethoxy]ethoxy}ethoxy)phthalonitrile (2.4d)

In a dried Schlenk flask, phthalonitrile **2.3d** (400 mg, 1.23 mmol) was added to a stirring solution of anhydrous dichloromethane (25 mL) and anhydrous trimethylamine (4 mL, 28.65 mmol) at 0 °C, under a nitrogen atmosphere. This solution was stirred for 10 minutes, and then a solution of methanesulfonyl chloride (2 mL, 25.84 mmol) in anhydrous dichloromethane (15 mL) was added dropwise, approximately for 1h 30 min. The mixture was allowed to warm up to room temperature and stirred for 16 h. The reaction was poured in NaHCO<sub>3</sub> solution (20%) and extracted with dichloromethane (2x 50 mL). The organic phase was dried with anhydrous sodium sulfate and filtered. After the removal of the solvent under reduced pressure, the residue was purified by column chromatography on silica gel, using, firstly, dichloromethane as eluent, and then a mixture of dichloromethane/ethanol (100:1) as eluent, which rendered the target compound **2.4d** as a colorless sticky oil, in 77% isolated yield (380 mg, 0.95 mmol). Spectroscopic data is in agreement with literature.<sup>13</sup>

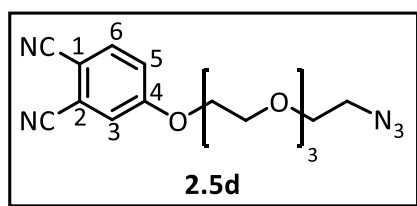


**<sup>1</sup>H-NMR (400 MHz, CDCl<sub>3</sub>), δ/ppm:** 7.70 (d, *J* = 8.8 Hz, 1H, H-6), 7.32 (d, *J* = 2.6 Hz, 1H, H-3), 7.23 (dd, *J* = 8.8, 2.6 Hz, 1H, H-5), 4.39–4.34 (m, 2H, CH<sub>2</sub>), 4.26–4.20 (m, 2H, CH<sub>2</sub>), 3.91–3.85 (m, 2H, CH<sub>2</sub>), 3.80–3.74 (m, 2H, CH<sub>2</sub>), 3.71–3.62 (m, 8H, CH<sub>2</sub>), 3.06 (s, 3H, CH<sub>3</sub>). **<sup>13</sup>C-NMR (100.61 MHz, CDCl<sub>3</sub>), δ/ppm:** 162.1 (C<sub>Ar</sub>-O), 135.3 (C<sub>Ar</sub>), 119.9 (C<sub>Ar</sub>), 119.8 (C<sub>Ar</sub>), 117.4 (C<sub>Ar</sub>), 115.8

(CN), 115.4 (CN), 107.4 (C<sub>Ar</sub>), 71.0 (C<sub>H2</sub>), 70.7 (2 x C<sub>H2</sub>), 70.6 (C<sub>H2</sub>), 69.4 (C<sub>H2</sub>), 69.3 (C<sub>H2</sub>), 69.1 (C<sub>H2</sub>), 68.7 (C<sub>H2</sub>), 37.8 (C<sub>H3</sub>).

### 3-(2-{2-[2-(2-Azidoethoxy-ethoxy)ethoxy]-ethoxy}phthalonitrile (2.5d)

In a dried Schlenk flask, a mixture of the mesylated phthalonitrile **2.4d** (180 mg, 0.45 mmol) and sodium azide (293 mg, 4.5 mmol) were stirred in anhydrous DMF (2.5 mL) at 60 °C for 6 h, under a nitrogen atmosphere. Then, reaction was stirred at room temperature for 16 h. After quenching with water, the product was extracted with ethyl acetate (3x 50 mL), and the organic layer was dried over anhydrous sodium sulfate, filtered and solvent was evaporated under reduced pressure. After purification by column chromatography on silica gel, using as eluent, firstly, dichloromethane, and then a mixture of dichloromethane/ethanol (100:1), the target compound **2.5d** was obtained as white solid, in 80% isolated yield (124 mg, 0.36 mmol). Spectroscopic data is in agreement with literature.<sup>13</sup>



**<sup>1</sup>H-NMR (400 MHz, CDCl<sub>3</sub>), δ/ppm:** 7.69 (d, *J* = 8.8 Hz, 1H, H-6), 7.30 (d, *J* = 2.6 Hz, 1H, H-3), 7.22 (dd, *J* = 8.8, 2.6 Hz, 1H, H-5), 4.21–4.18 (m, 2H, C<sub>H2</sub>), 3.90–3.84 (m, 2H, C<sub>H2</sub>), 3.71–3.63 (m, 10H, C<sub>H2</sub>), 3.36 (t, 2H,

N<sub>3</sub>C<sub>H2</sub>). **<sup>13</sup>C-NMR (100.61 MHz, CDCl<sub>3</sub>), δ/ppm:** 161.8 (C<sub>Ar</sub>-O), 134.9 (C<sub>Ar</sub>), 119.6 (C<sub>Ar</sub>), 119.3 (C<sub>Ar</sub>), 117.1 (C<sub>Ar</sub>), 115.5 (CN), 115.0 (CN), 107.1 (C<sub>Ar</sub>), 70.7 (C<sub>H2</sub>), 70.4 (2x C<sub>H2</sub>), 70.3 (C<sub>H2</sub>), 69.8 (C<sub>H2</sub>), 69.0 (C<sub>H2</sub>), 68.4 (C<sub>H2</sub>), 50.4 (N<sub>3</sub>C<sub>H2</sub>). **FT-IR [(ATR), ν<sub>max</sub>/cm<sup>-1</sup>]:** 3080 (aromatic C-H stretching vibration), 2875 (aliphatic C-H stretching vibration), 2230 (CN stretching vibration), 2099 (N<sub>3</sub> stretching vibration), 1596 (C=C stretching vibration), 1046–1130 (C-O-C stretching vibration). **HRMS (ESI-FIA-TOF):** *m/z* calcd. for C<sub>16</sub>H<sub>19</sub>N<sub>5</sub>O<sub>4</sub>Na [M+Na]<sup>+</sup>: 368.1300, found: 368.1332.

## 5.3.2 Synthesis of β-tetra-substituted phthalocyanines

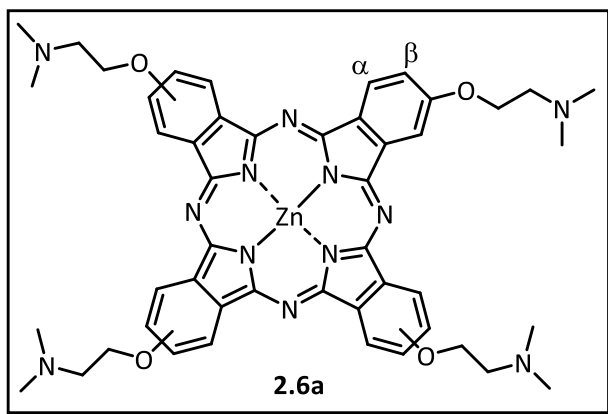
### General procedure for zinc(II) phthalocyanine complexes

In a dried Schlenk flask, the mixture of the 4-substituted phthalonitrile (1 equiv.) in DMAE/butan-1-ol solution (2:1, respectively) and zinc(II) acetate dihydrate (0.5 equiv.) was heated to 120 °C and stirred for the given time, under nitrogen atmosphere. The

reaction mixture was allowed to reach room temperature, and after the adequate work-up and purification procedures by column chromatography, the corresponding zinc(II) phthalocyanines were obtained.

**[2(3),9(10),16(17),23(24)-tetrakis-(2-Dimethylaminoethylethanol)phthalocyaninato] zinc(II) (2.6a)**

Phthalonitrile **2.3a** (500 mg, 2.32 mmol) was dissolved in a mixture of DMAE (0.7 mL) and butan-1-ol (0.35 mL). The reaction was deaerated and zinc(II) acetate dihydrate (254 mg, 1.16 mmol, 0.5 equiv.) was added. The reaction was stirred under nitrogen atmosphere for 24 h at 120 °C. After cooling, the reaction mixture was precipitated with hexane, the solid was filtered, washed with diethyl ether and dried under reduced pressure. The residue was extracted several times with dichloromethane/water and the organic phase was dried with anhydrous sodium sulfate, filtered and solvent was evaporated. After purification by column chromatography in neutral aluminum oxide (grade 2), using chloroform as eluent, the target compound **2.6a** was obtained as dark green waxy solid in 60% yield (322 mg), after being washed with hot hexane. Spectroscopic data is in agreement with literature.<sup>7,8</sup>



<sup>1</sup>H-NMR (400 MHz, DMSO-*d*<sub>6</sub>),  $\delta$ /ppm: 7.72 (br, 4H, Pc- $\alpha$ -H), 7.36-7.26 (br, 8H, Pc- $\alpha$ -H and Pc- $\beta$ -H), 4.22 (t, *J* = 5.7 Hz, 8H, OCH<sub>2</sub>), 2.66 (t, *J* = 5.7 Hz, 8H, OCH<sub>2</sub>CH<sub>2</sub>), 2.22 (s, 24H, C(CH<sub>3</sub>)<sub>2</sub>). HRMS (MALDI-TOF, DCTB): *m/z* calcd. for C<sub>48</sub>H<sub>53</sub>N<sub>12</sub>O<sub>4</sub>Zn [M+H]<sup>+</sup> 925.3600, found: 925.3598. UV-Vis

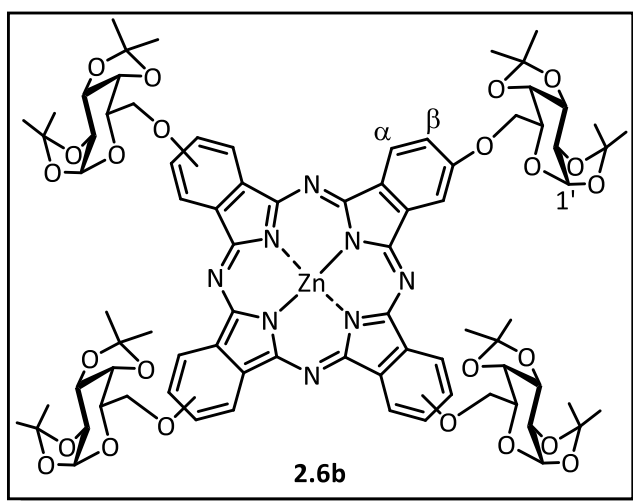
(DMSO)  $\lambda_{\text{max}}$ /nm: 350, 614, 681.

**[2,9(10),16(17),23(24)-tetrakis-(1,2:3,4-Di-O-isopropylidene- $\alpha$ -D-galactopyranos-6-O-yl)phthalocyaninato] zinc(II) (2.6b)**

Phthalonitrile **2.3b** (600 mg, 1.63 mmol) was dissolved in a mixture of DMAE (3 mL) and butan-1-ol (1.5 mL). The reaction was deaerated and zinc(II) acetate dihydrate (180 mg, 0.82 mmol, 0.5 equiv.) was added. The reaction was stirred under nitrogen atmosphere



for 24 h at 120 °C. After cooling, the reaction mixture was precipitated with methanol/H<sub>2</sub>O (1:3), the solid was filtered, washed with water and dried under reduced pressure. After purification by column chromatography on silica gel, using a mixture dichloromethane/ethyl acetate (5:1) as eluent, the target compound **2.6a** was obtained as dark blue solid, in 63% isolated yield (410 mg), after being washed with methanol. Spectroscopic data is in agreement with literature.<sup>10,11</sup>

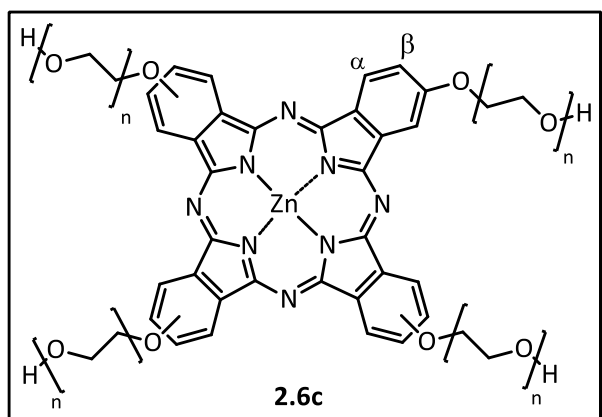


<sup>1</sup>H-NMR (400 MHz, CDCl<sub>3</sub> + Py-d<sub>5</sub>),  $\delta$ /ppm: 9.10-9.02 (m, 4H, Pc- $\alpha$ -H), 8.76-8.62 (m, 4H, Pc- $\alpha$ -H), 7.60-7.53 (m, 4H, Pc- $\beta$ -H), 5.63 (d,  $J$  = 3.5 Hz, 4H, H-1'), 4.69-4.51 (m, 16H, H-Galactose), 4.46-4.33 (m, 8H, H-Galactose), 1.63-1.51 (m, 24H, CH<sub>3</sub>), 1.38 (s, 12H, CH<sub>3</sub>), 1.31 (s, 12H, CH<sub>3</sub>). MS (MALDI-TOF, Dithranol):

$m/z$  calcd. for C<sub>80</sub>H<sub>90</sub>N<sub>8</sub>O<sub>24</sub>Zn [M+2H]<sup>+</sup> 1610.5, found: 1610.4. UV-Vis (DMSO)  $\lambda_{\max}$ /nm ( $\epsilon$ /M<sup>-1</sup> cm<sup>-1</sup>): 355 (7.4x10<sup>4</sup>), 613 (3.1x10<sup>4</sup>), 682 (1.6x10<sup>5</sup>).  $\Phi_F$  (DMSO): 0.19.

**[2(3),9(10),16(17),23(24)-tetrakis-(Polyethyleneglycoxy)phthalocyaninato] zinc(II) (2.6c)**

Following the above procedure, the phthalonitrile **2.3c** (1g, 3 mmol) was dissolved in a mixture of DMAE (1 mL) and butan-1-ol (0.5 mL). The reaction was deaerated and zinc(II) acetate dihydrate (0.33 g, 1.5 mmol, 0.5 equiv.) was added. The reaction was stirred under nitrogen atmosphere for 8 h at 120 °C. After cooling, the reaction mixture was extracted several times with dichloromethane/water and the organic phase was dried over anhydrous sodium sulfate, filtered and solvent was evaporated under reduced pressure. After purification by column chromatography on silica gel, using as eluent, firstly, a mixture chloroform/ethanol (10:1) and then chloroform/ethanol/triethylamine (10:1:0.5), the target compound **2.6c** was obtained as dark green oil, in 65% isolated yield (671.3 mg).

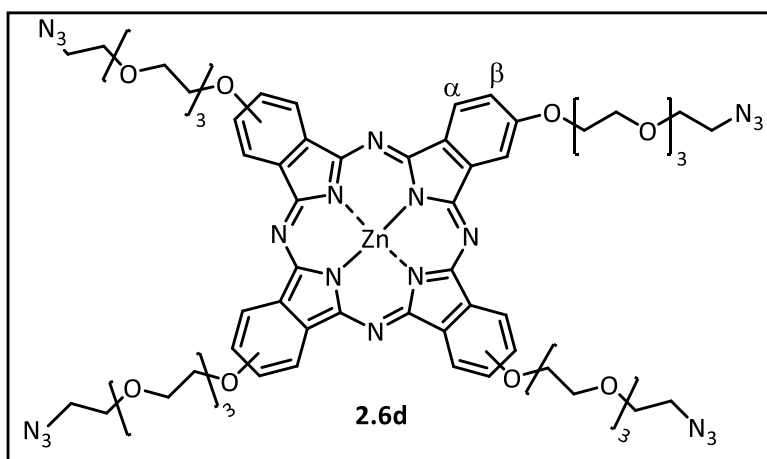


**<sup>1</sup>H-NMR (400 MHz, CDCl<sub>3</sub>), δ/ppm:**  
 7.68–7.59 (m, 4H, Pc-α-H), 7.24–7.20  
 (m, 4H, Pc-α-H), 7.15–7.09 (m, 4H,  
 Pc-β-H), 4.21–4.16 (m, CH<sub>2</sub>-PEG),  
 3.88–3.83 (m, CH<sub>2</sub>-PEG), 3.73–3.53  
 (m, CH<sub>2</sub>-PEG); **HRMS**  
**(ESI-TOF-INFUSION) (polydisperse**  
**distribution):** m/z calcd. for

C<sub>56</sub>H<sub>65</sub>N<sub>8</sub>O<sub>16</sub>Zn [M+H]<sup>+</sup>: 1169.3700, found: 1169.3807 (n=3); m/z calcd. for C<sub>64</sub>H<sub>81</sub>N<sub>8</sub>O<sub>20</sub>Zn [M+H]<sup>+</sup>: 1345.4800, found: 1345.4847 (n=4); m/z calcd. for C<sub>72</sub>H<sub>97</sub>N<sub>8</sub>O<sub>24</sub>Zn [M+H]<sup>+</sup>: 1521.5800 found: 1521.5942 (n=5). **FT-IR [(ATR), ν<sub>max</sub>/cm<sup>-1</sup>]:** 3403 (OH stretching vibration – broad band), 3060 (aromatic C-H stretching vibration), 2870 (aliphatic C-H stretching vibration), 1604 (C=C stretching vibration), 1034–1118 (C-O-C stretching vibration). **UV-Vis (DMSO) λ<sub>max</sub>/nm (ε/M<sup>-1</sup> cm<sup>-1</sup>):** 355 (5.1x10<sup>4</sup>), 613 (2.2x10<sup>4</sup>), 682 (1.1x10<sup>5</sup>). **Φ<sub>F</sub> (DMSO):** 0.18.

**[2,9(10),16(17),23(24)-tetrakis-[3-(2-[2-(2-(2-Azidoethoxy)-ethoxy]ethoxy)ethoxy)ethoxy]phthalocyaninato] zinc(II) (2.6d)**

Phthalonitrile **2.5d** (215 mg, 0.62 mmol) was dissolved in a mixture of DMAE (0.40 mL) and butan-1-ol (0.2 mL). The reaction was deaerated and zinc(II) acetate dihydrate (68 mg, 0.31 mmol, 0.5 equiv.) was added. The reaction was stirred under N<sub>2</sub> for 8 h at 120 °C. After cooling, the reaction mixture was precipitated with hexane, the solid was filtered, washed with diethyl ether and dried under reduced pressure. The reaction mixture was extracted several times with dichloromethane/water and the organic phase was dried over anhydrous sodium sulfate, filtered and solvent was evaporated under reduced pressure. After purification by column chromatography on silica gel, using as eluent, firstly, dichloromethane and then a mixture of dichloromethane/ethanol (40:1), the target compound **2.6d** was obtained as dark green waxy oil, in 52% isolated yield (114.0 mg). Spectroscopic data is in agreement with literature.<sup>13</sup>



**<sup>1</sup>H-NMR (400 MHz, CDCl<sub>3</sub>), δ/ppm:** 8.34 (br, 4H, Pc-α-H), 7.80 (br, 4H, Pc-α-H), 7.11 (br, 4H, Pc-β-H), 4.20 (br, 4H, Pc-β-H), 4.01 (br, 4H, CH<sub>2</sub>), 3.88 (br, 4H, CH<sub>2</sub>), 3.77–3.48 (m, 44H, CH<sub>2</sub>), 3.24 (br, 8H, CH<sub>2</sub>N<sub>3</sub>). **HRMS**

**(ESI-FIA-TOF):** m/z calcd. for C<sub>64</sub>H<sub>77</sub>N<sub>20</sub>O<sub>16</sub>Zn [M+H]<sup>+</sup>: 1445.5000, found: 1445.5111.

**FT-IR [(ATR), ν<sub>max</sub>/cm<sup>-1</sup>]:** 3077 (aromatic C–H stretching vibration), 2871 (aliphatic C–H stretching vibration), 2098 (N<sub>3</sub> stretching vibration), 1593 (C=C stretching vibration), 1041–1138 (C–O–C stretching vibration). **UV-Vis (DMSO) λ<sub>max</sub>/nm (ε/M<sup>-1</sup> cm<sup>-1</sup>):** 355 (4.8x10<sup>4</sup>), 613 (1.9x10<sup>4</sup>), 683 (9.9x10<sup>4</sup>). **Φ<sub>F</sub> (DMSO):** 0.16.

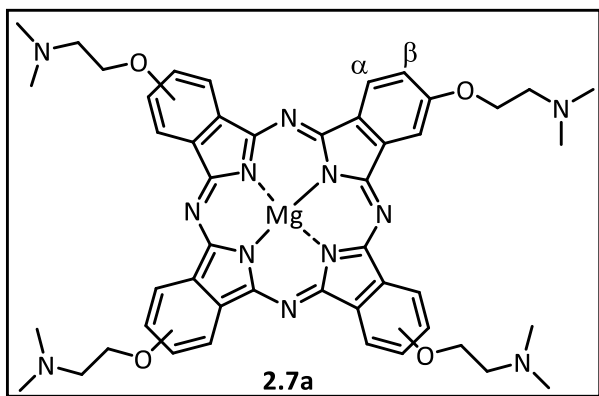
#### General procedure for magnesium(II) phthalocyanine complexes

In a dried Schlenk flask, magnesium turnings (4 equiv.) were suspended in pentan-1-ol. This suspension was heated to 150 °C (reflux) and maintained at that temperature until a light grey amalgam (*i.e.* magnesium bispentanolate) was formed (near 1 h). Then, octan-1-ol was added to this light grey amalgam, followed by 4-substituted phthalonitrile (1 equiv.). The reaction mixture was heated till 160 °C and stirred for the given time, under nitrogen atmosphere. The reaction mixture was allowed to reach room temperature, and after the adequate work-up and purification procedure by column chromatography, the corresponding magnesium(II) phthalocyanines were obtained.

#### [2,9(10),16(17),23(24)-tetrakis-(2-Dimethylaminoethylethanol)phthalocyaninato] magnesium(II) (2.7a)

Following the above procedure, 0.5 mL octan-1-ol and phthalonitrile **2.3a** (111 mg, 0.52 mmol) were added to the reaction mixture containing the light grey amalgam. The reaction mixture was heated till 160 °C and stirred for 4 h. After cooling, the reaction mixture was precipitated with hexane, the resulting green solid was filtered, washed with diethyl ether and dried under reduced pressure. After purification by column

chromatography on neutral aluminum oxide (grade 2), using a mixture chloroform/methanol (10:1) as eluent, the target compound **2.7a** was obtained as dark green waxy solid, in 44% isolated yield (50.6 mg), after being washed with hot hexane.

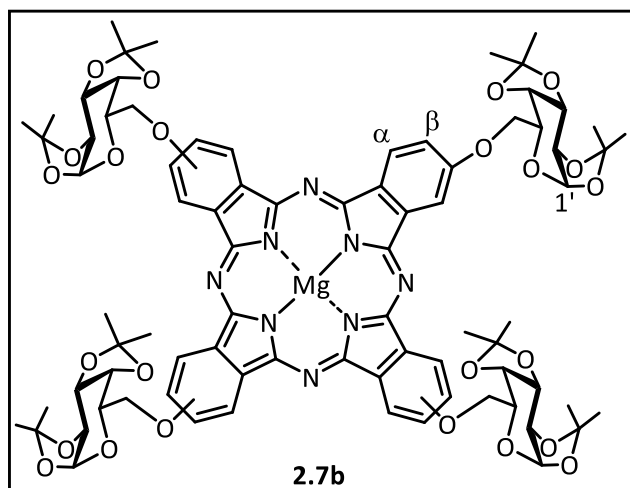


**<sup>1</sup>H-NMR (400 MHz, DMSO-*d*<sub>6</sub>),  $\delta$ /ppm:** 9.37 (br, 4H, Pc- $\alpha$ -H), 9.01 (br, 4H, Pc- $\alpha$ -H), 7.89 (br, 4H, Pc- $\beta$ -H), 5.10 (br, 8H, OCH<sub>2</sub>), 4.11 (br, 8H, OCH<sub>2</sub>CH<sub>2</sub>), 3.40 (s, 24H, C(CH<sub>3</sub>)<sub>2</sub>). **MS (MALDI-TOF, DCTB):** *m/z* calcd. for C<sub>48</sub>H<sub>53</sub>N<sub>12</sub>O<sub>4</sub>Mg [M+H]<sup>+</sup> 885.410, found: 885.407. **UV-Vis (DMSO)**

$\lambda_{\text{max}}/\text{nm}$  ( $\epsilon/\text{M}^{-1} \text{cm}^{-1}$ ): 355 ( $7.0 \times 10^4$ ), 613 ( $2.8 \times 10^4$ ), 681 ( $1.3 \times 10^5$ ).

**[2,9(10),16(17),23(24)-tetrakis-(1,2:3,4-Di-*O*-isopropylidene- $\alpha$ -D-galactopyranos-6-*O*-yl)phthalocyaninato] magnesium(II) (**2.7b**)**

Following the above procedure, 2 mL octan-1-ol and phthalonitrile **2.3b** (300 mg, 0.78 mmol) were added to the reaction mixture containing the light grey amalgam. The reaction mixture was heated till 160 °C and stirred for 7 h. After cooling the crude mixture was poured into a mixture of methanol/water (1:1), and the resulting green solid was filtered washed with methanol and dried under reduced pressure. After purification by column chromatography on silica gel, using as eluent, firstly, a mixture of hexane/ethyl acetate (1:1), and then a mixture of hexane/ethyl acetate (1:3), the target compound **2.7b** was obtained as dark green solid, in 42% isolated yield (129.5 mg).

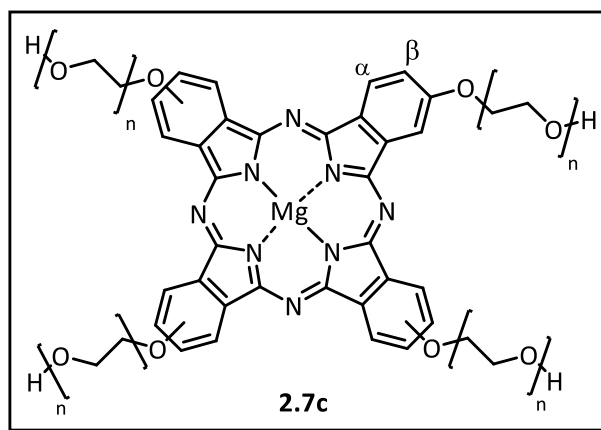


**<sup>1</sup>H-NMR (400 MHz, DMSO-*d*<sub>6</sub>),  $\delta$ /ppm:** 9.19 (br, 4H, Pc- $\alpha$ -H), 8.70–8.83 (br, 4H, Pc- $\alpha$ -H), 7.71 (br, 4H, Pc- $\beta$ -H), 5.68 (br, 4H, H-1'), 4.81–4.38 (m, 24H, H-Galactose), 1.53 (s, 24H, CH<sub>3</sub>), 1.44 (s, 12H, CH<sub>3</sub>), 1.35 (s, 12H, CH<sub>3</sub>). **HRMS (MALDI-TOF, Dithranol):** *m/z* calcd. for C<sub>80</sub>H<sub>88</sub>N<sub>8</sub>O<sub>24</sub>Mg [M]<sup>+</sup> 1568.5800,

found: 1568.57701;  $m/z$  calcd. for  $C_{80}H_{89}N_8O_{24}Mg$   $[M+H]^+$  1569.5800, found: 1569.58872. **UV-Vis (DMSO)**  $\lambda_{max}/nm$  ( $\epsilon/M^{-1} cm^{-1}$ ): 355 ( $9.3 \times 10^4$ ), 614 ( $3.6 \times 10^4$ ), 682 ( $1.8 \times 10^5$ ).  $\Phi_F$  (DMSO): 0.34.

**[2(3),9(10),16(17),23(24)-tetrakis-(Polyethyleneglycoxy)phthalocyaninato] magnesium(II) (2.7c).**

Following the above procedure, 1 mL octan-1-ol and phthalonitrile **2.3c** (190 mg, 0.59 mmol) were added to the reaction mixture containing the light grey amalgam. The reaction mixture was heated till 160 °C and stirred for 4 h. After cooling to room temperature, the crude mixture was poured into diethyl ether. The resulting green precipitate was washed with ethyl acetate, acetone and diethyl ether and dried under reduced pressure. After purification by column chromatography on silica gel, using as eluent a mixture of chloroform/ethanol/triethylamine (10:1:0.5), the target compound **2.7c** was obtained as dark green waxy oil, in 37% isolated yield (73.1 mg).



**$^1H$ -NMR (400 MHz, DMSO- $d_6$ ),  $\delta/ppm$ :** 9.14 (br, 4H, Pc- $\alpha$ -H), 8.75 (br, 4H, Pc- $\alpha$ -H), 7.71 (br, 4H, Pc- $\beta$ -H), 4.73–4.49 (m,  $CH_2$ -PEG), 4.03 (br,  $CH_2$ -PEG), 3.84–3.41 (m,  $CH_2$ -PEG).  
**HRMS (ESI-TOF-INFUSION) (polydisperse distribution):**  $m/z$  calcd. for  $C_{56}H_{65}N_8O_{16}Mg$   $[M+H]^+$ :

1129.4300, found: 1129.4345 ( $n=3$ );  $m/z$  calcd. for  $C_{64}H_{81}N_8O_{20}Mg$   $[M+H]^+$ : 1305.5300, found: 1305.5459 ( $n=4$ );  $m/z$  calcd. for  $C_{72}H_{97}N_8O_{24}Mg$   $[M+H]^+$ : 1481.6400, found: 1481.6465 ( $n=5$ ). **FT-IR [(ATR),  $\nu_{max}/cm^{-1}$ ]:** 3370 (OH stretching vibration - broad band), 3057 (aromatic C-H stretching vibration), 2867 (aliphatic C-H stretching vibration), 1603 (C=C stretching vibration), 1032–1122 (C-O-C stretching vibration). **UV-Vis (DMSO)**  $\lambda_{max}/nm$  ( $\epsilon/M^{-1} cm^{-1}$ ): 353 ( $6.7 \times 10^4$ ), 615 ( $2.7 \times 10^4$ ), 680 ( $1.2 \times 10^5$ ).  $\Phi_F$  (DMSO): 0.29.

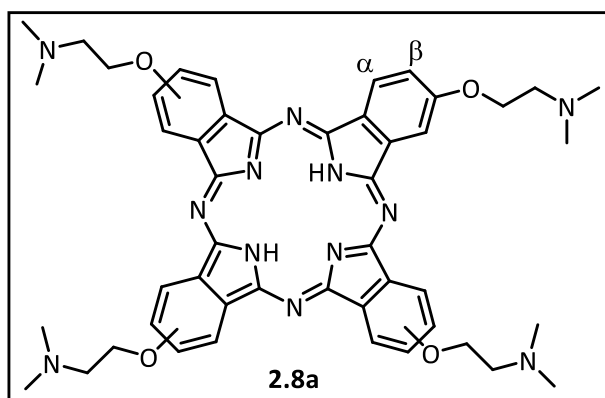
**General procedure for metal-free phthalocyanines**

The metal-free phthalocyanines were prepared by slight modification of a literature procedure.<sup>14</sup> In a dried Schlenk flask, a mixture of zinc(II) phthalocyanine (1 equiv.),

pyridine (450 equiv.) and pyridine-HCl (200 equiv.) was stirred at 110 °C for 17 h, under nitrogen atmosphere. The reaction mixture was allowed to reach room temperature, and after workup procedures, the corresponding metal-free phthalocyanines were obtained. The formation of metal-free derivative was confirmed by the formation of split Q-band in the UV-Vis spectrum of each compound.

### 2,9(10),16(17),23(24)-tetrakis-(2-Dimethylaminoethylethanol)phthalocyanine (2.8a)

Following the above procedure, zinc(II) phthalocyanine **2.6a** (82 mg, 0.087 mmol) was used. Workup was as follows: an aqueous solution of 1M NaOH was added (100 mL) and the resulting solution was left stirring for 30 min. The resulting dark green precipitate was filtered, washed with distilled water followed by water:methanol (1:1) and dried under reduced pressure. The target compound **2.8a** was obtained as dark green waxy solid, in 79% isolated yield (59.5 mg, 0.069 mmol), after being washed with hot pentane. Spectroscopic data is in agreement with literature.<sup>7,8</sup>



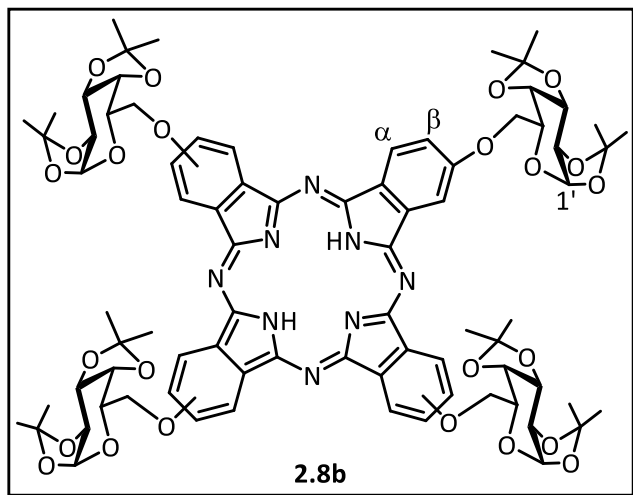
<sup>1</sup>H-NMR (400 MHz, CDCl<sub>3</sub>),  $\delta$ /ppm: 7.88 (br, 4H, Pc- $\alpha$ -H), 7.31 (br, 4H, Pc- $\alpha$ -H), 7.01 (br, 4H, Pc- $\beta$ -H), 4.23 (br, 8H, OCH<sub>2</sub>), 3.00 (br, 8H, OCH<sub>2</sub>CH<sub>2</sub>), 2.60 (s, 24H, N(CH<sub>3</sub>)<sub>2</sub>). MS (MALDI-TOF, DCTB): m/z calcd. for C<sub>48</sub>H<sub>55</sub>N<sub>12</sub>O<sub>4</sub> [M+H]<sup>+</sup>: 863.440, found:

863.440. UV-Vis (DMSO)  $\lambda_{\max}$ /nm ( $\epsilon$ /M<sup>-1</sup> cm<sup>-1</sup>): 341 (4.7x10<sup>4</sup>), 671 (7.9x10<sup>4</sup>), 703 (8.1x10<sup>4</sup>).

### 2,9(10),16(17),23(24)-tetrakis-(1,2:3,4-Di-O-isopropylidene- $\alpha$ -D-galactopyranos-6-O-yl)phthalocyanine (2.8b)

Following the above procedure, zinc(II) phthalocyanine **2.6b** (13.5 mg, 0.0084 mmol) was used. Workup was as follows: dichloromethane (100 mL) was added to mixture and extracted with water (5x50 mL). The organic phase was dried over anhydrous sodium sulfate, filtered and solvent was evaporated under reduced pressure. After purification by column chromatography on silica gel, using as eluent a mixture of

dichloromethane/ethyl acetate (3:1), the target compound **2.8b** was obtained as a dark blue solid, in 85% isolated yield (11 mg, 0.0071 mmol).



**<sup>1</sup>H-NMR (400 MHz, CDCl<sub>3</sub>), δ/ppm:**

8.78 (br, 4H, Pc-α-H), 8.31 (br, 4H, Pc-α-H), 7.53 (br, 4H, Pc-β-H), 5.82 (br, 4H, H-1'), 4.91–4.48 (m, 24H, H-Galactose), 1.79–1.68 (m, 20H, CH<sub>3</sub>), 1.65–1.52 (m, 18H, CH<sub>3</sub>), 1.47 (s, 10H, CH<sub>3</sub>), -3.11 (sl, NH, 2H).

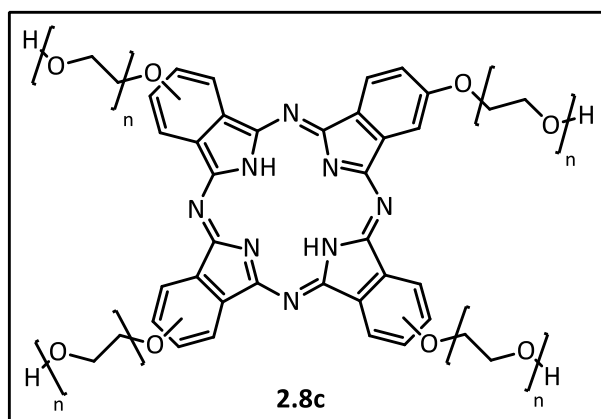
**HRMS (MALDI-TOF, Dithranol):** m/z

calcd. for C<sub>80</sub>H<sub>90</sub>N<sub>8</sub>O<sub>24</sub> [M]<sup>+</sup>:

1546.61000, found: 1546.61014; m/z calcd. for C<sub>80</sub>H<sub>91</sub>N<sub>8</sub>O<sub>24</sub> [M+H]<sup>+</sup>: 1547.61000, found: 1547.61152. **UV-Vis (DMSO) λ<sub>max</sub>/nm (ε/M<sup>-1</sup> cm<sup>-1</sup>):** 342 (6.3×10<sup>4</sup>), 672 (8.3×10<sup>4</sup>), 704 (8.5×10<sup>4</sup>). **Φ<sub>F</sub> (DMSO):** 0.22.

### 2(3),9(10),16(17),23(24)-tetrakis-(Polyethyleneglycoxy)phthalocyanine (**2.8c**)

Following the above procedure, zinc(II) phthalocyanine **2.6c** (100 mg, 0.073 mmol) was used. Workup was as follows: the solvent was removed under reduce pressure and the reaction mixture was placed in a dialysis membrane and dialyzed for three days in distilled water. After the dialysis, the mixture was concentrated and freeze-dried and compound **2.8c** was obtained as dark green waxy oil, in 81% yield (77.1 mg, 0.059 mmol).



**<sup>1</sup>H-NMR (400 MHz, DMSO-*d*<sub>6</sub>, 100 °C),**

**δ/ppm:** 8.56 (br, 4H, Pc-α-H), 8.15 (br, 4H, Pc-α-H), 7.56 (br, 4H, Pc-β-H), 4.62 (br, CH<sub>2</sub>-PEG), 4.17 (br, CH<sub>2</sub>-PEG), 3.92 (br, CH<sub>2</sub>-PEG), 3.83 (br, CH<sub>2</sub>-PEG), 3.76–3.39 (m, CH<sub>2</sub>-PEG), -3.23 (sl, NH, 2H). **HRMS (ESI-TOF-INFUSION)**

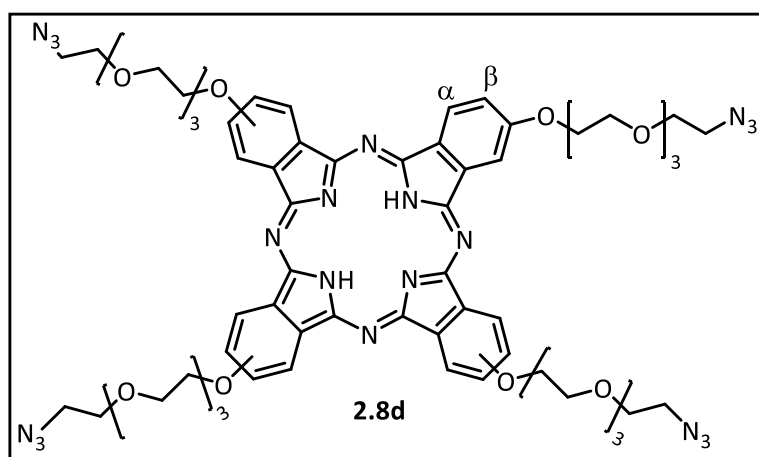
**(polydisperse distribution):** m/z

calcd. for C<sub>56</sub>H<sub>67</sub>N<sub>8</sub>O<sub>16</sub> [M+H]<sup>+</sup>: 1107.4600, found: 1107.4656 (n=3); m/z calcd. for C<sub>64</sub>H<sub>83</sub>N<sub>8</sub>O<sub>20</sub> [M+H]<sup>+</sup>: 1283.5600, found: 1283.5718 (n=4); m/z calcd. for C<sub>72</sub>H<sub>99</sub>N<sub>8</sub>O<sub>24</sub> [M+H]<sup>+</sup>: 1459.6700, found: 1459.6743 (n=5). **FT-IR [(ATR), ν<sub>max</sub>/cm<sup>-1</sup>]:** 3363 (OH

stretching vibration – broad band), 3051 (aromatic C-H stretching vibration), 2876 (aliphatic C-H stretching vibration), 1610 (C=C stretching vibration), 1038–1127 (C-O-C stretching vibration). **UV-Vis (DMSO)  $\lambda_{\max}/\text{nm}$  ( $\epsilon/\text{M}^{-1} \text{cm}^{-1}$ ):** 341 ( $5.5 \times 10^4$ ), 672 ( $7.2 \times 10^4$ ), 704 ( $7.3 \times 10^4$ ).  **$\Phi_F$  (DMSO):** 0.22.

**2,9(10),16(17),23(24)-tetrakis-[3-(2-{2-[2-(2-Azidoethoxy)-ethoxy]ethoxy}ethoxy)]  
phthalocyanine (2.8d)**

Following the above procedure, zinc(II) phthalocyanine **2.6d** (70 mg, 0.048 mmol) was used. Workup was as follows: dichloromethane (100 mL) was added to mixture and extracted with water (5x50 mL). The organic phase was then dried with anhydrous sodium sulfate, filtered and solvent was evaporated under reduced pressure. After purification by column chromatography on silica gel, using as eluent a mixture of dichloromethane/ethanol (20:1), compound **2.8d** was obtained as a dark green waxy solid in 85% yield (57 mg, 0.041 mmol).



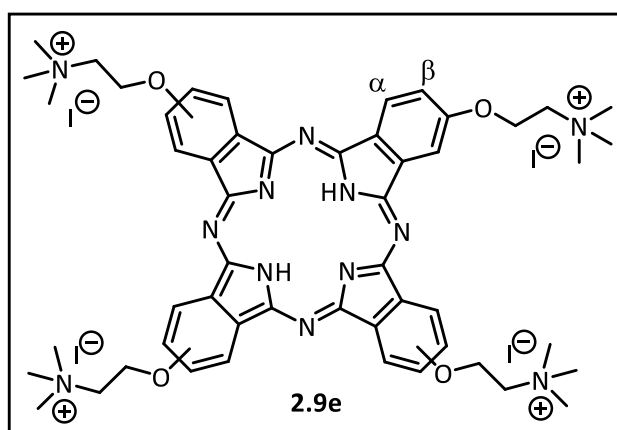
**$^1\text{H-NMR}$  (400 MHz, DMSO- $d_6$ , 100°C),  $\delta/\text{ppm}$ :** 8.50 (br, 4H, Pc- $\alpha$ -H), 8.03 (br, 4H, Pc- $\alpha$ -H), 7.53 (br, 4H, Pc- $\beta$ -H), 4.61 (br, 8H,  $\text{CH}_2$ ), 4.17 (br, 8H,  $\text{CH}_2$ ), 3.93 (br, 8H,  $\text{CH}_2$ ), 3.84 (br, 8H,  $\text{CH}_2$ ), 3.79–3.66

(m, 24H,  $\text{CH}_2$ ), 3.43 (br, 8H,  $\text{N}_3\text{CH}_2$ ), -3.36 (s, 2H,  $\text{NH}$ ). **MS (ESI, MeOH/ACN (1:1) + 0.1% formic acid):**  $m/z$  calcd. for  $\text{C}_{64}\text{H}_{79}\text{N}_{20}\text{O}_{16}$   $[\text{M}+\text{H}]^+$ : 1383.59, found: 1383.44. **FT-IR [(ATR),  $\nu_{\max}/\text{cm}^{-1}$ ]:** 3293 (NH stretching vibration), 3074 (aromatic C-H stretching vibration), 2866 (aliphatic C-H stretching vibration), 2096 ( $\text{N}_3$  stretching vibration), 1607 (C=C stretching vibration), 1039–1122 (C-O-C stretching vibration). **UV-Vis (DMSO)  $\lambda_{\max}/\text{nm}$  ( $\epsilon/\text{M}^{-1} \text{cm}^{-1}$ ):** 341 ( $6.5 \times 10^4$ ), 672 ( $8.8 \times 10^4$ ), 705 ( $8.8 \times 10^4$ ).  **$\Phi_F$  (DMSO):** 0.21.



**2,9(10),16(17),23(24)-tetrakis-(2-Trimethylaminoethylethanol)phthalocyanine tetraiodide (2.9e)**

Tetra-choline phthalocyanine tetraiodide was prepared by slight modification of a literature procedure.<sup>7,8</sup> Compound **2.8a** (60 mg, 0.070 mmol) was dissolved in 3.5 mL DMF and methyl iodide (3.97 g, 28 mmol, 400 equiv.) was added in small portions to this solution. The mixture was stirred for 24 h at 30 °C with methyl iodide additions at the beginning (100 equiv.), after 4 h (100 equiv.), after 8 h (100 equiv.) and after 12 h (100 equiv.). Then, the reaction mixture was precipitated by adding diethyl ether and kept in the fridge (3–5 °C) for 24 h. The resulting precipitate was filtered off and washed with acetone, ethyl acetate, dichloromethane and diethyl ether. The precipitate was dissolved in mixture acetonitrile/methanol (1:1) and dried under vacuum to give the corresponding cationic phthalocyanine **2.9e** in 86% (85.8 mg, 0.060 mmol). Spectroscopic data is in agreement with literature.<sup>7,8</sup>



**<sup>1</sup>H-NMR (400 MHz, DMSO-*d*<sub>6</sub>),**  
**δ/ppm:** 9.24 (br, 4H, Pc-α-H), 8.89  
 (br, 4H, Pc-α-H), 7.93 (br, 4H,  
 Pc-β-H), 5.12 (br, 8H, OCH<sub>2</sub>), 4.11 (br,  
 8H, OCH<sub>2</sub>CH<sub>2</sub>), 3.45 (s, 36H, C(CH<sub>3</sub>)<sub>2</sub>).  
**HRMS (ESI-FIA-TOF):** *m/z* calcd. for  
 C<sub>52</sub>H<sub>65</sub>N<sub>12</sub>O<sub>4</sub>K [M-4I+K]<sup>+</sup> 960.4900,  
 found: 960.3175; *m/z* calcd. for

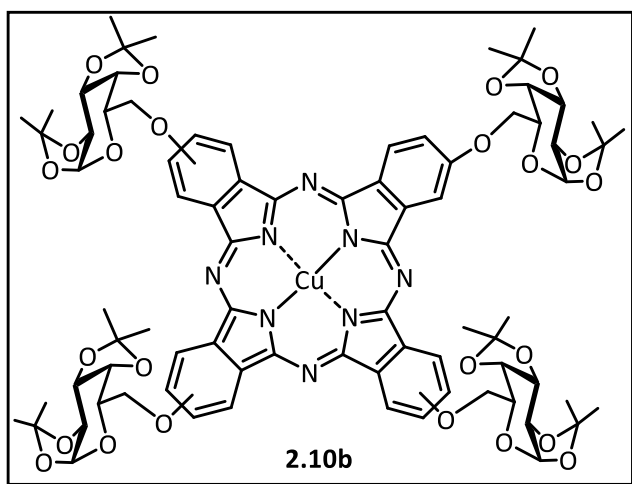
C<sub>50</sub>H<sub>60</sub>N<sub>12</sub>O<sub>4</sub> [M-4I-2CH<sub>3</sub>]<sup>+</sup> 891.4467, found: 891.4800; *m/z* calcd. for C<sub>49</sub>H<sub>57</sub>N<sub>12</sub>O<sub>4</sub> [M-4I-3CH<sub>3</sub>]<sup>+</sup> 877.4600, found: 877.4629. **UV-Vis (DMSO) λ<sub>max</sub>/nm (ε/M<sup>-1</sup> cm<sup>-1</sup>):** 341 (6.2x10<sup>4</sup>), 670 (1.0x10<sup>5</sup>), 703 (1.1x10<sup>5</sup>). **Φ<sub>F</sub> (DMSO):** 0.24.

**General procedure for copper(II) phthalocyanine complexes**

The mixture of the metal-free phthalocyanine (1 equiv.) in the given solvent (DMF or water) and copper(II) chloride (CuCl<sub>2</sub>) (2 equiv.) was heated to 75 °C and stirred for 15 minutes. The crude reaction was cooled to room temperature, and after the appropriated work-up and purification procedure, the corresponding copper(II) phthalocyanine complexes were obtained. The formation of copper(II) phthalocyanine was confirmed by the formation of one Q-band in the UV-Vis spectrum of this complex.

**[2,9(10),16(17),23(24)-tetrakis-(1,2:3,4-Di-O-isopropylidene- $\alpha$ -D-galactopyranos-6-O-yl)phthalocyaninato] copper(II) (2.10b)**

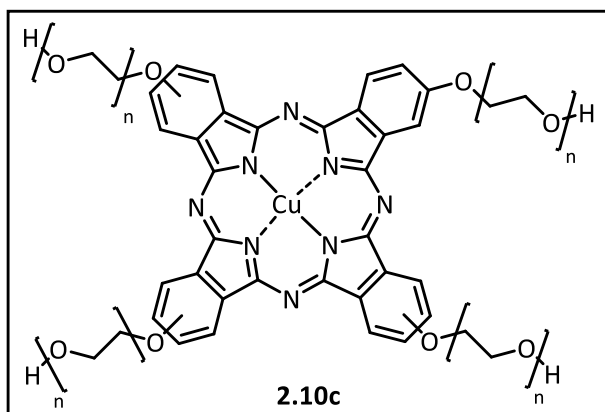
Following the above procedure, phthalocyanine **2.8b** (20 mg, 0.013 mmol) was dissolved in 3 mL DMF and CuCl<sub>2</sub> (3.5 mg, 0.026 mmol) was added to this solution. The reaction mixture was diluted in dichloromethane and washed with distilled water (3x 50 mL). The organic phase was dried over anhydrous sodium sulfate, filtered and evaporated. The target compound **2.10b** was obtained as a blue solid, in 92% isolated yield (19.3 mg, 0.012 mmol).



**HRMS (MALDI-TOF, Dithranol):** m/z calcd. for C<sub>80</sub>H<sub>89</sub>N<sub>8</sub>O<sub>24</sub>Cu [M+H]<sup>+</sup>: 1608.52000, found: 1608.51810.  
**Elem. Anal.** calcd. for [C<sub>80</sub>H<sub>88</sub>CuN<sub>8</sub>O<sub>24</sub> x 2H<sub>2</sub>O]: C: 58.40, H: 5.64, N: 6.81; found C: 58.64, H: 5.70, N: 6.95. **UV-Vis (DMSO)**  $\lambda_{\text{max}}/\text{nm}$  ( $\epsilon/\text{M}^{-1} \text{cm}^{-1}$ ): 347 (4.3x10<sup>4</sup>), 612 (2.5x10<sup>4</sup>), 680 (9.8x10<sup>4</sup>).

**[2(3),9(10),16(17),23(24)-tetrakis-(Polyethyleneglycoxy)phthalocyaninato] copper(II) (2.10c)**

Following the above procedure, phthalocyanine **2.8c** (20 mg, 0.015 mmol) was dissolved in 3 mL DMF and CuCl<sub>2</sub> (4.0 mg, 0.030 mmol) was added to this solution. The reaction mixture was precipitated with diethyl ether and filtered-off. The resulting precipitate was dissolved in distilled water and placed in a dialysis membrane, being dialyzed for two days in distilled water. After the dialysis the mixture was concentrated and freeze-dried, affording compound **2.10c** in 87% yield (17.8 mg, 0.013 mmol), as a dark bluish green waxy oil.

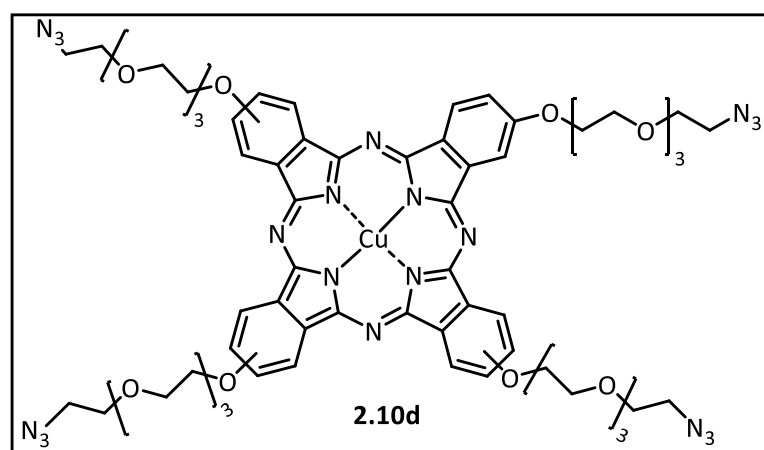


**HRMS (ESI-TOF-INFUSION), (polydisperse distribution):**  $m/z$  calcd. for  $C_{64}H_{81}N_8O_{20}Cu$   $[M+H]^+$ : 1344.4800, found: 1344.4859 ( $n=4$ );  $m/z$  calcd. for  $C_{72}H_{97}N_8O_{24}Cu^+$   $[M+H]^+$ : 1520.5800, found: 1520.5898 ( $n=5$ ). **FT-IR [(ATR),  $\nu_{max}/cm^{-1}$ ]:** 3390 (OH stretching vibration – broad band),

3062 (aromatic C-H stretching vibration), 2869 (aliphatic C-H stretching vibration), 1606 (C=C stretching vibration), 1033–1122 (C-O-C stretching vibration). **UV-Vis (DMSO)  $\lambda_{max}/nm$  ( $\epsilon/M^{-1} cm^{-1}$ ):** 348 ( $5.7 \times 10^4$ ), 613 ( $3.6 \times 10^4$ ), 680 ( $1.4 \times 10^5$ ).

**[2,9(10),16(17),23(24)-tetrakis-[3-(2-[2-(2-Azidoethoxy)-ethoxy]ethoxy)ethoxy]phthalocyaninato] copper(II) (2.10d)**

Following the above procedure, phthalocyanine **2.8d** (20 mg, 0.014 mmol) was dissolved in 3 mL DMF and  $CuCl_2$  (3.8 mg, 0.028 mmol) was added to this solution. The reaction mixture was diluted in dichloromethane and washed with distilled water (3x 50 mL). The organic phase was dried over anhydrous sodium sulfate, filtered and evaporated. The target compound **2.10d** was obtained as a bluish green waxy oil, in 86% isolated yield (17.3 mg, 0.012 mmol).

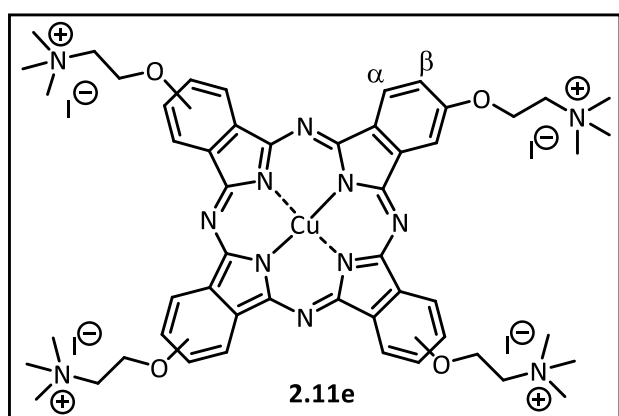


**HRMS (ESI-FIA-TOF):**  $m/z$  calcd. for  $C_{64}H_{77}N_{20}O_{16}Cu$   $[M+H]^+$ : 1444.5100, found: 1444.5112. **FT-IR [(ATR),  $\nu_{max}/cm^{-1}$ ]:** 3070 (aromatic C-H stretching vibration), 2866 (aliphatic C-H stretching vibration), 2099 ( $N_3$  stretching

vibration), 1601 (C=C stretching vibration), 1047–1129 (C-O-C stretching vibration). **UV-Vis (DMSO)  $\lambda_{max}/nm$  ( $\epsilon/M^{-1} cm^{-1}$ ):** 348 ( $5.8 \times 10^4$ ), 613 ( $3.3 \times 10^4$ ), 680 ( $1.4 \times 10^5$ ).

**[2,9(10),16(17),23(24)-tetrakis-(2-Trimethylaminoethylethanol)phthalocyaninato] copper(II) tetraiodide (2.11e)**

Following the above procedure, phthalocyanine **2.9e** (24 mg, 0.017 mmol) was dissolved in 3.5 mL water and CuCl<sub>2</sub> (4.6 mg, 0.034 mmol) was added to this solution. The reaction mixture was placed in a dialysis membrane and dialyzed for two days in distilled water. After the dialysis the mixture was concentrated and freeze-dried, affording compound **2.11e** in 94% (23.9 mg, 0.016 mmol), as a blue solid.



**HRMS (ESI-TOF-INFUSION):** m/z  
 calcd. for C<sub>52</sub>H<sub>66</sub>CuI<sub>2</sub>N<sub>12</sub>O<sub>4</sub>Na<sub>2</sub>  
 [M-2I+2Na+2H]<sup>+</sup>: 1285.2500, found:  
 1285.1499; m/z calcd. for  
 C<sub>50</sub>H<sub>58</sub>CuN<sub>12</sub>O<sub>4</sub> [M-4I-2CH<sub>3</sub>]<sup>+</sup>:  
 952.4000, found: 952.3814; m/z  
 calcd. for C<sub>49</sub>H<sub>57</sub>CuN<sub>12</sub>O<sub>4</sub>  
 [M-4I-3CH<sub>3</sub>+2H]<sup>+</sup>: 940.3900, found:

940.3451. **Elem. Anal.** calcd. for [C<sub>52</sub>H<sub>64</sub>CuI<sub>4</sub>N<sub>12</sub>O<sub>4</sub> x 2H<sub>2</sub>O]: C: 40.87, H: 4.48, N: 11.00; found C: 41.03, H: 4.65, N: 11.24. **UV-Vis (DMSO)** λ<sub>max</sub>/nm (ε/M<sup>-1</sup> cm<sup>-1</sup>): 350 (5.8x10<sup>4</sup>), 611 (3.1x10<sup>4</sup>), 678 (1.5x10<sup>5</sup>).

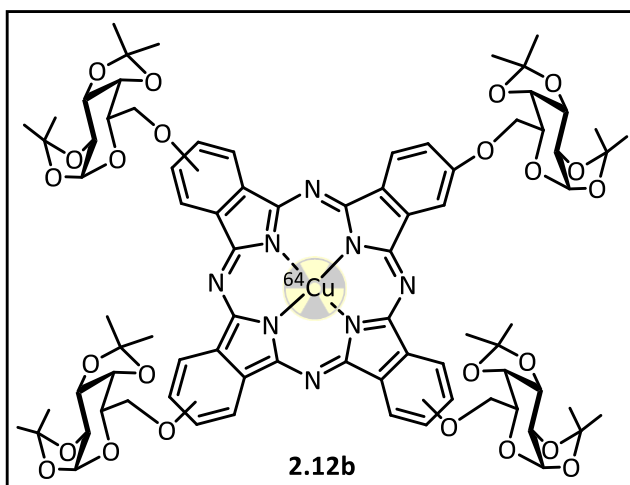
### 5.3.3 Radiolabelling studies with copper-64

#### General <sup>64</sup>Cu-labelling protocol of the metal-free phthalocyanines

Copper-64 was produced in an IBA Cyclone 18/9 cyclotron (IBA, Louvain-la-Neuve, Belgium) *via* the nuclear reaction <sup>64</sup>Ni(n,p)<sup>64</sup>Cu. The obtained copper-64 was dissolved in acidic medium and purified on an ion exchange column to produce [<sup>64</sup>Cu]CuCl<sub>2</sub> in 0.1 M HCl solution.<sup>15</sup> The resulting solution of [<sup>64</sup>Cu]CuCl<sub>2</sub> in 0.1 M HCl (200-300 μCi) was heated to dryness at 100 °C in a 3mL-borosilicate vial. To the dry <sup>64</sup>Cu-containing vial was added 100 μl of ammonium acetate buffer (0.1 M, pH ≈ 5.5), followed by the addition of 20 μl of metal-free phthalocyanine in selected solvent (1.8 nmol; [stock solution] = 9.0 x 10<sup>-4</sup> M) and 350 μl of selected solvent. The final solutions (pH ≈ 5.5; [labelling reaction] = 3.8 x 10<sup>-5</sup> M) were heated at 95 °C over a period of 5 minutes.

**[2,9(10),16(17),23(24)-tetrakis-(1,2:3,4-Di-*O*-isopropylidene- $\alpha$ -D-galactopyranos-6-*O*-yl)phthalocyaninato] copper-64 (2.12b)**

The  $^{64}\text{Cu}$ -labelling of metal-free phthalocyanine **2.8b** using DMF as selected solvent was

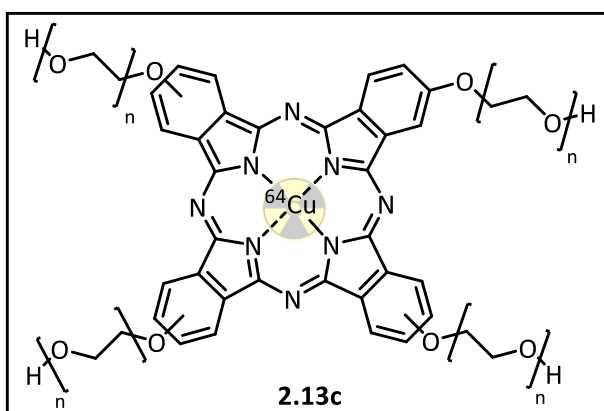


performed according to **5.3.3**. For purification of the  $^{64}\text{Cu}$ -labelled phthalocyanine **2.12b** a solid phase extraction (SPE) method was carried out. The post-reaction, after be diluted with 300  $\mu\text{l}$  of water, was applied to Sep-Pack<sup>®</sup> C18 cartridge column. The cartridge column was washed with 5 mL of water and the

$^{64}\text{Cu}$ -labelled phthalocyanine **2.12b** was eluted with 1 mL mixture of methanol/THF (1:1), being afforded in 37% radiochemical yield (non-decay corrected). The radiochemical purity was >98%, as checked by radio-TLC. For *in vitro* radiochemical stability studies, the solvents were removed by evaporation, and the resulting compound **2.12b** was taken up with 2% DMSO in physiological saline solution (NaCl 0.9% w/v).

**[2(3),9(10),16(17),23(24)-tetrakis-(Polyethyleneglycoxy)phthalocyaninato] copper-64 (2.13c)**

The  $^{64}\text{Cu}$ -labelling of metal-free phthalocyanine **2.8c** using DMF as selected solvent was



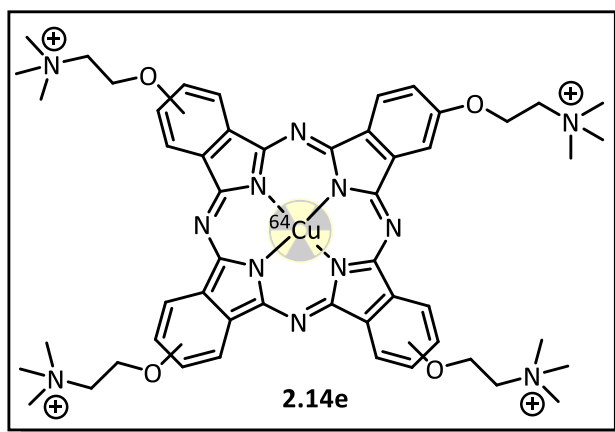
performed according to **5.3.3**. For purification of the  $^{64}\text{Cu}$ -labelled phthalocyanine **2.13c** a solid phase extraction (SPE) method was carried out. The post-reaction, after be diluted with 300  $\mu\text{l}$  of water, was applied to Sep-Pack<sup>®</sup> C18 cartridge column. The cartridge column was

washed with 5 mL of water and the  $^{64}\text{Cu}$ -labelled phthalocyanine **2.13c** was eluted with 1 mL of methanol, being afforded in 50% radiochemical yield (non-decay corrected). The

radiochemical purity was >98%, as checked by radio-TLC. For *in vitro* radiochemical stability studies, the solvents were removed by evaporation, and the resulting compound **2.13c** was taken up in physiological saline solution (NaCl 0.9% w/v).

**[2,9(10),16(17),23(24)-tetrakis-(2-Trimethylaminoethylethanol)phthalocyaninato] copper-64 (2.14e)**

The  $^{64}\text{Cu}$ -labelling of metal-free phthalocyanine **2.9e** using water as selected solvent was



performed according to **5.3.3**. Due to the almost quantitative radiochemical conversion (>99%),  $^{64}\text{Cu}$ -labelled phthalocyanine **2.14b** was further used in the *in vitro* radiochemical stability and *in vivo* PET imaging biodistribution studies without any purification. The solvent

(water/buffer) was removed by evaporation reaching a radiochemical yield of 98% (non-decay corrected). The resulting compound **2.14e** was taken up in physiological saline solution (NaCl 0.9% w/v).

***In vitro* radiochemical stability studies of  $^{64}\text{Cu}$ -labelled phthalocyanines**

All the *in vitro* radiochemical stability studies described in this thesis were performed in a similar manner in the presence of NaCl 0.9%, PBS 0.1 M (pH 7.4) and cell culture medium (DMEM – Dulbecco's Modified Eagle's Medium). Briefly, 30  $\mu\text{L}$  aliquots of aqueous solutions containing the  $^{64}\text{Cu}$ -labelled phthalocyanines under study (**2.12b**, **2.13c** and **2.14e**) were added to 80  $\mu\text{L}$  of each medium, and the mixtures were incubated at 37  $^{\circ}\text{C}$ . Analyses of the solutions were performed at specific time points by radio-TLC (incubation time: 1, 18 and 24 h).

## 5.4 Experimental (referring to Chapter 3)

In this section, the synthetic procedures of  $\beta$ -indolyketones (described in Chapter 3) are provided, as well as their full characterization. The chalcones **3.1a-e** were kindly provided by Professor Gilberto L. B. Aquino from Universidade Estadual de Goiás (Brazil). The *in vitro* cytotoxicity studies and ClogP determination of the compounds **3.3a-c** were performed by Hélder Soares (MSc) from the Photonics and Reactivity Laboratory of Coimbra Chemistry Center. The  $^{11}\text{C}$ -labelling experiments were performed in Radiochemistry and Cyclotron Laboratory at ICNAS-P. The production of carbon-11 radioisotope was performed by Ângela Neves (MSc) from ICNAS-P. The *in vivo* PET imaging and biodistribution studies in mice were performed by José Sereno (PhD) from ICNAS Pre-Clinical Imaging Facility.

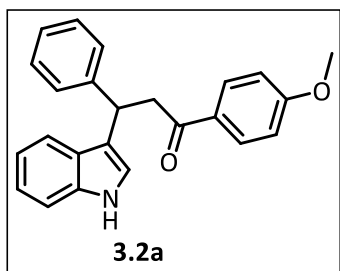
### 5.4.1 Synthesis of $\beta$ -indolyketones

#### General procedure for the synthesis of $\beta$ -indolyketones (**3.2a-e**)

A mixture of chalcone **3.1a-e** (1 mmol), indole (1.2 equiv.), *p*-TSOH (0.1 equiv.) and isopropanol (1 mL) was microwave-irradiated (200 W of power) in a closed vessel at 110 °C over a period of 5 min. Then, the reaction mixture was cooled to room temperature, and the solvent removed. After recrystallization with hot ethanol, the residue was purified through column chromatography on silica gel to afford the pure products **3.2a-e**.

#### **3-(1*H*-indol-3-yl)-1-(4-methoxyphenyl)-3-phenylpropan-1-one (3.2a)**

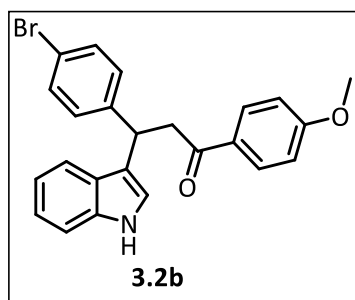
Following the above procedure, chalcone **3.1a** (239 mg, 1 mmol), indole (141 mg, 1.2 mmol) and *p*-TSOH (18 mg, 0.1 mmol) were dissolved in 1 mL of isopropanol. The residue was purified by column chromatography on silica gel using dichloromethane to obtain a light yellow solid (**3.2a**) in 88% yield (313 mg, 0.88 mmol). Spectroscopic data is in agreement with literature.<sup>16</sup>



**$^1\text{H-NMR}$  (400.13 MHz,  $\text{CDCl}_3$ ),  $\delta/\text{ppm}$ :** 7.98 (sl, 1H,  $\text{NH}$ ), 7.94–7.91 (m, 2H), 7.44 (d,  $J = 7.9$  Hz, 1H), 7.36–7.30 (m, 3H), 7.27–7.23 (m, 2H), 7.17–7.12 (m, 2H), 7.03–6.99 (m, 2H), 6.92–6.88 (m, 2H), 5.06 (t,  $J = 7.2$  Hz, 1H,  $\text{CH}$ ), 3.85 (s, 3H,  $-\text{OCH}_3$ ), 3.77 (dd,  $J = 16.4, 6.9$  Hz, 1H,  $\text{CH}_2$ ), 3.67 (dd,  $J = 16.4, 7.6$  Hz, 1H,  $\text{CH}_2$ ).  **$^{13}\text{C-NMR}$  (100.61 MHz,  $\text{CDCl}_3$ ),  $\delta/\text{ppm}$ :** 196.9 (C=O), 163.2, 144.2, 136.5, 130.2, 130.1, 128.2, 127.7, 126.5, 126.1, 121.9, 121.2, 119.4, 119.3, 119.2, 113.5, 110.9, 55.3, 44.7, 38.2. **GC/MS (EI):**  $m/z = 355.2$   $[\text{M}]^+$ .

### 3-(4-bromophenyl)-3-(1H-indol-3-yl)-1-(4-methoxyphenyl)propan-1-one (3.2b).

Following the above procedure, chalcone **3.1b** (318.0 mg, 1 mmol), indole (141 mg, 1.2 mmol) and *p*-TSOH (18 mg, 0.1 mmol) were mixed in 1 mL of isopropanol. The residue was purified by column chromatography on silica gel using dichloromethane/hexane (2:1) to obtain **3.2b** as a white solid in 90% yield (391 mg, 0.90 mmol).

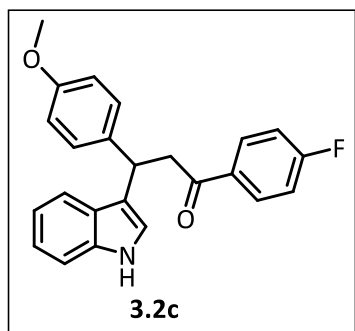


**$^1\text{H-NMR}$  (400.13 MHz,  $\text{CDCl}_3$ ),  $\delta/\text{ppm}$ :** 7.98 (sl, 1H,  $\text{NH}$ ), 7.93–7.80 (m, 2H), 7.41–7.32 (m, 4H), 7.22 (d,  $J = 8.4$  Hz, 2H), 7.16 (t,  $J = 7.6$  Hz, 1H), 7.05–6.99 (m, 2H), 6.92–6.89 (m, 2H), 5.02 (t,  $J = 7.2$  Hz, 1H,  $\text{CH}$ ), 3.86 (s, 3H,  $-\text{OCH}_3$ ), 3.74 (dd,  $J = 16.6, 6.4$  Hz, 1H,  $\text{CH}_2$ ), 3.64 (dd,  $J = 16.6, 8.1$  Hz, 1H,  $\text{CH}_2$ ).  **$^{13}\text{C-NMR}$  (100.61 MHz,  $\text{DMSO-d}_6$ ),  $\delta/\text{ppm}$ :** 196.5 (C=O), 163.1, 144.9, 136.4, 130.9, 130.4, 130.1, 129.8, 126.2, 122.0, 121.1, 118.7, 118.6, 118.4, 117.6, 113.9, 111.4, 55.5, 43.6, 37.2. **GC/MS (EI):**  $m/z = 435.1$   $[\text{M}+2\text{H}]^+$ .

### 1-(4-fluorophenyl)-3-(1H-indol-3-yl)-3-(4-methoxyphenyl)propan-1-one (3.2c)

Following the above procedure, chalcone **3.1c** (257 mg, 1 mmol), indole (141 mg, 1.2 mmol) and *p*-TSOH (18 mg, 0.1 mmol) were mixed in 1 mL of isopropanol. The residue was purified by column chromatography on silica gel using dichloromethane to obtain **3.2c** as a white solid in 87% isolated yield (325 mg, 0.87 mmol). Spectroscopic data is in agreement with literature.<sup>17</sup>





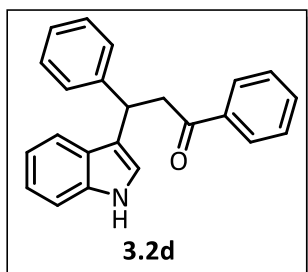
**$^1\text{H-NMR}$  (400.13 MHz,  $\text{CDCl}_3$ ),  $\delta/\text{ppm}$ :** 7.99 (sl, 1H,  $\text{NH}$ ), 7.99–7.92 (m, 2H), 7.43 (d,  $J = 7.9$  Hz, 1H), 7.32 (d,  $J = 8.2$  Hz, 1H), 7.27–7.24 (m, 2H), 7.17–7.13 (m, 1H), 7.12–7.06 (m, 2H), 7.05–7.01 (m, 1H), 6.97 (d,  $J = 1.7$  Hz, 1H), 6.82–6.78 (m, 2H), 5.00 (t,  $J = 7.2$  Hz, 1H,  $\text{CH}$ ), 3.78–3.73 (m, 4H,  $\text{CH}_2$  and  $-\text{OCH}_3$ ), 3.67 (dd,  $J = 16.5, 7.9$  Hz, 1H,  $\text{CH}_2$ ).

**$^{13}\text{C-NMR}$  (100.61 MHz,  $\text{CDCl}_3$ ),  $\delta/\text{ppm}$ :** 197.0 (C=O),

166.7, 164.2, 157.8, 136.5, 136.0, 133.5, 133.4, 130.6, 130.5, 128.5, 126.4, 122.0, 121.1, 119.4, 119.2, 115.6, 115.3, 113.7, 111.0, 55.0, 45.1, 37.4.  **$^{19}\text{F-NMR}$  (376 MHz,  $\text{CDCl}_3$ ),  $\delta/\text{ppm}$ :** -105.45 (s, 1F). **GC/MS (EI):**  $m/z = 373.1$   $[\text{M}]^+$ .

### 3-(1H-indol-3-yl)-1,3-diphenylpropan-1-one (3.2d)

Following the above procedure, chalcone **3.1d** (209 mg, 1 mmol), indole (141 mg, 1.2 mmol) and *p*-TSOH (18 mg, 0.1 mmol) were mixed in 1 mL of isopropanol. The residue was purified by column chromatography on silica gel using dichloromethane/hexane (1:1) to obtain a white solid (**3.2d**) in 82% yield (267 mg, 0.82 mmol). Spectroscopic data is in agreement with literature.<sup>16,17</sup>

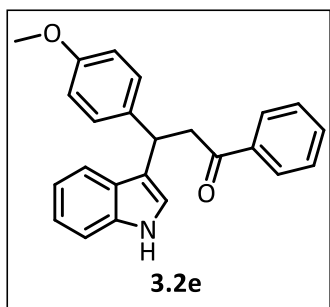


**$^1\text{H-NMR}$  (400.13 MHz,  $\text{CDCl}_3$ ),  $\delta/\text{ppm}$ :** 7.99 (sl, 1H,  $\text{NH}$ ), 7.95–7.91 (m, 2H), 7.57–7.52 (m, 1H), 7.46–7.42 (m, 3H), 7.38–7.35 (m, 2H), 7.32 (d,  $J = 8.2$  Hz, 1H), 7.28–7.25 (m, 2H), 7.19–7.13 (m, 2H), 7.04–6.99 (m, 2H), 5.08 (t,  $J = 7.2$  Hz, 1H,  $\text{CH}$ ), 3.83 (dd,  $J = 16.7, 6.8$  Hz, 1H,  $\text{CH}_2$ ), 3.74 (dd,  $J = 16.7, 7.6$  Hz, 1H,  $\text{CH}_2$ ).  **$^{13}\text{C-NMR}$  (100.61 MHz,  $\text{CDCl}_3$ ),  $\delta/\text{ppm}$ :** 198.7

(C=O), 144.4, 137.3, 136.8, 133.1, 128.7, 128.6, 128.2, 128.0, 126.8, 126.4, 122.3, 121.6, 119.7, 119.5, 119.4, 111.3, 45.4, 38.4. **GC/MS (EI):**  $m/z = 325.1$   $[\text{M}]^+$ .

### 3-(1H-indol-3-yl)-3-(4-methoxyphenyl)-1-phenylpropan-1-one (3.2e)

Following the above procedure, chalcone **3.1e** (239 mg, 1 mmol), indole (141 mg, 1.2 mmol) and *p*-TSOH (18 mg, 0.1 mmol) were dissolved in 1 mL of isopropanol. The residue was purified by column chromatography on silica gel using dichloromethane to obtain a light yellow solid (**3.2e**) in 85% yield (302 mg, 0.85 mmol). Spectroscopic data is in agreement with literature.<sup>18</sup>



**$^1\text{H-NMR}$  (400.13 MHz,  $\text{CDCl}_3$ ),  $\delta/\text{ppm}$ :** 7.95 (s, 1H,  $\text{NH}$ ), 7.94–7.92 (m, 2H), 7.56–7.52 (m, 1H), 7.45–7.41 (m, 3H), 7.32 (d,  $J = 8.1$  Hz, 1H), 7.28–7.24 (m, 2H), 7.17–7.13 (m, 1H), 7.04–6.99 (m, 2H), 6.81–6.78 (m, 2H), 5.02 (t,  $J = 7.2$  Hz, 1H,  $\text{CH}$ ), 3.79 (dd,  $J = 16.6, 6.6$  Hz, 1H,  $\text{CH}_2$ ), 3.75 (s, 3H,  $-\text{OCH}_3$ ), 3.69 (dd,  $J = 16.6, 7.9$  Hz, 1H,  $\text{CH}_2$ ).  **$^{13}\text{C-NMR}$  (100.61**

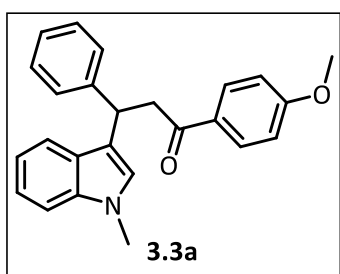
**MHz,  $\text{CDCl}_3$ ),  $\delta/\text{ppm}$ :** 198.9 (C=O), 158.1, 137.3, 136.8, 136.5, 133.1, 128.9, 128.7, 128.3, 126.8, 122.3, 121.4, 119.9, 119.8, 119.5, 114.0, 111.2, 55.3, 45.5, 37.6. **GC/MS (EI):**  $m/z = 355.1$   $[\text{M}]^+$ .

### General procedure for the synthesis of *N*-methylated $\beta$ -indolyketones (3.3a-e)

A mixture of chalcone **3.1a-e** (1 mmol), 1-methylindole (1.2 equiv.), *p*-TSOH (0.1 equiv.) and isopropanol (1 mL) was microwave-irradiated (200 W of power) in a closed vessel at 110 °C over a period of 5 min. Then, the reaction mixture was cooled to room temperature, and the solvent removed. After recrystallization with hot ethanol, the residue was purified by silica gel to afford the pure products **3.3a-e**.

### 1-(4-methoxyphenyl)-3-(1-methyl-1*H*-indol-3-yl)-3-phenylpropan-1-one (3.3a)

Following the above procedure, chalcone **3.1a** (239 mg, 1 mmol), 1-methylindole (158 mg, 1.2 mmol) and *p*-TSOH (18 mg, 0.1 mmol) were dissolved in 1 mL of isopropanol. The residue was purified by column chromatography on silica gel using dichloromethane/hexane (1:1) to obtain a light yellow solid (**3.3a**) in 90% yield (333 mg, 0.9 mmol). Spectroscopic data is in agreement with literature.<sup>16</sup>

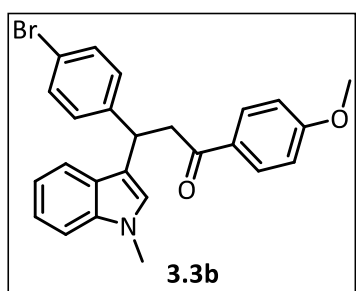


**$^1\text{H-NMR}$  (400.13 MHz,  $\text{CDCl}_3$ ),  $\delta/\text{ppm}$ :** 7.95 (d,  $J = 8.8$  Hz, 2H), 7.47 (d,  $J = 7.9$  Hz, 1H), 7.38 (d,  $J = 7.6$  Hz, 2H), 7.29–7.26 (m, 3H), 7.19 (q,  $J = 7.5$  Hz, 2H), 7.03 (t,  $J = 7.4$  Hz, 1H), 6.92 (d,  $J = 8.8$  Hz, 2H), 6.86 (s, 1H), 5.08 (t,  $J = 7.2$  Hz, 1H,  $\text{CH}$ ), 3.85 (s, 3H,  $-\text{OCH}_3$ ), 3.78 (dd,  $J = 16.6, 6.7$  Hz, 1H,  $\text{CH}_2$ ), 3.73–3.67 (m, 4H,  $\text{CH}_2$  and  $-\text{NCH}_3$ ).  **$^{13}\text{C-NMR}$  (100.61 MHz,**

**$\text{CDCl}_3$ ),  $\delta/\text{ppm}$ :** 197.2 (C=O), 163.5, 144.7, 137.5, 130.5, 130.4, 128.5, 127.9, 127.2, 126.4, 126.3, 121.8, 119.8, 118.9, 118.1, 113.8, 109.3, 55.57, 45.1, 38.4, 32.8. **GC/MS (EI):**  $m/z = 369.2$   $[\text{M}]^+$ .

**3-(4-bromophenyl)-1-(4-methoxyphenyl)-3-(1-methyl-1*H*-indol-3-yl)propan-1-one**  
**(3.3b)**

Following the above procedure, chalcone **3.1b** (318 mg, 1 mmol), 1-methylindole (158 mg, 1.2 mmol) and *p*-TSOH (18 mg, 0.1 mmol) were dissolved in 1 mL of isopropanol. The residue was purified by column chromatography on silica gel using dichloromethane/hexane (1:1) to obtain a white solid (**3.3b**) in 88% yield (395 mg, 0.88 mmol).



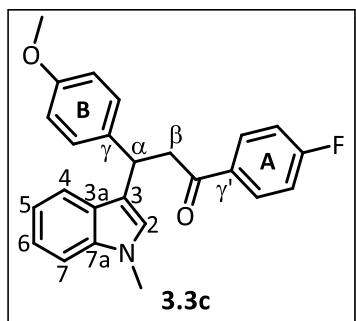
**<sup>1</sup>H-NMR (400.13 MHz, CDCl<sub>3</sub>), δ/ppm:** 7.93–7.90 (m, 2H), 7.41–7.34 (m, 3H), 7.27–7.25 (m, 1H), 7.24–7.17 (m, 3H), 7.04–7.00 (m, 1H), 6.92–6.89 (m, 2H), 6.82 (s, 1H), 5.01 (t, *J* = 7.2 Hz, 1H, CH), 3.86 (s, 3H, -OCH<sub>3</sub>), 3.75–3.70 (m, 4H, -NCH<sub>3</sub> and CH<sub>2</sub>), 3.64 (dd, *J* = 16.7, 8.1 Hz, 1H, CH<sub>2</sub>).

**<sup>13</sup>C-NMR (100.61 MHz, CDCl<sub>3</sub>), δ/ppm:** 196.8 (C=O),

163.7, 143.7, 137.5, 131.6, 130.5, 130.2, 129.8, 127.0, 126.3, 122.0, 120.1, 119.7, 119.1, 117.6, 113.9, 109.4, 55.6, 44.8, 37.8, 32.9. **GC/MS (EI):** *m/z* = 449.1 [*M*+2*H*]<sup>+</sup>.

**1-(4-fluorophenyl)-3-(4-methoxyphenyl)-3-(1-methyl-1*H*-indol-3-yl)propan-1-one**  
**(3.3c)**

Following the above procedure, chalcone **3.1c** (257 mg, 1 mmol), 1-methylindole (158 mg, 1.2 mmol) and *p*-TSOH (18 mg, 0.1 mmol) were dissolved in 1 mL of isopropanol. The residue was purified by column chromatography on silica gel using dichloromethane/hexane (2:1) to obtain a white solid (**3.3c**) in 85% yield (330 mg, 0.85 mmol).



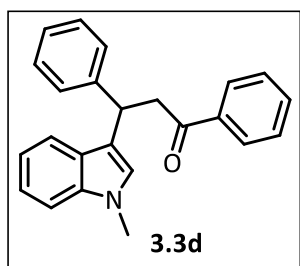
**<sup>1</sup>H-NMR (400.13 MHz, CDCl<sub>3</sub>), δ/ppm:** 7.97–7.92 (m, 2H, *H*<sub>ortho</sub> Ring **A**), 7.43 (d, *J* = 8.0 Hz, 1H, H<sub>4</sub>), 7.26–7.24 (m, 3H, *H*<sub>ortho</sub> Ring **B** and H<sub>7</sub>), 7.18 (t, *J* = 8.0 Hz, 1H, H<sub>6</sub>), 7.11–7.06 (m, 2H, *H*<sub>meta</sub> Ring **A**), 7.01 (t, *J* = 7.9 Hz, 1H, H<sub>5</sub>), 6.81–6.78 (m, 3H, *H*<sub>meta</sub> Ring **B** and H<sub>2</sub>), 4.98 (t, *J* = 7.2 Hz, 1H, H<sub>α</sub>), 3.77–3.72 (m, 7H, H<sub>β</sub>, -OCH<sub>3</sub> and -ONH<sub>3</sub>), 3.68 (dd, *J* =

16.5, 8.0 Hz, 1H, H<sub>β</sub>). **<sup>13</sup>C-NMR (100.61 MHz, CDCl<sub>3</sub>), δ/ppm:** 197.3 (C=O), 167.1 (C-F), 164.5 (C-F), 158.1 (*C*<sub>para</sub> Ring **B**), 137.5 (C<sub>7a</sub>), 136.5 (C<sub>γ</sub>), 133.8 (C<sub>γ'</sub>), 133.7 (C<sub>γ'</sub>), 130.9 (*C*<sub>ortho</sub> Ring **A**), 130.8 (*C*<sub>ortho</sub> Ring **A**), 128.8 (*C*<sub>ortho</sub> Ring **B**), 127.1 (C<sub>3a</sub>), 126.3 (C<sub>2</sub>), 121.9 (C<sub>6</sub>),

119.7 (C4), 119.0 (C5), 118.2 (C3), 115.9 ( $C_{meta}$  Ring A), 115.6 ( $C_{meta}$  Ring A), 114.0 ( $C_{meta}$  Ring B), 109.4 (C7), 55.3 ( $O\text{C}\underline{H}_3$ ), 45.5 ( $C\beta$ ), 37.6 ( $C\alpha$ ), 32.8 ( $N\text{C}\underline{H}_3$ ).  $^{19}\text{F-NMR}$  (376 MHz,  $\text{CDCl}_3$ ),  $\delta/\text{ppm}$ :  $\delta$  -105.49 (s, 1F).  $\text{GC/MS}$  (EI):  $m/z$  = 387.2  $[\text{M}]^+$ .

### 3-(1-methyl-1H-indol-3-yl)-1,3-diphenylpropan-1-one (3.3d)

Following the above procedure, chalcone **3.1d** (209 mg, 1 mmol), 1-methylindole (158 mg, 1.2 mmol) and *p*-TSOH (18 mg, 0.1 mmol) were dissolved in 1 mL of isopropanol. The residue was purified by column chromatography on silica gel using dichloromethane/hexane (1:2) to obtain a white solid (**3.3d**) in 91% yield (309 mg, 0.91 mmol). Spectroscopic data is in agreement with literature.<sup>18</sup>

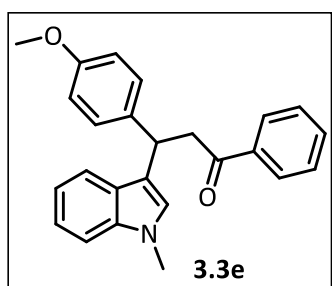


$^1\text{H-NMR}$  (400.13 MHz,  $\text{CDCl}_3$ ),  $\delta/\text{ppm}$ : 7.95–7.93 (m, 2H), 7.57–7.52 (m, 1H), 7.46–7.41 (m, 3H), 7.38–7.36 (m, 2H), 7.28–7.24 (m, 3H), 7.21–7.14 (m, 2H), 7.04–7.00 (m, 1H), 6.84 (s, 1H), 5.07 (t,  $J$  = 7.2 Hz, 1H,  $\text{CH}$ ), 3.82 (dd,  $J$  = 16.8, 6.7 Hz, 1H,  $\text{CH}_2$ ), 3.78–3.72 (m, 4H,  $\text{CH}_2$  and  $-\text{NCH}_3$ ).  $^{13}\text{C-NMR}$  (100.61

MHz,  $\text{CDCl}_3$ ),  $\delta/\text{ppm}$ : 198.7 (C=O), 144.5, 137.5, 137.3, 133.1, 128.7, 128.6, 128.2, 128.0, 127.1, 126.4, 121.8, 119.7, 119.0, 118.0, 109.3, 45.5, 38.3, 32.8.  $\text{GC/MS}$  (EI):  $m/z$  = 339.2  $[\text{M}]^+$ .

### 3-(4-methoxyphenyl)-3-(1-methyl-1H-indol-3-yl)-1-phenylpropan-1-one (3.3e)

Following the above procedure, chalcone **3.1e** (239 mg, 1 mmol), 1-methylindole (158 mg, 1.2 mmol) and *p*-TSOH (18 mg, 0.1 mmol) were dissolved in 1 mL of isopropanol. The residue was purified by column chromatography on silica gel using dichloromethane/hexane (1:1) to obtain a light yellow solid (**3.3e**) in 86% yield (318 mg, 0.86 mmol). Spectroscopic data is in agreement with literature.<sup>18</sup>



$^1\text{H-NMR}$  (400.13 MHz,  $\text{CDCl}_3$ ),  $\delta/\text{ppm}$ : 7.94–7.92 (m, 2H), 7.56–7.50 (m, 1H), 7.45–7.41 (m, 3H), 7.27–7.24 (m, 3H), 7.20–7.16 (m, 1H), 7.03–6.99 (m, 1H), 6.86–6.78 (m, 3H), 5.01 (t,  $J$  = 7.2 Hz, 1H,  $\text{CH}$ ), 3.80–3.67 (m, 8H,  $\text{CH}_2$ ,  $-\text{OCH}_3$  and  $-\text{NCH}_3$ ).  $^{13}\text{C-NMR}$  (100.61 MHz,  $\text{CDCl}_3$ ),  $\delta/\text{ppm}$ : 198.8 (C=O), 158.1, 137.5, 137.3, 136.6, 133.1, 128.9, 128.7, 128.3,

127.1, 126.3, 121.8, 119.8, 119.0, 118.3, 113.9, 109.3, 55.3, 45.6, 37.5, 32.8. **GC/MS (EI):**  
m/z = 369.1 [M]<sup>+</sup>.

## 5.4.2 Radiolabelling studies with carbon-11

### General <sup>11</sup>C-labelling protocol, purification and reformulation

In a sample flask, 3 mg (0.008 mmol) of compound **3.2c** was dissolved in dry DMF (348 µl, 23 mM) and vortexed for 1 min. To this solution was added 9 mg of KOH (0.16 mmol, 20 equiv.) and vortexed for 5 min. 100 µl (0.86 mg of compound **3.2c**) of the previous mixture was introduced in the 2 mL stainless loop of the carbon-11 automated radiosynthesis system. The [<sup>11</sup>C]CH<sub>3</sub>I produced in Synthra radiosynthesis module is driven to the loop and allowed to react with compound **3.2c** for 5 min at room temperature. The reaction product was isolated using a semi-preparative HPLC with Phenomenex Luna C<sub>18</sub> (10-15 µm, 10 x 250 mm) column and ACN/0.1 M ammonium format buffer solution (65:35) as a mobile phase with flow of 9 mL.min<sup>-1</sup>. Detection was made by UV (254 nm) and radioactivity. The <sup>11</sup>C-labelled product **3.4c** was collected for reformulation in a system installed at IBA Synthra® Extension automated module. The <sup>11</sup>C-labelled product **3.4c** was trapped in a SPE cartridge, and was washed with 10 mL of water to remove the acetonitrile from the mobile phase leaving only <sup>11</sup>C-labelled product **3.4c**. The loaded cartridge was eluted with 1 mL of ethanol, followed by 9 mL of NaCl 0.9% reaching the sterile final vial. The amount of radioactivity of the final vial was measured in a dose calibrator and a sample of the <sup>11</sup>C-labelled product **3.4c** was subject to quality control.

### Quality control of <sup>11</sup>C-labelled compound **3.4c**

The analytical HPLC was performed using a HPLC *Agilent Technologies 1200 series* with using Zorbax Eclipse XDB-C18 (5 µm, 4.6 x 150 mm) column using ACN/0.1 M ammonium format buffer solution (65:35) as a mobile phase with flow of 2 mL.min<sup>-1</sup>, controlled by UV (254 nm) and γ-detector. Levels of organic volatile impurities were analyzed through the injection of 2 µl of the final solution into a GC equipped with a FID and previously calibrated for the residual solvents in analysis. Since injection <sup>11</sup>C-labelled product **3.4c** vehicle is 10% ethanol and 90% saline and acetonitrile belongs of the mobile phase, two

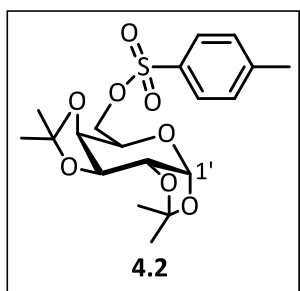
possible peaks could be expected in the chromatogram and their concentration in the final solution shall be, according to radiopharmaceutical preparations monograph of Ph. Eur., less than 4.1 mg/10 mL for acetonitrile and 2500 mg/10 mL for ethanol.<sup>19</sup> The pH of reformulated <sup>11</sup>C-labelled product **3.4c** solution was measured by potentiometry and should be between 4.5 and 8.5, in accordance with the radiopharmaceutical preparations monograph of Ph. Eur.<sup>19a</sup>

## 5.5 Experimental (referring to Chapter 4)

In this section, the synthetic procedures of phthalonitrile and the corresponding  $\alpha$ -octa-substituted phthalocyanines are provided, as well as, their full characterization.

### 1,2:3,4-Di-*O*-isopropylidene- $\alpha$ -D-galactopyranos-6-yl tosylate (**4.2**)

Toluene-azeotropically dried 1,2:3,4-di-*O*-isopropylidene-D-galactopyranose **4.1** (1.30 g, 5 mmol) was placed in a dried Schlenk flask, under nitrogen atmosphere, and dissolved in dry pyridine (10 mL). The solution was kept at room temperature and tosyl chloride (1.0 g, 5.25 mmol) was added, under nitrogen atmosphere. After stirring 1 h at room temperature, the reaction mixture was cooled to 0-5 °C and further stirred for 16 h. The final reaction mixture was filtered and the resulting filtrate was poured into distilled water and extracted with diethyl ether (4x 50 mL). The combined organic phases were washed successively with 0.1 M hydrochloric acid (2x 30 mL), brine (2x 30 mL), distilled water (2x 30 mL) and then dried over Na<sub>2</sub>SO<sub>4</sub>. After filtration and solvent removal by evaporation, product **4.2** was obtained in 80% isolated yield (1.66 g, 4 mmol). Spectroscopic data is in agreement with literature.<sup>20</sup>

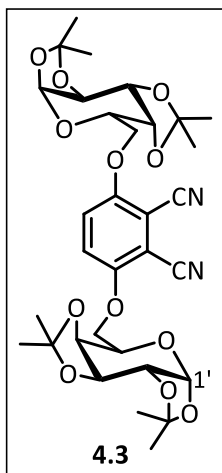


<sup>1</sup>H-NMR (400.13 MHz, CDCl<sub>3</sub>),  $\delta$ /ppm: 7.80 (d,  $J$  = 8.3 Hz, 2H, H-Ar), 7.32 (d,  $J$  = 8.3 Hz, 2H, H-Ar), 5.44 (d,  $J$  = 5.0 Hz, 1H, H-1'), 4.58 (dd,  $J$  = 7.9, 2.5 Hz, 1H, H-Galactose), 4.28 (dd,  $J$  = 5.0, 2.5 Hz, 1H, H-Galactose), 4.21–4.17 (m, 2H, H-Galactose), 4.12–4.03 (m, 2H, H-Galactose), 2.43 (s, 3H, Ph-CH<sub>3</sub>), 1.49 (s, 3H, CH<sub>3</sub>), 1.33 (s, 3H, CH<sub>3</sub>), 1.30 (s, 3H, CH<sub>3</sub>), 1.25 (s, 3H, CH<sub>3</sub>).

$^{13}\text{C-NMR}$  (100.61 MHz,  $\text{CDCl}_3$ ),  $\delta/\text{ppm}$ : 145.2, 133.3, 130.2, 128.6, 110.0, 109.4, 95.6, 71.0, 70.9, 70.8, 68.6, 66.3, 26.4, 26.3, 25.4, 24.8, 22.1.

### 3,6-bis(1,2:3,4-Di-*O*-isopropylidene- $\alpha$ -D-galactopyranos-6-yl)-phthalonitrile (**4.3**)

Toluene-azeotropically dried 2,3-dicyanohydroquinone (1.06 g, 6.67 mmol) and  $\text{PPh}_3$  (5.26 g, 20 mmol), were placed in a dried Schlenk flask and suspended in dry toluene (60 mL), under nitrogen atmosphere. At room temperature, 9.5 mL (20 mmol) of DEAD (40% in toluene) was added dropwise with stirring, over a period of 5 min. To this solution, 5.5 g (20 mmol) of 1,2:3,4-di-*O*-isopropylidene- $\alpha$ -D-galactopyranose **4.1** dissolved in 10 mL of dry toluene was added and the reaction was heated to 110 °C. After stirring for 24 h under nitrogen atmosphere, the solvent was evaporated under reduced pressure. Then, the residue was dissolved in dichloromethane and purified by a silica gel column chromatography, using dichloromethane/methanol (200:1) as eluent, and further purified by recrystallization in methanol, providing compound **4.3** in 39% isolated yield (1.7 g, 2.6 mmol). Spectroscopic data is in agreement with literature.<sup>21</sup>

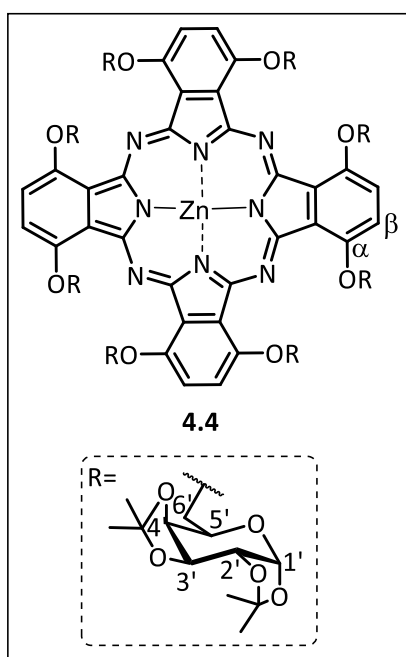


$^1\text{H-NMR}$  (400.13 MHz,  $\text{CDCl}_3$ ),  $\delta/\text{ppm}$ : 7.25 (s, 2H, H-Ar), 5.52 (d,  $J$  = 4.9 Hz, 1H, H-1'), 4.66 (dd,  $J$  = 7.9, 2.4 Hz, 2 H, H-Galactose), 4.40 (d,  $J$  = 8 Hz, 2H, H-Galactose), 4.34 (dd,  $J$  = 4.9, 2.4 Hz, 2H, H-Galactose), 4.28–4.15 (m, 6H, H-Galactose), 1.54 (s, 6H,  $\text{CH}_3$ ), 1.44 (s, 6H,  $\text{CH}_3$ ), 1.33 (s, 12H, 2x  $\text{CH}_3$ ).  $^{13}\text{C-NMR}$  (100.61 MHz,  $\text{CDCl}_3$ ),  $\delta/\text{ppm}$ : 155.4 ( $\text{C}_{\text{Ar-O}}$ ), 119.4, 112.9, 109.6, 109.2, 105.7, 96.4, 70.8, 70.7, 70.6, 68.9, 66.4, 26.2 ( $\text{CH}_3$ ), 26.1 ( $\text{CH}_3$ ), 25.0 ( $\text{CH}_3$ ), 24.5 ( $\text{CH}_3$ ). **HRMS (ESI-TOF)**:  $m/z$  calcd. for  $\text{C}_{32}\text{H}_{40}\text{N}_2\text{O}_{12}\text{Na}$  [ $\text{M}+\text{Na}$ ] $^+$ : 667.2497, found: 667.2474.

### [1,4,8,11,15,18,22,25-octakis-(1,2:3,4-Di-*O*-isopropylidene- $\alpha$ -D-galactopyranos-6-yl)phthalocyaninato] zinc(II) (**4.4**)

In a dried Schlenk flask, phthalonitrile **4.3** (250 mg, 0.39 mmol) was dissolved in pentan-1-ol (2.5 mL) and DBU (5  $\mu\text{L}$ , 0.039 mmol, 10 mol%) were added. The reaction was deaerated and zinc(II) acetate dihydrate (43.9 mg, 0.20 mmol, 0.5 equiv.) was added. The reaction was stirred at 150 °C (reflux) over a period of 6 h, under nitrogen atmosphere. The reaction mixture was allowed to reach room temperature and it was

poured into a 2:1 mixture of MeOH/H<sub>2</sub>O, and allow to precipitate at room temperature. The resulting precipitated was dissolved in dichloromethane and purified by a silica gel column chromatography, using first a mixture of dichloromethane/ethyl acetate (1:1) as eluent, and then ethyl acetate to collect the green fraction containing phthalocyanine **4.4**. After evaporation under reduced pressure the pure compound **4.4** was obtained in 25% yield (65 mg), as a light green solid.



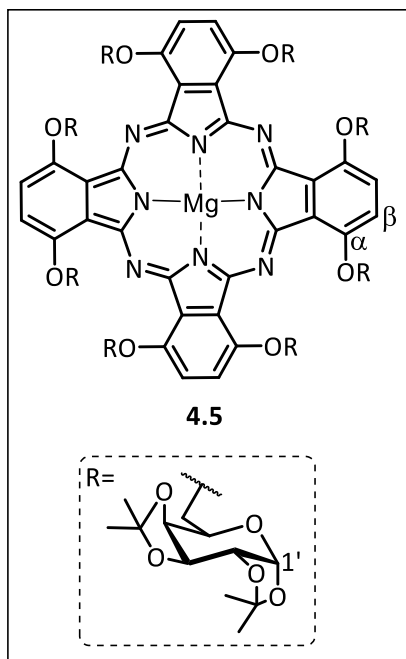
**<sup>1</sup>H-NMR (400.13 MHz, CDCl<sub>3</sub> + Py-*d*<sub>5</sub>), δ/ppm:** 7.55 (s, 8H, Pc-β-H), 5.37 (d, *J* = 5.0 Hz, 8H, H-1'), 5.14 (dd, *J* = 12.0, 5.4 Hz, 8H, H-6'a/b), 4.85 (dd, *J* = 12.0, 6.5 Hz, 8H, H-6'a/b), 4.47 (d, *J* = 8.1 Hz, 8H, H-4'), 4.34 (m, 8H, H-5'), 4.29 (dd, *J* = 8.0, 2.1 Hz, 8H, H-3'), 4.04 (dd, *J* = 5.0, 2.1 Hz, 8H, H-2'), 1.20 (s, 24H, CH<sub>3</sub>), 1.18 (s, 24H, CH<sub>3</sub>), 1.00 (s, 24H, CH<sub>3</sub>), 0.90 (s, 24H, CH<sub>3</sub>). **MS (MALDI-TOF, reflector mode):** *m/z* calcd. for C<sub>128</sub>H<sub>162</sub>N<sub>8</sub>O<sub>48</sub>Zn [M+2H]<sup>+</sup>: 2642.96, found: 2642.44. **UV-Vis (DMSO) λ<sub>max</sub>/nm (ε/M<sup>-1</sup> cm<sup>-1</sup>):** 326 (4.5x10<sup>4</sup>), 736 (1.1x10<sup>5</sup>). **Φ<sub>F</sub> (DMSO):** 0.17.

**[1,4,8,11,15,18,22,25-octakis-(1,2:3,4-Di-O-isopropylidene-α-D-galactopyranos-6-yl)phthalocyaninato] magnesium(II) (4.5)**

In a dried Schlenk flask, 48 mg of magnesium turnings (2 mmol) were suspended in 1 mL pentan-1-ol. This suspension was heated to 150 °C (reflux) and maintained at that temperature until a light grey amalgam was formed (near 1 hour). Then, 1 mL octan-1-ol was added to this amalgam, followed by 200 mg of phthalonitrile **4.3** (0.31 mmol). The reaction mixture was heated till 160 °C and stirred over a period of 3 h, under nitrogen atmosphere. After azeotropic removal of reactions solvents with toluene under reduced pressure, the crude mixture was poured into a mixture of dichloromethane/hexane (1:1) and filtered off. The green filtrate was evaporated under reduced pressure and, the resulting residue was subjected to silica gel column chromatography, using first a mixture of dichloromethane/ethyl acetate (1:1) as eluent, and then ethyl acetate to afford the green fraction containing phthalocyanine **4.5**. The solvent was removed, and



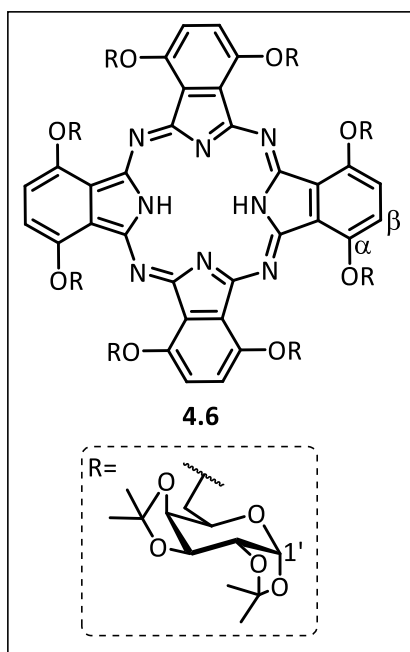
the green solid **4.5** was obtained in 15% yield (30 mg), after being washed with hot pentane and dried under reduced pressure.



**$^1\text{H-NMR}$  (400.13 MHz, DMSO- $d_6$ ),  $\delta$ /ppm:** 7.72 (s, 8H, Pc- $\beta$ -H), 5.52 (d,  $J = 5.0$  Hz, 8H, H-1'), 5.15 (br, 8H, H-Galactose), 4.89 (br, 8H, H-Galactose), 4.65 (d,  $J = 8.2$  Hz, 8H, H-Galactose), 4.54 (dd,  $J = 7.9, 1.6$  Hz, 8H, H-Galactose), 4.48–4.42 (m, 8H, H-Galactose), 4.33 (dd,  $J = 4.9, 1.9$  Hz, 8H, H-Galactose), 1.40 (s, 24H,  $\text{CH}_3$ ), 1.30 (s, 24H,  $\text{CH}_3$ ), 1.25 (s, 24H,  $\text{CH}_3$ ), 1.06 (s, 24H,  $\text{CH}_3$ ). **MS (MALDI-TOF, Dithranol):**  $m/z$  calcd. for  $\text{C}_{68}\text{H}_{71}\text{N}_8\text{O}_{23}\text{Mg}$  [ $\text{M}+\text{H}-5\text{Prot Gal}$ ] $^+$ : 1391.450, found: 1391.363, (\*Prot Gal = protected galactose residue). **UV-Vis (DMSO)  $\lambda_{\text{max}}$ /nm ( $\epsilon/\text{M}^{-1} \text{cm}^{-1}$ ):** 327 ( $4.6 \times 10^4$ ), 760 ( $9.7 \times 10^4$ ).  **$\Phi_{\text{F}}$  (DMSO):** 0.03.

#### 1,4,8,11,15,18,22,25-octakis-(1,2:3,4-Di-O-isopropylidene- $\alpha$ -D-galactopyranos-6-yl)phthalocyanine (4.6)

Lithium (50 mg, 7.1 mmol) and 1 mL of pentan-1-ol were placed in a dried Schlenk flask and the mixture was stirred, under nitrogen atmosphere, at 150 °C (reflux). After stirring for 1 h (*i.e.* when all the lithium was dissolved), 1 mL of pentan-1-ol was added, followed by 300 mg phthalonitrile **4.3** (0.47 mmol), and the reaction mixture was stirred over a period of 2 h at reflux, under nitrogen atmosphere. The reaction mixture was allowed to reach room temperature and it was poured into 25 mL THF. Glacial acetic acid (3 mL) was slowly added and the mixture was stirred at room temperature for 30 min. The reaction mixture was poured in a mixture of  $\text{H}_2\text{O}$ /methanol (2:1) and placed in a fridge until formation of a brown precipitate was observed. The solution was filtered, and the resulting precipitate was dissolved in dichloromethane and purified by a silica gel column chromatography, using first dichloromethane as eluent, and then a mixture dichloromethane/ethyl acetate (3:2) to collect the brown greenish fraction containing metal-free phthalocyanine **4.6**. After removal of solvent the compound **4.6** was obtained in 9% yield (28.1 mg), after being dried under reduced pressure.



**$^1\text{H-NMR}$  (400.13 MHz,  $\text{DMSO-}d_6$ ,  $100^\circ\text{C}$ ),  $\delta/\text{ppm}$ :** 7.80 (br, 8H, Pc- $\beta$ -H), 5.50 (br, 8H, H-1'), 4.80–4.14 (m, 48H, H-Galactose), 1.52–0.92 (m, 96H,  $\text{CH}_3$ ). **MS (MALDI-TOF, Dithranol):**  $m/z$  calcd. for  $\text{C}_{104}\text{H}_{127}\text{N}_8\text{O}_{38}$   $[\text{M}+\text{H}-2\text{Prot Gal}]^+$ : 2095.820, found: 2095.895;  $m/z$  calcd. for  $\text{C}_{92}\text{H}_{109}\text{N}_8\text{O}_{33}$   $[\text{M}+\text{H}-3\text{Prot Gal}]^+$ : 1853.710, found: 1853.785, (\*Prot Gal = protected galactose residue). **UV-Vis (DMSO)  $\lambda_{\text{max}}/\text{nm}$  ( $\epsilon/\text{M}^{-1} \text{cm}^{-1}$ ):** 332 ( $5.7 \times 10^4$ ), 782 ( $9.4 \times 10^4$ ).  **$\Phi_{\text{F}}$  (DMSO):** 0.02.

## 5.6 References

- <sup>1</sup> Fery-Forgues, S.; Lavabre, D., *Journal of Chemical Education* **1999**, 76 (9), 1260–1264.
- <sup>2</sup> Chauke, V.; Durmus, M.; Nyokong, T., *Journal of Photochemical and Photobiology A: Chemistry* **2007**, 192 (2-3), 179–187.
- <sup>3</sup> Rurack, K.; Spieles, M., *Analytical Chemistry* **2011**, 83 (4), 1232–1242.
- <sup>4</sup> (a) Larsen, P.; Ulin, J.; Dahlstrom, K.; Jensen, M., *Applied Radiation and Isotopes* **1997**, 48 (2), 153–157; (b) Link, J. M.; Krohn, K. A.; Clark, J. C., *Nuclear Medicine and Biology* **1997**, 24 (1), 93–97.
- <sup>5</sup> Shriver, D. F.; Drezdson, M. A., *The Manipulation of Air-Sensitive Compounds*, Wiley and Sons, New York, **1986**.
- <sup>6</sup> Burrows, H. D.; Pereira, M. M., *Química: Síntese e Estrutura - Uma abordagem prática*, Escolar Editora, Coimbra, **2006**.
- <sup>7</sup> Pinto, S. M. A.; Tomé, V. A.; Calvete, M. J. F.; Pereira, M. M., Burrows, H. D., Cardoso, A. M. S.; Pallier, A.; Castro, M. M. C. A.; Tóth, E. M.; Geraldés, C. F. G. C., *Journal of Inorganic Biochemistry* **2016**, 154, 50–59.
- <sup>8</sup> Zhang, L.; Huang, J.; Ren, L.; Bai, M.; Wu, L.; Zhai, B.; Zhou, X., *Bioorganic & Medicinal Chemistry* **2008**, 16 (1), 303–312.
- <sup>9</sup> Choi, C. F.; Huang, J. D.; Lo, P. C.; Fong, W. P.; Ng, D. K., *Organic & Biomolecular Chemistry* **2008**, 6 (12), 2173–2181.
- <sup>10</sup> Soares, A. R. M.; Tomé, J. P. C.; Neves, M. G. P. M. S.; Tomé, A. C.; Cavaleiro J. A. S., Torres, T., *Carbohydrate Research* **2009**, 344 (4), 507–510.
- <sup>11</sup> Kimani, S. G.; Shmigol, T. A.; Hammond, S.; Phillips, J. B.; Bruce, J. I.; MacRobert, A. J.; Malakhov, M. V.; Golding, J. P., *Photochemistry and Photobiology* **2013**, 89 (1), 139–149.
- <sup>12</sup> (a) Kumru, U.; Ermeydan, M. A.; Dumoulin, F.; Ahsen, V., *Journal of Porphyrins and Phthalocyanines* **2008**, 12 (10), 1090–1095; (b) Karabörk, M.; Serin, S., *Synthesis and Reactivity in Inorganic and Metal-Organic Chemistry* **2002**, 32 (9), 1635–1647.
- <sup>13</sup> Koç, V.; Topal, S. Z.; Aydın Tekda, D.; Ate, Ö. D.; Önal, E.; Dumoulin, F.; Gurek, A. G.; Ahsen, V., *New Journal of Chemistry* **2017**, 41 (18), 10027–10036.
- <sup>14</sup> Alzeer, J.; Roth, P. J. C.; Luedtke, N. W., *Chemical Communications* **2009**, 15, 1970–1971.
- <sup>15</sup> Alves, F.; Alves, V. H. P.; Do Carmo, S. J. C.; Neves, A. C. B.; Silva, M.; Abrunhosa, A. J., *Modern Physics Letters A* **2017**, 32 (17), 1740013-1–1740013-21.
- <sup>16</sup> Xu, L.-W.; Zhou, W.; Yang, L.; Xia, C.-G., *Synthetic Communications* **2007**, 37 (18), 3095–3104.
- <sup>17</sup> Tetsu, T.; Yuichiro, K.; Yasuhiro, Y.; Shue, K., *Chemistry - An Asian Journal* **2010**, 5 (9), 1974–1977.
- <sup>18</sup> Li, S. S.; Lin, H.; Zhang, X. M.; Dong, L., *Organic & Biomolecular Chemistry* **2015**, 13(4), 1254–1263.

---

<sup>19</sup> (a) European Pharmacopoeia, *Guide for the elaboration of monographs on radiopharmaceutical preparations*, Edition 2018, **2018**; (b) European Pharmacopoeia, 9<sup>th</sup> Edition, Vol. 1, **2017**, chapter 5.4 – Residual Solvents, 07/2016:50400, 665–672.

<sup>20</sup> (a) Benati, L.; Rino, L.; Minozzi, M.; Nanni, D.; Scialpi, R.; Spagnolo, P.; Strazzari, S.; Zanardi, G., *Angewandte Chemie International Edition*, **2004**, 43 (27), 3598–3601; (b) May Jr, J. A.; Sartorelli, A. C., *Journal of Medicinal Chemistry* **1979**, 22 (8), 971–976.

<sup>21</sup> Crucius, G.; Hanack, M.; Ziegler, T., *Journal of Porphyrins and Phthalocyanines* **2013**, 17 (8-9), 808–813.